A HIGH-PRECISION RADIAL-VELOCITY SEARCH FOR SUBSTELLAR COMPANIONS TO SOUTHERN SOLAR-TYPE STARS

A THESIS
SUBMITTED IN PARTIAL FULFILMENT
OF THE REQUIREMENTS FOR THE DEGREE
OF
DOCTOR OF PHILOSOPHY IN ASTRONOMY
IN THE
UNIVERSITY OF CANTERBURY
by

Kaylene A. Murdoch

University of Canterbury
1992

Contents

Appendices

List of Tables

List of Figures

Abstract

A system has been developed at the Mt John University Observatory to enable relative radial velocities of solar-type stars to be obtained with a characteristic random error of 55 m/s. The high radial-velocity precision has been achieved by interfacing a single optical fibre feed between the telescope and spectrograph, which has enabled the spectrograph to be mounted in a thermally and mechanically stable configuration and has virtually eliminated guiding errors.

Using this system, a programme of observation of 29 solar-type stars and 10 giant International Astronomical Union radial-velocity standard stars was carried out over 2.5 years with a view to the detection of low-mass companions to the dwarf stars. One star, HR 3220, turned out to have a previously-undiscovered stellar companion but no dwarfs showed obvious radial-velocity variability suggesting the presence of sub-stellar companions, although β Hyi showed a possible variation. This is despite the programme's sensitivity to the discovery of companions of mass 20 $M_{\mathcal{Q}}$ or greater in orbits of periods less than about 8 years (and larger masses in longer period orbits). In contrast, at least half the giant 'standard' stars were variable in radial velocity. Four and possibly five of the giant standards are probably intrinsic (pulsating) red or yellow (Walker *et al.* 1989) variables. Two further standards, β Aqr and δ Sgr, showed long-period variability suggestive of companions of indeterminable but low mass.

The lack of brown dwarfs observed in this programme is consistent with the results of other recent surveys. High-mass brown dwarfs appear to be rare as companions to stars and are probably rare in the field as well. They are unlikely to contribute significantly to the local mass density. Low-mass brown dwarfs (or high-mass planets) seem to be rare in orbits closer than 10 AU but could yet be found to abound in wider orbits or in the field.

Chapter 1

Introduction

The observed mass range of stars spans three orders of magnitude. However, between stars of about a tenth of a solar mass and the most massive *planet* in the solar system (Jupiter), there is no certain evidence of any objects at all. Jupiter, nevertheless, is two orders of magnitude less massive than the least massive known stars. The question arises whether or not this lack of objects with masses intermediate between stars and planets is real. It is with this question that this thesis is concerned. The discovery of even a single object in this mass range would have implications for several areas in astronomy — among them the physics of star formation at low masses, the relationship between planet and star formation and the dynamical implications of possible large populations of presently invisible substellar objects. The techniques required for searching for such objects are, however, exercises in advancing the technical limits of astronomy, since faint, sub-massive objects are difficult to detect.

1.1 Brown dwarfs: theoretical predictions

It is unlikely that all objects formed like stars do actually become stars. Only if the objects formed from the collapse of interstellar molecular clouds[1] have sufficient mass will they be able to sustain the hydrogen fusion reactions which characterize a main-sequence star. The theoretical hydrogen-burning minimum mass was first determined about 30 years ago (Kumar 1963; Grossman 1970; Grossman, Mutschlecner & Pauls 1970; Grossman & Graboske 1971) and now is agreed to be about 0.080 $M_{\odot}$ (solar masses) (*e.g.* D'Antona & Mazzitelli

[1]Star formation scenarios are reviewed by Shu, Adams & Lizano (1987).

1985; Nelson, Rappaport & Joss 1986; Burrows, Hubbard & Lunine 1989)— approximately 80 $M_{\mathcal{U}}$ (Jupiter masses)[2]. The core of an object formed with a mass less than this will never reach the temperature and pressure necessary to maintain significant thermonuclear hydrogen burning. The object may burn deuterium for a short time if it has sufficient mass, but will spend most of its lifetime cooling and fading, radiating only the virialized energy of its gravitational collapse. Such hypothetical failed 'stars' have been named *brown dwarfs* (Tarter 1975). The term 'dwarf' acknowledges formation in the manner of stars, that is, by the collapse and fragmentation of interstellar clouds. The colour 'brown' was chosen as being intermediate between 'red' — implying a main-sequence *star* — and 'black' — implying emission of no radiation at all — since although formed like stars, brown dwarfs would be cool and therefore intrinsically faint enough that even nearby ones would be invisible to most instruments. Brown was also thought to be appropriate as not a true colour, since predicting the colours of brown dwarfs has proved difficult because of the probable presence of complex opacity sources.

While the upper mass limit for brown dwarfs is defined by the end of the stellar main sequence, the lower mass limit is usually defined by the lowest mass that can result from the fragmentation of a protostellar cloud. This lower limit has been variously estimated to be between 3 $M_{\mathcal{U}}$ (Low & Lynden-Bell 1976) and 20 $M_{\mathcal{U}}$ (Boss 1986). On the other hand, recent star-formation models suggest that the onset of deuterium burning may be a necessary stage in star-like formation (see the review by Shu *et al.* 1987) and therefore the lower mass limit for brown dwarfs might be defined by the lower mass limit for the onset of deuterium burning — 15 $M_{\mathcal{U}}$ (Burrows *et al.* 1989). Although the value of this lower limit to the mass of brown dwarfs is uncertain, it is significant that all estimations are well below the hydrogen-burning minimum mass. Unless there is a serious problem with the modelling, theory admits the possibility of the existence of brown dwarfs.

Planets, while being of similar observational interest in that they are also substellar in mass, are probably distinct from the theoretical impression of a brown dwarf because of a different manner of formation. Evidence from the solar system (*e.g.* rocky planet cores, small orbital eccentricities, roughly coplanar orbits) suggests that planets form by accretion in a disk of cold matter, rather than by collapse and fragmentation of a molecular cloud[3]. Although there is no

[2] $1\ M_{\mathcal{U}} \approx 0.001\ M_{\odot}$.

[3] Planet formation scenarios are reviewed by Wetherill (1980) and Pollack (1984).

Mass					Formation process
			80 $M_{\mathcal{Q}}$	< star	Fragmentation
	20 $M_{\mathcal{Q}}$	< brown dwarf <	80 $M_{\mathcal{Q}}$		Fragmentation
planet <	?				Accretion
		⟵ substellar objects |			

Figure 1.1: Distinction between stars, brown dwarfs and planets.

overlap in the mass range of stars and in the mass range of brown dwarfs, in the lack of knowledge of the maximum planetary mass, there seems to be no reason why there should not be an overlap in the mass range between *planets* and brown dwarfs, because of the different formation processes. Figure 1.1 summarizes the differences outlined here between stars, brown dwarfs and planets.

1.2 The stellar mass function

Over and above the theoretical likelihood of the existence of brown dwarfs, observational evidence leads to the conclusion that they might exist in very large numbers. It is a well-known fact that the observed number density of stars in the Galaxy at a given mass increases towards lower masses. In a given volume of space, there are relatively few of the massive O-type dwarfs but much larger numbers of the low-mass M-type dwarfs which dominate the total mass of stars in the solar neighbourhood (*e.g.* Bahcall & Soneira 1980). Since brown dwarfs are still lower in mass than these stars, the possibility arises that since stars and brown dwarfs are formed by the same process, perhaps the trend continues and brown dwarfs are present in numbers even exceeding M stars.

The present-day *mass function* is the observed frequency distribution of stellar masses. For stars in the Galaxy with masses less than 0.9 $M_{\odot}$, this is the same as the initial mass function (IMF) — the frequency distribution of stellar masses at birth — since such stars can not have evolved away from the main sequence during the lifetime of the Galaxy. The classic IMF is that of Salpeter (1955) who, using data for stars between 0.4 $M_{\odot}$ and 10 $M_{\odot}$, described the frequency distribution ξ of stellar masses M as a power law:

$$\xi(M)dM = 0.013M^{-2.35}dM,$$

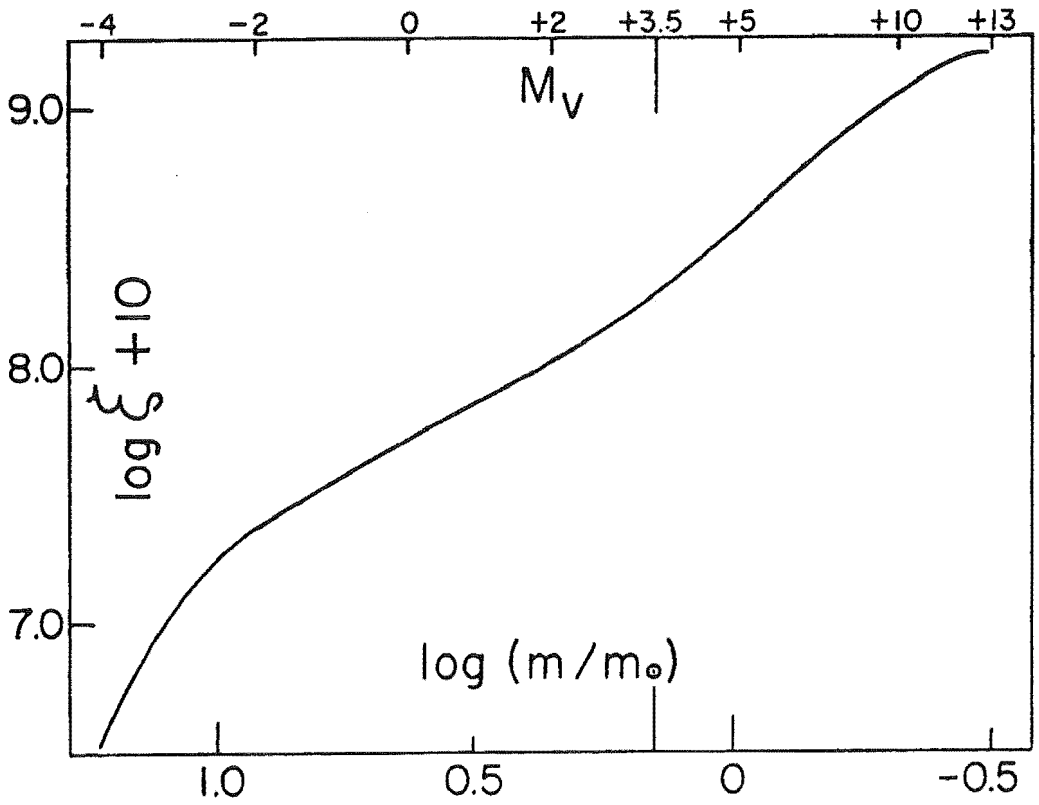

Figure 1.2: Salpeter's IMF which approximates a power law between 0.4 $M_\odot$ and 10 $M_\odot$ (adapted from Salpeter 1955).

which is illustrated in Figure 1.2. This increase in the frequency of stars towards low masses was interpreted, on extrapolation to even lower masses, to imply the existence of a large population of brown dwarfs, dominating the total mass of stars (Kumar 1972; Ostriker & Peebles 1973; Stevenson 1978).

Determination of the mass function involves combining an observational luminosity function with an observational mass-luminosity relationship. Both are difficult to determine for faint stars, but the uncertainties in particularly the mass-luminosity relationship are such that even the most modern results for the mass function at low masses should be treated with caution. Some recent determinations of the mass function of low-mass stars below the 0.4 $M_\odot$ sample limit of Salpeter suggest that a unique power law is in fact not appropriate to describe the numbers of stars in the substellar range. Reid & Gilmore (1984); Scalo (1986) and Kroupa, Tout & Gilmore (1990) find that the frequency of stars flattens out or even decreases at around 0.3 $M_\odot$. Others still find the frequency of stars increasing through the hydrogen-burning limit at 0.08 $M_\odot$ (Hawkins &

Bessell 1988; Leggett & Hawkins 1988). In a review, Liebert & Probst (1987) tentatively summarize that on balance, the IMF appears to be flat or increasing near the hydrogen-burning mass limit. Brown dwarfs are still very likely to exist by mass-function arguments and furthermore could, by any evidence, be present in large numbers.

1.3 The 'missing mass' problems

> *Unseen bodies may, for aught we can tell, predominate in mass over the sum-total of those that shine; they supply possibly the chief part of the motive power of the universe.*
>
> — Agnes Clerke, *Problems in Astrophysics*, 1903.

The prediction of large numbers of brown dwarfs in the Galaxy provides an attractive solution to one of the long-standing 'missing mass' problems of astronomy. These problems refer to the fact that on a variety of scales, the mass of a system derived from its dynamics exceeds the mass of the luminous matter — stars and gas. This suggests the presence of previously unaccounted-for 'dark' matter which could at least in part comprise brown dwarfs.

The first missing-mass problem came to light in the 1930s when Oort (1932, 1960) compared the mass density of visible matter in the solar neighbourhood to the mass implied by the force of gravity pulling stars back into the Galactic disk. He deduced that as much as 50 per cent of the mass in the solar neighbourhood is unaccounted for by luminous material and must be made up of dark matter of some form. This conclusion was upheld in much later studies, most notably by Bahcall (1984a, 1984b).

Later, in the 1970s, it was discovered (Roberts 1976; Krum & Salpeter 1976, 1977; Rubin, Ford & Thonnard 1978) than normal spiral galaxies have rotation curves[4] that, instead of dropping off with increasing radius[5], are flat out to the optical radius and far beyond it[6], suggesting the presence of dark matter at large radii. Ostriker & Peebles (1973) postulated on early hints of these flat rotation curves that such galaxies are embedded in massive, dark halos, outweighing the luminous matter by a factor of ten, the nature of this second 'missing mass' being again unknown.

[4] Galactic rotation curves represent the circular velocity of galactic material as a function of radial distance from the galactic centre.

[5] As is expected if the galactic mass is centrally concentrated.

[6] Rotation curves beyond the optical radius were determined using HI 21 cm observations.

On a larger scale again, in the 1930s Zwicky (1933) and Smith (1936) deduced that if the Coma and Virgo clusters were gravitationally bound then more mass had to exist in the clusters than is apparent in the form of luminous matter. This conclusion holds even if the mass of the dark galactic halos is taken into account. Furthermore, this same problem has been detected on the scale of superclusters of galaxies.

The nature of the dark matter is uncertain. A review of the observational constraints on its nature is given by Trimble (1987). In short, the missing mass is likely to be made up of some combination of baryonic and non-baryonic particles. In the realm of baryons, large numbers of brown dwarfs provide a plausible solution to at least the problem of the local missing mass.

1.4 Detection of brown dwarfs

To date, there have been no certain detections of brown dwarfs and all current brown-dwarf candidates have been isolated within only the last 5 years. This is hardly surprising since brown dwarfs represent a considerable observational, and hence technological, challenge. Their faintness and redness (thermal spectrum peak in the infrared) mean that they are selected against in surveys — they require detectors that are sensitive in the infrared, but infrared detectors tend to be somewhat smaller and less sensitive than optical detectors. Furthermore their masses are low enough that brown dwarfs in binary systems would induce only very small and difficult-to-detect gravitational perturbations on their more visible stellar primaries.

The methods for detecting brown dwarfs can be divided into two general categories: direct techniques — whereby light from the brown dwarf itself is detected, and indirect techniques — whereby the existence of the brown dwarf is inferred from its influence on the more easily detected light from a star. These techniques are described below, with more attention being paid to the indirect techniques which are of more importance to this thesis. Specific results from the individual studies that are referred to will be discussed in more detail in Chapter 8.

1.4.1 Direct techniques

In this category fall techniques whereby the brown dwarf is to be imaged, such as infrared speckle interferometry[7] (*e.g.* Henry & McCarthy 1990), infrared array searches (*e.g.* Skrutskie, Forrest & Shure 1989) and deep photographic (*e.g.* Hawkins 1986) or CCD (*e.g.* Jameson & Skillen 1989; Stauffer *et al.* 1989) sky surveys. Also in the category of direct techniques fall infrared photometric surveys of white dwarfs (*e.g.* Zuckerman & Becklin 1987a) in order to look for brown-dwarf companions. The idea in the latter kind of survey is to look for an excess of infrared emission over the little normally expected from a white dwarf.

The main problem with surveys using direct techniques is that they rely heavily on comparison with theoretical models to see whether the observational quantities (colour, luminosity, spectra) are in agreement with those predicted for a brown dwarf. In a review, Stevenson (1991) expresses some confidence in the models for brown dwarfs in the degenerate cooling phase but admits that models are unreliable for earlier epochs. A further difficulty in the identification of young brown dwarfs is that there is a considerable overlap in their predicted luminosities with the predicted luminosities of lower main-sequence stars (D'Antona 1987), creating confusion as to which are brown dwarfs and which are stars (D'Antona & Mazzitelli 1985). These problems are particularly important as newly-formed non-degenerate brown dwarfs are the brightest brown dwarfs which makes searches for them in star-forming regions very attractive. In practice, only older, degenerate brown dwarfs are distinctive (Stevenson 1991) but these are faint and therefore more difficult to detect.

There are some considerable advantages in using direct techniques for searching for brown dwarfs. Significant scientific contributions can be made by short-term projects, for example. Imaging techniques are the only techniques suitable for looking for isolated ('free-floating') brown dwarfs. However, the main disadvantage is that the primary parameter characterizing a brown dwarf is its mass and this cannot be directly determined from observational parameters such as luminosity and colour.

[7] For a review of the technique of speckle interferometry see McAlister (1988).

1.4.2 Indirect techniques

Someone saw Nasrudin searching for something on the ground.

"What have you lost, Mulla?", he asked. "My key", said the Mulla. So they both went down on their knees and looked for it.

After a time the other man asked: "Where exactly did you drop it?"

"In my house."

"Then why are you looking here?"

"There is more light here than in my house!"

— Indries Shah, *The exploits of the incomparable Mulla Nasrudin.*

Indirect techniques avoid the problem of trying to detect the sparse light from the brown dwarf itself and instead look for changes in more easily-detectable starlight which might betray the presence of a brown-dwarf companion. The two major indirect techniques — astrometry and radial velocities — involve looking for the tiny gravitational perturbation that would be induced in the motion of a star were it in orbit with a brown dwarf. Although both techniques require that observing programmes be long-term (of the order of the maximum orbital period to be detected), their great advantage over direct techniques is that the mass of the companion arises as a direct interpretation of the observations, requiring no intermediate modelling.

Astrometry

Astrometric techniques[8] (*e.g.* Heintz 1989) involve the long-term observations of the positions of stars in order to look for the periodic 'wobble' of a star's motion in the plane of the sky as it moves in orbit about the centre-of-mass of the system (see Figure 1.3). The mass of a companion in a circular orbit in the plane of the sky is given by

$$M_2 = \left(\frac{M_1}{P}\right)^{2/3} \frac{\theta}{\pi_p} \ ,$$

where the mass of the primary M_1 (the star) and the mass of the secondary M_2 (the brown dwarf) are in $M_\odot$, the period P is in years and the parallax π_p and the angular perturbation θ are in arc s. From this equation, which is simplification in that it ignores projection and eccentricity effects, it can be seen that astrometric studies are most sensitive to the detection of low-mass companions for small primary star masses, long periods and nearby systems. The astrometric

[8] Astrometric techniques are reviewed by Lippincott (1978).

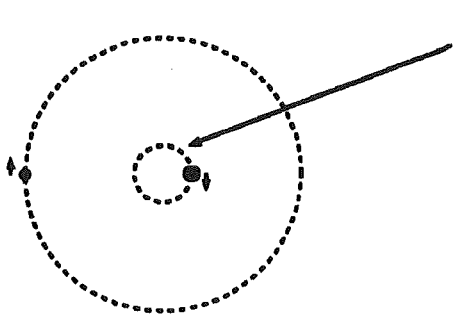

Miniature reflex orbit of star due to a sub-stellar companion is detected as ...

...a periodic change in the star's radial velocity.

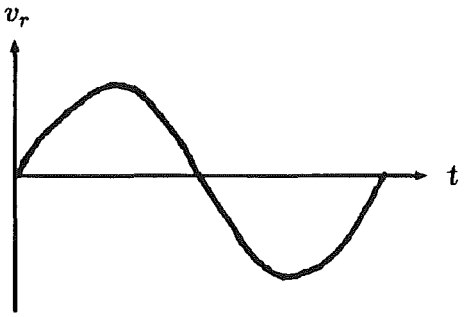

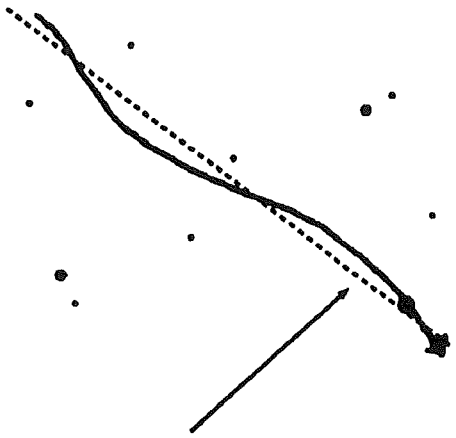

...a periodic astrometric deviation of the star's path in the sky relative to background stars.

Path if no companion

Figure 1.3: Schematic description of the astrometric and radial-velocity techniques.

Period	⟸Brown dwarfs⟹				
(years)	1 $M_{\mathcal{Q}}$	20 $M_{\mathcal{Q}}$	50 $M_{\mathcal{Q}}$	80 $M_{\mathcal{Q}}$	100 $M_{\mathcal{Q}}$
0.1	0.02	0.4	1.1	1.7	2.2
0.5	0.06	1.3	3.2	5.0	6.3
1.0	0.10	2.0	5.0	8.0	10.0
2.0	0.16	3.2	7.9	12.7	15.9
5.0	0.29	5.8	14.6	23.4	29.2
10.0	0.46	9.3	23.2	37.1	46.4

Table 1.1: Maximum amplitude of astrometric perturbation (in marcsec) of a 1 $M_{\odot}$ star at a distance of 10 pc orbited by a companion of given mass and period in a circular orbit.

perturbation θ in a nearby star induced by a brown dwarf would typically be of the order of marcsec (see Table 1.1). Not only do techniques then need to have positional accuracies of marcsec or better to be able to detect brown dwarfs (fractions of marcsec for searches for planets), but they also need to be able to maintain such accuracies over many years.

Radial velocities

A stellar radial velocity is the velocity of a star along the observer's line of sight and is measured from the Doppler shifts of absorption lines in the stellar spectrum. Radial-velocity techniques (*e.g.* Campbell & Walker 1979; Marcy & Benitz 1989) involve the long-term observations of the radial velocity of a star in order to look for periodic changes in that velocity indicative of orbital motion.

In the case of a star with a stellar companion of similar luminosity, the spectral lines of both components of the system are visible and the radial-velocity curve of both stars can be determined. In such *double-lined spectroscopic binaries*, one is able to determine the ratio of the masses in the system. In the case where the spectrum of only the primary star can be observed, as would be the case for a brown-dwarf companion, only one spectrum is visible and only a single velocity curve can be determined. In this case of the *single-lined spectroscopic binary*, the companion mass is related to the derivable orbital parameters by:

$$f(M) = \frac{M_2^3 \sin^3 i}{(M_1 + M_2)^2} = \frac{P}{2\pi G}(1 - e^2)^{3/2} K_1^3,$$

where i is the inclination of the orbit to the plane of the sky, K_1 is the radial-velocity semi-amplitude of the star and G is the universal gravitational constant.

$f(M)$ is called the spectroscopic *mass function.* For $M_2 << M_1$, the approximation can be made that $M_1 + M_2 \approx M_1$ so that

$$M_2 \sin i \approx \left(\frac{1}{2\pi G}\right)^{1/3} (1-e^2)^{1/2} P^{1/3} K_1 M_1^{2/3}$$

From this equation it can be seen that the radial-velocity technique is most sensitive to the detection of low-mass companions for small primary star masses and short period orbits. The technique is thus somewhat complementary to astrometry in that it is most sensitive to short periods while astrometry is most sensitive to long periods. Furthermore the perturbation in radial velocity K_1 is independent of the system distance, while the astrometric perturbation θ is inversely proportional to distance. Lastly, the radial-velocity technique detects most easily those orbits perpendicular to the plane of the sky (along the line of sight) while astrometry selects for orbits in the plane of the sky.

The biggest drawback of the radial-velocity technique is that the derivable quantity is not M_2 but $M_2 \sin i$, and there is usually no knowledge of the orbital inclination, i. Since the companion mass must be equal to or more than $M_2 \sin i$, the technique provides only a lower limit to M_2. In the search for brown dwarfs, this means that radial-velocity evidence alone does not form a strong case for the companion being substellar, since a stellar mass can be implied by any suitably small inclination. Orbital inclinations of single-lined spectroscopic binaries are in general difficult to determine, although statistical analyses or occultation studies (see Section 1.4.2) may provide probabilities that the companion is below stellar mass.

Serkowski (1976) was one of the first to recognize the potential of the radial-velocity technique in the detection of substellar companions to stars. In order to search for brown dwarfs however, one must have very high radial-velocity precision. The maximum velocity displacement K_1 of a solar-type primary star would typically be of the order of only several hundreds of metres per second for a brown-dwarf mass secondary. Table 1.2 shows the typical maximum velocity semi-amplitude in metres per second of a 1 $M_\odot$ star with a companion in a circular orbit of varying mass and period. Because of this small displacement, one therefore requires that the radial-velocity error is no more than about 100 m/s or so in order to be serious about looking for brown dwarfs. Compared to traditional techniques of obtaining radial velocities where the precision is typically about 1 km/s, this is a challenging goal. Furthermore, Table 1.2 indicates that searches

Period	⇐Brown dwarfs⇒				
(years)	1 $M_{\mathcal{U}}$	20 $M_{\mathcal{U}}$	50 $M_{\mathcal{U}}$	80 $M_{\mathcal{U}}$	100 $M_{\mathcal{U}}$
0.1	64	1282	3206	5130	6412
0.5	37	749	1875	3000	3750
1.0	30	595	1488	2381	2976
2.0	24	472	1811	1889	2362
5.0	17	348	870	1392	1740
10.0	14	276	690	1105	1381

Table 1.2: Maximum semi-amplitude of radial velocity perturbation (in m/s) of a 1 $M_{\odot}$ star orbited by a companion of given mass and period in a circular orbit.

for Jupiter-mass companions require precisions of metres per second, since low-mass companions in long-period orbits induce perturbations at the metre-per-second level. High-precision radial velocities are the subject of this thesis and are discussed more fully below.

Other techniques

Three other techniques deserve mentioning. The periodic motion of a pulsar with an unseen companion about the centre-of-mass of the system will cause, if the plane of the orbit is not face-on-to the observer, a periodic change in the timing of the radio signal emitted from the star. Although the question arises as to how a low-mass object would survive the supernova explosion that led to the pulsar, to date one group (Wolszczan & Frail 1992) has observed such periodicities and has ascribed them to substellar mass companions.

Secondly, if the plane of the orbit of a substellar companion to a star is sufficiently parallel to the line-of-sight, the object may occult some of the light from the star. This photometric signal may be interpreted to infer the existence of the companion. Although this is too much of a 'long shot' technique to be used in *surveys* to find low-mass companions, since such occultation would be rare, it has already proved useful in putting a constraint on the inclination of an orbit (an hence on the secondary mass) determined from the radial-velocity technique (Robinson *et al.* 1990).

Finally, the gravitational lensing of light from a compact object by another compact object will create two or more images, the combined brightness of which is greater than that if the single, unlensed image. If the two images are not resolved, then the effect of this *microlensing* is just an increase in brightness of

the source object. Intensive searches for gravitational microlensing by brown dwarfs or planets have been suggested as a means for detecting substellar objects in the galactic halo (Gott 1981) or disk (Paczyński 1991). In the former case the source object might most easily be Magellanic Cloud stars, in the latter case, galactic bulge stars.

1.4.3 Case: detection of Jupiter

As techniques for looking for brown dwarfs become more sensitive, they will become more appropriate in the search for objects of planetary mass. An example often used (*e.g.* Brown 1989) to illustrate the difficulty of detecting a planet in orbit about a star is the case of trying to detect Jupiter in orbit about the sun from the favourable distance of 5 pc. The challenge to direct detection would be trying to detect an object which is only 26th magnitude in the visual which is at maximum separation, only 1 arc s away from a 4th magnitude star. Even at 20 μm, the wavelength of Jupiter's thermal spectrum peak, the magnitude difference reduces to a still-formidable 11.5 magnitudes. The challenge to indirect searches would be to astrometry — detecting the maximum 1 marcsec reflex displacement; to radial-velocity searches — detecting the maximum 13 m/s reflex velocity; to occultations — detecting the 1 per cent dimming in sunlight which would occur for only 30 hours in every 12 years for only 0.1 per cent of the celestial sphere.

1.5 High-precision radial velocities

The astrophysical merits of obtaining stellar radial velocities to a precision of hundreds or even tens of metres per second are without doubt, with applications in the fields of stellar seismology and stellar pulsation as well as in the search for extra-solar planets or brown dwarfs. However, attaining such precision is not a simple matter, let alone maintaining it over the years necessary for a search for brown dwarfs. It is only in the last decade or two that errors in measured radial velocities below ± 1 km/s have been achieved routinely, chiefly due to the improved efficiency of obtaining velocities since the advent of solid-state detectors (Reticon diode arrays, CCDs) and cross-correlation techniques. Table 1.5 reviews a sample of radial-velocity programmes over the course of the history of stellar radial velocities, showing the typical precision in each case. As this thesis is

Year	Principal observer	Method	Error (m/s)
1870	Huggins, Secchi	visual	40000
1892	Vogel	photographic	4000
1894	Keeler	visual (3 bright stars only)	3000
~1910	Frost	photographic (B stars)	13000
1910	Pickering	objective prism	15000
1913	Schwarzschild	objective prism	10000
~1920	Campbell, Moore, Wright, Adams, Joy, Plaskett	photographic	1000–4000
1921	Plaskett	photographic (early Sp types)	2500–10000
1955	Fehrenbach	objective prism	4000–10000
1967	Griffin	photoelectric coudé scanner	< 1000
1980	Mayor	photoelectric, Cassegrain échelle	200–400
1989	Latham	digital cross correlation	250
1989	Marcy	digital cross correlation	230
1989	Scarfe	photographic, image slicer	145
1989	Campbell	HF cell	13
1992	Marcy	I_2 cell	25

Table 1.3: Review of radial-velocity programmes in the past 120 years.

concerned mostly with the application of radial-velocity measurements to brown-dwarf searches, Table 1.5 lists only those programmes conducted over a time-scale of at least a year.

1.5.1 The problem of obtaining high-precision velocities

In an ideal system, the positions of stellar lines relative to the lines of some comparison spectrum[9] at rest relative to the observer are a result only of the difference in radial velocity between the star and the observer. In this case the precision with which the radial velocity can be measured is limited solely by the finite amount of noise in the two spectra. Theory indicates (Chapter 2) that the radial-velocity information content in a high-dispersion late-type stellar spectrum of even modest coverage and signal-to-noise implies a spectral-noise limited random error-bar of typically only a few metres per second. This precision would be ideal for most conceivable applications.

The problem is that typically it is not photon noise which limits radial-velocity precision. In practice the position of stellar spectrum relative to a reference

[9]Traditionally an emission lamp mounted in the spectrograph.

spectrum is affected also by instrumental factors which cause the stellar spectrum to shift on the detector, mimicking a Doppler shift. These factors include:

- *Changes in air temperature or pressure in the spectrograph* which alter the air's refractive index and hence the lines' wavelengths.
- *Changes in spectrograph temperature* which cause expansion or contraction of components of the spectrograph.
- *Mechanical flexure* of a Cassegrain spectrograph as the telescope tracks.
- *Guiding errors.* Non-uniform illumination of the spectrograph slit through irregular guiding results in asymmetrical line profiles and therefore apparent shifts of the line centres.
- *Difference in ray path between starlight and comparison lamp light.* Zonal optical aberrations may cause light of the same wavelength to be focussed in different places on the detector causing a shift between stellar and comparison light of the same wavelength (Tull 1969).

The spurious shifts from these instrumental sources are difficult both to control and to measure and have in practice limited the precision of many radial-velocity programmes. In a classic paper Griffin & Griffin (1973) summarize the problem as being due to the nature of the reference source. An emission lamp reference spectrum cannot be affected in exactly the same way as the stellar spectrum by instrumental shifts. They suggested the solution of a wavelength reference superimposed on the stellar spectrum such as telluric O_2. In principle such lines must be affected in the same manner as the stellar lines.

1.5.2 Techniques of radial-velocity measurement

Techniques using an emission lamp as a reference source

Early stellar radial velocities were obtained from the *measurement of the positions of individual stellar absorption lines.* A stellar spectrum is recorded (traditionally photographically) along with a reference emission lamp spectrum which provides a dispersion relation. The Doppler-shifted wavelengths of stellar lines with known laboratory rest wavelengths are then obtained from measurement of the line positions. The difference in wavelength of a line from its rest wavelength gives the apparent radial velocity of the star. Any one spectral line provides a

radial velocity but in practice, the radial-velocity precision is improved through the measurement of many lines.

While a Doppler shift in a stellar spectrum can be measured line by line, the method involves laborious reduction and ignores the information content of lines of unknown wavelength or which are too weak to measure. Furthermore, for the accurate measurement of individual line positions a high signal-to-noise spectrum and precise laboratory rest-wavelengths of the lines are required. Modern programmes often favour *cross-correlation techniques*, where the stellar spectrum is cross correlated with a 'mask' or 'template' spectrum. The result is a function with a maximum (or minimum, depending on whether the mask is positive or negative) corresponding to the relative radial velocity of the two spectra. The advantage of cross correlation is that it exploits the redundancy of radial-velocity information found in the lines of a spectrum by condensing *all* the line information into the cross-correlation function peak (or dip) while automatically weighting the contribution of each line according to its strength. Laboratory rest wavelengths of stellar lines are not needed and the required signal-to-noise (and therefore exposure time) is much less than for measuring the positions of individual lines for the same quality radial velocity, allowing observations of more and fainter stars.

Griffin (1967) pioneered the first analogue cross-correlation device, whereby the spectrum is cross correlated with a physical mask[10] and the resulting cross-correlation function was recorded photo-electrically. This instrument was used with a coudé spectrograph, while later devices have also used échelle spectrographs (*e.g.* CORAVEL: Baranne, Mayor & Poncet 1979). The early 1980s brought solid-state detectors to the fore and thus also the possibility of determining radial velocities by means of *digital* cross correlation, as discussed by Simkin (1974). In this case the spectrum is imaged and cross correlated later in a computer (Da Costa *et al.* 1977; Hill 1982; Latham 1985; Marcy & Benitz 1989).

In both individual-line measurement and cross-correlation schemes, the wavelength reference is typically provided by an emission lamp in the spectrograph. In order to reduce the effect on radial-velocity precision of flexure and temperature and pressure changes, comparison spectra are usually obtained both before and after the stellar exposure in order to estimate the zero point of the system at the mid-exposure time (Marcy & Benitz 1989; Latham 1985). Guiding errors can be reduced by using an autoguider (Baranne *et al.* 1979), an image slicer (Scarfe,

[10]The mask is opaque except where there are spectral lines.

Batten & Fletcher 1989) or a narrow spectrograph slit (Marcy, Lindsay & Wilson 1987) or by observing in 'poorer' seeing conditions, since all these result in more even illumination of starlight on the slit.

Despite these precautions, all the programmes listed in this section are limited principally by guiding and flexure errors to a radial-velocity error of a couple of hundred metres per second or so. The main problem is that the reference spectrum is affected in a different way than the stellar spectrum by instrumental shifts.

Techniques with wavelength reference on the stellar spectrum

The most precise velocities have been obtained by those who have attempted to track the instrumental shifts in the spectrum using a calibration spectrum *superimposed* on the stellar spectrum. The theory is that the stellar spectrum and the calibration spectrum will be subject to the same instrumental shifts.

Cochran (1988) and Smith (1982, 1983) have employed the suggestion of Griffin and Griffin (1973) of telluric O_2 as a wavelength reference with success, obtaining random errors of between ± 5 m/s and ± 20 m/s over a few nights. The reduction technique in these cases does not lend itself to automation in that blends of telluric and stellar lines must be fitted on a case-by-case basis. The precision is ultimately limited by atmospheric winds.

Campbell, Walker & Yang (1988) have employed a similar rationale by placing a cell of HF gas ahead of the slit of a coudé spectrograph, imposing reference HF absorption lines on the stellar spectrum. Again, the procedure ensures that the stellar and reference lines are recorded simultaneously and under identical conditions and has resulted in a random error of only ± 13 m/s over several years. This is the only technique involving a wavelength reference superimposed on the stellar spectrum which has demonstrated such precise stellar radial velocities over the matter of years required for a search for substellar companions to stars. Nevertheless, the instrumental and reduction requirements are demanding. HF is a highly noxious gas requiring careful handling, reduction procedures are complex and the high signal-to-noise spectra and short exposure times needed mean that a large telescope is required. The Canada-France-Hawaii 3.6 m was used, for which there is great competition for observing time.

A similar technique, but with molecular iodine as the captive gas, has been used by two groups, Marcy & Butler (1992) and Cochran & Hatzes (1990). In

the former case, an échelle spectrograph and large-format CCD is used to obtain stellar radial velocities with a random error of 25 m/s over one year. In the latter case, a coudé spectrograph and smaller format CCD acquire spectra at higher resolution and from observations of the Moon, radial velocities appear to be stable to about 10 m/s in the long term.

Finally, a Fabry-Perot etalon has been used to impress wavelength calibration on starlight by McMillan *et al.* (1985) with resulting random errors of about ±10 m/s but only over a matter of days.

1.6 The Mt John radial-velocity programme

The distinguishing feature of the radial-velocity programme at the University of Canterbury's Mt John University Observatory is that radial velocities of high precision are obtained not by mapping instrumental shifts precisely with a special reference source but simply by reducing the magnitude of the instrumental shifts.

The instrumentation for the programme is generally unremarkable: it comprises the Observatory's 1 m telescope, high-dispersion échelle spectrograph and Reticon diode array detector. The reference source is a Th-Ar hollow-cathode emission lamp. If the spectrograph were mounted on the telescope at the traditional Cassegrain focus the precision would be limited to a few hundred metres per second, principally by guiding errors and the difference in ray paths between the starlight and Th-Ar lamp light. Instead, the programme is distinguished by the spectrograph being mounted vertically on a trolley in a room adjacent to the dome. Light is fed from the focus to the spectrograph via a single optical fibre feed. This configuration has many advantages for reducing instrumental shifts. Light scrambling in the fibre produces a uniformly illuminated output at the spectrograph slit (Kapany 1967), eliminating guiding errors. A Th-Ar calibration lamp is mounted at the fibre input module, so that this light also passes down the fibre. Starlight and comparison lamp light enter the spectrograph in the same way ensuring that the ray paths are virtually identical. Furthermore, since the spectrograph no longer moves as the telescope does, there is no flexure of the spectrograph throughout an exposure, eliminating flexure errors. Finally, the fact that the spectrograph is stationary has allowed it to be enclosed in a thermally-insulated cabinet, reducing errors from thermal effects. This set-up has enabled radial velocities of bright solar-type stars to be obtained by the method of digital cross correlation, with all the method's simplicity of implementation

and throughput advantages, with a typical external error of only 55 m/s.

The Mt John system has been used to observe a sample of 40 solar-type stars and International Astronomical Union radial-velocity standard stars monthly over a period of 2.5 years. The aim was to search for the very low-amplitude velocity variations suggestive of reflex motion due to unseen substellar companions. Estimating that this time frame might allow the discovery of orbits with a period of up to 5 years and that the precision of the system might allow the detection of orbits with a semi-amplitude as small as 100 m/s, the capability of the programme can be estimated to be the detection of companions of mass 6 $M_{\mathcal{Y}}$ and over, if within at least 3 astronomical units of the primary star, and still smaller masses if in closer orbits.

1.7 Introduction to the thesis

This thesis discusses the high-precision radial-velocity programme at the Mt John University Observatory and its application to a search for low-mass companions to a sample of southern solar-type stars.

Chapter 2 describes the technique of cross correlation to obtain stellar radial velocities and analyses its potential for the measurement of radial velocities of high precision. To do this, the ideal system where the error in radial velocity arises only from noise in the stellar spectrum is considered. A theoretical derivation is provided of the ultimate limit to the precision of radial velocities by cross correlation from the presence of spectral noise. The relationship is used to establish spectrograph settings for maximizing the radial-velocity precision for a given object, exposure time and observing instrument. The results are applicable for various detectors and for fibre-fed or Cassegrain-mounted spectrographs, so are of general interest. There are several mathematical symbols used in this chapter and so definitions for these, and also for symbols used in other chapters, are listed in Appendix A.

In Chapter 3 the instrumentation and reduction software (much of which is listed in Appendix B) for the Mt John high-precision radial-velocity programme are described. The set-up of the system is then considered in the light of the recommendations of Chapter 2 for maximizing the rate of acquisition of radial-velocity information. The observing programme, designed to search for low-mass companions to solar type stars, is described.

The velocities obtained for the sample of stars in the Mt John programme

are displayed in Chapter 4 and tabulated in Appendix C. Since some of the stars were spectroscopic binaries with stellar companions, these orbits are discussed and the orbital motion is subtracted from the data. In subsequent chapters only the residuals of these orbits are considered in analysing for the presence of smaller scale velocity variations.

In Chapter 5 the performance of the system is analysed while in Chapter 6 tests are applied to the data to determine which stars are intrinsically variable in radial velocity. In Chapter 7 the class of variable giant which became apparent over the course of the programme is discussed. Chapter 8 discusses the constraints on the masses of possible companions of the Mt John programme stars as well as discussing the implications for the existence of brown dwarfs. Finally, Chapter 9 summarizes the findings of this thesis and presents suggestion for further work in the fields of high-precision radial velocities and searches for low-mass companions to stars.

Chapters 2 and 3 have been based on papers been published back-to-back in an issue of *Astrophysics and Space Science* (Murdoch & Hearnshaw 1991a, 1991b), while a paper on the variability of the M-giant γ Cru, similar to the section on γ Cru in Chapter 7, has appeared in *Monthly Notices of the Royal Astronomical Society* (Murdoch, Clark & Hearnshaw 1992). These three papers were prepared before the completion of the programme and thus, where radial velocities were presented, the more up-to-date results are contained in this thesis.

Chapter 2

High-precision radial velocities from the cross-correlation technique

In this chapter, the technique of spectral cross correlation is introduced as a means for obtaining stellar radial velocities and other stellar parameters. The technique's potential for obtaining radial velocities of solar type stars of *high precision* is then examined in Section 2.2 by considering the ultimate limit to the precision of radial velocities from this method. Finally, in Section 2.3, this derived precision is used to make recommendations for the spectrograph set-up in order to obtain the best radial-velocity precision in a given exposure time.

2.1 The cross-correlation function of stellar spectra

Mathematically, the cross correlation of discretely sampled spectra $G(x_i)$ and template $T(x_i)$, the lth normalized cross-correlation coefficient C_l (lth normalized element of the discrete cross-correlation function) is defined as

$$C_l = \frac{1}{(N-l)R_T R_G} \sum_{i=1}^{N-l} T(x_i)G(x_{i+l}) \tag{2.1}$$

where l is the correlation lag, N is the number of points in each spectrum and R_T and R_G are the root mean squared (rms) values of the signals in the spectra T and G respectively.[1]

[1]For the sake of mathematical simplicity continuum-subtracted fluxes will be used in the following derivations.

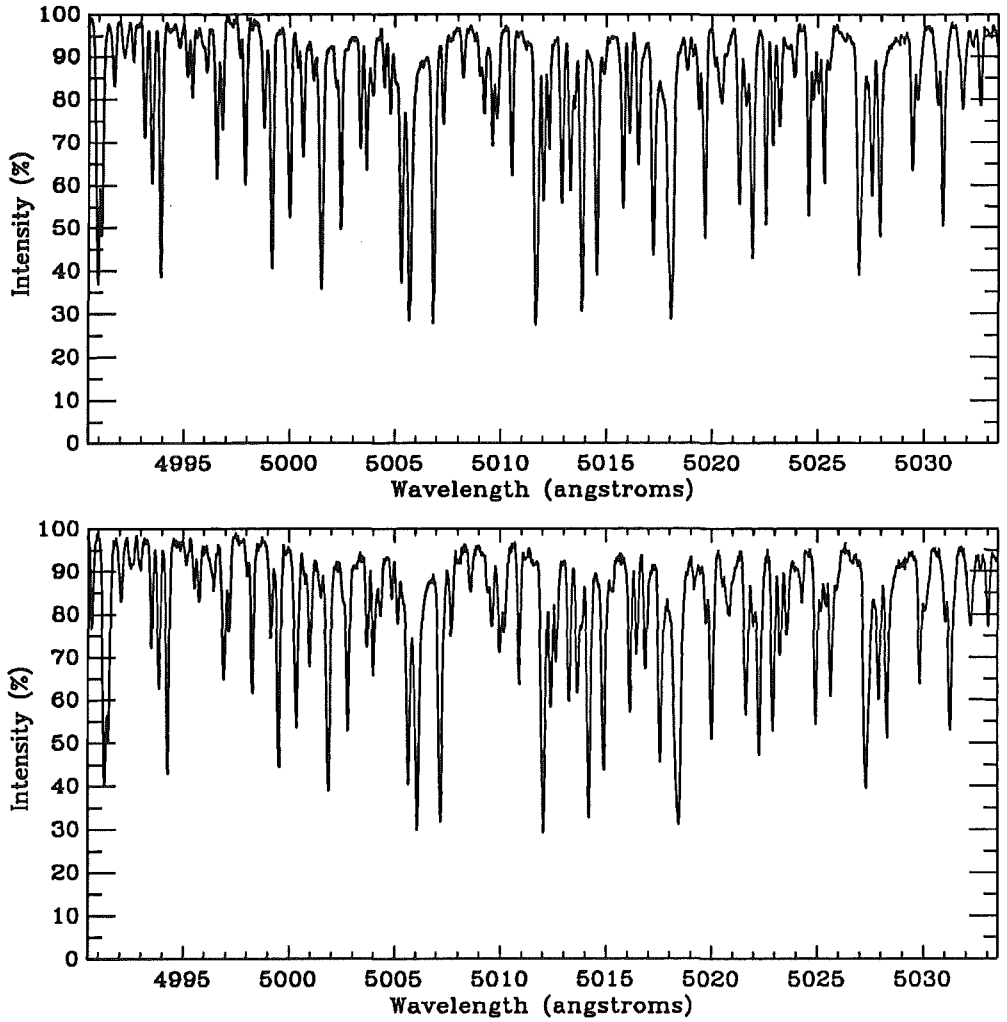

Figure 2.1: Two high-dispersion late-type stellar spectra. Both are of α Cen A (G2V) but were obtained at different epochs.

Graphically, the cross correlation of two spectra is illustrated in Figures 2.1 and 2.2. In Figure 2.1 the two high-dispersion late-type spectra are plotted while Figure 2.1 shows the result of their cross correlation.

The main feature of the cross-correlation function is that it exhibits a peak at a value equal to the lag between the two spectra. Furthermore the peak height is a measure of the linear correlation between the spectra and the shape of the peak is indicative of the mean line profile of the spectra. Benz (1979) has shown that the cross-correlation function peak of late-type spectra tends towards a Gaussian shape, principally because of the statistical effect of line blending. Even without this blending effect, a Gaussian shape might be expected anyway from the instrumental profile, which is typically the dominant line-broadening

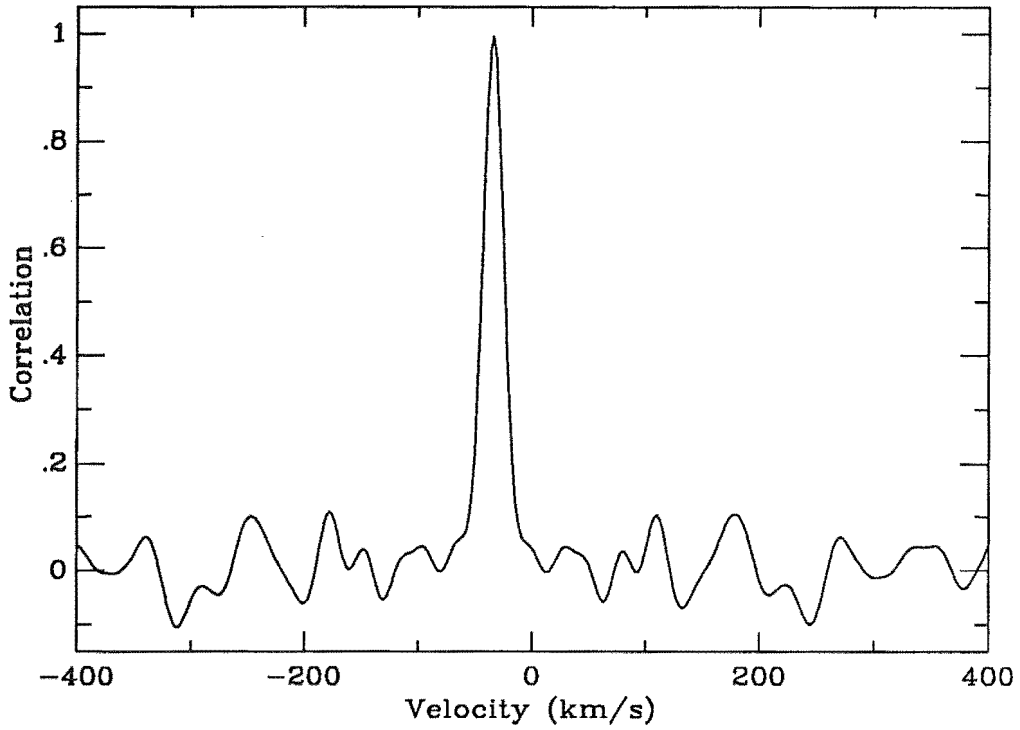

Figure 2.2: The cross-correlation function of the two spectra. The peak position corresponds to the difference in apparent radial velocity of α Cen A between the two epochs.

source.

The cross-correlation function peak is effectively a condensation of any positional and morphological information that is redundant in the lines of a stellar spectrum and thus is, in terms of reduction effort, a very efficient source of information compared to studying individual lines. The popularity of spectral cross correlation lies in this efficiency, which permits observations of more and fainter stars and makes the technique ideal for survey-type programmes.

2.1.1 Radial velocities

A stellar radial velocity is only obtained by measuring the Doppler shift of lines in a star's spectrum and then correcting for the motion of the observer[2]. The effect of a Doppler shift is to multiply all wavelengths in the spectrum by the amount $(1 + v/c)$ as is seen in the Doppler formula which relates wavelengths in the spectrum of an object with the object's velocity v

$$\frac{\lambda' - \lambda}{\lambda} = \frac{v}{c} \tag{2.2}$$

[2]By convention stellar radial velocities are expressed relative to the solar-system barycentre.

where c is the speed of light, λ is the rest wavelength of a spectral line and λ' is the corresponding Doppler-shifted wavelength.

For the cross-correlation technique to be applicable to the precise measurement of Doppler shifts, strictly speaking, the spectra must be re-mapped such that the Doppler shift is uniform across the spectrum. Equation 2.2 can be rewritten

$$\begin{aligned} \frac{\lambda'}{\lambda} - 1 &= \frac{v}{c} \\ \ln\lambda' - \ln\lambda &= \ln\left(1+\frac{v}{c}\right) \\ \Delta\ln\lambda &= \ln\left(1+\frac{v}{c}\right) \quad . \end{aligned}$$

The right-hand side of this equation is constant for all λ, so that the Doppler shift *is* uniform across a spectrum re-mapped in terms of $\ln\lambda$. A cross correlation of two spectra rebinned in this way will have a peak at lag value $\Delta\ln\lambda$ which is approximately proportional to the apparent relative radial velocity of the two source objects.[3] The task of obtaining an apparent relative radial velocity from the method of cross correlation is thus reduced to obtaining the cross-correlation peak centroid. This may be accomplished by the fitting of an appropriate function, such as a Gaussian, to the peak. A barycentric correction is then applied in the usual way.

2.1.2 Other stellar parameters

Parameters other than radial velocity may be determined from the cross-correlation technique, again with the advantage of the reduction efficiency of the technique and consequent potential for studying large numbers of faint stars. Although these parameters are of secondary interest to the work in this thesis, they deserve mention because they show the versatility of the cross-correlation method.

The broadening of spectral lines as a result of factors such as turbulence or rotation is mirrored in the cross-correlation peak. Mayor (1985) has shown that by calibrating the cross-correlation dip[4] width against these parameters, macroturbulent or rotational velocities (multiplied by the sine of the angle of the rotational axis to the line of sight) of stars may be determined.

[3] The x_is in Equation 2.1 may thus be referred to in units of velocity.

[4] Cross correlation produces a dip rather than a peak in the CORAVEL system because of a negative mask.

Similarly, metallicity and temperature may be compared between similar stars from the area of the cross-correlation function peak — a measure of mean equivalent width (Mayor 1985) — or from the peak's height. In the latter case, it must be recalled that the height of the cross-correlation peak is a measure of the linear correlation between the two spectra and ranges between -1 (perfect anti-correlation) and $+1$ (perfect correlation, for example for a spectrum *auto*-correlated with itself). A spectrum's unknown temperature or metallicity may be found from correlation with a grid of template spectra of known temperature and metallicity. The best correlation will be with the template corresponding to a temperature and metallicity which is close to that of the spectrum (see Carney *et al.* 1987).

2.2 The noise-limited radial-velocity error, ϵ_p

The precision of the determination of a stellar radial velocity is usually limited by errors from instrumental sources. Factors described in Chapter 1 such as guiding errors and thermal, barometric and mechanical instabilities all produce pseudo-random shifts of the spectrum on the detector which mimic the Doppler shift one is trying to measure. However, if these instrumental effects were able to be removed, the precision would still be finite, being limited by the noise in the spectrum.

In this section a formula is derived for the random error in the determination of a radial velocity by cross correlation in the presence of spectral noise only. This has been done to some extent before (Connes 1985) but in this case, by using some approximations, care has been taken to develop the relationship in terms of simple parameters of the recording of a stellar spectrum (such as recorded signal-to-noise, number of recorded spectral lines, resolution etc.). The formula represents the smallest radial-velocity error attainable and gives observers a practical indication of the factors influencing the limiting error in their radial velocities. In particular, it provides a simple means of determining the spectral-noise limited error for a given signal-to-noise. This is vital to know in order to improve the throughput of a system — care can be taken to record spectra with the minimum signal-to-noise (exposure time) so that spectral noise still affects the overall precision negligibly.

2.2.1 The cross-correlation function error, ϵ_C

First the error in the cross-correlation function arising from spectral noise in the two contributing spectra will be calculated.

General expression for ϵ_C

If the noise associated with template $T(x_i)$ and spectrum $G(x_i)$ is uncorrelated and described by normal distributions[5] with standard deviations ϵ_{T_i} and ϵ_{G_i} respectively, then the square of the uncertainty ϵ_X in the product $X = T(x_i)G(x_{i+l})$ from Equation 2.1 defining the cross-correlation function is

$$\begin{aligned} \epsilon_X^2 &= \epsilon_{T_i}^2 \left(\frac{\partial X}{\partial T}\right)^2 + \epsilon_{G_{i+l}}^2 \left(\frac{\partial X}{\partial G}\right)^2 \\ &= \epsilon_{T_i}^2 G^2(x_{i+l}) + \epsilon_{G_{i+l}}^2 T^2(x_i) \ . \end{aligned}$$

The net noise from N processes with noise described by Gaussians with standard deviations ϵ_i is itself a Gaussian of standard deviation

$$\left(\sum_{i=1}^{N} \epsilon_i^2\right)^{\frac{1}{2}} \ .$$

It follows then from Equation 2.1 that the uncertainty in the lth cross-correlation coefficient C_l from noise in $T(x_i)$ and $G(x_i)$ only is

$$\epsilon_{C_l} = \frac{1}{(N-l)R_T R_G} \left(\sum_{i=1}^{N-l} \epsilon_{T_i}^2 G^2(x_{i+l}) + \epsilon_{G_{i+l}}^2 T^2(x_i)\right)^{\frac{1}{2}} \ , \qquad (2.3)$$

where R_T and R_G are the rms values of spectra T and G and N is the number of points in each spectrum.

For a readout-noise limited detector, ϵ_T and ϵ_G are constant for all i. This is also approximately true for the case of a photon-noise limited system where, given that the continuum signal[6] (defined as F_T for spectrum T and F_G for spectrum G) has been subtracted, $\epsilon_{T_i} = \sqrt{F_T + T(x_i)}$ and $\epsilon_{G_i} = \sqrt{F_G + G(x_i)}$ ($T(x_i)$, $G(x_i) < 0$). The continuum signal will dominate the noise terms and the approximation can be made that $\epsilon_{T_i} \approx \sqrt{F_T}$ and $\epsilon_{G_i} \approx \sqrt{F_G}$, constants for all i.

For small shifts ($l \ll N$), a general formula can be constructed from Equation 2.3 for the random error in the cross-correlation function for the case of noise

[5] The assumption that the noise has a normal (Gaussian) probability distribution is justified by the large number of random events causing the noise.

[6] Assumed to be constant over the window of observation.

from either readout sources or from photon statistics.

$$\begin{aligned}\epsilon_C &= \frac{1}{NR_TR_G}\left(\epsilon_T^2\sum_{i=1}^{N}G^2(x_i)+\epsilon_G^2\sum_{i=1}^{N}T^2(x_i)\right)^{\frac{1}{2}} \\ &= \frac{1}{\sqrt{N}}\left(\frac{\epsilon_T^2}{R_T^2}+\frac{\epsilon_G^2}{R_G^2}\right)^{\frac{1}{2}} \quad . \end{aligned} \tag{2.4}$$

Alternative expressions for R_T and R_G

In practice most lines in solar-type spectra have approximately equal recorded widths. Consider then the continuum-subtracted recorded signal in spectrum $T(x_i)$ as a sum of N_{lines} Gaussian-shaped lines P_{ij} with half-$\frac{1}{e}$-widths σ_{line}.

$$\begin{aligned}T(x_i) &= \sum_{j=1}^{N_{\text{lines}}} P_{ij} \\ &= \sum_{j=1}^{N_{\text{lines}}} -F_T D_j e^{-\left(\frac{x_i-z_j}{\sigma_{\text{line}}}\right)^2}\end{aligned}$$

where D_j is the central line depth of the jth line as a fraction of the continuum signal F_T and z_j is the line's position. Using this formula an approximate expression can be derived for the rms value of the signal.

$$\begin{aligned}R_T^2 &= \frac{1}{N}\sum_{i=1}^{N}T^2(x_i) \\ &= \frac{1}{N}\sum_{i=1}^{N}\left(\sum_{j=1}^{N_{\text{lines}}}P_{ij}\right)^2 \\ &\simeq \sum_{j=1}^{N_{\text{lines}}}\frac{1}{N\Delta x}\sum_{i=1}^{N}P_{ij}^2\Delta x \qquad \text{assuming well-separated lines} \\ &= \sum_{j=1}^{N_{\text{lines}}}\frac{1}{N\Delta x}\sum_{i=1}^{N}\left(-F_T D_j e^{-\left(\frac{x_i-z_j}{\sigma_{\text{line}}}\right)^2}\right)^2\Delta x \\ &= \sum_{j=1}^{N_{\text{lines}}}\frac{F_T^2}{N\Delta x}\sum_{i=1}^{N}D_j^2 e^{-2\left(\frac{x_i-z_j}{\sigma_{\text{line}}}\right)^2}\Delta x \\ &\simeq \frac{F_T^2}{N\Delta x}\left(\sum_{j=1}^{N_{\text{lines}}}D_j^2\right)\int_{-\infty}^{+\infty}e^{-2\left(\frac{x_i-z_j}{\sigma_{\text{line}}}\right)^2}dx \\ &= \frac{F_T^2}{N\Delta x}\left(\sum_{j=1}^{N_{\text{lines}}}D_j^2\right)\frac{\sqrt{\pi}\sigma_{\text{line}}}{\sqrt{2}} \\ &= \sqrt{\frac{\pi}{2}}\frac{F_T^2 D_T^2 N_{\text{lines}}\sigma_{\text{line}}}{N\Delta x} \qquad \text{substituting } D_T^2 = \frac{1}{N_{\text{lines}}}\sum_{j=1}^{N_{\text{lines}}}D_j^2 \ ,\end{aligned}$$

where D_T is the rms line depth as a fraction of the continuum and Δx is the sampling interval in velocity space. Similarly,

$$R_G^2 = \sqrt{\frac{\pi}{2}} \frac{F_G^2 D_G^2 N_{\rm lines} \sigma_{\rm line}}{N \Delta x} \ .$$

The requirement in one of the steps above that the spectral lines are well-separated means that these expressions for R_T and R_G are approximations for solar-type stars as they have blended lines. Blends will increase the rms value for a continuum-subtracted spectrum. Comparison of these approximate formulae with the true calculated rms value of a 40Å window of a solar-type spectrum shows that they are good to about 5%.

ϵ_C in terms of simple spectral parameters

Equation 2.4 can now be expressed as

$$\epsilon_C = \left(\sqrt{\frac{2}{\pi}} \frac{\Delta x}{\sigma_{\rm line}} \left(\frac{\epsilon_T^2}{(DF\sqrt{N_{\rm lines}})_T^2} + \frac{\epsilon_G^2}{(DF\sqrt{N_{\rm lines}})_G^2} \right) \right)^{\frac{1}{2}} \ . \qquad (2.5)$$

By defining the spectral signal-to-noise ratio F/ϵ as S/N, Equation 2.5 becomes

$$\epsilon_C = \left(\sqrt{\frac{2}{\pi}} \frac{\Delta x}{\sigma_{\rm line}} \left(\frac{1}{(D(S/N)\sqrt{N_{\rm lines}})_T^2} + \frac{1}{(D(S/N)\sqrt{N_{\rm lines}})_G^2} \right) \right)^{\frac{1}{2}} \ . \qquad (2.6)$$

It may now be illustrated how cross correlation condenses the information content in the spectral lines into the cross-correlation function peak. Consider a spectrum recorded at a signal-to-noise ratio of only 20:1 containing 60 lines with rms fractional depth 60 per cent of the continuum and characteristic line width 10 detector resolution elements. When correlated with a spectrum with no random noise, the implied signal-to-noise ratio in the centre of the cross-correlation function peak (say the peak height is about 1) from Equation 2.6 is over 300:1.

2.2.2 Error in radial velocity from least-squares fitting

It has been seen how the photon noise in the spectra translates into a random error in the cross-correlation function. Now it remains to be determined how the error in the cross-correlation function translates into the random error in radial velocity, $\epsilon_{\rm p}$[7]. To do this, the theory of fitting by the method of least squares

[7]The subscript p stands for the source of this error — photon noise.

must be considered since the radial velocity is found by the fitting of a function to the cross-correlation peak. The least-squares procedure is appropriate where the error in the fitted function is the same for each data point — it was found in Section 2.2.1 that in both the readout-noise limited and photon-noise limited cases the ϵ_Cs were at least approximately constant with lag l.

Accordingly it is found that the error, $\epsilon_{\rm p}$, in the determination of v, is related to ϵ_C by

$$\frac{1}{\epsilon_{\rm p}^2} = \frac{1}{\epsilon_C^2} \sum_{i=1}^{N_{\rm fit}} \left(\frac{\partial y(l_i)}{\partial v} \right)^2 \tag{2.7}$$

where $N_{\rm fit}$ is the number of data points in the peak to be fitted and y is the fitting function (Press *et al.* 1988).

The fitting function

The relevant fitting function y to the cross-correlation peak (as justified in Section 2.1) is the Gaussian function,

$$y(l) = Ae^{-\left(\frac{l-v}{\sqrt{2}\sigma_{\rm line}}\right)^2} . \tag{2.8}$$

The geometric interpretation of A is as the height of the Gaussian but recall that it may also be interpreted as the linear correlation coefficient between the two spectra of the correlation. v is the position of the Gaussian in the lag coordinate l and hence is the apparent relative radial velocity of the star. $\sigma_{\rm line}$ is the half-$\frac{1}{e}$-width of the mean Gaussian line profile of one spectrum. The cross-correlation peak is a convolution of the average line profiles of the two stars so its half-$\frac{1}{e}$-width is $\sqrt{2}$ times $\sigma_{\rm line}$, hence the factor of $\sqrt{2}$ in the exponent of Equation 2.8.

Equation 2.7 implies that most of the radial-velocity information in the peak is where the gradient $(\frac{\partial y}{\partial v})^2$ is largest. These steep parts are fitted well by a Gaussian. Although departures of the cross-correlation peak from the Gaussian profile may occur in the wings of the peak, the equation implies that these departures will have little effect on the radial-velocity error since the gradient there is small. Some cross-correlation programmes fit a parabola rather than a Gaussian to the peak (Latham 1985; Hill 1982), but because of the mis-match in shape they are unable to fit below about half the peak height. A Gaussian is thus the superior fitting function — it can fit more of the peak better and can thus utilize more of the available radial-velocity information.

2.2.3 Expression for ϵ_p in terms of simple parameters

Δx, the detector resolution in velocity space, is equal to Δl, the detector resolution in velocity lag space. It follows from Equation 2.7 that

$$\begin{aligned}
\frac{1}{\epsilon_p^2} &= \frac{1}{\epsilon_C^2}\frac{1}{\Delta l}\sum_{i=1}^{N_{\rm fit}}\left(\frac{\partial y(l_i)}{\partial v}\right)^2 \Delta l \\
&\approx \frac{1}{\epsilon_C^2}\frac{1}{\Delta x}\int_{-\infty}^{+\infty}\left(\frac{\partial y(l_i)}{\partial v}\right)^2 dl \\
&\approx \frac{1}{\epsilon_C^2}\frac{1}{\Delta x}\int_{-\infty}^{+\infty}\frac{A^2(l-v)^2}{\epsilon_{\rm line}^4}e^{-\left(\frac{l-v}{\sigma_{\rm line}}\right)^2} dl \\
&= \frac{1}{\epsilon_C^2}\frac{A^2\sqrt{\pi}}{2\sigma_{\rm line}\Delta x} \; . \qquad (2.9)
\end{aligned}$$

Combining Equations 2.6 and 2.9, the radial-velocity error in the presence of spectral noise only is

$$\epsilon_p = \frac{\sqrt{2\sqrt{2}}\Delta x}{A\sqrt{\pi}}\left(\frac{1}{(D(S/N)\sqrt{N_{\rm lines}})_T^2}+\frac{1}{(D(S/N)\sqrt{N_{\rm lines}})_G^2}\right)^{\frac{1}{2}} \; , \qquad (2.10)$$

an expression in terms of basic parameters of the recording of the stellar spectra: detector resolution, signal-to-noise, rms line depth, number of spectral lines and degree of correlation between the two spectra.

Consider briefly the special case of a single spectrum T always being the 'template' in a series of correlations with other spectra G. ϵ_T is equal to zero since although the spectrum is recorded with a certain amount of noise, it contributes no *random* noise from correlation to correlation. An example of this situation is the correlation of spectra of a particular star against a single spectrum of that same star (which, as shall be seen later, is the relevant case for the programme in this thesis). In this case,

$$\epsilon_p = \sqrt{\frac{2\sqrt{2}}{\pi}}\frac{\Delta x}{AD(S/N)_G\sqrt{N_{\rm lines}}} \; . \qquad (2.11)$$

Considering again the case where $(S/N) = 20$, $N_{\rm lines} = 60$, $D = 0.6$, $A = 1$ and setting $\Delta x = 1.5$ km/s, the implied random error in radial velocity from spectral noise is $\epsilon_p = \pm 15$ m/s. If such observations had an error in radial velocity limited to say 100 m/s by instrumental factors, the overall radial-velocity error would be $\sqrt{100^2+15^2} = \pm 101$ m/s. The signal-to-noise could be halved increasing the radial-velocity error to only $\sqrt{100^2+30^2} = \pm 104$ m/s. In this case the exposure times would be reduced and more stars could be observed.

For the purpose of clarity, throughout the remainder of this chapter Equation 2.11 will be used for the radial-velocity random error rather than the more general Equation 2.10. The results for optimum slit width and spectral region which follow are unaffected.

2.3 Optimizing the precision

In this section, Equation 2.11 for the spectral-noise limited random error from cross correlation is used to consider how the performance of a system can be optimized for a *fixed* exposure time, by choosing the best instrumental set-up for the system. Considering the cases of detectors limited by readout noise and detectors limited by noise from photon statistics, the qualitative effect on the radial-velocity precision (defined as the inverse square of the spectral noise limited random error) of the choice of spectral region and resolution for a solar-type star is shown. To further aid the observer, simple formulae are derived for the optimum slit width for radial-velocity work for the case of a Cassegrain spectrograph mounted directly on the telescope and for a fibre-fed spectrograph. In Chapter 3 these results will be put to use in assessing the setting up of the Mt John high-precision radial-velocity system.

2.3.1 General considerations

From Equation 2.11 the noise limited radial-velocity *precision* can be defined as

$$\frac{1}{\epsilon_{\rm p}^2} = \frac{A^2 W^2 (S/N)^2 N_{\rm lines}}{2\sqrt{2}\pi\sigma_{\rm line}^2 (\Delta x)^2} \tag{2.12}$$

where the rms fractional line depth D has been substituted by $D = \frac{W}{\pi\sigma_{\rm line}}$ where W is the rms fractional line area (equivalent width)[8]. From this equation it can be seen that there are three ways in which the radial-velocity precision can be maximized for a given observing instrument, object and exposure time.

Firstly, one can choose the optimum spectral region for radial-velocity work. This involves maximization of the product $W^2(S/N)^2 N_{\rm lines}$ that is, choosing an area of spectrum with a large number of deep lines and a high photon flux.

Secondly, one can choose the optimum slit width by maximizing the ratio of S/N to $\sigma_{\rm line}$. Higher precision is implied by a smaller $\sigma_{\rm line}$ and larger S/N but

[8]The substitution will facilitate consideration of the optimum slit width since it separates out that aspect of the line profile directly dependent on the slit width — $\sigma_{\rm line}$, from that which is independent of it — W.

the two are not independent. Narrowing the slit (decreasing $\sigma_{\rm line}$) will permit the entry of fewer photons in a given exposure time, lowering S/N. Widening it will raise S/N. A slit width can be chosen which optimizes the radial-velocity precision in a given exposure time.

Thirdly, it is desirable to have the linear correlation coefficient between the two spectra A as close as is feasible to 1. This is done by ensuring that the template spectrum is as similar in spectral type as possible to the other spectrum in the correlation. It may be another spectrum of the same star, in which case $A \simeq 1$.

2.3.2 Choice of spectral region

The spectral region containing the maximum amount of radial-velocity information is the one in which the product $W^2(S/N)^2 N_{\rm lines}$ is maximized over the window of observation. In this section the relative radial-velocity information content throughout the solar spectrum is determined by considering the Beckers, Bridges & Gilliam (1976) solar flux atlas. A 40 Å window of observation has been assumed, which is relevant to high-dispersion studies using detectors of modest size.

Maximization of $W^2(S/N)^2 N_{\rm lines}$, although simple as a concept, is more difficult to compute from data in digital format than is the more rigorous equivalent

$$\sum_{\rm window} (S/N)^2 \left(\frac{\partial I_\lambda}{\partial v}\right)^2 = \sum_{\rm window} \frac{(S/N)^2 \lambda^2}{c^2} \left(\frac{\partial I_\lambda}{\partial \lambda}\right)^2 , \qquad (2.13)$$

which is also proportional to the radial-velocity precision (see Merline 1985). I_λ is the spectral intensity at wavelength λ. In order to differentiate between cases of detectors limited by readout noise and detectors limited by noise from photon statistics, new definitions are introduced. These are $T_{\rm slit}$ — the fractional transmission of starlight through the spectrograph slit and T_λ — the fractional transmission of light through the atmosphere and all optical elements other than the slit. For photon-noise-limited detectors $S/N \propto \sqrt{T_\lambda T_{\rm slit}}$, while for readout-noise-limited detectors, $S/N \propto T_\lambda T_{\rm slit}$. Expression 2.13 now becomes

$$\sum_{\rm window} \frac{T_{\rm slit} T_\lambda \lambda^2}{c^2} \left(\frac{\partial I_\lambda}{\partial \lambda}\right)^2 \qquad (2.14)$$

for the photon-noise-limited case and

$$\sum_{\rm window} \frac{T_{\rm slit}^2 T_\lambda^2 \lambda^2}{c^2} \left(\frac{\partial I_\lambda}{\partial \lambda}\right)^2 \qquad (2.15)$$

for the readout-noise-limited case.

Expressions 2.14 and 2.15, proportional to the radial velocity precision, were calculated for the solar spectrum over spectral windows 40 Å wide with the $T_{\rm slit}$ constant in both cases. T_λ was calculated using terms for the atmospheric transmission for 1 airmass (Borchers & Schmidt 1964) and four aluminium reflections (Allen 1973). In practice the transmission T_λ is also affected by the particular observing instrument. I_λ was calculated from combination of the Beckers *et al* (1976) Atlas data and the relative flux from the solar atmosphere of Kurucz (1979). Figure 2.3 and Figure 2.4 show the intrinsic radial-velocity information available at the resolution of the Beckers *et al.* (1976) atlas (14 mÅ) and also at a resolution degraded to 200 mÅ using a square instrumental profile. It can be seen that for both kinds of detector a lower resolution implies relatively more radial-velocity information at the red end of the spectrum where the effects of instrumental blending arising from the decreased resolving power are less than in the blue. Data beyond 6300 Å have been omitted because of excessive contamination by telluric lines.

Figures 2.3 and 2.4 are only intended as a qualitative guide to the radial-velocity information content in the solar spectrum and its change with changing resolution. In practice, choice of spectral region for a particular instrument requires that the transmission properties of the instrument be included in the above calculation. Such a calculation is carried out for the Mt John system in Chapter 3.

Furthermore, for radial-velocity work a well-defined dispersion solution from a comparison spectrum is required. The number density of the comparison spectrum lines varies with wavelength, so the choice of spectral region will also affect the precision with which the dispersion solution can be determined. The weight of this consideration as a constraint on the choice of spectral region again depends on the particular instrument. A very linear dispersion may be defined as well as a non-linear dispersion by observation of fewer lines.

2.3.3 Choice of spectrograph slit width

Now the optimum slit width for a given detector, star, spectral region and exposure time is considered.

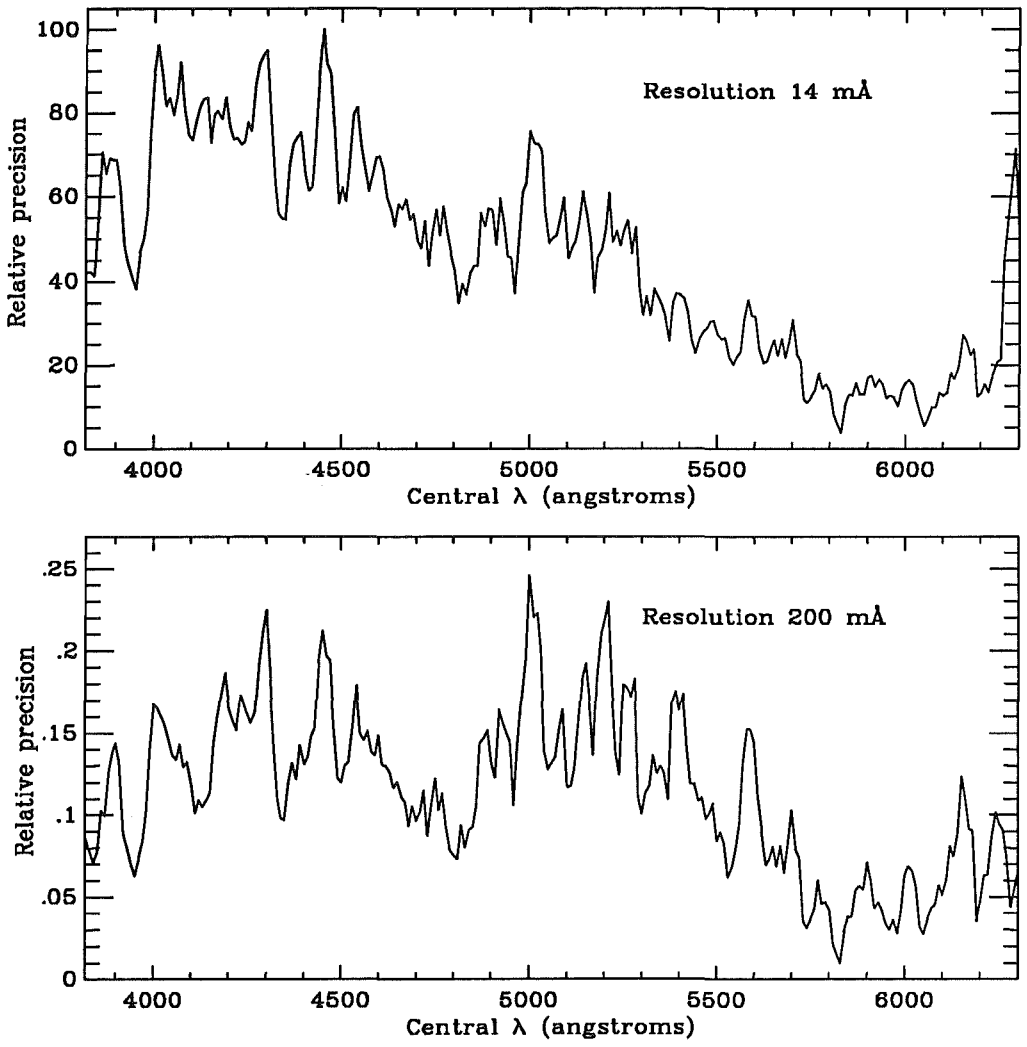

Figure 2.3: Intrinsic radial-velocity information in the solar spectrum for a photon-noise-limited detector calculated in a 40 Å wide travelling window.

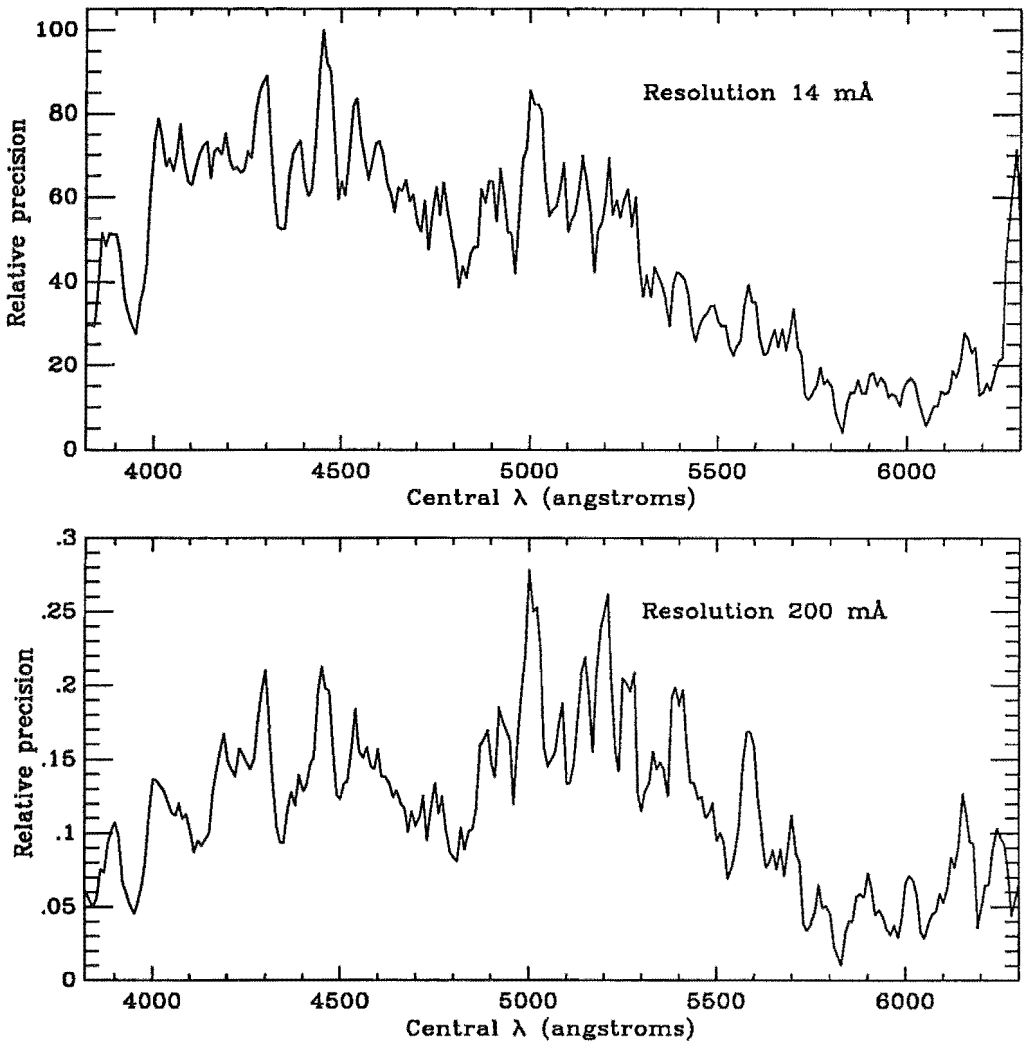

Figure 2.4: Intrinsic radial-velocity information in the solar spectrum for a readout-noise-limited detector calculated in a 40 Å wide travelling window.

Alternative expression for $\sigma_{\rm line}$

Since a spectral line is a convolution of the instrumental profile and the stellar line profile, for solar-type stars (negligible rotation and lines dominated by Doppler broadening from thermal and turbulent sources), the recorded line width, $\sigma_{\rm line}$, can be expressed as

$$\sigma_{\rm line}^2 = \sigma_{\rm instr}^2 + \sigma_{\rm Dopp}^2 \tag{2.16}$$

where $\sigma_{\rm instr}$ is the half-$\frac{1}{e}$-width of the instrumental profile and $\sigma_{\rm Dopp}$ is the half-$\frac{1}{e}$-width of the intrinsic Doppler line profile. $\sigma_{\rm instr}$ can further be divided into a term dependent on the slit width, $\sigma_{\rm slit}$, and a term due to the finite pixel size of the detector and any other factors, $\sigma_{\rm pixel}$.

$$\sigma_{\rm instr}^2 = \sigma_{\rm slit}^2 + \sigma_{\rm pixel}^2$$

$\sigma_{\rm slit}$ is proportional to the slit width. Defining a proportionality constant ρ, $\sigma_{\rm instr}$ is given by

$$\sigma_{\rm instr}^2 = (\rho w)^2 + \sigma_{\rm pixel}^2 \ .$$

ρ may be calculated as

$$\rho \simeq 0.41 m \ , \tag{2.17}$$

where m is the magnification between the slit and its image at the detector. The 0.41 factor relates the slit width to the half-$\frac{1}{e}$-width of the Gaussian approximation to the instrumental profile (Allen 1973).

Equation 2.16 can now be written as

$$\sigma_{\rm line}^2 = (\rho w)^2 + \sigma_{\rm pixel}^2 + \sigma_{\rm Dopp}^2 \ .$$

Defining a further parameter $\sigma_0^2 = \sigma_{\rm pixel}^2 + \sigma_{\rm Dopp}^2$ allows Equation 2.16 to be rewritten in terms of $\sigma_{\rm slit}$ (dependent on slit width) and σ_0 (independent of slit width). That is

$$\sigma_{\rm line}^2 = (\rho w)^2 + \sigma_0^2 \ .$$

Expression for relative radial-velocity precision

For a given detector, star, spectral region and exposure time, A, W, $N_{\rm lines}$, Δx, T_λ and σ_0 are all constant. From Equations 2.14 and 2.15 it follows that

$$\frac{1}{\epsilon_{\rm p}^2} \propto \frac{T_{\rm slit}}{(\rho w)^2 + \sigma_0^2} \tag{2.18}$$

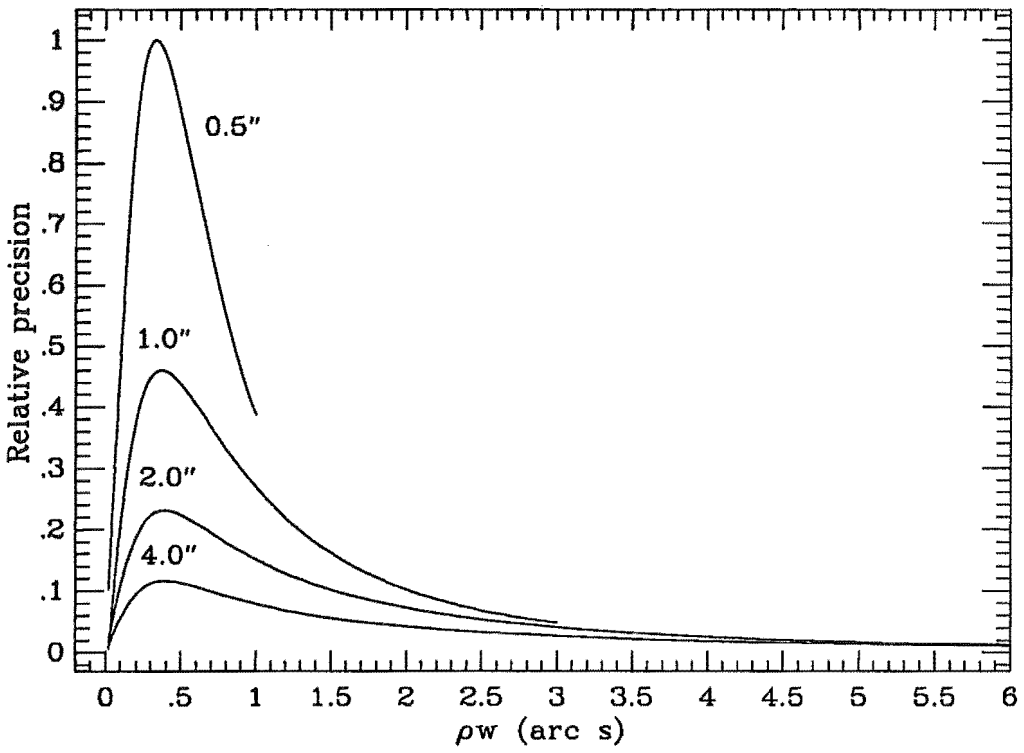

Figure 2.5: Family of curves showing precision as a function of slit image width for a photon-noise limited detector and $\sigma_0 = 0.4$ arc s, for seeing σ_* as labelled.

in the photon-noise limited case and

$$\frac{1}{\epsilon_p^2} \propto \frac{T_{slit}^2}{(\rho w)^2 + \sigma_0^2} \tag{2.19}$$

in the readout-noise limited case.

Case of spectrograph mounted on telescope

T_{slit} for 0.5, 1, 2 and 4 arc s seeing images and long slits from Diego (1985) was used to calculate Expressions 2.19 and 2.18. The results take the form of the family of curves in Figures 2.5 and 2.6. In these figures, the precision is expressed as a function of slit width for various values of the seeing and for the example of $\sigma_0 = 0.4$ arc s, which in practice is a plausible value for high-dispersion observations of solar-type stars[9]. The optimum slit width w_{opt} was determined by inspection of the peak values of these curves and curves for other values of σ_0.

In Figure 2.7 the optimum slit width is expressed as a function of seeing σ_* for both the readout-noise limited case and the photon-noise limited case. w_{opt}

[9]Based on $\sigma_{Dopp} = 0.1$ arc s, $\sigma_{pixel} = 0.39$ arc s.

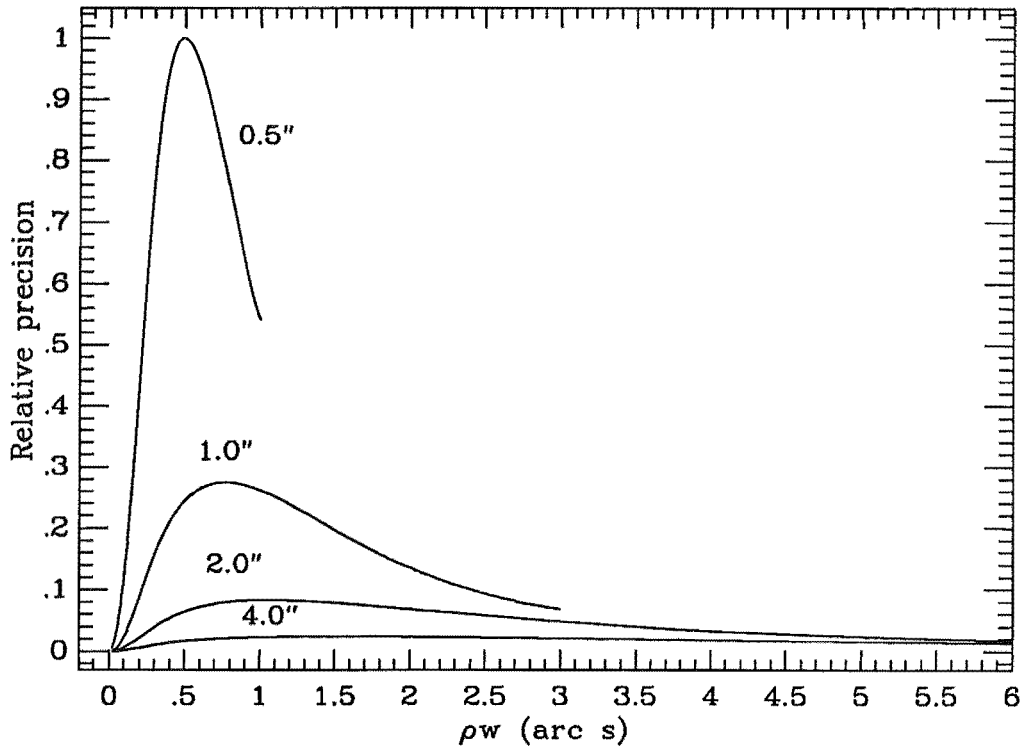

Figure 2.6: Family of curves showing precision as a function of slit image width for a read-out-noise limited detector and $\sigma_0 = 0.4$ arc s, for seeing σ_* as labelled.

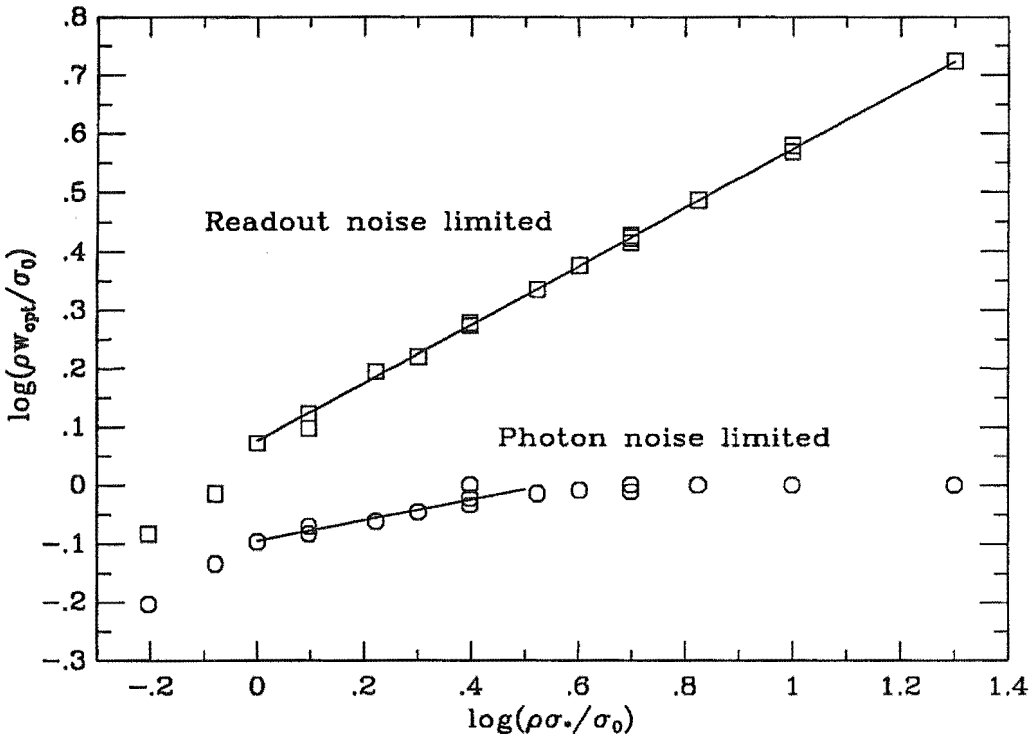

Figure 2.7: Relationship between optimum spectrograph slit width and seeing for radial-velocity studies with a long slit and the spectrograph mounted directly on the telescope.

and σ_* are expressed as fractions of σ_0. Bearing in mind the limitations of these relationships — that they are dependent on the assumed form of the stellar image profile and are valid for long slits — it is possible to construct semi-empirical relationships between $w_{\rm opt}$, σ_*, ρ and σ_0 via least-squares fitting. These fits are shown as solid lines in Figure 2.7.

It can be seen in Figure 2.7 that the optimum slit width for radial-velocity work is fairly insensitive to the seeing for a photon-noise limited detector, particularly for large $\rho\sigma_*/\sigma_0$, where

$$w_{\rm opt} \simeq \frac{\sigma_0}{\rho} \ .$$

This could represent the case of poor seeing (say for a typical detector $\sigma_* >$ 3 arc s) and few or no external error sources in the system. On the other hand, for the more common situation of smaller $\rho\sigma_*/\sigma_0$ (better seeing, presence of external error sources broadening the spectral lines) a least-squares fit for $0 < \log(\rho\sigma_*/\sigma_0) < 0.5$ gave the following relationship for $w_{\rm opt}$ with $w_{\rm opt}$, σ_0 and σ_* in arc s:

$$w_{\rm opt} \simeq 0.8 \left(\frac{\sigma_0}{\rho}\right)^{1.2} \sigma_*^{0.2} \ .$$

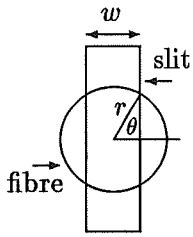

Figure 2.8: Geometry of the fibre and spectrograph slit.

A least-squares fit to the part of the readout-noise limited data in Figure 2.7 obtained for $\log(\rho\sigma_*/\sigma_0) > 0$ gave the following relationship for all commonly encountered seeing and σ_0 with $w_{\rm opt}$, σ_0 and σ_* in any units:

$$w_{\rm opt} \simeq 1.2\sqrt{\frac{\sigma_*\sigma_0}{\rho}} \ .$$

Case of fibre-fed spectrograph

The transmission of light $T_{\rm slit}$ through a slit of width w centred on a uniformly illuminated fibre of radius r is equal to the fraction of the cross-sectional area of the fibre that the slit exposes. If the slit height $\geq 2r$ then parameterizing with $w = 2r\cos\theta$,

$$T_{\rm slit} = 1 - \frac{2\theta}{\pi} + \frac{2}{\pi}\cos\theta\sin\theta \ ,$$

where the symbols are shown diagramatically in Figure 2.8.

Using this expression for $T_{\rm slit}$, differentiating Expressions 2.18 and 2.19 with respect to w and setting the result to zero yields relationships between σ_0 and the optimum slit width $w_{\rm opt}$ (parameterized by $\theta_{\rm opt}$) for each of the two cases. The results are

$$\frac{\pi - 2\theta_{\rm opt}}{\tan\theta_{\rm opt}} - 2\cos^2\theta_{\rm opt} = \left(\frac{\sigma_0}{\rho r}\right)^2 \qquad (2.20)$$

for the readout-noise case and

$$\frac{\pi - 2\theta_{\rm opt}}{\tan\theta_{\rm opt}} = \frac{1}{2}\left(\frac{\sigma_0}{\rho r}\right)^2 \qquad (2.21)$$

for the photon-noise case. These relationships are plotted in Figure 2.9.

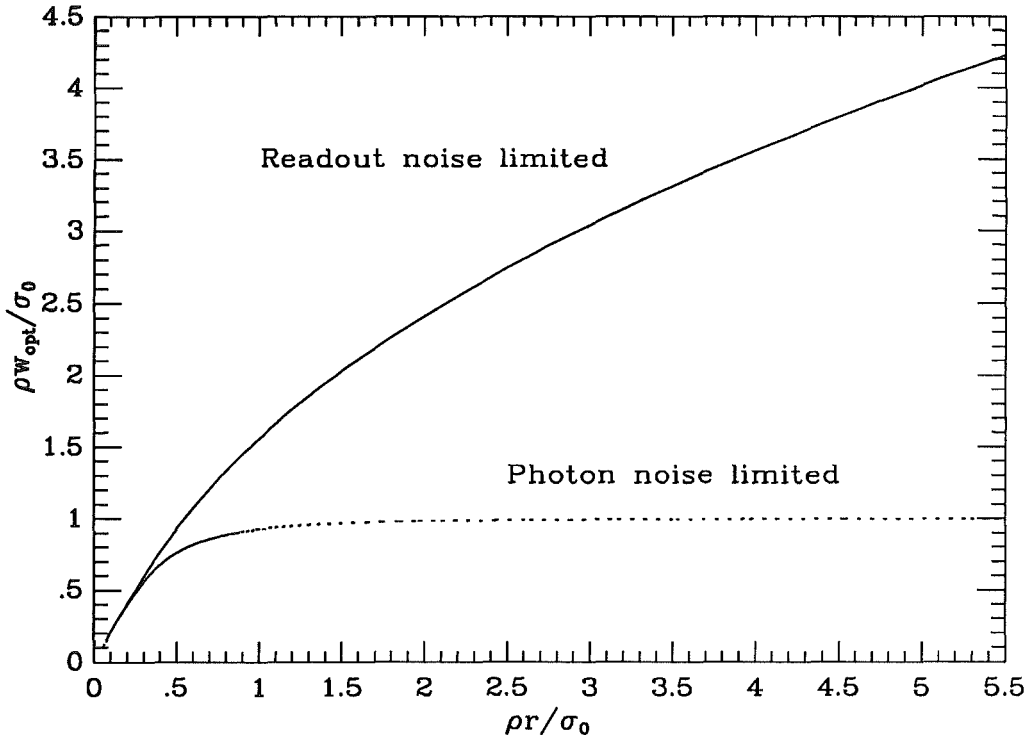

Figure 2.9: Relationship between optimum slit width and fibre radius for radial-velocity studies with a long slit and a fibre-fed spectrograph.

Note in the photon-noise limited case the insensitivity of the optimum slit width to the fibre radius. The optimum slit width is again given by

$$w_{\rm opt} = \frac{\sigma_0}{\rho} \ .$$

2.3.4 Choice of template spectral type

If both spectra in a correlation are of the same star then, in the absence of noise, there is a perfect linear correlation between them and A in Expression 2.12 equals 1. Any difference in spectral type between the spectrum and template will imply $A < 1$ and the radial-velocity random error $\epsilon_{\rm p}$ will increase in inverse proportion.

A cannot be expressed as a simple function of difference in spectral type as it also depends on the actual spectral types, wavelength coverage and signal-to-noise of each spectrum. It is to be recommended however that for high-precision work the template be as similar in spectral type as possible to the other spectrum in the correlation.

Chapter 3

The Mt John high-precision radial-velocity system

3.1 Instrumentation

The Mt John radial-velocity programme uses the following instrumentation:

- 1 m f/8 Cassegrain telescope,
- optical fibre input module, with facility for remote acquisition and guiding,
- 25 m length of UV transmitting optical fibre,
- fibre-spectrograph interface,
- high dispersion échelle spectrograph in a temperature-controlled environment,
- liquid-nitrogen-cooled Reticon linear diode array,
- a 6809 Gimix computer for diode array control and data acquisition.

The whole system from telescope to detector was designed and constructed in the Physics Department at the University of Canterbury, except for the spectrograph, which was built at Canterbury from Harvard-Smithsonian drawings. The physical layout of the system is illustrated in Figure 3.1.

3.1.1 Optical fibre input module

The fibre input module is mounted at the f/8 Cassegrain focus of the Mt John 1 m McLellan reflector. This telescope has a Dall-Kirkham optical configuration.

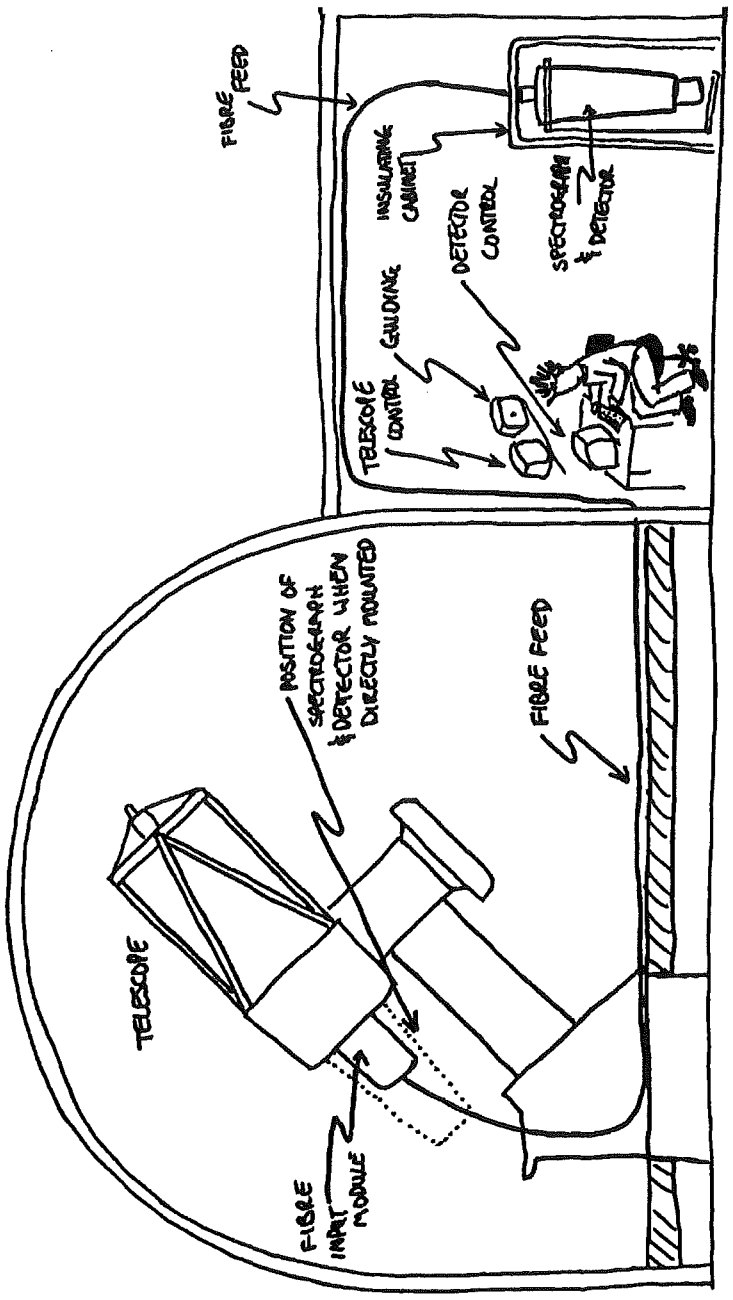

Figure 3.1: Instrumentation for the Mt John high-precision radial-velocity programme.

The light traverses two field corrector lenses (Nankivell & Rumsey 1986) mounted ahead of the Cassegrain focus, even when used for on-axis observations, as in this programme. The focal plane scale is 25 arc s/mm.

The star to be observed is acquired and set onto the fibre by viewing it in a Sanyo CCD camera (572 x 485 pixels) linked to a 3-stage 18 mm image intensifier. The module can operate either in acquisition mode or guiding mode. In the former, the telescope beam is changed to about f/3.2 using an f/2.5 camera lens just in front of the CCD, to give a field of view on the monitor of about 20 arc minutes.

In guiding mode the observer sees a field of view of about 3 arc minutes centred on the fibre input. The f/8 beam from the telescope is focussed directly onto the fibre. It does so by entering a small optically polished wedge with a 6.6° angle between its plane faces. The rear surface is aluminized and lies in the focal plane of the telescope. A 120 μm pinhole in the centre of the aluminizing allows most of the starlight to pass through the wedge and into the fibre. The latter is connected to the wedge by a small refractive index-matching glycerine drop. The fibre end is cleaved but not polished. In this guiding mode a small part of the peripheral stellar image is reflected by the wedge aluminizing into an f/2.8 camera lens, which transfers a magnified image of the star and pinhole to the intensified CCD camera for display on the monitor. The optical arrangement for the fibre input resembles that described by Enard, Lund & Tarenghi (1983) for the fibre input from the prime focus of the ESO 3.6 m telescope.

Normally starlight enters the fibre. However a system of rotating mirrors allows light from either a Th-Ar hollow cathode lamp or from a quartz halogen white lamp to be passed into the fibre with the same f/8 focal ratio. These lamps are used respectively for the dispersion solutions of the spectra and for flat-fielding of the diode-array.

A fuller description of the fibre input module has been given by Kershaw & Hearnshaw (1989).

3.1.2 Optical fibre and the fibre-spectrograph interface

The fibre chosen was a 25 m length of Spectran 820 step index 105 μm core diameter UV-transmitting fibre. This carries starlight from the Cassegrain focus to the échelle spectrograph in the adjoining control room. The diameter corresponds

to 2.5 arc s in the focal plane of the telescope. In 2 arc s seeing and assuming a 2-dimensional Lorentzian distribution of the starlight, the fibre diameter intercepts 72 per cent of the photons in the stellar image (Diego 1985). For wavelengths greater than 4000 Å attenuation within the fibre is about 6 per cent.

The light emerges from the fibre at approximately f/5.2. Since this no longer matches the f/8.9 spectrograph collimator, the fibre end is re-imaged using an f/1.8 camera lens which produces a magnified image of the fibre output of diameter 180 μm. The light is then passed through a rectangular slit of width 115 μm in the collimator focal plane.

3.1.3 Echelle spectrograph and Reticon diode array

The échelle spectrograph has been described by Hearnshaw (1977, 1978). It gives a dispersion of 1.75 Å/mm in diffraction order 46, for which the nominal order centre is 5020 Å. The instrument is based on a 79 groove/mm échelle grating with a blaze angle of $\theta_B = 63°26' = \arctan 2$. A first order grating cross disperser is placed after the échelle.

The linear diode array system (MacQueen 1986) is based on a RL1872F chip with 1872 pixels each $15 \times 750\,\mu$m in a 28 mm long array. For the radial-velocity programme the array is centred on 5012 Å in order 46, giving a coverage of 45 Å from 4989 to 5034 Å. The width of each pixel corresponds to a Doppler shift of about 1550 m/s. The array is operated at $-128.0\,°$C and thermostatically controlled to $\pm 0.01\,°$C. The spectra in Figure 2.1 are in fact examples of spectra from this system.

The spectrograph is mounted in a vertical orientation on a trolley, with the fibre entering from above. It is housed in a thermally controlled chamber in one corner of the control room. The chamber is insulated with thick fibreglass walls lined with aluminium reflecting foil. The échelle grating temperature is monitored to the nearest $0.01\,°$C using a precise temperature sensor cemented to the échelle grating cell with output to a digital display. The temperature of the échelle is controlled to within about $0.02\,°$C drift during a full night by intermittently supplying heat from two 60 W incandescent light bulbs mounted inside the thermal chamber in close proximity to the spectrograph, which is completely light tight. The liquid nitrogen in the dewar is replenished about one hour before sunset and lasts all night, thereby ensuring that the thermal stability of the spectrograph is maintained during observations. The dewar boil-off is vented to the chamber's

exterior for the same reason.

3.2 Reduction procedures

Fixed pattern subtraction, flat-field division and baseline corrections of the spectra are performed on the 6809 Gimix computer at Mt John. These processes are described more fully by MacQueen (1986). All further reductions are performed on either an AT computer at Mt John or on a 386 machine at Canterbury University with software written in Turbo Pascal. The techniques follow the recommendations of Simkin (1974) for cross correlating digital spectra using Fourier transformations. The reduction programmes are listed in Appendix B.

The first stage in a correlation is to obtain the dispersion solution relevant to each exposure. A second order polynomial was found to be adequate for description of the dispersion behaviour of the Mt John system since the values of coefficients of higher order are of the order of the errors in those same coefficients. This polynomial is calculated automatically from consultation of a list of the 14 Th-Ar comparison line wavelengths and approximate positions. A mean of the two dispersion solutions is obtained before and after the stellar exposure in order to characterize the mean dispersion of the stellar spectrum.

The next stage is the correlation itself. The structure of the programme which performs the cross correlations is illustrated in Figure 3.2. Each spectrum is prepared for correlating by first rebinning in terms of $\log \lambda$ using the appropriate dispersion solution. The rebinning is effected by preserving the total number of counts in the original spectrum, but then scaling the counts in the rebinned spectrum in order to keep the continuum flat. Parts of the stellar spectrum that lie outside the range of the first (λ = 4989.31 Å) and last (λ = 5029.893 Å) Th-Ar lines in the window are not used. The accuracy of the dispersion solution is critical for high-precision stellar radial velocities, and it is necessary to avoid the region of the spectrum where the dispersion solution is an extrapolation, even though this region is small.

The cross correlation is performed in the Fourier domain. A Fast Fourier Transform (FFT) algorithm is used, thereby reducing the number of required calculations[1]. The Fourier transform also allows for spectral filtering.

The mean value of the spectrum is subtracted to avoid a low-frequency spike

[1]The number of calculations is $4N\log N$ where N is the number of points in the correlation versus N^2 if performing the cross correlation as a sum of multiplications — see Wyatt (1985).

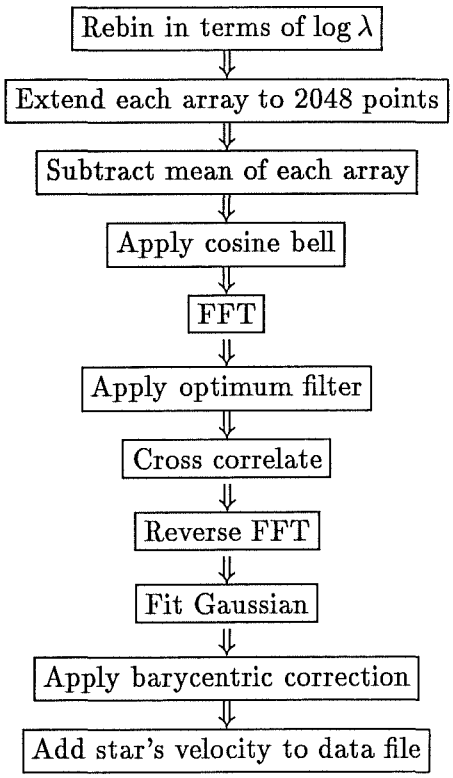

Figure 3.2: Structure of the cross-correlation programme.

in Fourier space (Simkin 1974). The ends then are masked with a cosine bell in order to eliminate discontinuities in the periodic spectrum. Finally the spectral array is extended with zeros. This is for two reasons. Firstly the FFT algorithm requires that the array has a number of points that is a power of two (here the extension is to 2048 points). Secondly, zeros between the periodic sections of spectrum ensure that the opposite ends of the spectra are not cross correlated with each other.

The Fourier transform algorithm used is the TWOFFT procedure from Press *et al.* (1988). Here the two spectra are transformed in the same array, which is more efficient for cross correlating than transforming two separate arrays. The spectra are filtered using an optimum filter (high frequencies only) of the form described by Brault & White (1971), cross correlated, normalized and then inverse transformed.

The cross-correlation peak centroid is found from the fitting of a Gaussian function to the peak using procedures from Press *et al.* (1988). The function is fit to 80 per cent of the peak height and for all but the 4 stars of latest spectral type, assuming a baseline value of zero for the fitted Gaussian. Blended lines in the later spectral types lowering the apparent continuum level in the spectrum account for a higher baseline level being required for the fitting of the Gaussian to the cross-correlation function peak. In Figure 3.3 it can be seen that a zero continuum level gives a good fit for α Cen A (G2V) but a poor fit for γ Cru (M3.5III) which requires a continuum level of 0.15 for a good fit (both γ Cru fits are illustrated). The 80 per cent level is chosen as it is found that by fitting to this level the Gaussian approximation to the peak shape is excellent, those parts of the peak with the most radial-velocity information (greatest slope) are included and there is less sensitivity at this level to the small asymmetries resulting from alignment of the fibre output end on the slit, dispersion solution uncertainties etc. The quality of a fit can be quantified by the goodness-of-fit parameter Q of Press *et al.* (1988). It was found that if the line of the fitted Gaussian and the line of the cross-correlation function peak appear to overlap completely on the screen then that corresponds to a centroid of the peak no more than about 5 m/s different from the centroid from the fitted Gaussian with the best possible Q. So in summary, it was found to be sufficient that the Gaussian *appeared* to fit the cross-correlation function peak.

The final step is the correction of the apparent relative velocity to the solar

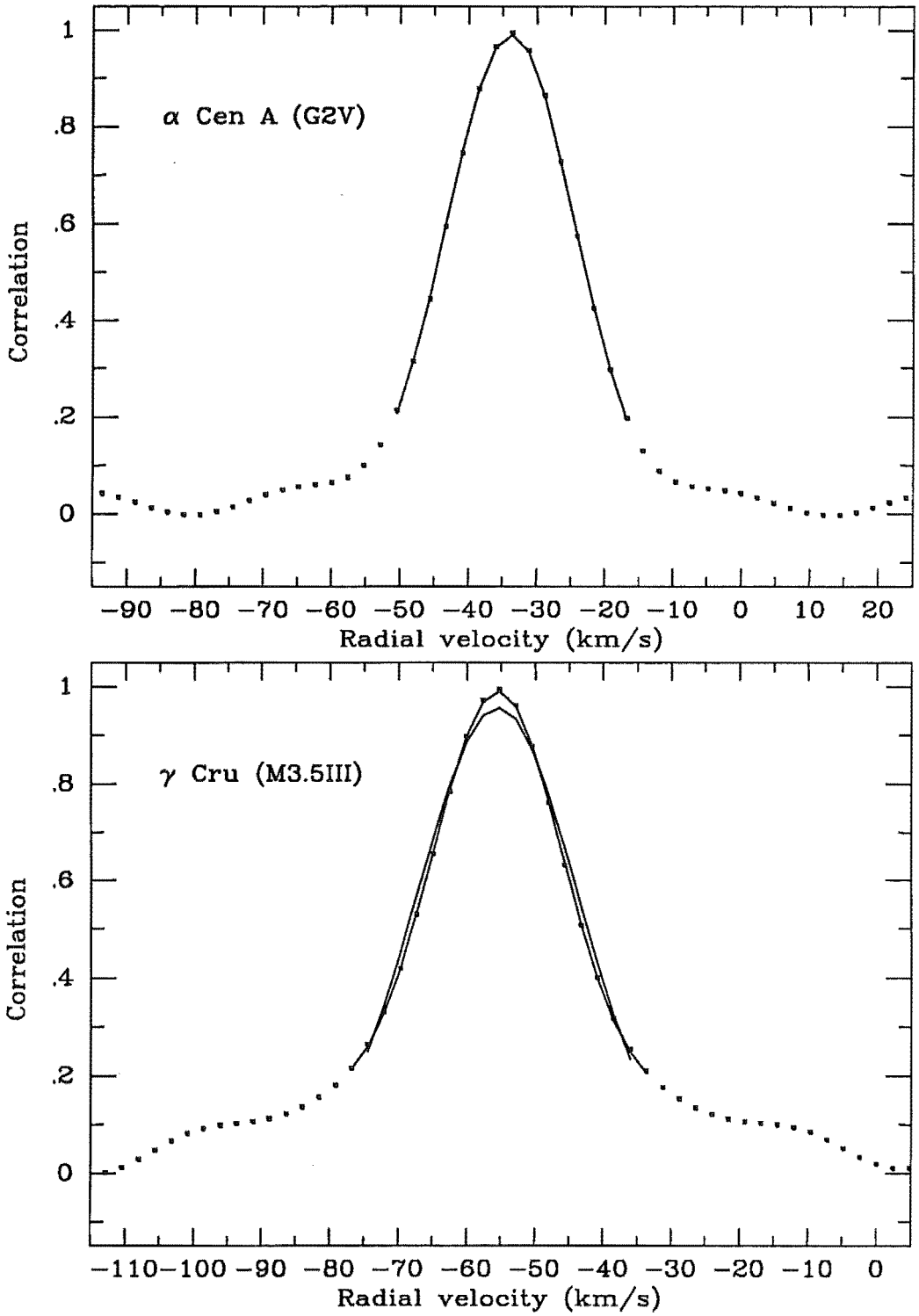

Figure 3.3: Fitting a Gaussian function to typical cross-correlation peaks in the Mt John programme. The better fit to the peak of γ Cru is for a Gaussian continuum level of 0.15, the poorer fit is with the usual continuum level of 0.00.

system barycentre. The routine used is an adaptation of a Pascal translation by V. J. McIntyre to a Fortran code by Ball (1976). The original code was in error in several places. Correction of these as well as substituting an improved precession procedure and the addition of a term concerning the motion of the Sun about the Sun-Jupiter barycentre, resulted in an absolute error of at most than 1 m/s during a night or 6 m/s over the 2.5 year duration of the Mt John programme. This has been determined from comparison with corrections for stars at various positions (star on ecliptic pole, star on ecliptic with low declination, star of high declination) calculated from the routine of Stumpff (1980) whose barycentric correction routines have an accuracy of ± 42 cm/s. Stumpff's routines were not used in the Mt John cross-correlation software as they are written in Fortran and the Pascal translation of the Ball code was already available. Finally, the Mt John programme calculates the Heliocentric Julian Date of each spectral observation, to be used later in analysis of the time series of radial velocities for each star.

In practice, the processing of data from an observing run involves the cross correlation of many pairs of spectra. The process is streamlined to minimize interactive input. The dispersion solutions for all comparison spectra on a floppy disk are calculated and averaged one after the other automatically upon initial setting of a file containing parameters for the fit (such as source and destination directories and whether the Gaussian fits were to be displayed graphically, an option which slows the process down). The cross-correlation process is similarly streamlined. The first step is to write a file containing the names of pairs of spectra that are to be cross correlated. Upon setting up the parameters controlling the fit (name of the file with the names of the pairs of spectra, directories, continuum level of Gaussian), all the correlations are performed. The new velocities and other information on the correlation are added to each star's data file. Strictly speaking, the parameter files could be eliminated entirely but they allow more easily for experimentation, and where no experimentation is required, default values are adopted.

3.3 Implied optimal performance

In Chapter 2, it was shown that for a given instrument and star, the rate of acquisition of radial-velocity information is optimized through the choice of spectral region of observation, slit width of the spectrograph and spectral type of correlation template. In this section it will be examined how these parameters

are (almost) optimized in the set-up of the Mt John programme. The implied optimum performance for the system (in the absence of uncertainties other than spectral noise) is then calculated.

3.3.1 Slit width

Equation 2.20 is the relationship relevant to the Mt John system between the optimum slit width and the fibre radius for radial-velocity studies with a long slit and fibre-fed spectrograph. Values of ρ and σ_0 for the Mt John system are required in order to determine the implied optimum slit width from Figure 2.9.

Calculation of ρ and σ_0

In the Mt John system, the magnification between the slit and the detector is 1, so $\rho = 0.41$ from Equation 2.17.

σ_0 is a combination of the intrinsic broadening of the stellar lines, $\sigma_{\rm Dopp}$ and the instrumental broadening due to factors other than the slit width, $\sigma_{\rm pixel}$. Fe lines in the solar spectrum (which dominate the spectrum) have total thermal and microturbulent broadening of 1.8 km/s while the solar macroturbulence is about 3.1 km/s (Gray 1976). These values are typical (Soderblom 1982) for the solar-type stars the Mt John system is designed for, so the total Doppler line width $\sigma_{\rm Dopp}$ is taken to be $\sqrt{1.8^2 + 3.1^2} = 3.6$ km/s ($\approx 36\,\mu$m on the detector).

The instrumental broadening in the system due to factors other than the slit $\sigma_{\rm pixel}$ was expected to be at least 15μm, the detector pixel width. It was calculated more accurately from observation of the line widths of Th-Ar comparison lamp lines for various spectrograph slit widths. The Th-Ar lines have negligible intrinsic width and thus

$$\sigma_{\rm line}^2 \approx (\rho w)^2 + \sigma_{\rm pixel}^2 \ .$$

The implied line width for a slit width of zero will equal $\sigma_{\rm pixel}$ for the system. Figure 3.4 shows a plot of $(\rho w)^2$ versus $\sigma_{\rm line}^2$ where the intercept implies that $\sigma_{\rm pixel} = 23\,\mu$m for the Mt John system. To construct this figure, Th-Ar spectra were obtained at different spectrograph slit widths. The mean line width $\sigma_{\rm line}$ was obtained from measurement of the width of the autocorrelation function peak for each spectrum.

Thus $\sigma_0 = \sqrt{\sigma_{\rm Dopp}^2 + \sigma_{\rm pixel}^2} = \sqrt{36^2 + 23^2} = 43\,\mu$m.

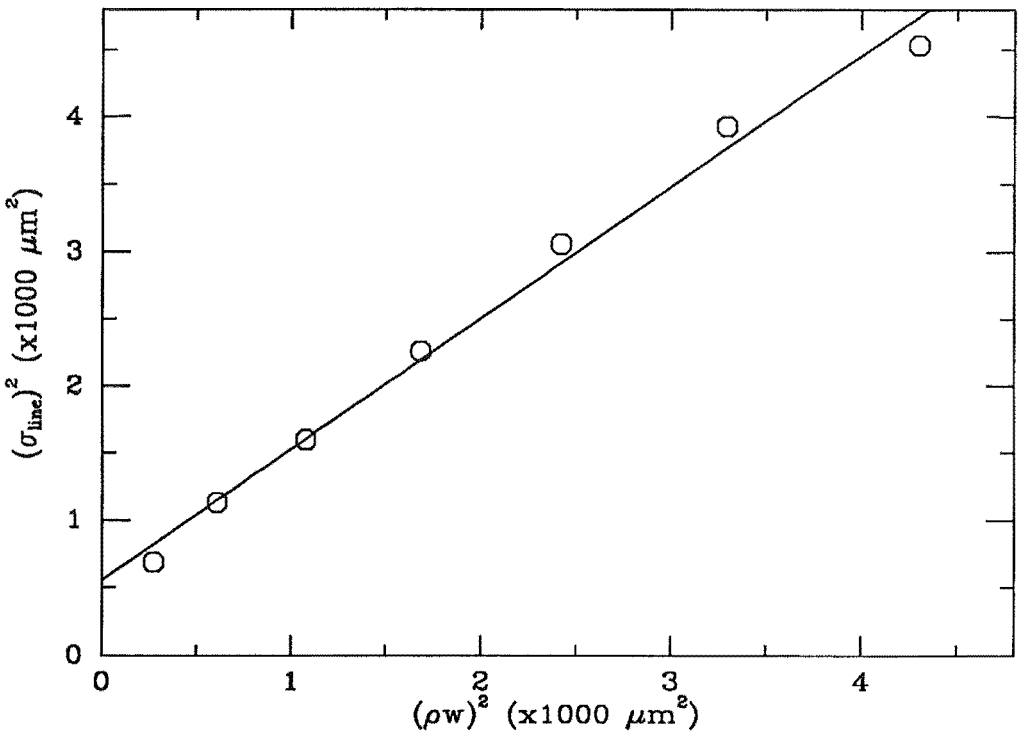

Figure 3.4: Estimation of σ_{pixel} in the Mt John system from observation of the width of Th-Ar lines. The intercept is the square of σ_{pixel}.

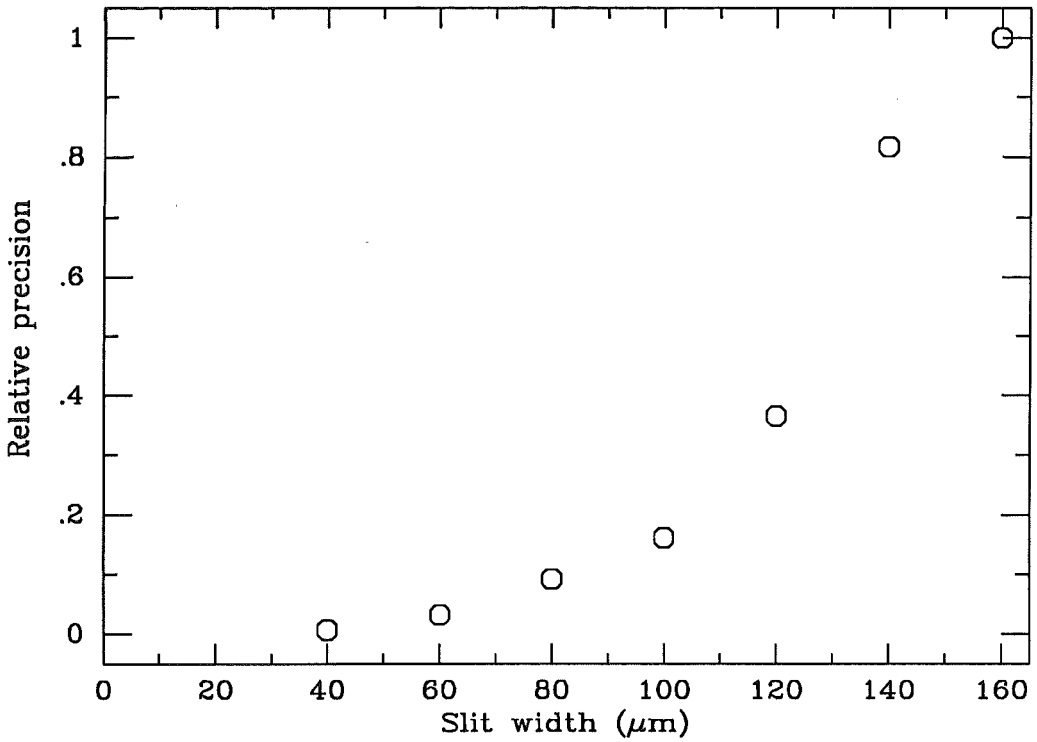

Figure 3.5: Semi-empirical calculation of the optimum slit width.

The optimum slit width

Using these results and noting that the fibre image at the slit has a radius of 90 μm, from Figure 2.9 the optimum spectrograph slit width for observation of a solar-type star with our system is calculated to be about 150 μm.

A semi-empirical test of this value for the optimum slit width was carried out by observing the star α Cen A with different spectrograph slit widths but with a constant exposure time (3 minutes). The observations were made one after the other so atmospheric conditions are unlikely to have changed much over the course of the procedure. A cross-correlation was obtained of each spectrum in the normal way and the photon-noise limited uncertainty in the resulting velocity was calculated from the uncertainty in the Gaussian fit. This is equivalent to the photon-noise limited error from Equation 2.7. The resulting precision was plotted against slit width in Figure 3.5. Unfortunately such a high optimum slit width was not anticipated and an insufficient range in slit width was sampled to give an accurate estimate of the optimum slit width. Nevertheless it can be seen that towards the end of the sampling range the curve is drawing towards

a maximum value. The maximum value is probably somewhere around 150–160 μm, in agreement with the above calculation.

The actual slit width

In practice, the spectrograph slit width was set to 115 μm corresponding to a resolution of 205 mÅ in order 46. The implication is that radial-velocity information was collected at about a third the optimum rate because of this difference between the actual and the calculated optimum slit width. This would be true in the absence of instrumental error sources in the system. However, a wider spectrograph slit appeared to magnify the radial-velocity error from instrumental sources and opening the slit to the optimum value would have been detrimental to the performance of the system. The particular error concerned is probably due to asymmetrical placement of the fibre output end on the slit and is discussed in Chapter 5.

About 25 per cent of the light is rejected by passing it through the slit. An image slicer would improve this wasteful situation. The overall fibre efficiency is 47 per cent in 2.5 arc s seeing (or 62 per cent in 1 arc s, 13 per cent in 4 arc s), taking into account losses at the input end, the output end (that is the slit) and the absorption loss in the fibre itself.

3.3.2 Spectral region

Having set the optimum slit width, the optimum spectral region can be determined. A calculation of Expression 2.19 (relevant to the Mt John programme's readout noise limited detector) was performed on the Beckers, Bridges & Gilliam (1976) solar flux atlas as in Section 2.3.2. In this case however, the transmission of the Mt John system was included (the extra transmission terms were those for the grating, échelle and fibre), the window of observation corresponded to the length of the diode array and the resolution of the atlas was degraded to 205 mÅ using a square instrumental profile.

A plot of Expression 2.19 calculated in 10 Å steps across orders 37 to 60 is shown in Figure 3.6. The overlapping segments are the separate échelle orders. Again, the plot does not extend beyond 6300 Å due to contamination of the atlas by telluric lines.

It is apparent from Figure 3.6 that the optimum wavelength region for radial-velocity studies of solar type stars with the Mt John system is at the centre of

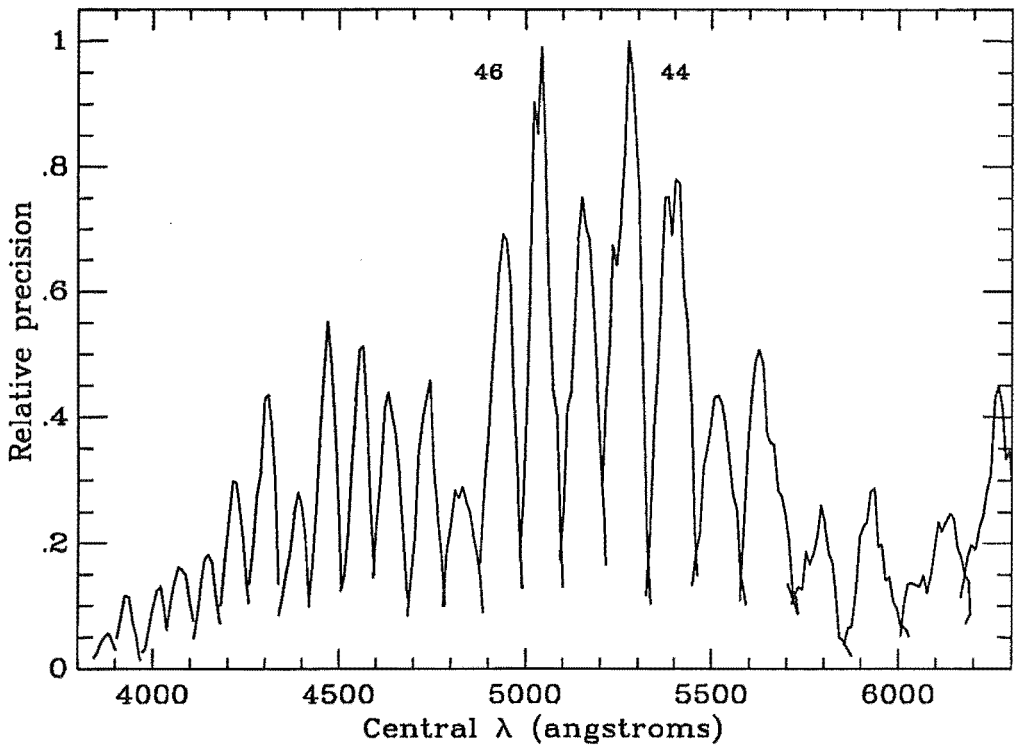

Figure 3.6: Intrinsic radial-velocity information in the solar spectrum for the Mt John system. The échelle orders containing the most information are orders 46 and 44.

order 46 (5040 Å) or the centre of order 44 (5275 Å). The system was actually set up near the centre of order 46, centred on 5010 Å.

It was mentioned in Chapter 2 that the number and strength of *comparison* spectrum lines could be a further consideration when choosing in which spectral region to set up a system. In this case, where two échelle orders are obviously equally suitable in terms of information in the stellar spectrum, the deciding factor should indeed be in which of these orders the comparison spectrum provides more information. Where the Mt John system was set up, at 5010 Å, there are 14 Th-Ar comparison lines available. In contrast, near the centre of order 44 about twice this many comparison spectrum lines could have been used.

3.3.3 Correlation template

Originally it was planned to cross correlate each dwarf star in the Mt John programme against a particular International Astronomical Union (IAU) standard star always observed on the same night. Equation 2.12 implies that a better radial-velocity precision is obtained by cross correlating a star's spectrum against a template spectrum of itself, since the correlation between the two spectra, A,

will be close to 1 and also there will be no *random* noise contribution from the template spectrum. This development also makes the observing procedure simpler, as there is no longer a constraint to necessarily observe a given standard star in conjunction with a programme star when in fact 1) that part of the sky in which the standard is to be found might be cloudy, 2) the standard star may not be above the horizon, since IAU standards tend to be at equatorial declinations and 3) the standard star is unlikely to match the programme dwarf star in spectral type because most IAU radial-velocity standards are giants. One further simplification in not using IAU radial-velocity standard stars as templates is that at high levels of radial-velocity precision many of them are variable (Mayor & Maurice 1985; Walker *et al.* 1989). Removing the template variability could prove complicated.

3.3.4 Spectral noise limited precision

With the system thus set up, the radial-velocity error in the presence of the readout noise alone can be calculated. Using Equation 2.11 for a signal-to-noise ratio of 100:1, the limiting radial-velocity error is about 5 m/s for a star of solar spectral type. This represents the smallest radial-velocity error possible with this system for a signal-to-noise of 100:1, but ignores the presence of other error sources in the system.

3.4 Observing Programme

3.4.1 Description

Between 1988 November and 1991 September, 40 stars were observed for the Mt John radial-velocity programme. They are listed in Table 3.1. Ten of the stars are giant IAU radial-velocity standards from the revised list of Mayor & Maurice (1985). One further star, the spectroscopic binary HR 4492, was added to the observing list towards the end of the programme in order to confirm its orbit. The other 29 stars, including two further IAU radial-velocity standards, were the programme stars. The programme stars were chosen to be dwarfs[2], the object for which was the detection of low-mass companions. They are all brighter than

[2]Although these stars are all listed as luminosity class V in the *Bright Star Catalogue* (Hoffleit 1982), further investigation showed that some are more accurately considered to belonging luminosity classes such as IV (Houk and Cowley 1975), with one even belonging to class III. This explains the slight spread in the luminosity classes of the 'dwarf' sample in Table 3.1.

HR number	Name	Spectral type	V mag	α_{2000} h	m	s	δ_{2000} °	′	″
77	ζ Tuc	G0V	4.23	0	20	4	−64	52	30
98	β Hyi	G1IV	2.80	0	25	45	−77	15	16
188*	β Cet	G9III	2.04	0	43	35	−17	59	12
370†	ν Phe	G0V	4.96	1	15	11	−45	31	54
911*	α Cet	M1.5IIIa	2.53	3	2	17	+ 4	5	23
1008†	82 Eri	G8V	4.27	3	19	56	−43	4	11
1083	κ Ret	F3IV/V	4.72	3	29	23	−52	56	16
1136	δ Eri	K0+IV	3.54	3	43	15	− 9	45	48
1674	ζ Dor	F6/7V	4.72	5	5	31	−57	28	22
1743†	o Col	K0/1IV/V	4.83	5	17	29	−34	53	43
1829*†	β Lep	G5II	2.84	5	28	15	−20	45	34
1983	γ Lep	F6V	3.60	5	44	28	−22	26	54
2906		F6IV	4.45	7	34	3	−22	17	46
2943	α CMi	F5IV/V	0.38	7	39	18	+ 5	13	30
3220		F5V	4.76	8	9	1	−61	18	7
3748*	α Hya	K3II/III	1.98	9	27	35	− 8	39	31
3862		F9V	4.94	9	42	14	−23	54	56
4134		F5V	4.89	10	31	22	−53	42	56
4492		K2III	5.17	11	39	30	−65	23	52
4523		G3V	4.91	11	46	31	−40	30	1
4540*†	β Vir	F9V	3.61	11	50	42	+ 1	45	53
4763*	γ Cru	M3.5III	1.63	12	31	10	−57	6	47
4786*†	β Crv	G5IIb	2.65	12	34	23	−23	23	48
4979†		G3V	4.85	13	12	3	−37	48	11
5019	61 Vir	G6.5V	4.74	13	18	24	−18	18	41
5459	α Cen A	G2V	−0.01	14	39	36	−60	50	7
5460	α Cen B	K1V	1.33	14	39	36	−60	50	7
5777†	37 Lib	K1III/IV	4.62	15	34	11	−10	3	53
6056*	δ Oph	M0.5III	2.74	16	14	21	− 3	41	40
6102†	γ Aps	G8/K0III	3.89	16	33	27	−78	53	49
6603*†	β Oph	K2III	2.77	17	43	28	+ 4	34	2
6859*†	δ Sgr	K2.5IIIa	2.70	18	21	0	−29	49	41
7597	ω Sgr	G5IV	4.70	19	55	50	−26	17	58
7602†	β Aql A	G8IV	3.71	19	55	19	+ 6	24	24
7665†	δ Pav	G6/8IV	3.56	20	8	43	−66	10	56
8181	γ Pav	F7V	4.22	21	26	27	−65	21	59
8232*	β Aqr	G0Ib	2.91	21	31	33	− 5	34	16
8387†	ϵ Ind	K4/5V	4.69	22	3	21	−56	47	10
8447	τ PsA	F6V	4.92	22	10	9	−32	32	55
8969*	ι Psc	F7V	4.13	23	39	57	+ 5	37	35

* IAU radial-velocity standard star.

† Apparently constant in radial velocity so chosen to define run zero points.

Table 3.1: Stars in the Mt John programme.

visual magnitude 5.0 with spectral class between F5 and K5, but exclude fast rotators and in general, known spectroscopic binaries. The line profiles of fast rotating stars were not well-enough defined for precise radial velocities to be obtained in the Mt John programme. Stable orbits are less likely in binary systems, however the two bright components of the α Cen system and Procyon (α CMi) which were too bright to resist inclusion. ω Sgr is also a known spectroscopic binary but slipped through the initial selection process.

Observations were made monthly and since about two-thirds of the stars are circumpolar, a good year-round radial-velocity coverage was possible of most of them. Unfortunately no data could be obtained between Julian dates 2447780 and 2447980 because of failure of the diode array detector.

3.4.2 Correction for run-to-run zero point variations

It became apparent during the course of the programme that there was some degree of correlation between the time series of relative radial velocities of several of the stars in the Mt John programme. An example of the raw radial velocities of three of the stars is shown in Figure 3.7. The stars all show a drop in velocity towards later dates. This pattern was mirrored in about a dozen other stars where more subtle correlation effects were also apparent. It was suspected that these stars are intrinsically constant in radial velocity and that different observing runs (different instrumental set-ups) had different velocity zero-points. This possibility was investigated. The mean velocity of all except the most obviously variable stars in a given run was calculated and compared to similar mean velocities of a few other runs. The runs in question were 1990 July, August, September and October and 1991 January. A t-test was used to determine whether the run-to-run means were significantly different. In some cases, for example July compared with August and September compared with October, the probability of such a large difference between the mean values happening by chance was statistically very small. It was concluded that for all runs in the programme, the zero point defined by each individual run should be corrected for.

A subset of stars with assumed constant velocity was used to define the zero point of each run. These stars were chosen as those whose raw velocities showed the smallest scatter overall but also showed a star-to-star correlation between velocities obtained in the same run, as in Figure 3.7. These 14 stars are marked

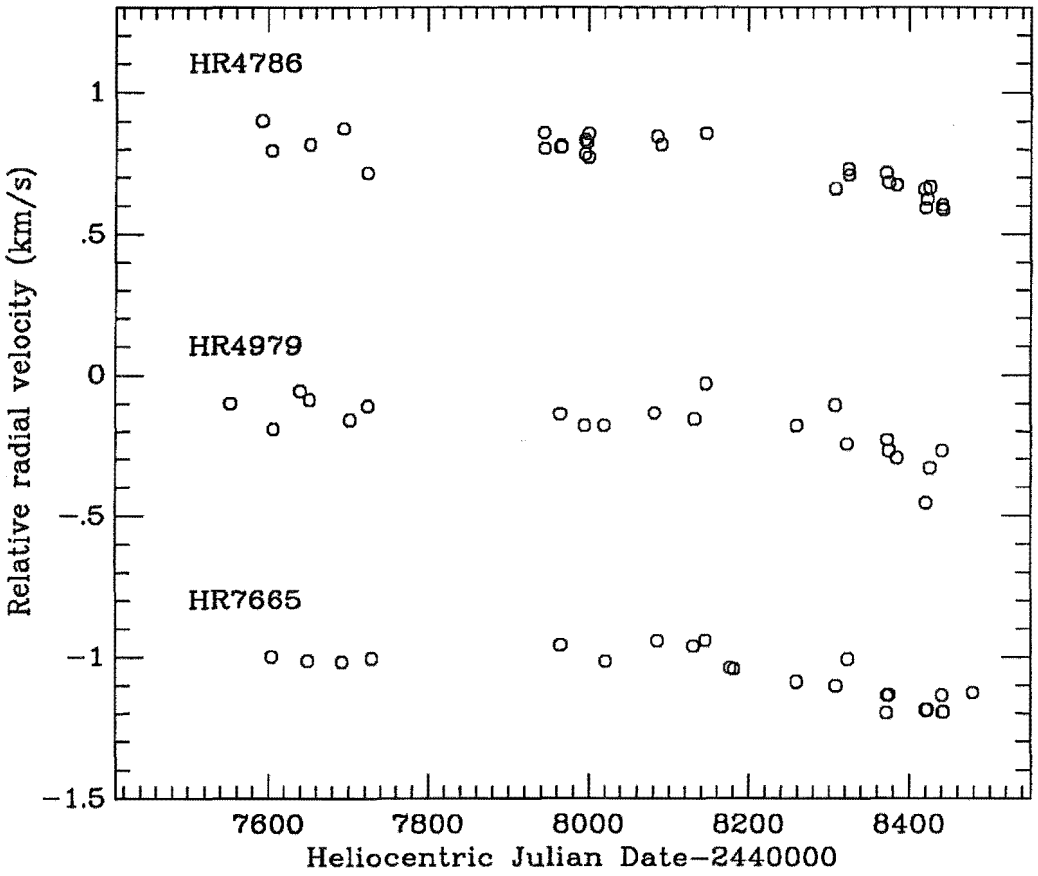

Figure 3.7: Velocities of three stars in the Mt John radial-velocity programme, uncorrected for run-to-run zero-point variations.

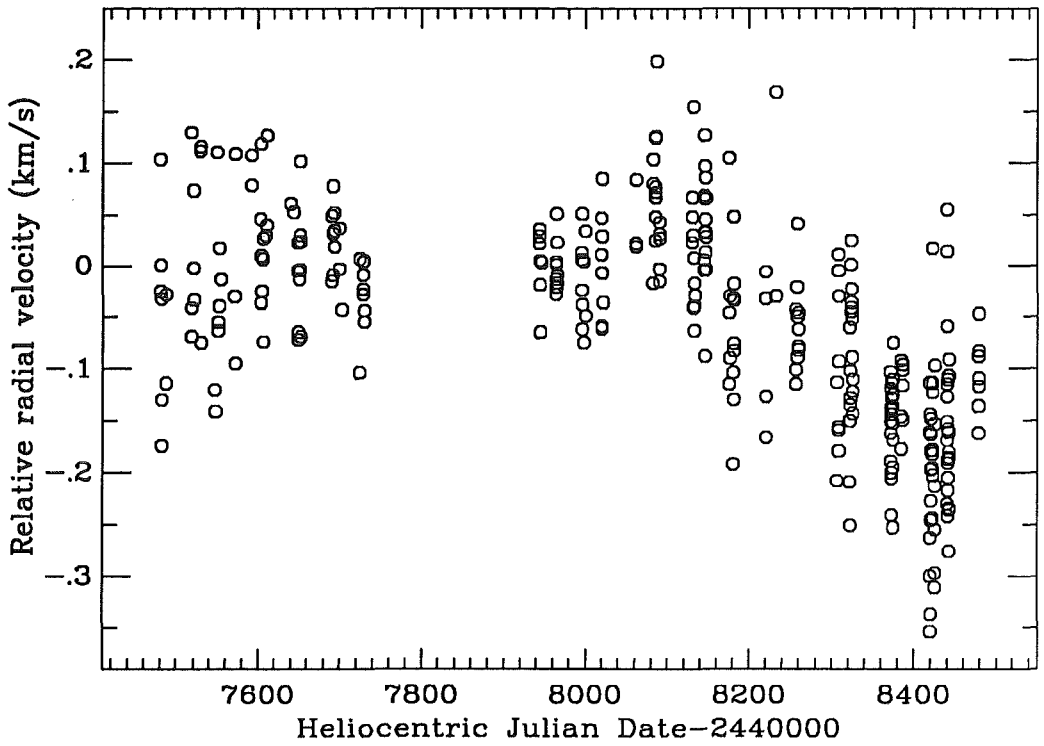

Figure 3.8: Relative radial velocities of the 14 assumed non-varying stars in the Mt John programme, showing the run-to-run changes in zero point.

with a † in Table 3.1. Figure 3.8 shows the raw velocities from the 14 assumed non-varying stars, showing the run-to-run trends. The mean value of the velocities of the non-varying stars was subtracted from all velocity observations for a given run.

The probable cause of the run-to-run zero-point variations will be discussed in Chapter 5.

Chapter 4

Results of the Mt John programme

4.1 Individual relative velocities

The relative radial velocities obtained for all the stars in the Mt John programme are tabulated in Appendix C. Here those same velocities, except with zero points altered for the convenience of plotting, are displayed in graphical form in Figures 4.11 to 4.10. Recall that the absence of data between Julian Dates 2447780 and 2447980 was due to equipment failure.

The velocity data for all stars but one are plotted to the same scale, in order to give an idea of the relative values of the scatter in velocity. The exception is HR 4492, the data for which are presented last. For this star the range in velocities is somewhat larger than the range in velocities of the other stars, requiring a more expanded graphical scale.

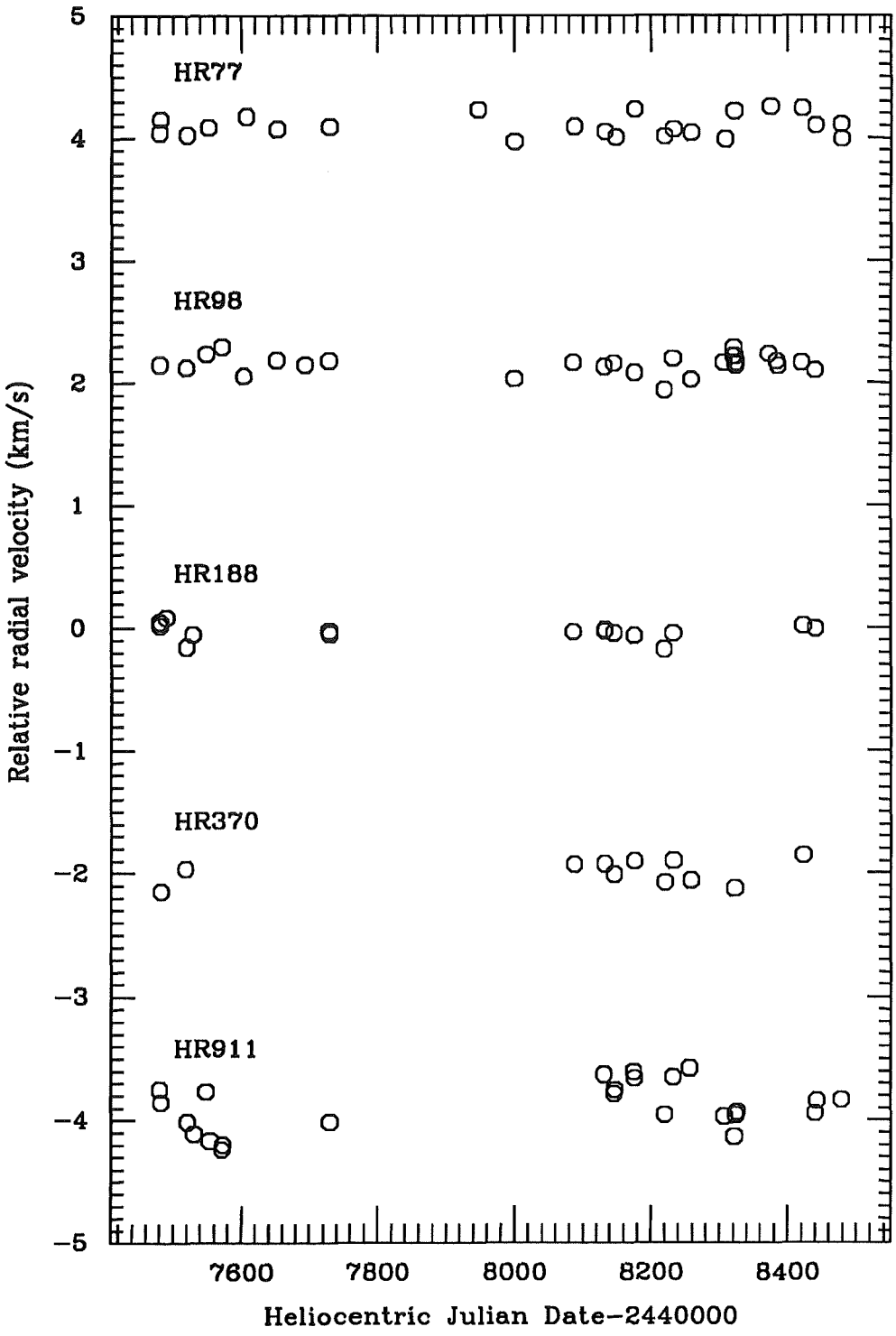

Figure 4.1: Relative radial velocities for HR 77 (ζ Tuc), HR 98 (β Hyi), HR 188 (β Cet), HR 370 (ν Phe) and HR 911 (α Cet).

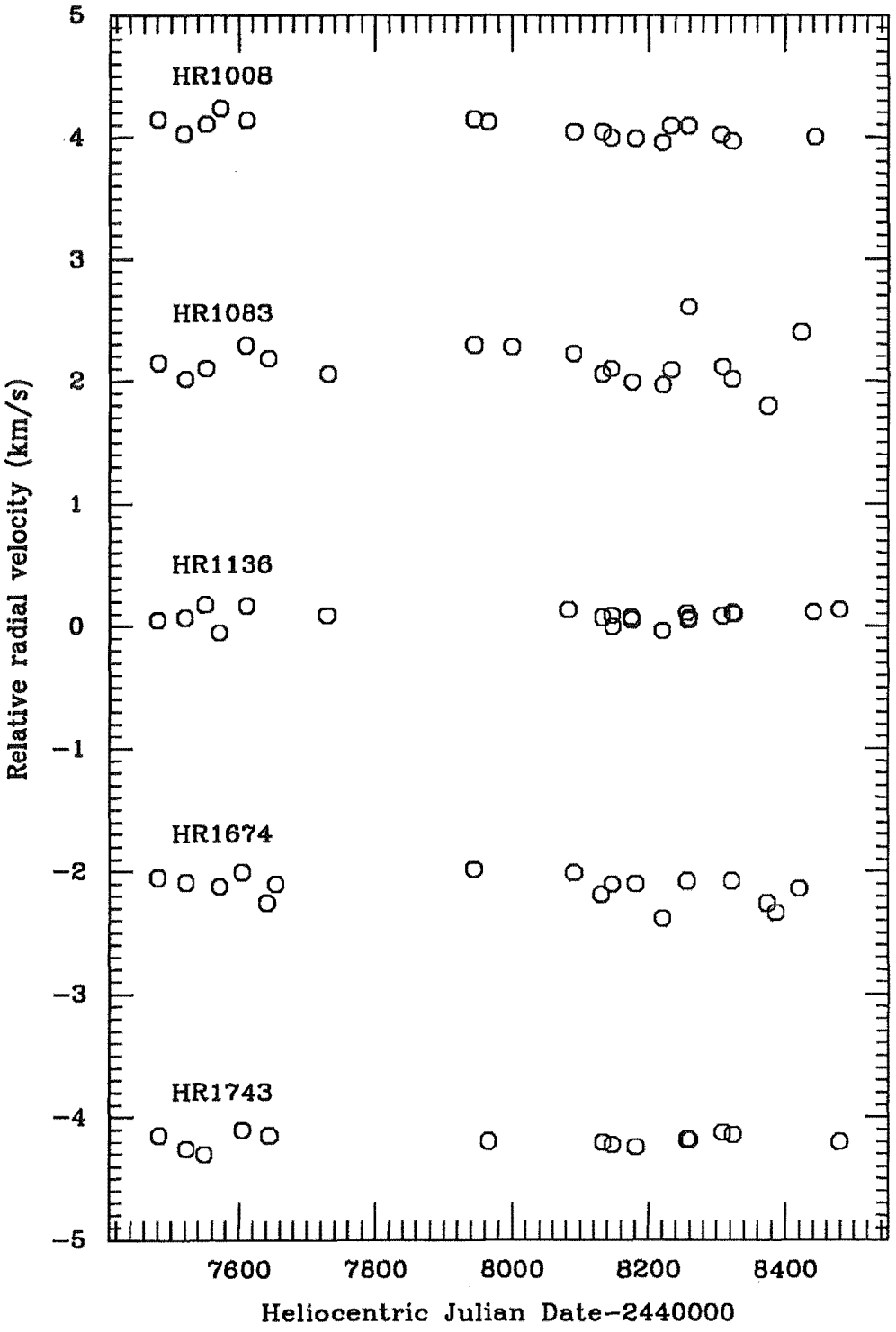

Figure 4.2: Relative radial velocities for HR 1008 (82 Eri), HR 1083 (κ Ret), HR 1136 (δ Eri), HR 1674 (ζ Dor) and HR 1743 (o Col).

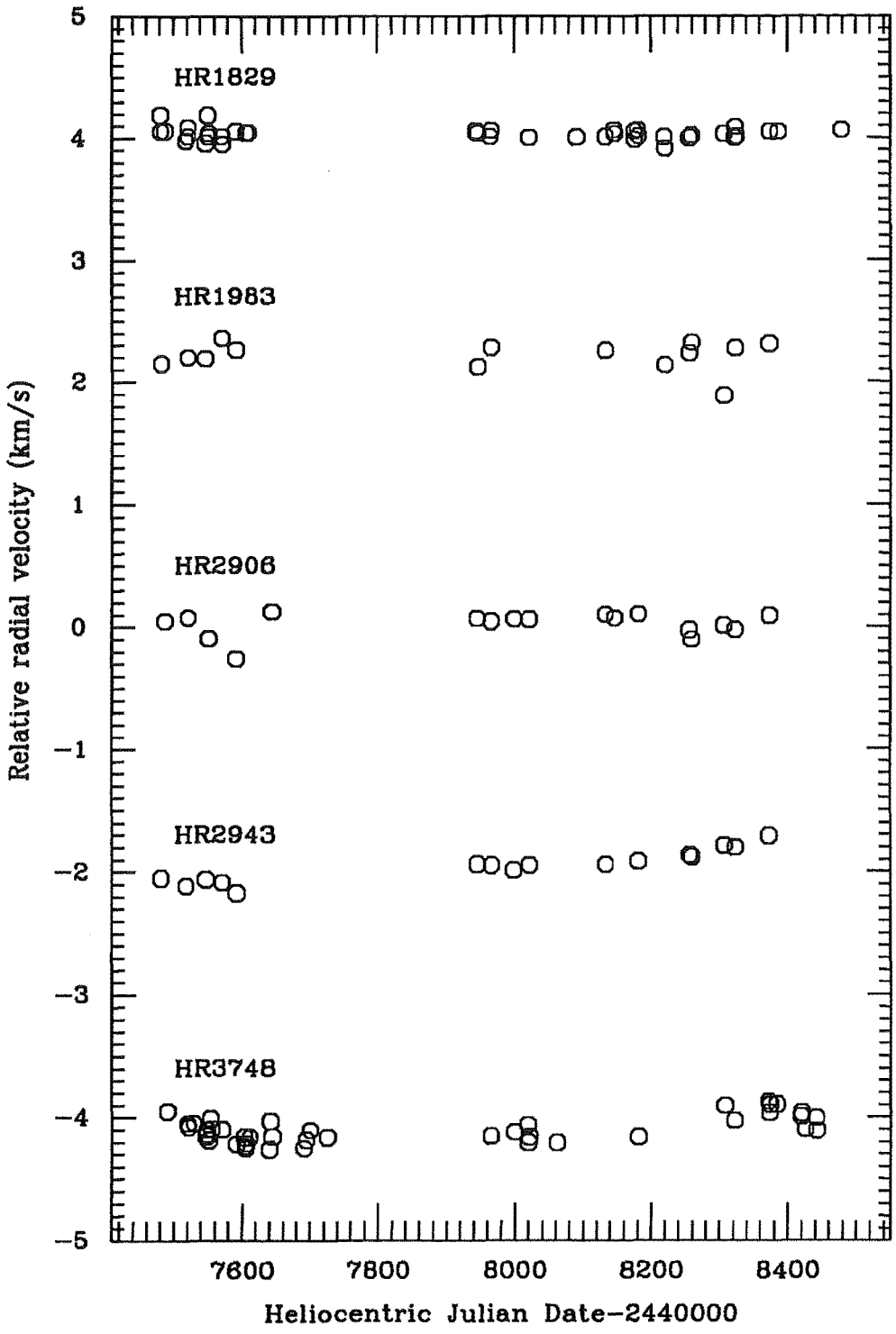

Figure 4.3: Relative radial velocities for HR 1829 (β Lep), HR 1983 (γ Lep), HR 2906, HR 2943 (α CMi) and HR 3748 (α Hya).

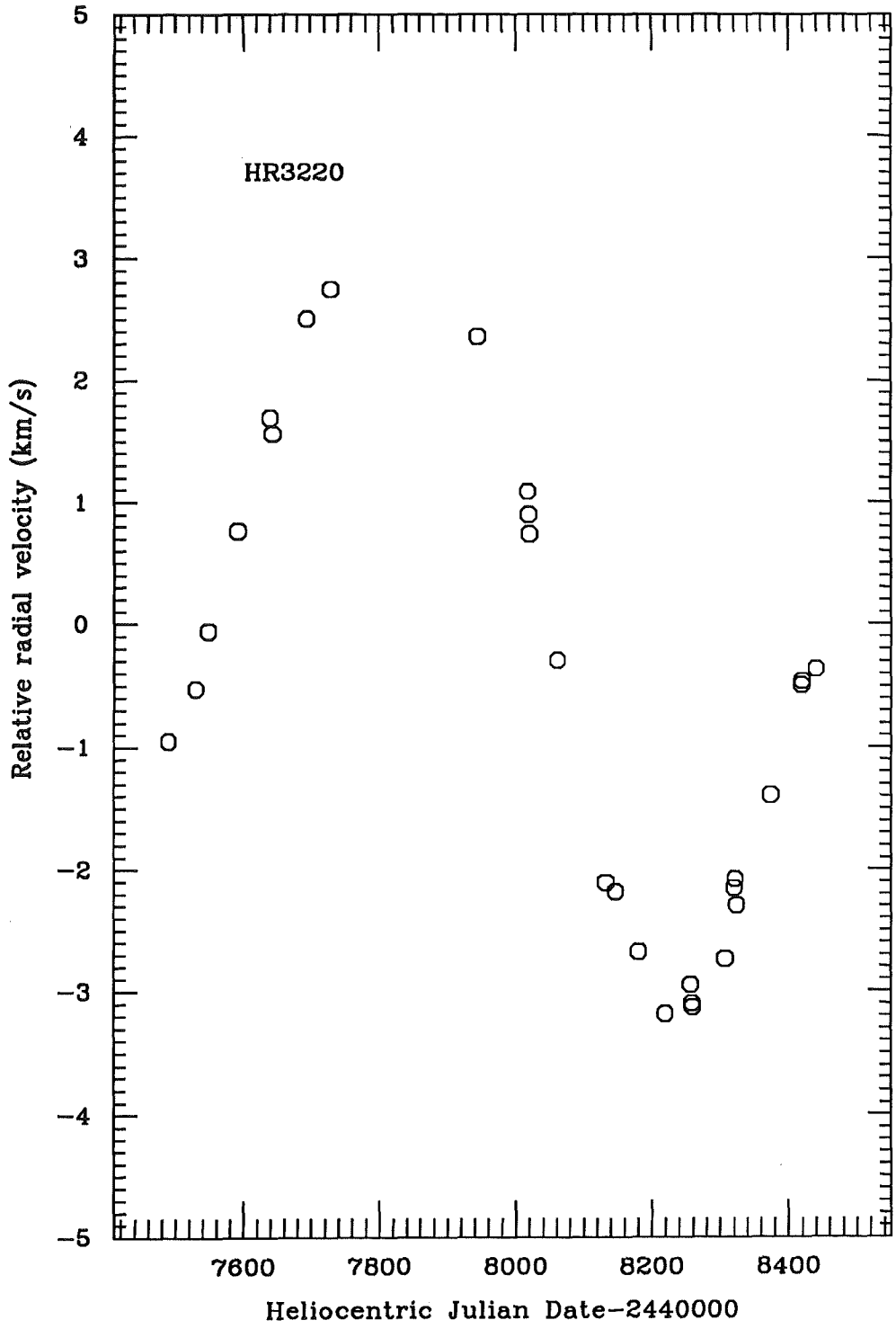

Figure 4.4: Relative radial velocities for HR 3220.

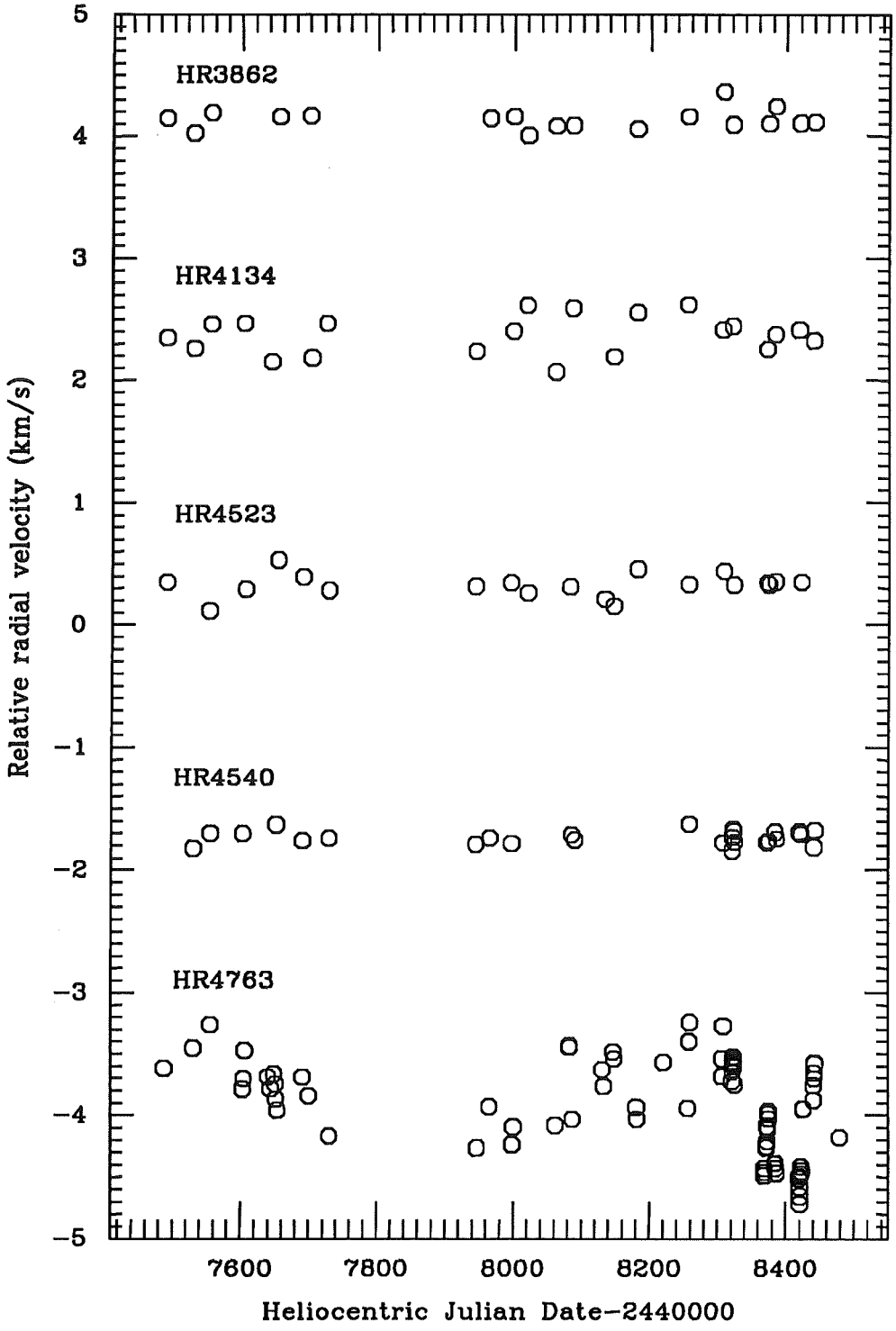

Figure 4.5: Relative radial velocities for HR 3862, HR 4134, HR 4523, HR 4540 (β Vir) and HR 4763 (γ Cru).

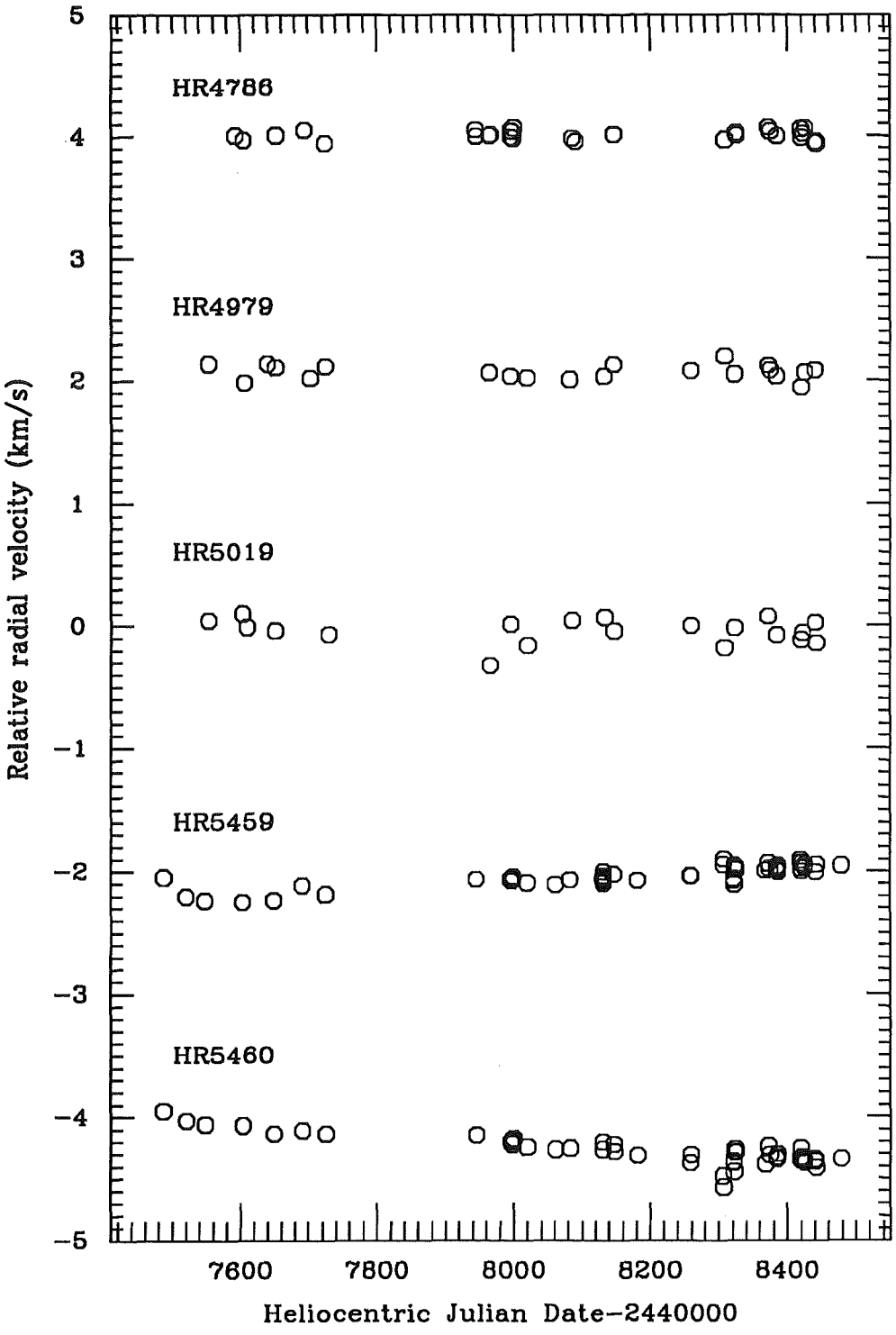

Figure 4.6: Relative radial velocities for HR 4786 (βCrv), HR 4979, HR 5019 (61 Vir), HR 5459 (α Cen A) and HR 5460 (α Cen B).

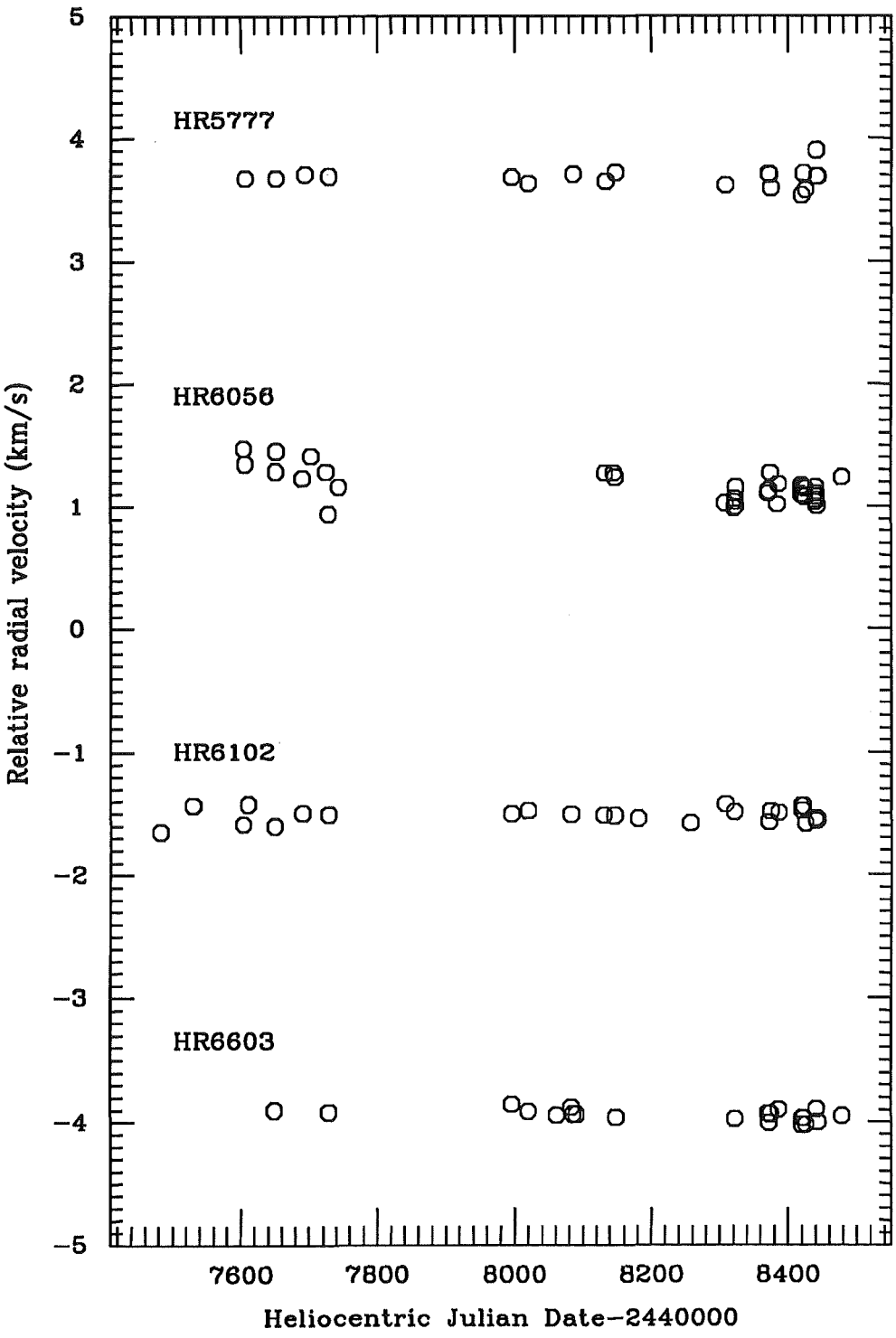

Figure 4.7: Relative radial velocities for HR 5777 (37 Lib), HR 6056 (δ Oph), HR 6102 (γ Aps) and HR 6603 (β Oph).

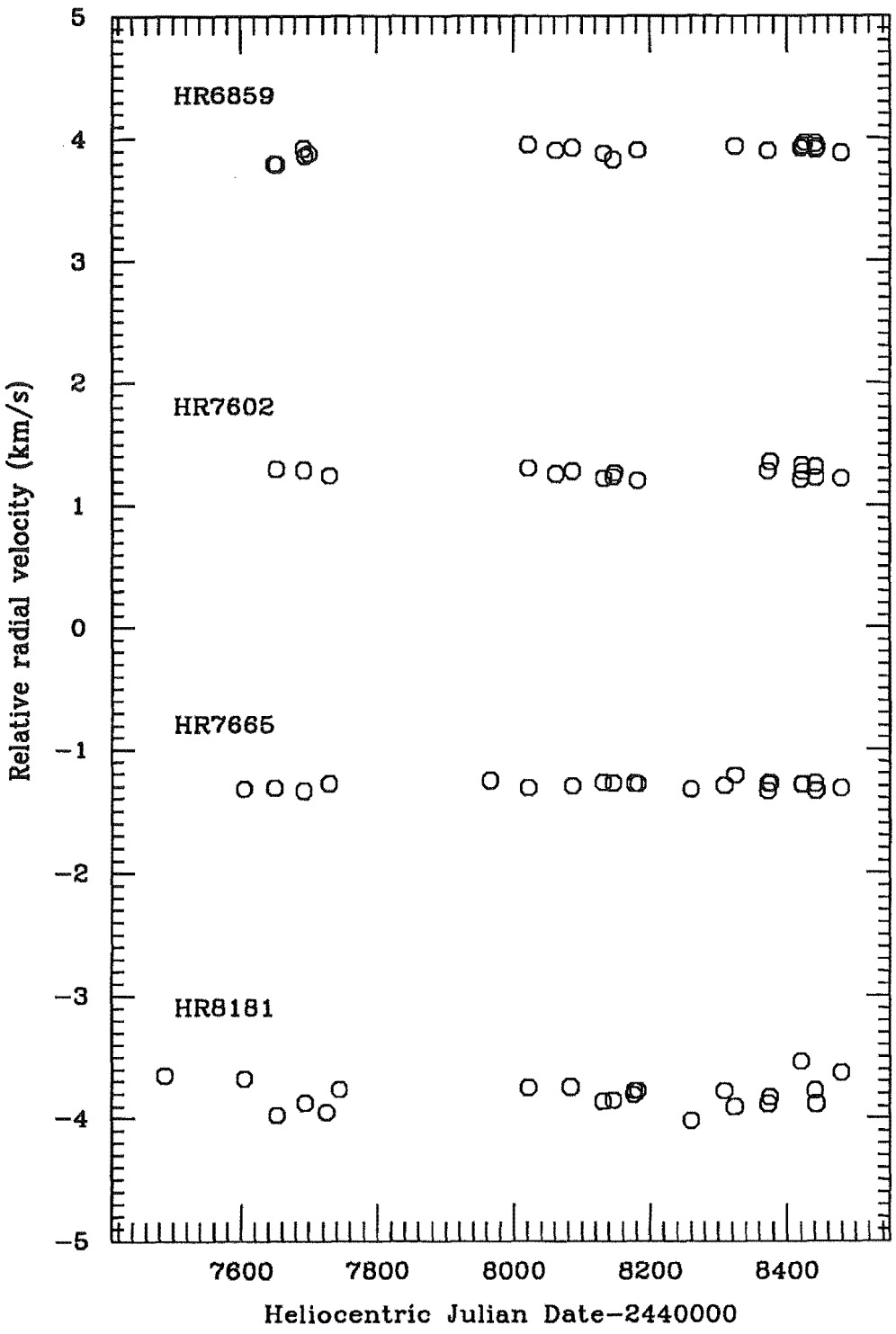

Figure 4.8: Relative radial velocities for HR 6859 (δ Sgr), HR 7602 (β Aql), HR 7665 (δ Pav) and HR 8181 (γ Pav).

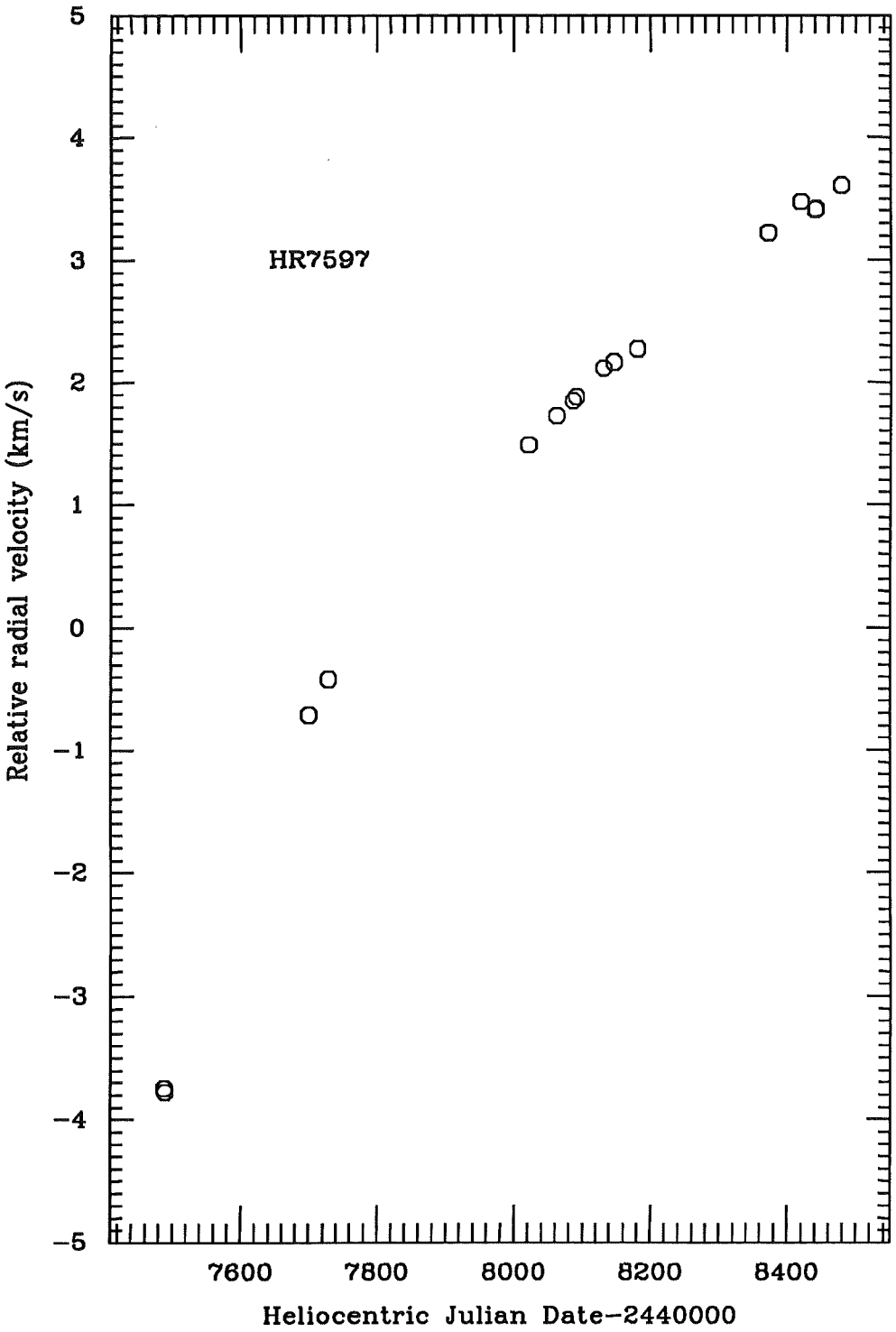

Figure 4.9: Relative radial velocities for HR 7597 (ω Sgr).

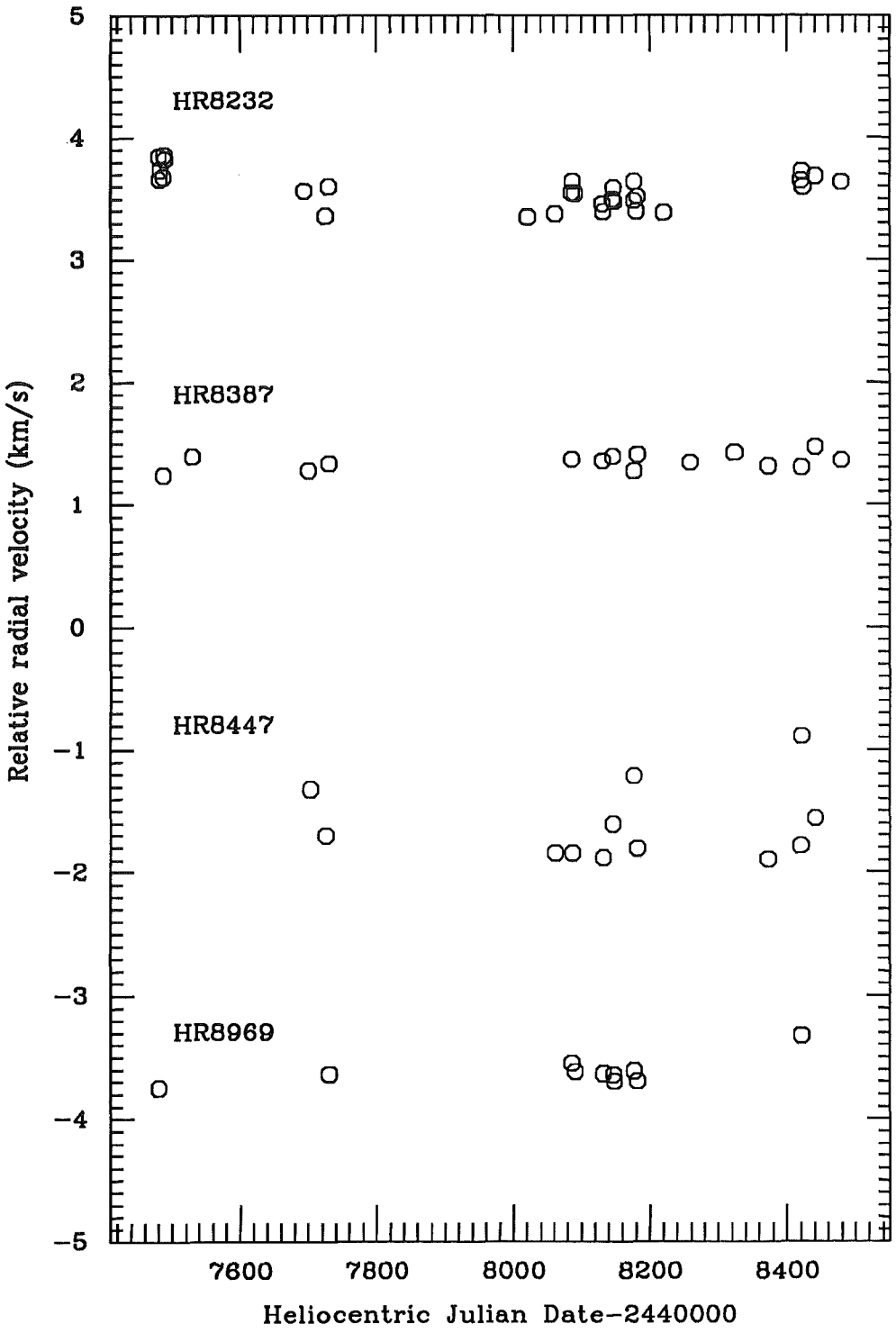

Figure 4.10: Relative radial velocities for HR 8232 (β Aqr), HR 8387 (ϵ Ind), HR 8447 (τ PsA) and HR 8969 (ι Psc).

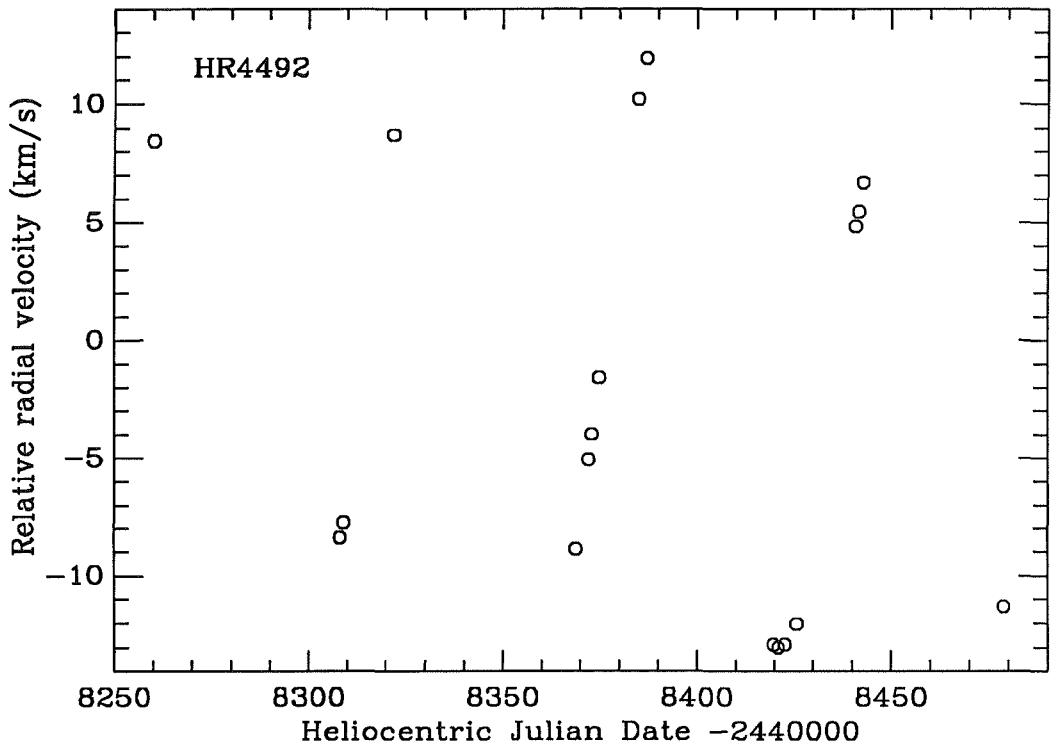

Figure 4.11: Relative radial velocities for HR 4492.

4.2 Conversion to absolute velocities

Although this thesis is concerned only with changes in the radial velocities of stars, it is recognized that at some stage other researchers may wish to compare their radial velocities to the Mt John radial velocities. For this purpose, corrections have been determined which allow conversion of the Mt John relative radial velocities, listed in Appendix C, to absolute radial velocities. To do this, the spectral template of each star in the Mt John programme has been cross correlated with the template of one of three IAU standard stars. The actual IAU standard star template chosen is the one closest in spectral type to the star itself, in order to minimize the probable systematic error resulting from cross correlation of spectra of different spectral type (see Chapter 5). The IAU standard stars (Table 4.1) chosen to calculate the absolute velocities had radial velocities that appeared to be constant with time and represented the range of spectral types of stars in the programme. The resulting radial-velocity difference between each pair of templates, combined with the respective run correction for each template, the difference of the mean of the standard star velocities from the standard-star template and the IAU-accepted absolute radial velocity for the standard, results in a correction which should be added to each velocity for the star in order to convert it to a frame of reference relative to the solar system barycentre. These velocity corrections are listed in Table 4.2.

4.3 The obvious binaries

Six stars in the Mt John programme have obvious stellar companions. These stars comprise those already known as spectroscopic binaries and which already had determined orbits — α Cen A, α Cen B, Procyon (α CMi) and HR 4492; the star already known as a spectroscopic binary but without a determined orbit —

Star	Spectral type	IAU radial velocity (km/s)
β Vir	F9V	$+ 5.0 \pm 0.2$
β Crv	G5IIb	$- 7.0 \pm 0.0$
β Oph	K2III	-12.0 ± 0.1

Table 4.1: IAU-accepted radial velocities for the three IAU standard stars used to determine the absolute velocity corrections for the Mt John programme stars.

HR	Name	Correction (km/s)	Ref.	HR	Name	Correction (km/s)	Ref.
77	ζ Tuc	+ 9.671	β Vir	4763	γ Cru	+23.018	β Oph
98	β Hyi	+23.531	β Vir	4786	β Crv	− 7.092	β Crv
188	β Cet	+13.578	β Oph	4979		−12.450	β Crv
370	ν Phe	+12.098	β Vir	5019	61 Vir	− 6.908	β Crv
911	α Cet	−25.147	β Oph	5459	α Cen A	−23.793	β Crv
1008	82 Eri	+88.205	β Oph	5460	α Cen B	−19.366	β Oph
1083	κ Ret	+14.318	β Crv	5777	37 Lib	+49.139	β Oph
1136	δ Eri	− 6.988	β Oph	6056	δ Oph	−18.650	β Oph
1674	ζ Dor	− 0.740	β Vir	6102	γ Aps	+ 6.262	β Oph
1743	o Col	+20.306	β Oph	6603	β Oph	−11.954	β Oph
1829	β Lep	−13.687	β Crv	6859	δ Sgr	−19.864	β Oph
1983	γ Lep	− 8.864	β Vir	7597	ω Sgr	−22.783	β Crv
2906		+61.540	β Vir	7602	β Aql A	−39.876	β Oph
2943	α CMi	− 3.249	β Vir	7665	δ Pav	−21.132	β Crv
3220		+24.305	β Vir	8181	γ Pav	−29.340	β Vir
3748	α Hya	− 3.167	β Oph	8232	β Aqr	+ 6.964	β Vir
3862		+35.140	β Vir	8387	ϵ Ind	−39.636	β Oph
4134		+21.678	β Vir	8447	τ PsA	−15.525	β Vir
4523		+17.475	β Crv	8969	ι Psc	+ 5.946	β Vir
4540	β Vir	+ 4.936	β Vir				

Table 4.2: Corrections required to be added to the Mt John relative radial velocities in Appendix C in order to convert them to absolute radial velocities. The 'Ref.' column indicates the standard star whose template was used in the cross correlation to obtain the correction.

ω Sgr; and the star discovered to be a spectroscopic binary in the course of this survey — HR 3220. The aims of this section are to compare the present data with previous orbital solutions if any, to present new orbital solutions if possible and from the orbital solutions to determine the velocity residuals for investigation in a later chapter of the existence of yet lower mass companions.

4.3.1 The α Cen system

The two bright components of this system have a well-known 80-year-period visual orbit but no computed spectroscopic orbit[1]. Data from the Mt John programme reveal an apparently linear change in radial velocity for both components (see Figure 4.6), consistent with what is to be expected from orbital motion of the pair alone — the programme was in progress for only about 3 per cent of a cycle so velocity changes should appear approximately linear. Although this is not enough information from which to compute a spectroscopic orbit, it is possible to verify that the slope in the data is in agreement with the visual orbit. Furthermore the Mt John data are sufficient for the determination of a spectroscopic mass ratio for the system.

Orbital motion of components A and B

The visual-orbit elements and parallax for the α Cen system from Heintz (1982) have been used to derive the corresponding spectroscopic elements. Using these elements and the computer program BXT2 of T. Mazeh, the expected values of the velocity of α Cen B relative to α Cen A ($v_B - v_A$) over the course of the Mt John programme have been calculated. The mean slope of the predicted velocities was measured in order to compare to the slope of the Mt John observations of $v_B - v_A$. The predicted slope is -0.62 m/s/day.

Although for the α Cen system each velocity was calculated relative to a single spectrum of the same star (as is the case for all other stars in the programme), in this case cross correlations were also performed of α Cen B with α Cen A on every occasion when they were observed one after the other. This procedure, which eliminated the need for run-to-run corrections, enabled the most accurate calculation of $v_B - v_A$. Using a least-squares fitting procedure it was found that the change in $v_B - v_A$ over the course of the Mt John programme was

[1]The third component, Proxima, is distant enough and of sufficiently small mass that its effect on the orbital motion of components A and B can be neglected.

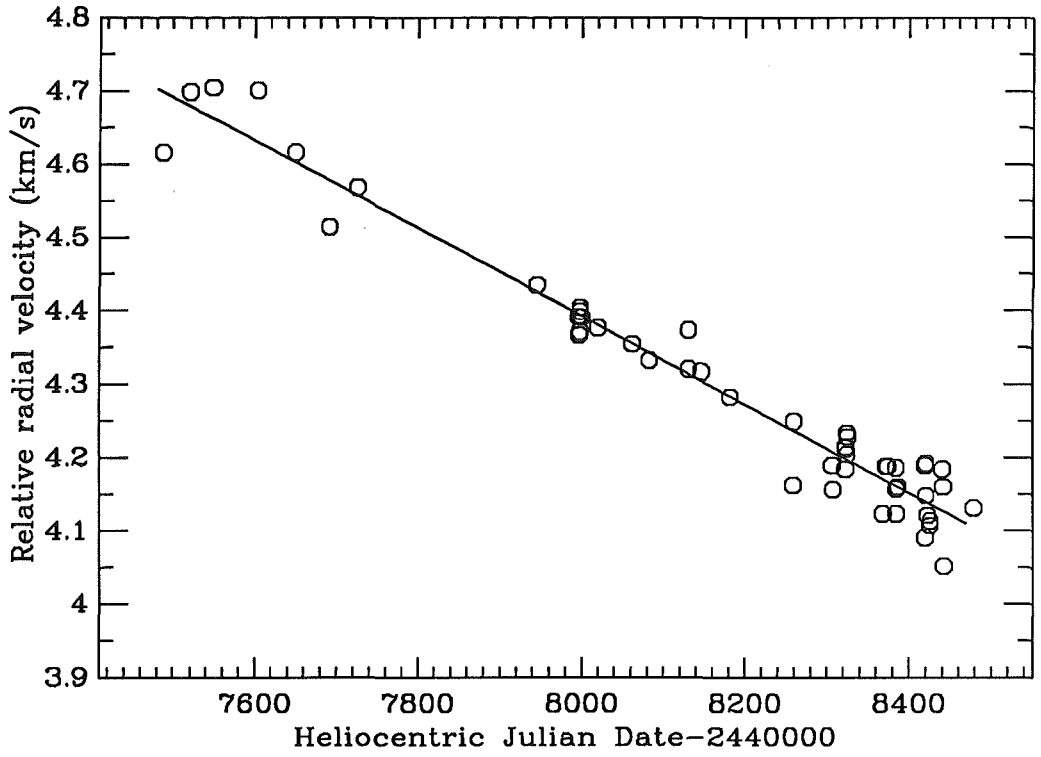

Figure 4.12: Velocity record of α Cen B relative to α Cen A showing least-squares fit to the data.

(-0.60 ± 0.02) m/s/day. It was concluded that the measured slope in the α Cen radial velocities was consistent with that expected from a modern visual orbit for the system. The data and the least-squares fit are displayed in Figure 4.12.

In future chapters, the changes in velocity from orbital motion of the A-B pair, represented by the best-fit slopes to the data of A and of B, have been subtracted from the original data. It is noted here that the absolute values of $v_B - v_A$ are not compared with those predicted from the astrometric orbit because of a suspected systematic error in the cross correlation of two stars of different spectral class. This subject will discussed in Chapter 5.

Spectroscopic mass ratio of components A and B

The Mt John programme was the first to undertake a systematic high-precision radial-velocity study of the α Cen system. In the past, the lack of a systematic radial-velocity study coupled with the poor distribution in time of existing radial-velocity data resulted in a spectroscopic mass ratio m_B/m_A of very poor accuracy which disagreed with the results obtained from the well-known visual

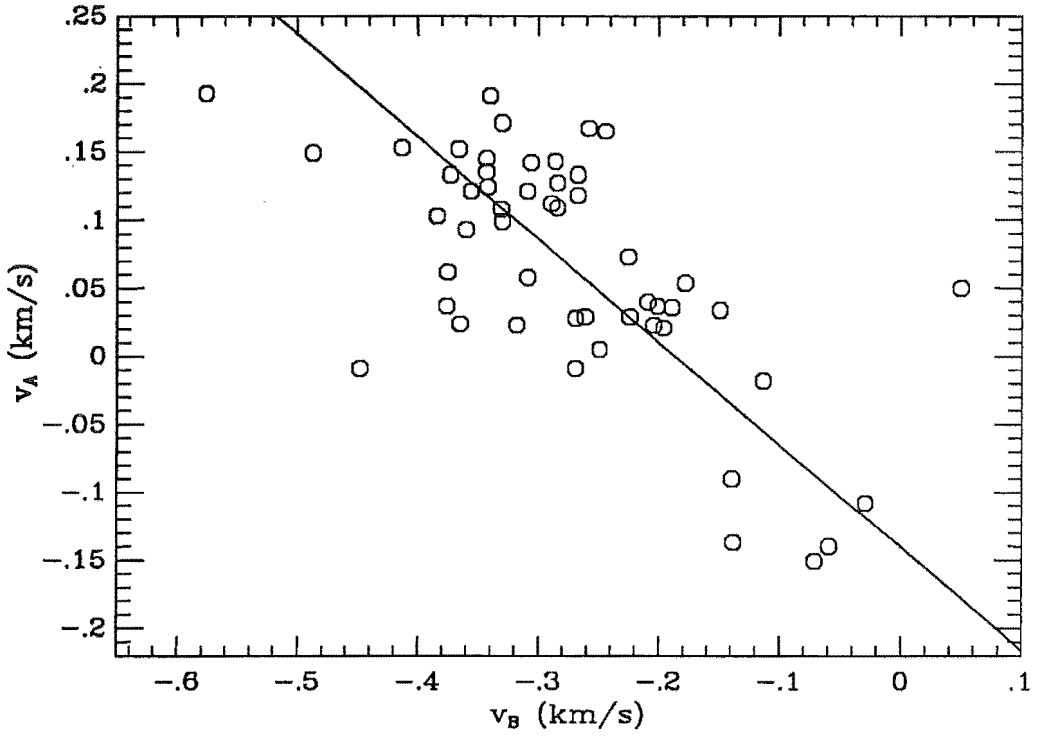

Figure 4.13: Relative radial velocities v_A of α Cen A plotted against relative radial velocities v_B of α Cen B.

orbit. Heintz (1982) addresses this discordance between mass-ratio results, comparing 0.82 from astrometric observations with 0.4 (!) from radial velocities. Since all positional data for the stars are known to an accuracy of 1 per cent whilst past radial-velocity data are sparse, there is good reason to doubt the spectroscopic value.

Although only a small fraction of one orbit of the α Cen system was observed in the Mt John programme, sufficient data was obtained for the calculation of an improved mass ratio. Wilson (1941) describes how if the velocity of both components v_A and v_B of a binary system are obtained at a minimum of two epochs, the negative slope of a plot of v_A (ordinate) versus v_B (abscissa) gives the mass ratio m_B/m_A of the system. Figure 4.13 contains a plot of v_A versus v_B for the α Cen system, using the Mt John velocities.

A linear least-squares fit was carried out on the data in Figure 4.13 in order to derive the slope. Since, unlike many least-squares problems, there is significant error in *both* coordinates, the usual simple regression of x on y or y on x was not appropriate. Instead, the recommendations of Isobe *et al.* (1990) were applied,

calculating the best-fit line as the bisector of the y on x regression and the x on y regression. This line is plotted in Figure 4.13.

From the slope of this line a spectroscopic mass ratio for the α Cen system was derived as

$$\frac{m_B}{m_A} = 0.75 \pm 0.09.$$

This spectroscopic value is in agreement with the mass ratio calculated from astrometric data (0.82) and represents a considerable improvement in precision on the previous spectroscopic mass ratio.

4.3.2 Procyon (α CMi)

This is another long-period system whose radial-velocity changes could be expected to be approximately linear over the course of the Mt John programme. The orbital elements of J. M. Fletcher quoted by Batten, Fletcher & MacCarthy (1989) (which, except for the period derived from the visual orbit, are all derived spectroscopically) have been used to predict the rate of change in radial velocity over the course of the Mt John programme. The prediction is 0.36 m/s/day compared to a measured slope from the Mt John velocities of (0.35 ± 0.04) m/s/day. The observed velocity changes for this star are again consistent with those expected from orbital motion due to the known (white dwarf) companion alone. Again, the best-fit slope was deemed representative of the orbital motion of the primary pair of stars and was subtracted from the data for further analysis in later chapters.

4.3.3 HR 4492

This star was not a foundation member of the Mt John programme, but was added during the course of the programme as an exercise in testing the capability of the system and also to verify the star's orbit. Consequently it is not included in analyses beyond this section.

HR 4492 is a K giant RS CVn type single-lined spectroscopic binary separated by 0.22 arc s from an eclipsing binary comprising two early A-type stars (Collier 1982). Spectra of HR 4492 obtained at Mt John are clearly dominated by light from the K giant since it is 0.8 magnitude brighter in the visual than the eclipsing binary. The radial velocities obtained of HR 4492 were thus of the K star only and represent its orbital motion with the spectroscopic companion. Using again

the computer program BXT2, a spectroscopic orbit was obtained for the K giant. The computed elements were as follows:

$$P = 61.323 \pm 0.067 \text{ d}$$
$$K = 13.3 \pm 0.3 \text{ km/s}$$
$$e = 0.017 \pm 0.021$$
$$\omega = 143 \pm 30 \text{ degrees}$$
$$T_0 = 8355 \pm 7 \text{ d}$$
$$a \sin i = 11.2 \pm 0.3 \text{ Gm}$$
$$f(M) = 0.0150 \pm 0.0011 \ M_\odot$$

where P is the period, K is the radial-velocity semi-amplitude, e is the orbital eccentricity, ω is the longitude of periastron, T_0 is the Julian day of periastron passage -2440000, a is the semi-major axis, i is the orbital inclination and $f(M)$ is the mass function. The large error in ω and the large error in T_0 relative to the length of the period are a result of the small eccentricity of the orbit which renders its orientation in space somewhat uncertain. No value of the systemic velocity is given because of the relative nature of the recorded velocities.

These elements agree well with those derived by Balona (1987) and are of equal or better precision. However, in Balona's case, the orbit was derived from 55 radial velocities well distributed in phase and each determined with a random error of about 2 km/s, compared to the Mt John case where only 18 spectra were recorded and the phase coverage was poor (spanning only half a cycle). The Mt John case shows the advantage of a smaller radial-velocity error. The calculated orbit and Mt John velocities are plotted modulo orbital phase in Figure 4.14.

4.3.4 ω Sgr

This G5 dwarf was already suspected to be a spectroscopic binary (Hoffleit 1982). An insufficient fraction of the star's orbit (see Figure 4.9) was observed in the Mt John programme in order to be able to derive an orbital solution for the system. Nevertheless, approximate lower limits can be placed on P and K for the system:

$$P \geq 2000 \text{ d}$$
$$K \geq 4 \text{ km/s}.$$

These limits imply a minimum companion mass of around 0.3 $M_\odot$, that is, the companion is a star.

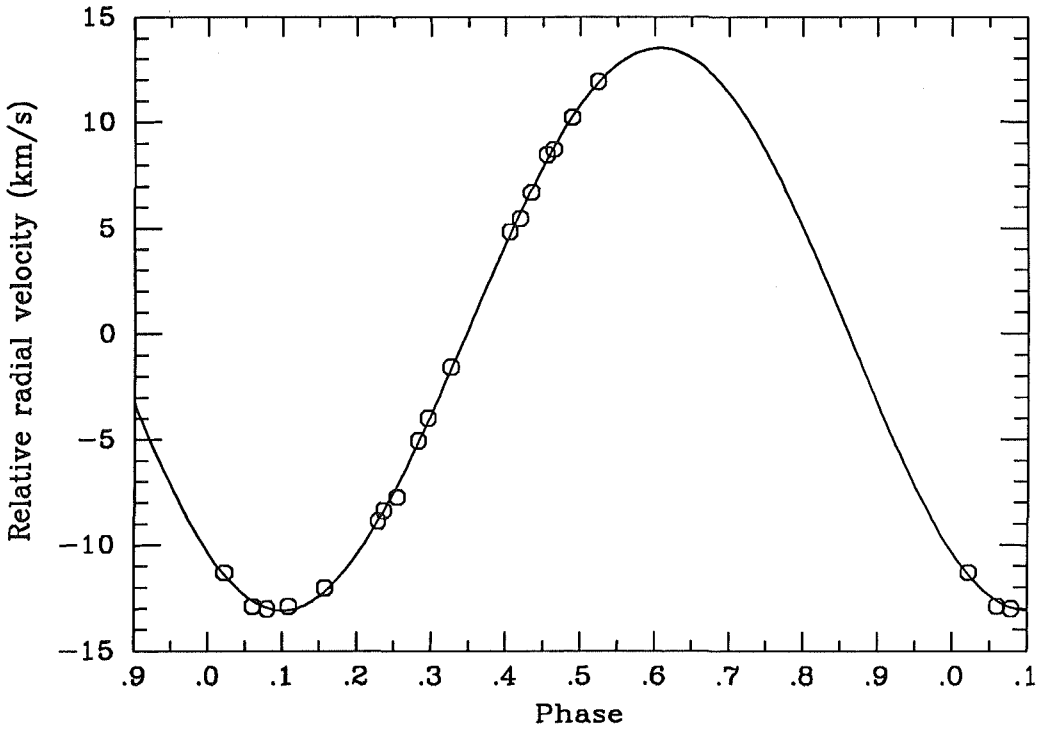

Figure 4.14: Radial velocities and calculated orbit for HR 4492 plotted modulo orbital phase. The period is 61.32 d.

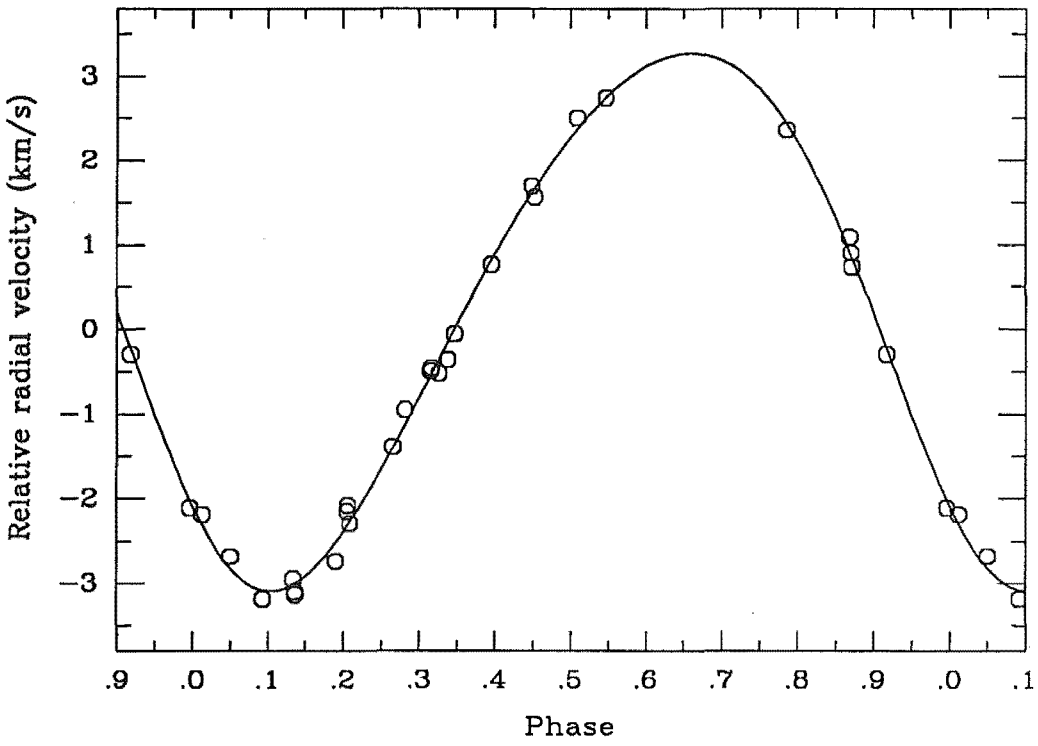

Figure 4.15: Radial velocities and calculated orbit for HR 3220 plotted modulo orbital phase. The period is 901 d.

A best-fit 5th order polynomial was subtracted from the data so that the residuals could be analysed for evidence of a further companion.

4.3.5 HR 3220

HR 3220 is an F5 dwarf star which prior to this programme was thought to be single. Hoffleit (1982) does not even mark this star as a possible radial-velocity variable. In the Mt John programme however, the record of radial velocities for the star (Figure 4.4) quickly revealed that the system is a single-lined spectroscopic binary. Over the course of the programme 29 spectra were obtained over more than one cycle, enabling the computation of an orbit of good quality. This is shown as a phased plot in Figure 4.15. The computed elements are as follows:

$$P = 900.6 \pm 5.3 \text{ d}$$
$$K = 3.18 \pm 0.06 \text{ km/s}$$
$$e = 0.119 \pm 0.012$$
$$\omega = 133 \pm 5 \text{ degrees}$$
$$T_0 = 8136 \pm 19 \text{ d}$$

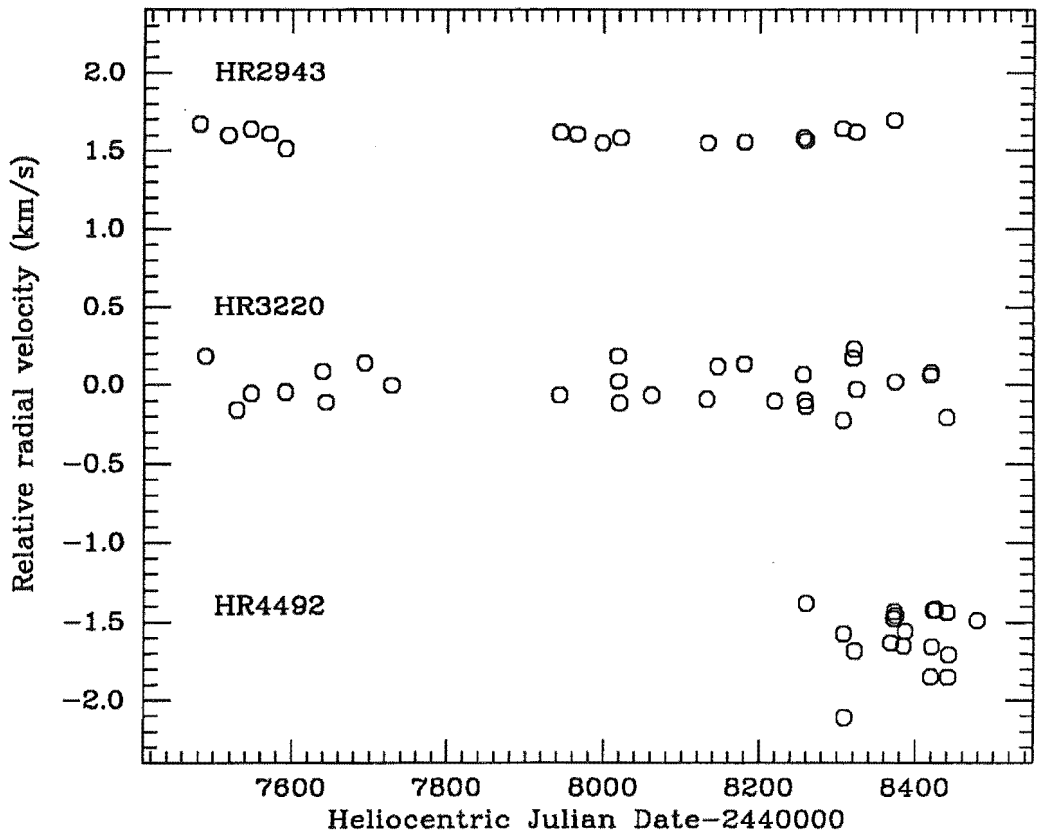

Figure 4.16: Velocity residuals of α CMi, HR 3220 and HR 4492 after subtraction of orbital motion due to their respective stellar companions.

$$a \sin i = 39.1 \pm 0.7 \text{ Gm}$$
$$f(M) = 0.00294 \pm 0.00016 \, M_{\odot}$$

The symbols are as defined in section 4.3.3. Assuming a mass of about 1.4 $M_{\odot}$ for HR 3220, which is of spectral type F5V (Allen 1973), the calculated mass function implies a lower limit to the secondary mass of about 0.20 $M_{\odot}$.

4.3.6 Summary of velocity residuals

Figures 4.16 and 4.17 show the velocity residuals of the six stars in this section after subtraction of the orbital solutions or best-fit slopes described above. It is these residuals, along with the velocities of the other stars in the programme, which will be used to characterize the precision of the system in the next chapter and which will be analysed for smaller amplitude radial velocity variation in

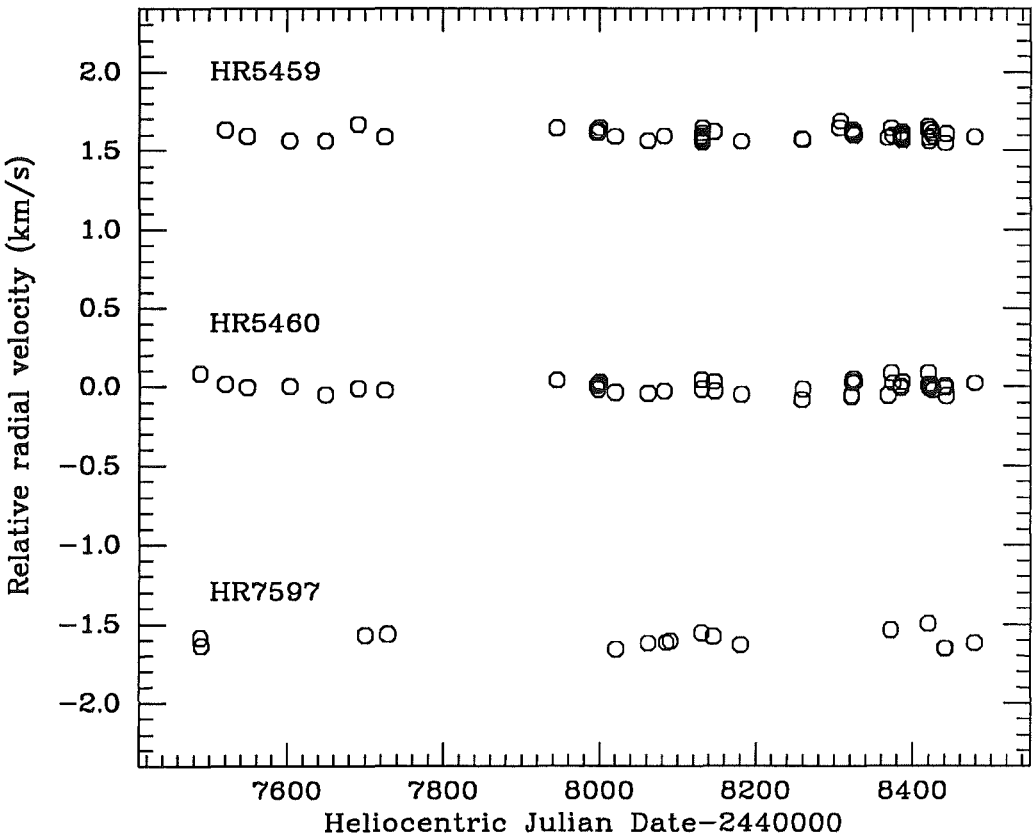

Figure 4.17: Velocity residuals of α Cen A, α Cen B and ω Sgr after subtraction of orbital motion due to their respective stellar companions.

HR	Name	σ_{obs} (m/s)	HR	Name	σ_{obs} (m/s)
77	ζ Tuc	89	4763	γ Cru	381
98	β Hyi	78	4786	β Crv	39
188	β Cet	67	4979		61
370	ν Phe	99	5019	61 Vir	103
911	α Cet	197	5459	α Cen A	32
1008	82 Eri	78	5460	α Cen B	38
1083	κ Ret	179	5777	37 Lib	53
1136	δ Eri	58	6056	δ Oph	132
1674	ζ Dor	115	6102	γ Aps	59
1743	o Col	55	6603	β Oph	46
1829	β Lep	38	6859	δ Sgr	49
1983	γ Lep	75	7597	ω Sgr	46
2906		98	7602	β Aql A	43
2943	α CMi	49	7665	δ Pav	32
3220		124	8181	γ Pav	117
3748	α Hya	106	8232	β Aqr	147
3862		82	8387	ϵ Ind	63
4134		160	8447	τ PsA	318
4523		96	8969	ι Psc	117
4540	β Vir	56			

Table 4.3: Root mean squared scatter σ_{obs} for observations of each star in the Mt John programme.

subsequent sections.

4.4 Observed scatter

In Table 4.3 the observed rms scatter in velocity, σ_{obs}, has been tabulated for each star in the programme. In the cases of α CMi (HR 2943), HR 3220, α Cen A (HR 5459), α Cen B (HR 5460) and ω Sgr (HR 7597), orbital motion due to the companion has been subtracted as described in Section 4.3.

Chapter 5

Performance of the Mt John system

In this chapter the radial-velocity performance of the Mt John system is scrutinized. Initially the possible sources of error in the system are considered and then the magnitude and principal sources of error are identified from observation of the observed scatter in the radial velocities of stars in the Mt John programme.

5.1 Possible sources of error

The random error in the measurement of a radial velocity in the Mt John programme, ϵ_v, results from the uncertainty in the determination of the zero point of the dispersion solution $\epsilon_{\rm disp}$, the uncertainty in the determination of the run correction $\epsilon_{\rm run}$, perturbations from instrumental effects $\epsilon_{\rm instr}$, the uncertainty in the barycentric correction $\epsilon_{\rm bc}$ and the uncertainty from spectral noise $\epsilon_{\rm p}$. If these sources of uncertainty are independent and normally distributed and the various ϵ represent the standard deviations of the noise Gaussians then ϵ_v is given by

$$\epsilon_v^2 = \epsilon_{\rm p}^2 + \epsilon_{\rm disp}^2 + \epsilon_{\rm run}^2 + \epsilon_{\rm instr}^2 + \epsilon_{\rm bc}^2 \ .$$

The nature and probable magnitude of these contributing error sources are now discussed individually.

5.1.1 Error from spectral noise, ϵ_p

The source of this error was discussed in more detail in Chapter 2. During most of the Mt John programme, the aim was to record spectra with a signal-to-noise ratio of 30:1 in order to expose for the minimum time and yet have a spectral-noise limited radial-velocity error of only about $\epsilon_p \approx 15$ m/s. Accurate calculation of the implied spectral-noise limited error for real exposures during the observing runs in 1991 March and April showed that ϵ_p was at most 10 m/s even for the broader lined stars, probably because observers tended to err on the side of obtaining a higher signal-to-noise than the target of 30:1, often recording spectra with a signal-to-noise ratio as high as 100:1.

5.1.2 Error in the dispersion solution, ϵ_{disp}

The dispersion polynomial,

$$n = a_0 + a_1\lambda + a_2\lambda^2 \ ,$$

relates the pixel number n to the central wavelength λ of that pixel. Of the coefficients a_0, a_1 and a_2, the most important for high-precision radial velocities is a_0. This term quantifies the zero point of the stellar spectrum on the array and is therefore crucial in determining the position of the cross-correlation function peak and ultimately, the stellar relative radial velocity. Random error in a_0 will translate into a random error in the measured velocity. In contrast, errors in higher-order coefficients will merely broaden the cross-correlation function — a much smaller, second-order effect in decreasing the precision.

In the Mt John system, the dispersion polynomial is obtained by first least-squares fitting Gaussian functions to the 14 individual Th-Ar reference emission spectrum lines to obtain their positions and then chi-squared fitting those line positions against the known line wavelengths. The source of random error in this process is the photon noise in the Th-Ar spectrum, which translates into uncertainty in the line positions.

The precision with which the position of each Th-Ar emission line is determined depends on the strength of the line. The quadratic weighting favours the stronger lines which have better-defined positions so that although some line positions are determined to a precision of only ± 300 m/s, the precision with which a_0 is determined from two comparison spectra corresponds typically to about ± 8 m/s.

5.1.3 Error in run zero point, $\epsilon_{\rm run}$

The need for a run correction to be applied to the Mt John velocities, as described in Chapter 3, implies that the instrumental set-up for each run induces a systematic error into the radial velocities of that run.

The most likely variation in the run-to-run set-up of the system that could plausibly affect the relative radial velocities is the way the fibre end is imaged relative to the spectrograph slit. The fibre end is interfaced to the spectrograph by a plate attached by three sets of antagonistic screws. The placement of the fibre-end image on the slit is adjusted by the 'tweaking' of these screws so that the image is apparently centred on the slit, as judged by the appearance of the fibre end image reflected off the slit jaws into the slit viewing microscope. In practice however, the position of the fibre-end image on the slit will not be symmetrical because of the difficulty of fine adjustment of the screws and because the placement is done by eye. The asymmetry of the placement across the width of the slit will be different from run to run. The effect on the spectra in a run will be a characteristic asymmetry in the instrumental profile and therefore in the line profiles as well. Since in the Mt John system of obtaining relative radial velocities, spectra are cross correlated with a spectrum obtained at an earlier epoch, in general the cross correlations of spectra from a given run involve spectra of two different asymmetries. The result will be asymmetrical cross-correlation peaks and a systematic radial-velocity error for velocities in the run because of the fitting of symmetrical Gaussian functions to the peaks to obtain the velocities.

A more subtle effect that may also contribute to the difference between run zero points is that of uneven radial distribution of light at the fibre output end. Barden (1988) notes the near-'perfect' azimuthal scrambling of light at the output end of a fibre, but the poorer radial scrambling. For example, an off-axis spot of light at the input end may appear as a ring of light at the output end. This may introduce zonal errors in the spectrograph which have a characteristic effect from run to run.

This systematic error for velocities in a given run is in part corrected for by determining the mean value of the radial velocities of presumed constant radial-velocity stars, as described in Chapter 3. The value of the systematic error for each run is determined with a random error, which over all the runs translates into a pseudo-random error contribution $\epsilon_{\rm run}$ to ϵ_v. On average, 10 velocities are used to establish the zero point for each run. From the scatter in these velocities

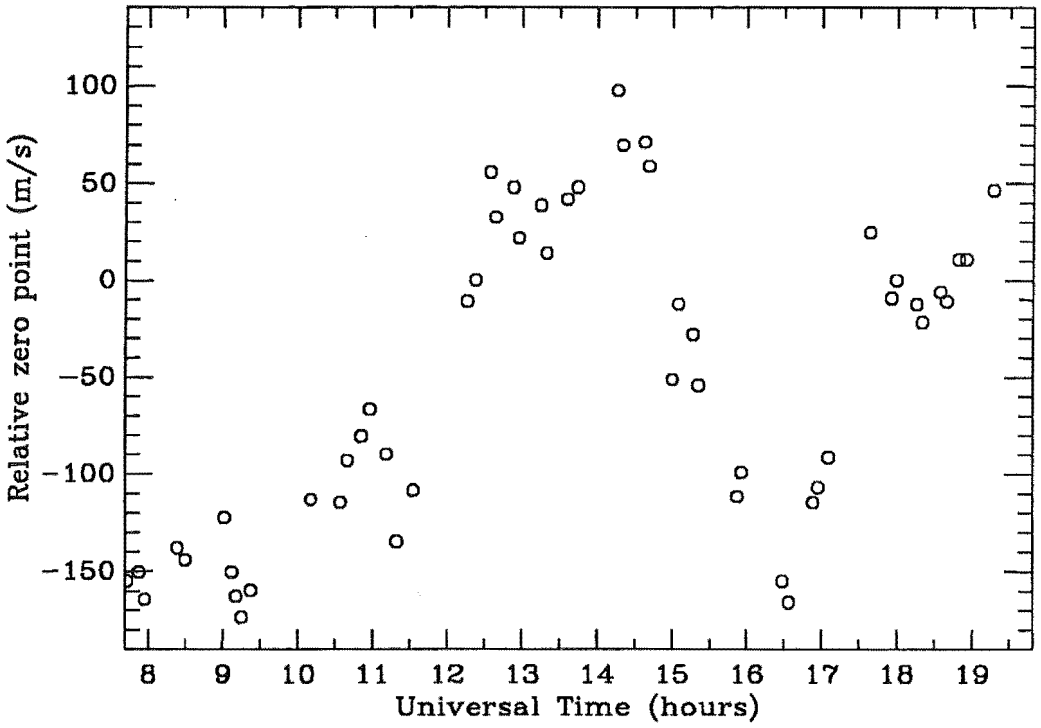

Figure 5.1: Drifts in the zero point of the Mt John system during a night (3/7/91).

about the implied run correction (mean value of these velocities) it is found that the mean error in the run correction ϵ_{run} is about 17 m/s.

5.1.4 Errors from instrumental sources, ϵ_{instr}

Although the idea of the optical fibre feed is to reduce the errors from the instrumental sources outlined in Chapter 1, some still exist and contribute to the uncertainty in the determination of radial velocities. These are mainly thermal and barometric changes which cause shifts in the zero point of the system. Figure 5.1 illustrates the drift in the Mt John system zero point during a night where the zero-point variations were fairly extreme. The figure plots the shift (as determined by cross correlation) between Th-Ar spectra obtained throughout the night and a single Th-Ar spectrum taken on the same night. The extent to which this drifting zero point causes an instrumental radial-velocity error ϵ_{instr} depends on the ability of the mean dispersion solution, obtained from the Th-Ar reference spectra exposed before and after each stellar spectrum, to represent the actual changing dispersion solution throughout the stellar exposure. The magnitude of ϵ_{instr} is therefore expected to be somewhat dependent on the exposure

time, since one might expect a linear interpolation between dispersion solutions to be a good approximation over short exposures, but a poorer one over longer exposures, especially if the sky transparency or extinction was changing during the exposure.

Air pressure and air temperature stability

As demonstrated by Innis, Isaak & Isaak (1990), atmospheric pressure or temperature changes cause a change in the refractive index of the air and thus a corresponding change in the wave speed and hence wavelength of light. This will lead to a shift in the positions of spectral lines on the detector.

Gray (1972) gives the formula for the dependence of the refractive index of air n on temperature in degrees Celsius T and pressure P in mm Hg as

$$n_{T,P} - 1 = (n_{15,760} - 1)\frac{P}{760}\frac{(1 + P\beta_T)}{(1 + 760\beta_{15})}\frac{(1 + 15\alpha)}{(1 + T\alpha)}$$

where $\alpha = 0.00366$, $\beta_T = (1.049 - 0.0157T)\,10^{-6}$. Using this formula, the effect of a moderate pressure change at an atmospheric pressure of one atmosphere and 24°C (the approximate operating pressure and temperature of the Mt John spectrograph) can be calculated. Using the fact that $n\lambda$ is constant when n changes, for the 5010 Å wavelength region in the Mt John programme it turns out that an increase in pressure of 1 millibar (≈ 0.75 mm Hg) mimics a velocity shift of about -80 m/s.

Similarly, one can calculate the effect of a change in the air's refractive index from a moderate change in temperature. It turns out that at a constant atmospheric pressure of one atmosphere an increase in temperature from 24°C to 25°C mimics a velocity shift of about +270 m/s. Both the temperature-induced shift and the pressure-induced shift are approximately constant over a short length of spectrum so that the net effect for the Mt John programme in both cases is an overall linear shift of the spectrum on the detector.

Spectrograph temperature stability

Temperature drifts may also cause expansion or contraction of the components in the échelle spectrograph. The most likely origin of a shift in the zero point of the Mt John system from this effect is a change in the tilt of the échelle grating. One side of the grating is attached to the aluminium body of the spectrograph by an aluminium bracket while the opposite side is supported by a steel micrometer

which allows adjustment of the grating's tilt. The thermal expansion coefficients of the two metals are markedly different so that the effect of heating or cooling of the spectrograph is a change in the échelle tilt and a subsequent linear shift of the spectrum on the detector. The effect is a shift of about 2000 m/s/C°.

A further effect is that of the thermal expansion and contraction of the échelle grating itself. This will change the groove spacing, therefore also changing the dispersion.

5.1.5 Error in barycentric correction, $\epsilon_{\rm bc}$

The *maximum* absolute error in the barycentric correction (see Chapter 3) was calculated to be 6 m/s over the duration of the Mt John programme. The *random* error in the barycentric correction is only about ±4 m/s.

Consideration must also be made, however, of the fact that in the Mt John programme the barycentric correction is calculated for the mid-time of the stellar exposure, rather than the flux-weighted mid-time of the exposure. The two times may be different by a few minutes for rising or setting stars (due to extinction changes) or if observing is done through patchy cloud. For the most part, the mid-exposure time was expected to be within 5 minutes of the mean exposure time. Over this time scale it is the component in the direction to the star of the earth's motion due to rotation that changes the fastest. This is given by

$$v_{\rm rot} = 465 \cos\delta \sin H \cos\phi \qquad \text{m/s},$$

where δ is the star's declination, H is the hour angle and ϕ is the observer's latitude. At Mt John $\cos\phi \approx 1/\sqrt{2}$, so the rate of change of barycentric correction is $\partial v_{\rm rot}/\partial H = 329 \cos\delta \cos H$ m/s^2.

Considering the worst case at Mt John of an equatorial star at meridian passage with an error in the flux-weighted mean exposure time of 5 minutes (a change in hour angle $\delta H = \frac{2\pi}{12\times 24}$ radians), then the error in the barycentric correction would be

$$\begin{aligned} \epsilon_{\rm bc} &= \frac{\partial v_{\rm rot}}{\partial H}\delta H \\ &= 329\cos(0)\cos\left(\frac{2\pi}{288}\right)\frac{2\pi}{288} \\ &\approx 7 \quad \text{m/s} \ . \end{aligned}$$

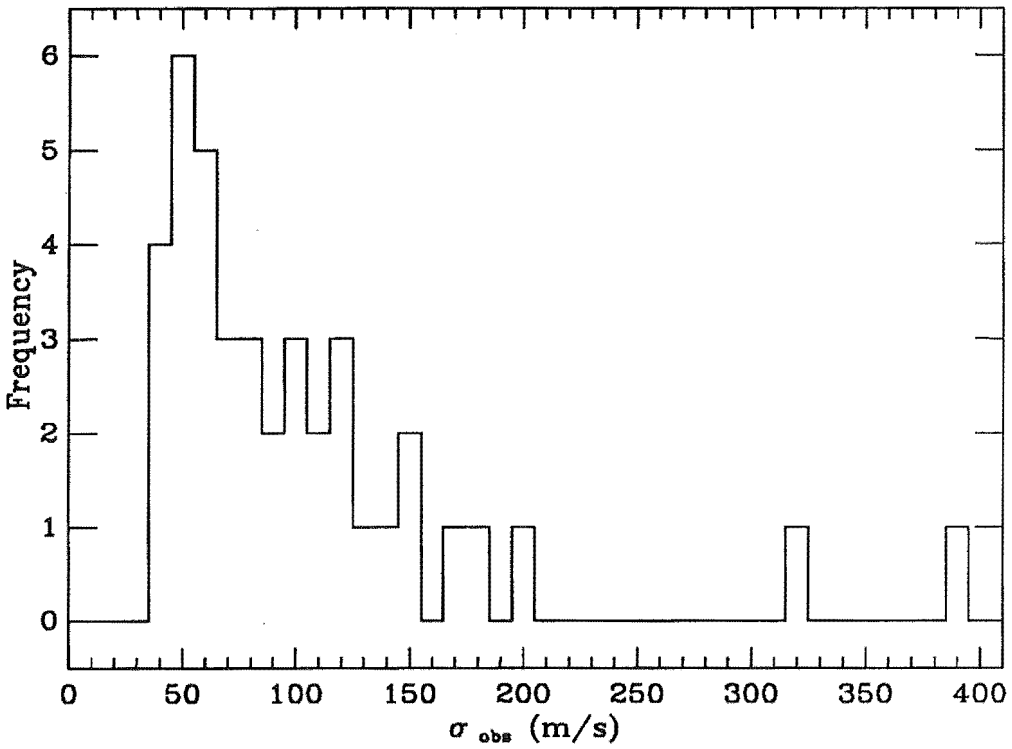

Figure 5.2: Histogram showing the distribution of root-mean-squared scatters of the velocities in the Mt John programme.

This is certainly a worst-case error, especially since about two-thirds of the stars in the Mt John programme are circumpolar. Estimating the random error from this source as ±5 m/s, the total error in the barycentric correction is still only $\epsilon_{bc} = \sqrt{4^2 + 5^2} = 6$ m/s.

5.2 Observed errors

5.2.1 Main features

In order to get an initial look at the behaviour of the Mt John system, a histogram is displayed in Figure 5.2 which shows the distribution of observed root-mean-squared (rms) scatters of the velocities σ_{obs} for all the stars (including variables) in the Mt John programme. The values of σ_{obs} were listed in Table 4.3.

The main features of the distribution are a peak at 55 m/s, a distinct lower bound at around 40 m/s and an irregular trailing off towards larger rms scatters. The majority of stars have small scatters, which is to be expected if these are intrinsically non-variable to a few metres per second and the observed scatter is

due entirely to the finite precision of the system. The stars towards the right of the histogram are possibly variable or are less precisely observed for some reason. The lower bound represents the best performance of the system — a random error of around ±40 m/s. Because of the position of the peak, a more typical radial-velocity error for the system might be described as being about ±55 m/s.

5.2.2 Actual sources of error

In no case is the observed rms scatter of radial velocities for a star in the Mt John programme below around 40 m/s over the 2.5 years of the observing programme. This immediately eliminates $\epsilon_{\rm p}$, $\epsilon_{\rm disp}$ and $\epsilon_{\rm bc}$ as major contributors to ϵ_v, since their total contribution to the overall error is only about $\sqrt{10^2+8^2+6^2} = 14$ m/s. Thus

$$\epsilon_v^2 \approx \epsilon_{\rm run}^2 + \epsilon_{\rm instr}^2 \ .$$

If the $\epsilon_{\rm run}$ is the major contributor then one expects to see radial-velocity errors independent of exposure time. If $\epsilon_{\rm instr}$ is the major contributor, then one expects to see a dependence on exposure time.

In order to see if there is some exposure-time dependence of the precision of the determination of a radial velocity, Figure 5.3 shows the rms scatters over the 2.5 year duration of the programme of all the stars plotted against stellar magnitude. Since spectra of all stars were recorded with about the same signal-to-noise ratio, dependences on exposure time should be apparent in this figure. Although Figure 5.3 is no doubt confused by the presence of stars with variable radial velocity, again a distinct lower bound in rms scatter is obvious. The points bounding the lower part of the figure can most plausibly be explained as being for those stars which are intrinsically non-variable. It is apparent that the smaller rms scatters in velocity occur mainly for the brighter stars ($V < 4$) while the fainter stars may show larger rms scatters, suggesting that there is some exposure-time dependence of the radial-velocity precision. On the other hand, the brightest stars (α Cen A, α Cen B, α CMi and γ Cru) were usually observed with exposures of 10 minutes or less. $\epsilon_{\rm instr}$ for these stars is expected to be negligible. It is surmised that $\epsilon_{\rm run}$ is the dominant source of error for brighter stars.

In order to verify that run corrections are the source of the error in radial velocity for bright stars, the rms scatter of velocities of α Cen A, α Cen B and γ Cru obtained within a single run were calculated. These velocities should be

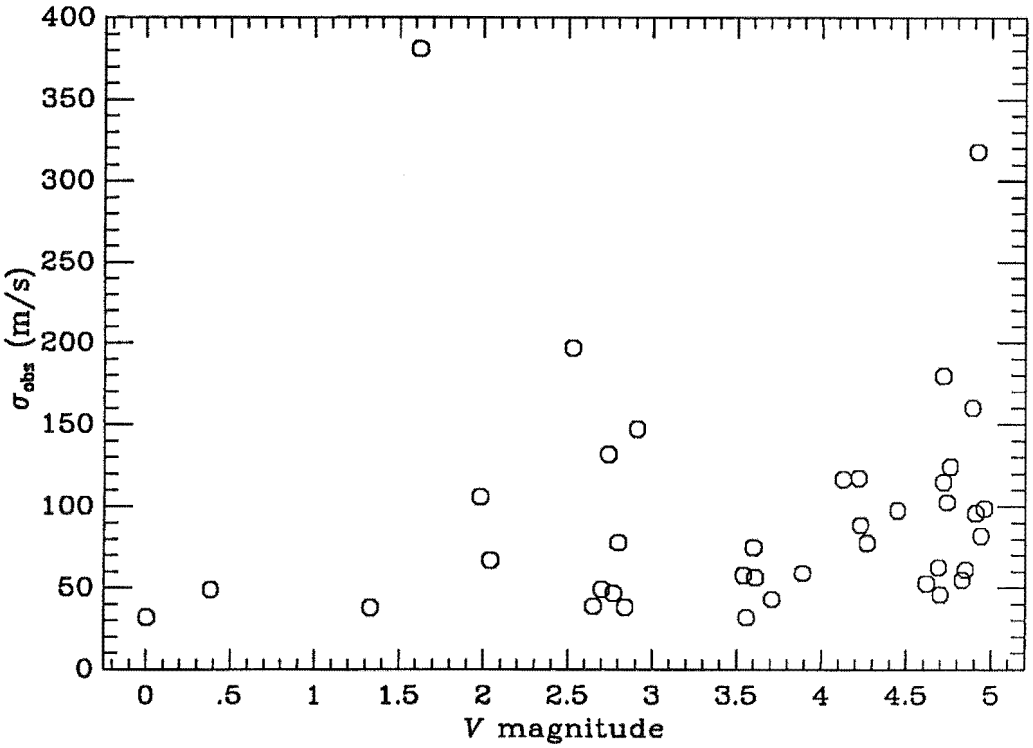

Figure 5.3: Root-mean-squared scatters of the stars over the duration of the Mt John programme plotted against V magnitude.

Star name	Range in HJD -2440000	Number of observations	Rms scatter (m/s)
α Cen A	8130.83–8131.85*	9	16
	8323.13–8325.95	6	13
α Cen B	8323.14–8325.96	6	10
γ Cru	8324.89–8325.14	4	15

*The six further observations obtained on HJD 2448131 were not included as spectrograph settings were being altered as a test.

Table 5.1: Root-mean-squared scatter of velocities of the brightest stars obtained over small time scales.

immune to run correction errors and are displayed in Table 5.1. During no run was α CMi observed many times so it is not included here, and, as will be seen in the next chapter, γ Cru is variable and so the night analysed for that star was chosen as one where the apparent rate of change of velocity was small.
From just these four examples, it seems likely that the radial-velocity error for the system for bright stars and short time-scales is a mere 15 m/s. This is of the order expected if the only sources of error are $\epsilon_{\rm p}$, $\epsilon_{\rm disp}$ and $\epsilon_{\rm bc}$. The only explanation for the increase in radial-velocity error for bright stars to about 35–40 m/s over longer time-scales is that run corrections must be applied. Although $\epsilon_{\rm run}$ was estimated to be about 17 m/s, it must be actually closer to 26 m/s to account for the observed scatter in velocity.

5.3 Systematic errors

The aim of the Mt John programme was the detection of *changes* in stellar radial velocities, however some effort was made in Chapter 4 to determine absolute radial velocities of the stars, for the convenience of other researchers who might like to use the Mt John programme velocities for their own purposes. In programmes which are specifically designed to determine absolute radial velocities, it is important to characterize the systematic errors, which include the zero point of the system (determined through observations of radial-velocity standard stars, observations of asteroids or perhaps the sun) and any spectral-type dependence of the radial velocities. Because of the Mt John programme's emphasis on relative radial velocities, no measure was made of the absolute zero point of the system.

However in the course of the Mt John programme some note was made of a systematic error dependent on spectral type. Although this error is unimportant to the scientific programme in this thesis, it is relevant to the interpretation of the corrections to absolute velocities listed in Chapter 4 and thus is discussed briefly here.

In the Mt John programme, each spectrum was cross correlated with a template spectrum of the same star. However, in the case of the α Cen binary system, whenever both components were always observed in immediate succession, the spectrum of the A component was also cross correlated with the spectrum of the B component obtained at the same epoch. In this way a record of the difference in velocity between the two components of the system was obtained. However, these velocities appeared to be about 160 m/s greater than expected from the published elements of the rather well-defined astrometric orbit (Heintz 1982). A systematic error was suspected, due to the cross correlation of a G2V type spectrum with a K1V spectrum.

Among the radial velocity standard stars in the programme are four of early G spectral type (G0 – G5 and thus very similar to α Cen A) and three of early K spectral type (K2 – K3 and thus very similar to α Cen B). Using the set of template spectra for the G- and K- type radial velocity standard stars, a simple test was carried out to investigate the possibility of a spectral type dependence of the radial velocities. The G-type standard templates in the programme were cross correlated with each other in all possible combinations. Similar cross correlations were performed among the three K type templates. Using the published IAU radial velocities for these stars, the predicted values of the radial-velocity differences between the stars were compared to the values obtained from the cross correlations. Small adjustments were made to give self-consistent absolute velocities for each star in the Mt John system. Using these modified IAU radial velocities, a prediction was made of the result of cross correlating the K stars with the G stars in all possible combinations. On comparing these values with the velocities obtained from cross correlating the G stars with the K stars it was found that in every case, the velocity of the K star minus that of the G star was between 100 m/s and 200 m/s more positive than predicted. This is of the correct sign and about the same magnitude as the effect suggested in the α Cen case. It was concluded that a spectral-type dependent systematic error in radial velocity differences probably exists in the Mt John system.

It was observed that in all cases where an early G-type star was cross correlated with an early K-type star, the cross-correlation function appeared to the eye as asymmetrical in the side-lobes compared to a cross-correlation function obtained from spectra of identical spectral type. Presumably this asymmetry exists also in the main peak itself and hence the fitting of a symmetric (in this case, Gaussian) function to the peak necessarily results in a systematic error in the centroid position.

Chapter 6

Tests for radial-velocity variability

This chapter is concerned with the detection of variations in the radial velocities of the stars in the Mt John programme. Firstly, a value of the random error in velocity for each star is adopted. This enables the overall scatter of the radial-velocity observations for each star to be scrutinized using the F-test to see if some portion of the scatter is likely to be due to some real variation. Then the power spectrum of the velocities of each star is examined for significant peaks representative of real periodic signals in the data. Finally, in order to improve detectability of longer-period orbits, the velocities of each star are examined for a significant slope or curvature with time.

6.1 F-test

The F-test determines whether or not the variances of two distributions are significantly different. F_0 is the ratio of the two variances such that $F_0 > 1$ and is associated with a probability $P(F > F_0)$ that one would observe F to be of magnitude F_0 or larger given the number of samples in each distribution and based on the null hypothesis that the variances are equal but F_0, the ratio of the estimates of the variances, was the observed value by chance. If the probability $P(F > F_0)$ is large then the variances can be said to be statistically indistinguishable. If the probability is below a set threshold level then the variances are statistically different.

6.1.1 Application to the Mt John velocities

In the context of determining whether or not a star in the Mt John programme is variable in radial velocity, it is required to be known whether the observed variance $\sigma^2_{\rm obs}$ of the velocities of each star is significantly different to the variance ϵ^2_v defined by the presumed random error in radial velocity. F_0 is defined in this case as:

$$\begin{aligned} F_0 &= \frac{\sigma^2_{\rm obs}}{\epsilon^2_v} \text{ if } \sigma_{\rm obs} > \epsilon_v \\ \text{or} \quad F_0 &= \frac{\epsilon^2_v}{\sigma^2_{\rm obs}} \text{ if } \sigma_{\rm obs} < \epsilon_v \ . \end{aligned}$$

If $\sigma_{\rm obs} > \epsilon_v$ then a small value of $P(F > F_0)$, say $P(F > F_0) < 0.01$, implies that the variance of the observations $\sigma_{\rm obs}$ is too large to have arisen from an underlying distribution of variance ϵ^2_v, and the star is a candidate radial-velocity variable.

In the Mt John system the value of ϵ_v for each star is not known *a priori* but it *is* known (see Chapter 5) that it arises principally from a constant error from the run corrections $\epsilon_{\rm run}$ and an instrumental error dependent on exposure time $\epsilon_{\rm instr}$. It is assumed here that $\epsilon_{\rm instr}$ is proportional to the square root of the exposure time. In this case it may be expressed as

$$\begin{aligned} \epsilon_{\rm instr} &\propto \sqrt{t} \\ &= \alpha\sqrt{10^{\frac{m}{2.5}}} \ , \end{aligned}$$

where t is the exposure time and m is the magnitude of the star in the bandwidth of observation[1], since $10^{\frac{m}{2.5}}$ is proportional to the exposure time. The functional form of ϵ_v is then known and it may be written as

$$\begin{aligned} \epsilon^2_v &= \epsilon^2_{\rm run} + \epsilon^2_{\rm instr} \\ &= \epsilon^2_{\rm run} + \alpha^2 10^{\frac{m}{2.5}} \ . \end{aligned}$$

ϵ_v will therefore be known if $\epsilon_{\rm run}$ and α can be determined. Since for non-variable stars, on average $\sigma_{\rm obs} = \epsilon_v$, $\epsilon_{\rm run}$ and α could be found empirically by fitting the relationship

$$\sigma^2_{\rm obs} = \epsilon^2_{\rm run} + \alpha^2 10^{\frac{m}{2.5}} \tag{6.1}$$

to the points corresponding to non-variable stars in Figure 5.3. Although the points forming a lower bound in Figure 5.3 probably correspond to non-variable

[1] V magnitude is close enough for the Mt John system.

stars, it is unclear exactly which points should be included in the fit and which should not be. Indeed there is danger in selecting the points, since if variables are included then the fitted ϵ_v will be too large and the F-test will interpret the $\sigma_{\rm obs}$ of many stars as being improbably low. On the other hand if some of the non-variable stars with higher values of $\sigma_{\rm obs}$ are excluded then the value of the fitted ϵ_v will be too low and the F-test will interpret the $\sigma_{\rm obs}$ of too many stars as being improbably high (that is, the F-test will predict too many variables). A situation between these two extremes is required and this will be the case where the smallest number of stars have low F-test probabilities. The following procedure was executed:

1. Fit Equation 6.1 to the ($\sigma_{\rm obs}$,m) database for all the stars in order to determine $\epsilon_{\rm run}$ and α and hence ϵ_v.
2. Apply F-test and isolate star with lowest $P(F > F_0)$ because of large $\sigma_{\rm obs}$.
3. Discard the star identified in Item 2 from the ($\sigma_{\rm obs}$,m) database and repeat from Item 1.

The best-fit ϵ_v was deemed to be the case where there were the minimum number of stars with $P(F > F_0) < 0.01$.

The final fitted ϵ_v was calculated to be

$$\epsilon_v = \sqrt{38^2 + 8^2 10^{\frac{m}{2.5}}} \text{ m/s} .$$

This relationship is plotted in Figure 6.1. The implied values of $P(F > F_0)$ for each star are listed in Table 6.1, which shows that fourteen stars had $P(F > F_0) < 0.01$. Since there is no physical explanation for a star with an improbably *low* velocity scatter ($\sigma_{\rm obs} < \epsilon_v$ and $P(F > F_0) < 0.01$), it was expected that all of the stars with $P(F > F_0) < 0.01$ would have improbably high values of $\sigma_{\rm obs}$. In fact, one star (δ Pav — HR 7665) did have an improbably small value of $\sigma_{\rm obs}$. However since this was only marginally improbable ($P(F > F_0) = 0.0018$), this single anomaly was ignored. The remaining thirteen stars were found by this process to be candidate radial-velocity variables, although marginally so in the cases of HR 188 (β Cet) and HR 8969 (ι Psc). It is interesting to note that the most convincing variables identified by the F-test are giant or supergiant radial-velocity 'standard' stars HR 911 (α Cet), HR 3748 (α Hya), HR 4763 (γ Cru), HR 6056 (δ Oph) and HR 8232 (β Aqr).

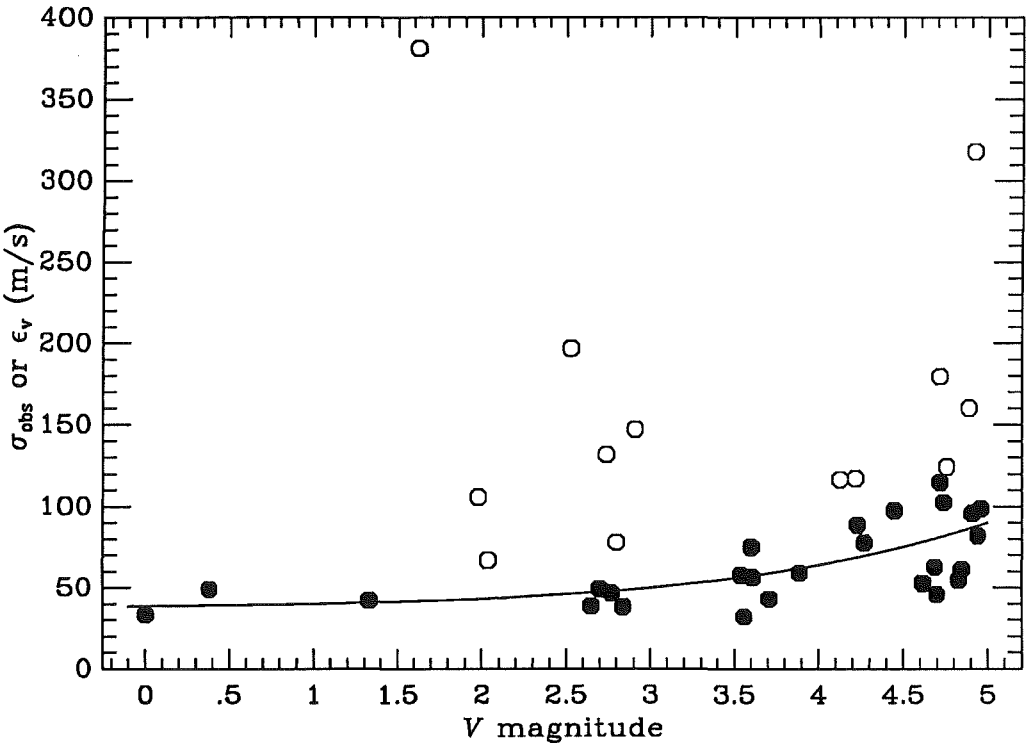

Figure 6.1: Fitted radial-velocity error ϵ_v as a function of stellar V magnitude (solid line). The solid dots are the σ_{obs} values of stars used in the fit. The open dots are σ_{obs} values of stars not used in the fit.

F-test probabilities	
Star	$P(F > F_0)$
HR 77	5.219×10^{-2}
HR 98*	1.780×10^{-5}
HR 188*	2.829×10^{-3}
HR 370	5.231×10^{-1}
HR 911*	infinitesimal
HR 1008	4.514×10^{-1}
HR 1083*	3.623×10^{-11}
HR 1136	7.962×10^{-1}
HR 1674	2.008×10^{-2}
HR 1743	7.214×10^{-2}
HR 1829	6.363×10^{-2}
HR 1983	1.154×10^{-1}
HR 2906	6.471×10^{-2}
HR 2943	1.539×10^{-1}
HR 3220*	2.753×10^{-4}
HR 3748*	4.620×10^{-31}
HR 3862	7.735×10^{-1}
HR 4134*	3.459×10^{-7}
HR 4523	4.780×10^{-1}
HR 4540	9.580×10^{-1}
HR 4763*	infinitesimal
HR 4786	1.844×10^{-1}
HR 4979	7.361×10^{-2}
HR 5019	1.061×10^{-1}
HR 5459	5.066×10^{-2}
HR 5460	4.896×10^{-2}
HR 5777	5.428×10^{-2}
HR 6056*	3.330×10^{-38}
HR 6102	8.103×10^{-1}
HR 6603	9.461×10^{-1}
HR 6859	7.405×10^{-1}
HR 7597	1.262×10^{-2}
HR 7602	1.222×10^{-1}
HR 7665†	1.781×10^{-3}
HR 8181*	1.512×10^{-5}
HR 8232*	2.042×10^{-37}
HR 8387	2.775×10^{-1}
HR 8447*	1.695×10^{-25}
HR 8969*	2.205×10^{-3}

*Variable by this test. †See note in text.

Table 6.1: Probabilities $P(F > F_0)$ that the rms scatter $\sigma_{\rm obs}$ of the radial velocities of stars in the Mt John programme could be as large as observed, if the radial-velocity error is $\epsilon_v = \sqrt{38^2 + 8^2 10^{\frac{m}{2.5}}}$ and the scatter in the data is due to noise only.

6.1.2 Sensitivity

In order to assess the sensitivity of the F-test method to the detection of low-mass companions to the stars in the survey, a series of simulations was performed. Considering the case of a 1 $M_{\odot}$ primary star, an average orbital inclination ($< \sin i >= \pi/4$ — see Gray 1976) and circular orbits, radial-velocity curves were generated for a range of periods and companion masses, including an additive Gaussian noise term of 65 m/s (the mean external radial-velocity error for stars in this programme). Each orbit was assigned a random phase and was sampled at 25 epochs which corresponded to the times of the observing runs in the Mt John radial-velocity programme. For each grid point corresponding to a single period P and companion mass M_2, 100 orbits were calculated, the difference between them being due to the random phases and the random noise.

For each orbit F and $P(F > F_0)$ were calculated. If, for a particular grid point, $P(F > F_0)$ was less than 0.01 for more than 95 per cent of the trials, that particular (P, M_2) was considered 'detectable' by this method. In this manner, the area on the P-M_2 plane detectable by the F-test was determined and is shown in Figure 6.2.

6.2 Power spectra

In order to test for embedded periodicities, one can investigate the data in the frequency domain via a Fourier technique. Significant power at a particular frequency in a power spectrum may indicate a signal at that frequency.

Power spectra (periodograms) are usually obtained via some kind of FFT (fast Fourier transform) algorithm. The problem when the data are unevenly sampled is that FFT methods require the data to be evenly spaced. Compensation by interpolation or some other means distorts the information in the power spectrum. In addition, in order to assess the significance of peaks in the power spectrum, a false-alarm criterion is required. FFT methods do not provide this.

The method of Lomb (1976) and Scargle (1982) addresses both of these issues. Specifically developed for the search for weak signals in unevenly spaced data, the method involves calculation of the power spectrum only at the times of observation. Furthermore, the power spectrum is normalized by the variance of the noise in the data ϵ^2, allowing the height of a peak to be assigned to a probability that it could have arisen from a spectrum of pure noise ϵ. More specifically, if

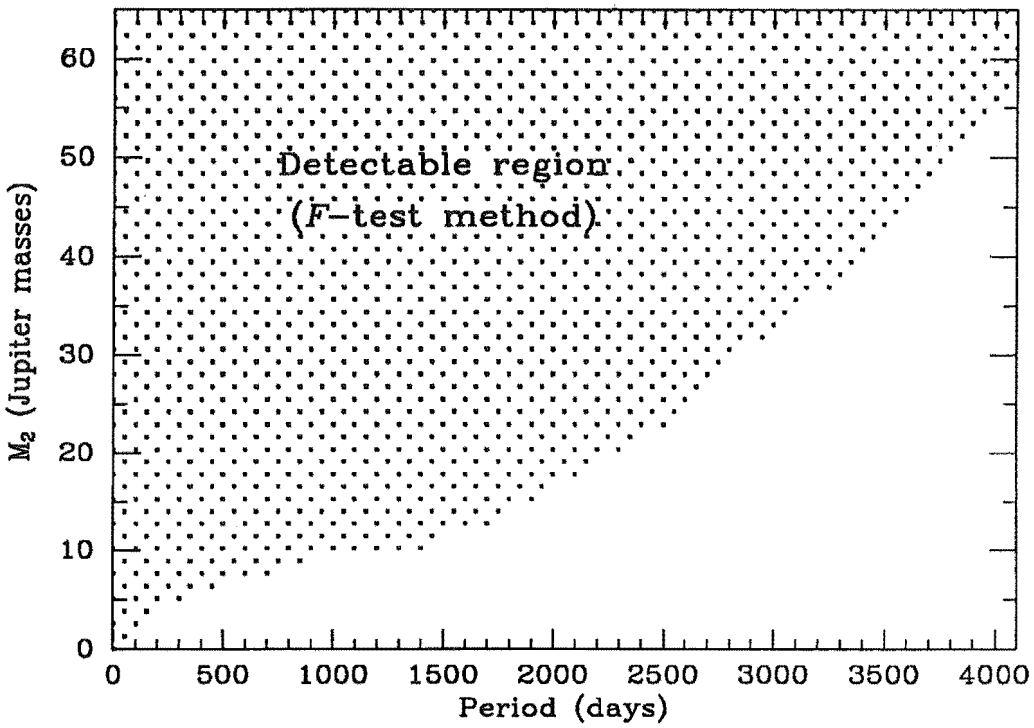

Figure 6.2: Region of detectability of low-mass companions by the F-test method, assuming circular orbits, a primary star of 1 $M_\odot$, an average orbital inclination ($\sin i = \pi/4$) and Gaussian noise of 65 m/s.

M independent frequencies are scanned in a power spectrum of white noise, the probability that a peak will have a height of z or greater is

$$P(> z) = 1 - (1 - e^{-z})^M \ .$$

A low 'false-alarm' probability (say below 0.01) indicates only a small chance that the peak arises by chance from noise.

The two variables affecting the value of the false-alarm probability are the power spectrum signal-to-noise ratio z and the number of independent frequencies M. It turns out that the false-alarm probability is rather insensitive to M, when it is considered that a fairly large error in $P(> z)$ can be tolerated, given the practical difference between the probabilities of significant and insignificant signals (see Press & Teukolsky 1988). Some researchers employ numerical simulations to determine M for their data, but a general rule is that if the sampling is up to the mean Nyquist frequency of the data set (that is, the Nyquist frequency were the data evenly spaced), then the number of independent frequencies M is about equal to the number of data points N. M will increase in proportion to the number of times greater than the mean Nyquist frequency the sampling is up to[2], and will decrease in proportion to the clumping of the data in time (*e.g.* will decrease by a factor of two if the sampling is in clumps of two). These approximations are discussed in more detail by Press & Teukolsky (1988).

The power signal-to-noise ratio of the peak z is defined (Scargle 1982) as

$$z = \frac{N}{4}\left(\frac{x}{\epsilon}\right)^2 \ ,$$

where N is the number of samples in the data set, x is the signal amplitude and ϵ is the noise level[3]. The value of z, and also the value of $P(> z)$, is very sensitive to the noise value ϵ used in the normalization, since ϵ appears as a squared quantity. A correct estimate of the false-alarm probability therefore rests on a correct assessment of the noise level.

If there exists a good *a priori* knowledge of the noise in the data then the false-alarm probability may be calculated with some confidence. However, this

[2]In the case of non-equally spaced data, information can be obtained up to the Nyquist frequency defined by the smallest time spacing between two successive data points.

[3]A sub-culture of a defining z as $z = (x/\epsilon)^2$ has arisen in the literature (see for example Martinez 1989; Kurtz & Marang 1987). This definition is clearly in error. Qualitatively, the $N/4$ factor in the definition of z describes the fact that the significance of a peak at a given amplitude signal-to-noise ratio of x/ϵ will be greater for a greater number of data points. Omitting the $N/4$ factor will result in erroneously higher (less significant) false-alarm probabilities.

is often not the case. If there is some knowledge of the source of errors then ϵ can be estimated from the characteristics of the data set (*e.g.* the way ϵ was calculated for the Mt John programme radial velocities in Section 6.1.1). In the case of data comprising white noise only (no signal), ϵ can be determined from the total variance of the data. However in the practical case when there is a possible signal in the data, the partitioning of noise and putative signal must often be assessed from the power (or amplitude) spectrum itself. One might for example, determine the noise ϵ from the typical amplitude spectrum peak height around the peak of interest. However, if the signal is real, the 'noise level' may have been greatly enhanced by the window-function of the signal. Removing the 'signal' to examine the noise level may result in an underestimated ϵ if the original signal wasn't real at all.

In summary, construction of a power spectrum via the Lomb-Scargle method is a useful tool for examining a time series in order to see in what frequencies the greatest power lies. However, when it comes to assessing the *significance* of a peak, unless there is some very good independent estimate of the noise in the data, great caution must be exercised in using the false-alarm probability because of the difficulty in determining the level of noise from the power or amplitude spectrum alone.

6.2.1 Application to the Mt John velocities

Power spectra were calculated using the Lomb-Scargle method for all the stars in the Mt John programme using the computer program of W. A. Lawson (Lawson *et al.* 1990). They are displayed in Figures 6.3 to 6.7. To preserve objectivity, these plots are not normalized (by the assumed noise variance in each case). Most of the plots are to the same scale. In those plots where a more expanded scale was necessary, the star name which labels the plot has been asterisked.

Lomb-Scargle probabilities

The Lomb-Scargle false-alarm probabilities for the single highest peaks in the periodograms of the Mt John programme stars have been calculated assuming underlying noise values ϵ_v equal to those calculated in Section 6.1. That is, the probabilities have been calculated assuming $\epsilon_v = \sqrt{38^2 + 8^2 10^{\frac{m}{2.5}}}$, where m is the V-magnitude of the star. These probabilities are listed in Table 6.2. For many stars, there were several occasions when the spacing between observations

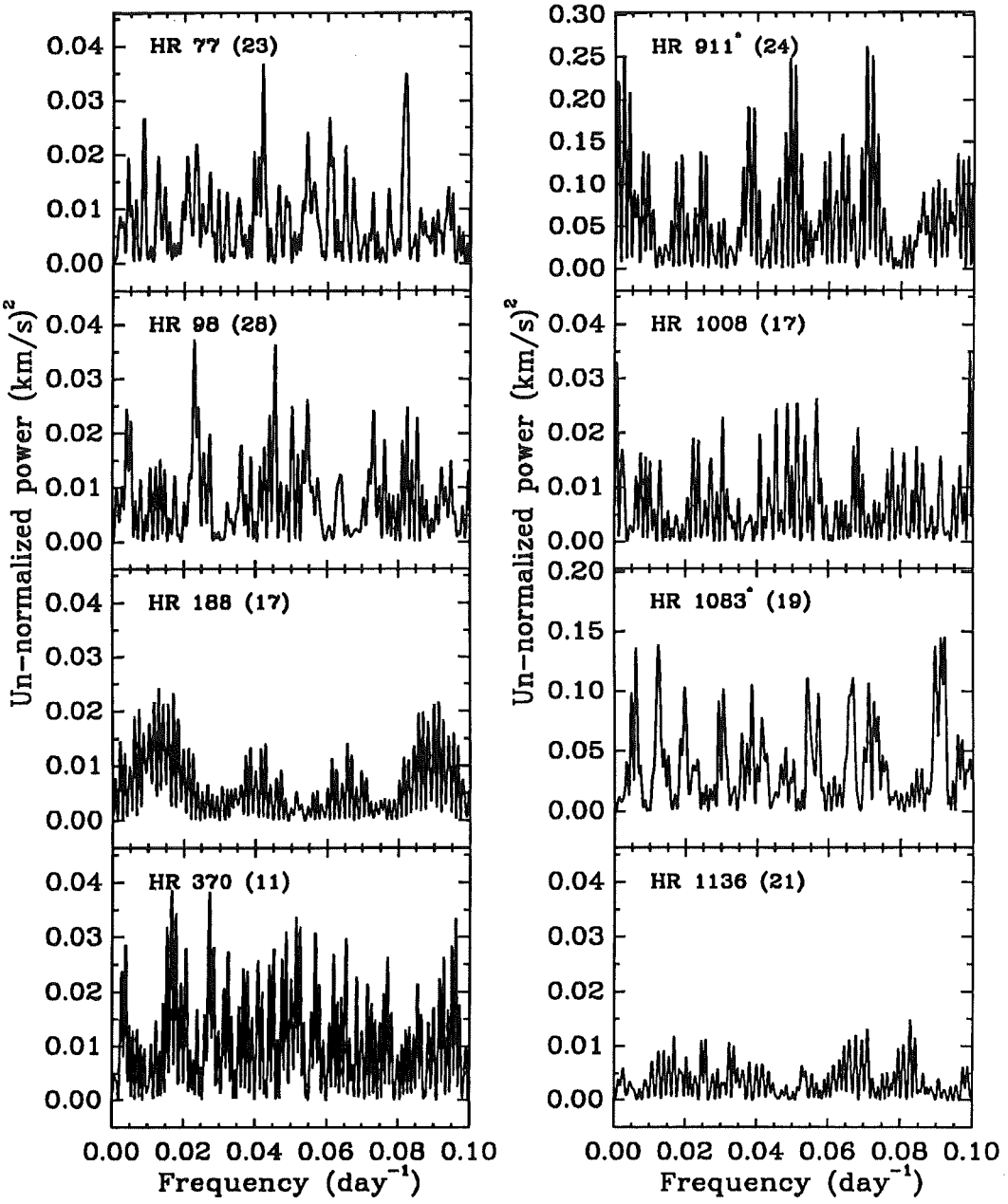

Figure 6.3: Power spectra of HR 77, HR 98, HR 188, HR 370, HR 911, HR 1008, HR 1083 and HR 1136. The number of observations is shown in parentheses and plots with more expanded scales have been asterisked.

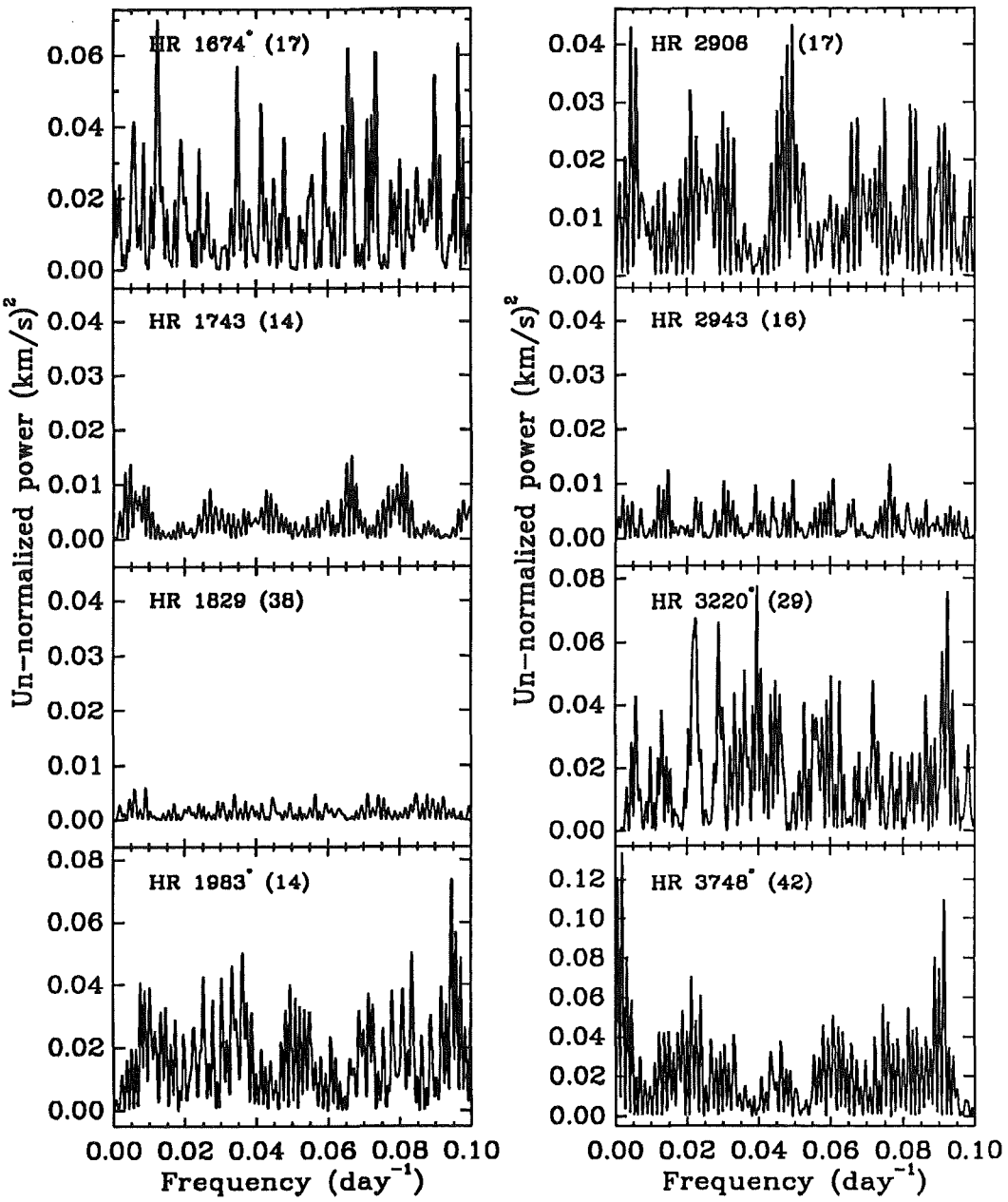

Figure 6.4: Power spectra of HR 1674, HR 1743, HR 1829, HR 1983, HR 2906, HR 2943, HR 3220 and HR 3748. The number of observations is shown in parentheses and plots with more expanded scales have been asterisked.

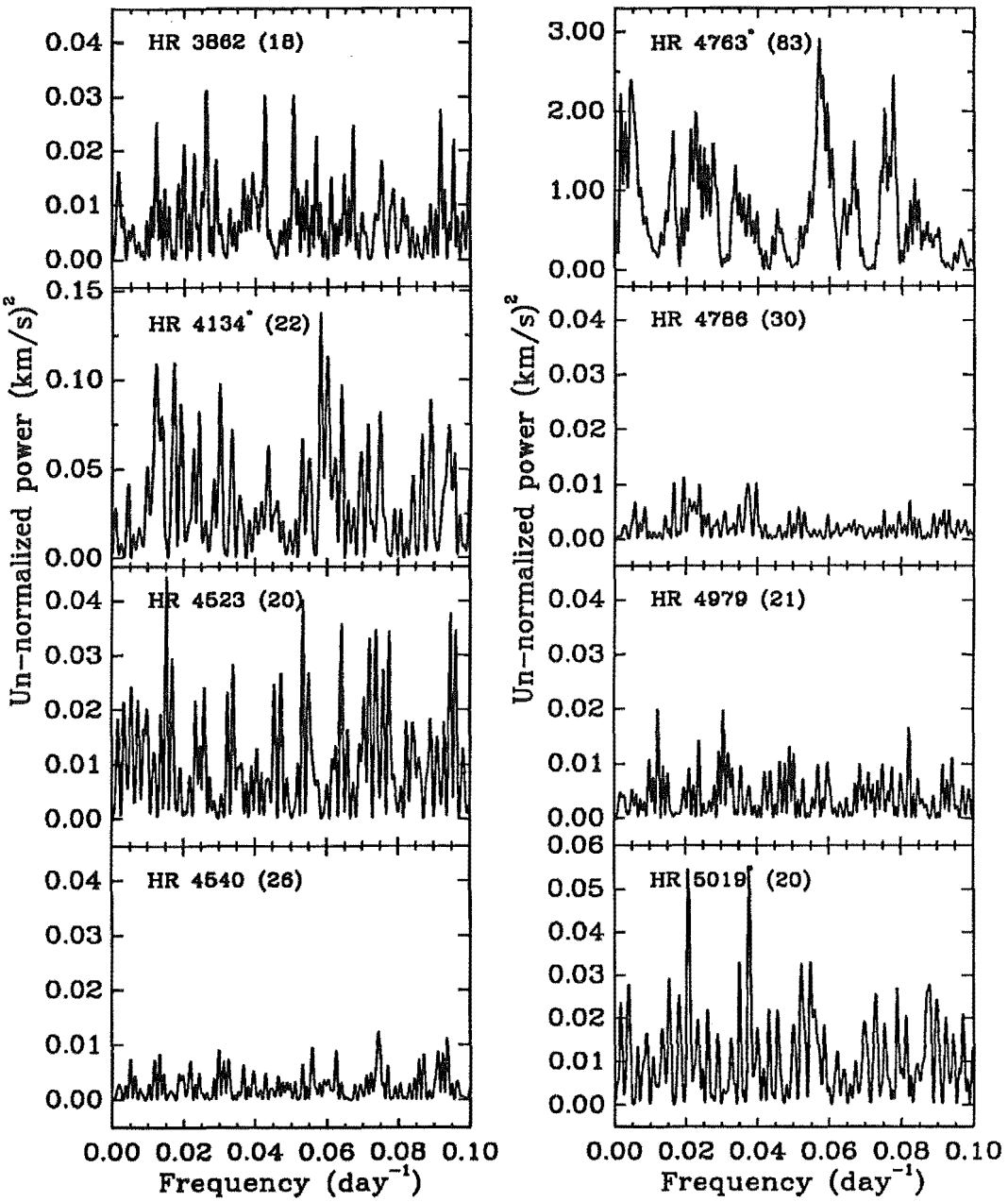

Figure 6.5: Power spectra of HR 3862, HR 4134, HR 4523, HR 4540, HR 4763, HR 4786, HR 4979 and HR 5019. The number of observations is shown in parentheses and plots with more expanded scales have been asterisked.

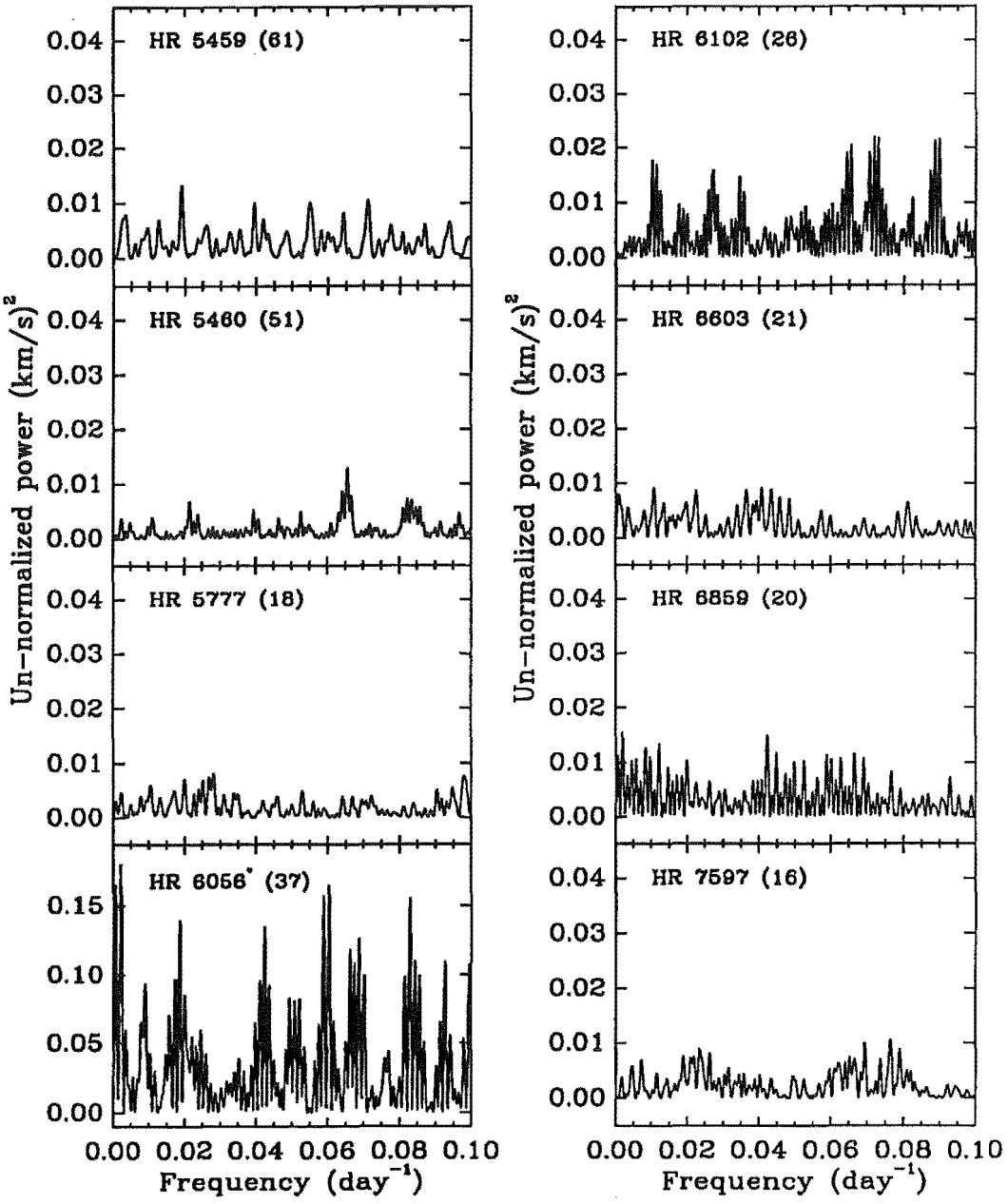

Figure 6.6: Power spectra of HR 5459, HR 5460, HR 5777, HR 6056, HR 6102, HR 6603, HR 6859 and HR 7597. The number of observations is shown in parentheses and plots with more expanded scales have been asterisked.

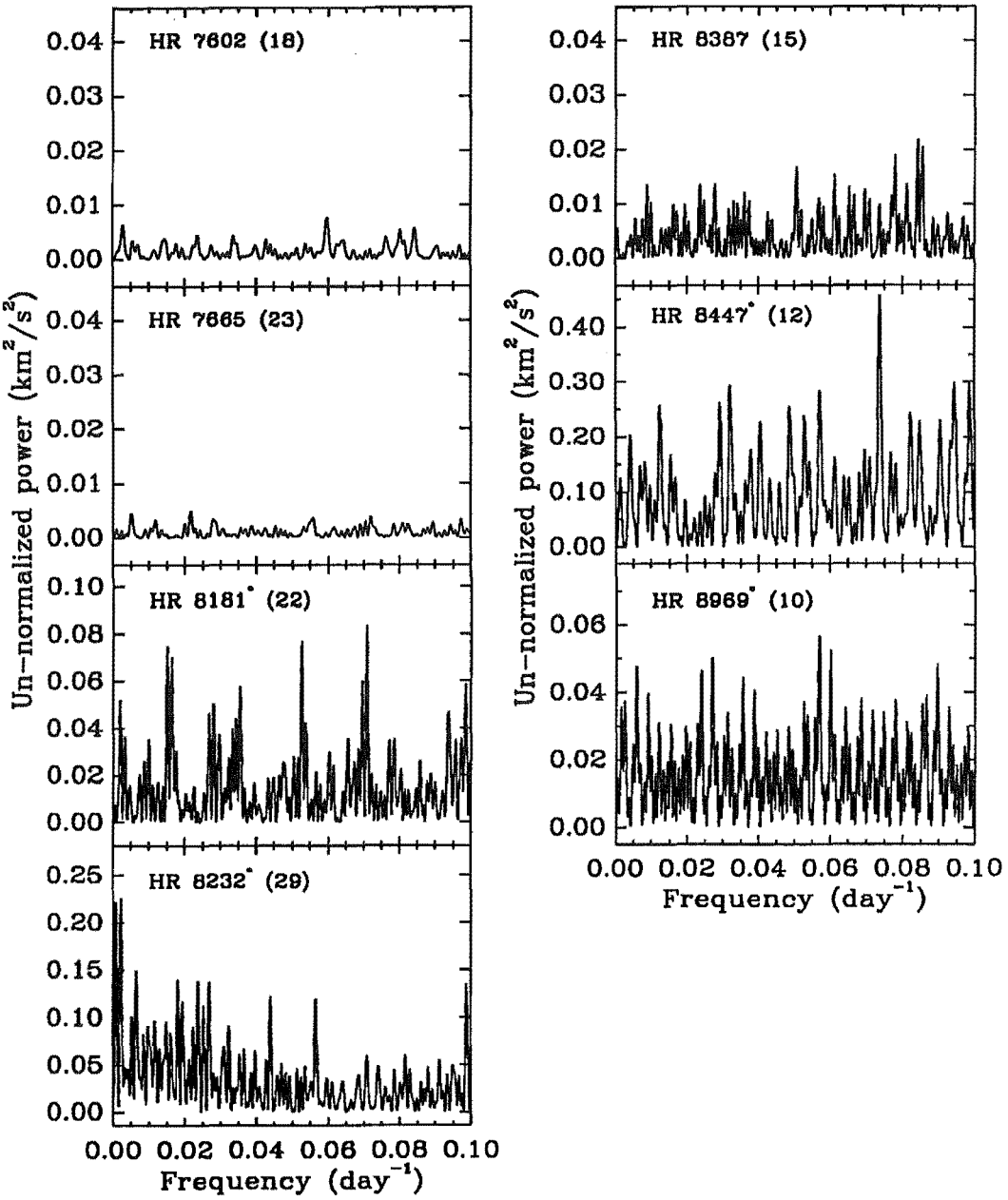

Figure 6.7: Power spectra of HR 7602, HR 7665, HR 8181, HR 8232, HR 8387, HR 8447 and HR 8969. The number of observations is shown in parentheses and plots with more expanded scales have been asterisked.

was only a day or so. For these stars, in calculating the false-alarm probability, the power spectrum up to a frequency of 0.10 day^{-1} (period of 10 days) was considered, implying $M \approx 200$. Stars sampled mostly once per run had several observations spaced by about 12 or 13 days, so in calculating false-alarm probabilities for these stars, frequencies only up to 0.04 day^{-1} (period of 25 days) were considered, implying $M \approx 80$.

Since the same underlying noise levels were assumed, it is perhaps not surprising that the Lomb-Scargle false-alarm probabilities are low for nearly exactly the same stars that the F-test probabilities were low. The exceptions are that HR 3220 and HR 8969 were marginally non-variable in the Lomb-Scargle case, and HR 1674 was marginally variable.

Randomization test

The problem with both the Lomb-Scargle probability test and the F-test is that their effectiveness in detecting radial-velocity variability relies on the accuracy in the determination of the underlying radial-velocity error ϵ_v. In order to obtain results that are independent of an assumed ϵ_v, the power spectra obtained above are examined in a slightly different way.

This time, false-alarm probabilities are obtained in a randomization scheme. Retaining the time spacings of the observations of a star, the radial velocities were randomly redistributed amongst the times. One hundred randomized data sets were created for each star and the periodogram of each of these data sets was calculated. The fraction of times the highest peaks in the periodograms of the randomized data sets exceeded the highest peak in the periodogram of the true data set was recorded. This is the false-alarm probability $P_2(> z)$. If the highest peak in the periodogram of the real data is due to a real signal, then the chance that the highest peaks in the 100 randomized data sets are larger is extremely small (small false-alarm probability $P_2(> z)$). A small false-alarm probability is therefore an indication of a significant peak.

The false-alarm probabilities $P_2(> z)$ for the stars in the Mt John programme are tabulated in Table 6.2. The stars which appeared as the most striking variables in the previous tests — HR 911, HR 3748, HR 4763 and HR 8232 — are also detected as variables in this test. However, none of the other stars previously detected to be variable are marked as being significant. On the other hand, HR 5459, HR 5460 (α Cen A and α Cen B) and HR 4523 are deemed to be

Periodogram probabilities				
Star	*	z	$P_1(>z)$	$P_2(>z)$
HR 77	1	5.8	2.1×10^{-1}	7.4×10^{-1}
HR 98	2	16.1	1.9×10^{-5}	$2. \times 10^{-2}$
HR 188	2	12.4	7.6×10^{-4}	$5. \times 10^{-2}$
HR 370	2	3.8	8.3×10^{-1}	8.7×10^{-1}
HR 911	2	119.2	3.3×10^{-50}	0
HR 1008	1	4.5	5.9×10^{-1}	7.3×10^{-1}
HR 1083	1	19.5	2.7×10^{-7}	6.3×10^{-1}
HR 1136	2	4.7	8.5×10^{-1}	3.7×10^{-3}
HR 1674	1	9.6	5.4×10^{-3}	1.7×10^{-1}
HR 1743	1	3.5	1.0	1.0×10^{-1}
HR 1829	2	2.5	1.0	4.4×10^{-1}
HR 1983	1	8.7	1.3×10^{-2}	3.4×10^{-1}
HR 2906	1	8.0	2.7×10^{-2}	1.0×10^{-1}
HR 2943	1	8.4	1.9×10^{-2}	7.3×10^{-1}
HR 3220	2	8.5	4.1×10^{-2}	9.5×10^{-1}
HR 3748	2	64.0	3.1×10^{-26}	0
HR 3862	1	4.1	7.6×10^{-1}	3.0×10^{-2}
HR 4134	1	12.5	2.9×10^{-4}	2.7×10^{-1}
HR 4523	1	5.9	2.1×10^{-1}	0
HR 4540	2	3.8	9.9×10^{-1}	5.8×10^{-1}
HR 4763	2	1644.1	infinitesimal	0.00
HR 4786	2	6.1	3.6×10^{-1}	4.7×10^{-1}
HR 4979	1	2.7	1.0	3.0×10^{-2}
HR 5019	1	7.8	3.4×10^{-2}	9.9×10^{-1}
HR 5459	2	8.6	3.7×10^{-2}	0.
HR 5460	2	7.9	7.2×10^{-2}	0.
HR 5777	2	1.4	1.0	2.3×10^{-1}
HR 6056	2	61.8	2.6×10^{-25}	$4. \times 10^{-2}$
HR 6102	2	5.3	6.2×10^{-1}	$5. \times 10^{-2}$
HR 6603	2	3.9	9.9×10^{-1}	1.7×10^{-1}
HR 6859	2	5.4	6.0×10^{-1}	1.8×10^{-1}
HR 7597	1	1.3	1.0	$6. \times 10^{-2}$
HR 7602	2	1.9	1.0	5.5×10^{-1}
HR 7665	2	1.4	1.0	1.2×10^{-1}
HR 8181	1	15.6	1.3×10^{-5}	3.8×10^{-1}
HR 8232	2	92.4	1.4×10^{-38}	0.
HR 8387	1	2.1	1.0	3.6×10^{-1}
HR 8447	1	39.3	6.7×10^{-16}	$9. \times 10^{-2}$
HR 8969	1	7.6	4.0×10^{-2}	9.9×10^{-1}

*'1' denotes maximum frequency considered $f_{\max} = 0.04\,\mathrm{day}^{-1}$, $M = 80$; '2' denotes $f_{\max} = 0.10\,\mathrm{day}^{-1}$, $M = 200$.

Table 6.2: False-alarm probabilities of the single highest periodogram peaks for the stars in the Mt John programme. $P_1(>z)$ is the Lomb-Scargle false-alarm probability assuming ϵ_v as derived in Section 6.1. $P_2(>z)$ is the false-alarm probability derived from the randomization procedure described in the text.

significant variables.

The random error in radial-velocity occurs chiefly on two time scales, as described in Chapter 5 — a random error from observation to observation and a pseudo-random error from run to run (a systematic error for a given run). This means that those stars for which there were several observations within a run (Case '2' in column 2 of Table 6.2) might be flagged as 'variable' due to the time-scale of the variations between runs. In fact, the low probabilities of three of the case '2' stars — HR 5459, HR 5460 and HR 1136 — are due to peaks at around 40–60 d, about the typical time interval between runs. The low probabilities for these stars are therefore discounted as indicators of variability.

Furthermore, a similar analysis of the periodogram of HR 4523, having removed the data point with the most positive relative velocity, shows that the periodicity formerly deemed significant all but disappears. Since one point is not a good foundation for a claim of variability, the star is not considered to be variable within the bounds of this test.

6.2.2 Sensitivity

Limited calculation was performed of the region of detectability of orbits in the period - companion mass plane by the power spectrum methods. This showed that the region of detectability is very similar to the region of detectability for the F-test, except with a few subtle features due to the window function imposed by the data spacing. Because the detectability simulations were very computer-time intensive and there seemed to be little difference from the F-test result, complete calculations were not performed. Marcy & Benitz (1989) also noted the similarity in detectability between F-test and periodogram methods but did note in the latter case a slightly enhanced detectability over the F-test of lower companion masses for a given period.

6.3 Slope and curvature

Neither the F-test nor the periodogram method is particularly sensitive to long-term trends in the data. To improve overall detectability, the slope and curvature in each time-series of radial velocities can be analysed. If S and C are defined respectively as the slope ($\dot{v}$) and curvature ($\ddot{v}$) of the radial-velocity data for a star, determined from independent fits and measured with respective uncertainties ϵ_S

and ϵ_C, then the ratios

$$\frac{|S|}{\epsilon_S}$$

and

$$\frac{|C|}{\epsilon_C}$$

are measures of the significance of S and C. These ratios are associated with probabilities $P(> S)$ and $P(> C)$ that the ratios would occur were the data just pure noise. A low value of $P(> S)$ or $P(> C)$ will indicate a candidate variable.

6.3.1 Application to the Mt John velocities

$|S|/\epsilon_S$ and $|C|/\epsilon_C$ were determined for each of the stars in the Mt John programme by the independent fitting of a straight line and a parabola to each time series of radial velocities. The values of ϵ_S and ϵ_C were determined from the scatter of the velocities about the fitted line or curve.

The probabilities $P(> S)$ and $P(> C)$ were determined in a randomization scheme. Retaining the time spacing of the observations of a given star, the radial velocities were randomly redistributed amongst the times. 1500 thus randomized data sets were created for each star. $|S|/\epsilon_S$ and $|C|/\epsilon_C$ were calculated for each of these sets. The probability $P(> S)$ was determined as the fraction of randomized data sets for which $|S|/\epsilon_S$ exceeded the $|S|/\epsilon_S$ of the original data. Similarly $P(> C)$ was defined as the fraction of randomized data sets for which $|C|/\epsilon_C$ exceeded the $|C|/\epsilon_C$ of the original data. This approach has the advantage that no assumptions are made on the distribution of velocity errors.

The resulting values of $P(> S)$ and $P(> C)$ for each star are listed in Table 6.3, where variables were taken to be those stars for which $P(> S)$ or $P(> C)$ is less than 0.01. Again, HR 3748, HR 6056 and HR 8232 were found to be variable, but also HR 6859 (δ Sgr) was found to have a significant slope.

6.3.2 Sensitivity

The simulated data sets described in Section 6.1.2 were again used, this time to estimate the sensitivity of the slope/curvature significance method to the detection of low-mass companions.

For each of the simulated data sets, $P(> S)$ and $P(> C)$ were determined by a randomization procedure similar to that described in Section 6.1.2. A particular (P, M_2) grid point was deemed 'detectable' by the slope/curvature method if

Slope/curvature probabilities		
Star	$P(> S)$	$P(> C)$
HR 77	0.740	0.725
HR 98	0.759	0.125
HR 188	0.302	0.171
HR 911	0.029	0.215
HR 370	0.473	0.738
HR 1008	0.025	0.419
HR 1083	0.944	0.677
HR 1136	0.904	0.342
HR 1674	0.193	0.344
HR 1743	0.670	0.843
HR 1829	0.864	0.551
HR 1983	0.492	0.548
HR 2906	0.525	0.350
HR 2943	0.996	0.023
HR 3220	0.970	0.981
HR 3748*	0.005	0.001
HR 3862	0.683	0.511
HR 4134	0.351	0.592
HR 4523	0.639	0.653
HR 4540	0.973	0.727
HR 4763	0.385	0.159
HR 4786	0.975	0.327
HR 4979	0.759	0.595
HR 5019	0.377	0.329
HR 5459	0.995	0.477
HR 5460	1.000	0.137
HR 5777	0.254	0.691
HR 6056*	0.000	0.291
HR 6102	0.529	0.455
HR 6603	0.017	0.469
HR 6859*	0.001	0.392
HR 7597	0.997	0.977
HR 7602	0.836	0.507
HR 7665	0.803	0.065
HR 8181	0.867	0.105
HR 8232*	0.028	0.000
HR 8387	0.133	0.888
HR 8447	0.836	0.284
HR 8969	0.091	0.079

*Variable by this test.

Table 6.3: Probabilities $P(> S)$ and $P(> C)$ that a more significant slope/curvature would exist in the radial-velocity data, were the data pure noise only.

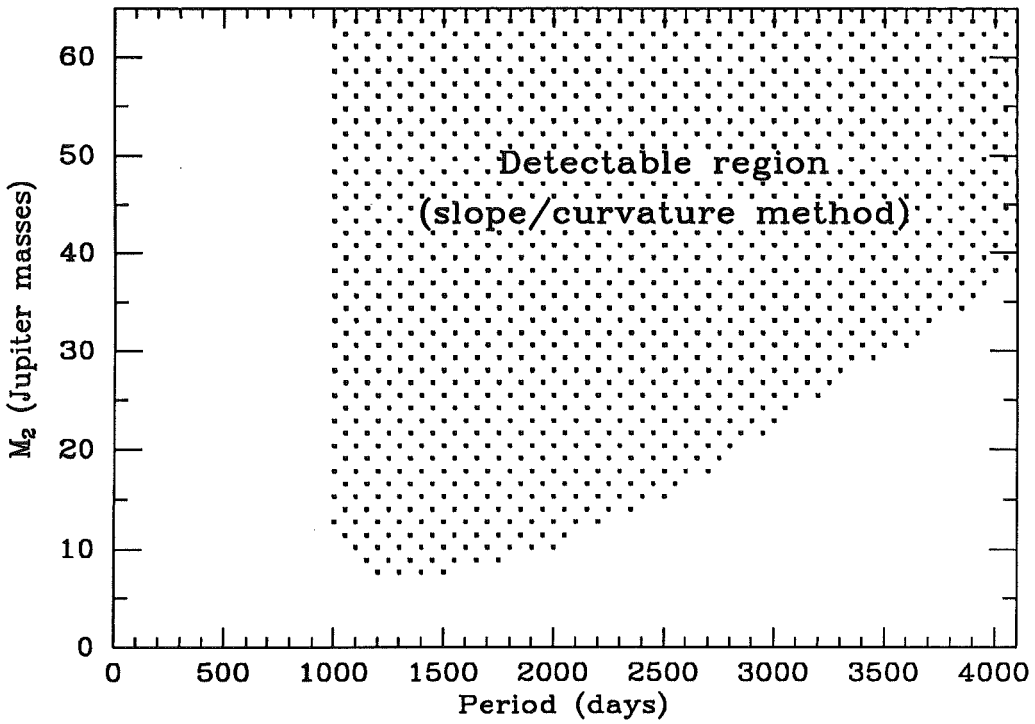

Figure 6.8: Region of detectability of low-mass companions by the slope/curvature method, assuming circular orbits, a primary star of 1 $M_\odot$, an average orbital inclination ($\sin i = \pi/4$) and Gaussian noise of 65 m/s.

$P(> S)$ or $P(> C)$ was less than 0.01 for 95 per cent or more of the trials for that point. The detectable region in the P-M_2 plane is displayed in Figure 6.8. As expected, the method is more sensitive than is either the F-test or period-search method to longer period orbits for companions of a given mass. The method cannot detect orbits with periods shorter than the length of the data set, since in such cases the overall slope and curvature will tend towards zero.

6.4 Summary of variables

None of the tests in this section is completely suitable on its own for a definitive analysis for the presence of orbital motion in the radial-velocity data for the Mt John programme. The F-test relies on an accurate estimation of the random error ϵ_v in radial velocity, as does the periodogram analysis if the Lomb-Scargle probability is to be relied upon. The randomization procedure adopted to analyse the periodograms of the data is not dependent on an assumed value for ϵ_v but it does select against finding irregular variations (multiple signals will appear

as noise) and it also picks out as a signal the slowly-varying error in the run corrections. Finally, the slope and curvature analysis is also independent of an assumed error bar but is only sensitive to the longer periods.

Of the earliest spectral type dwarfs found to be variable by the F-test — HR 1083 (κ Ret; F3), HR 3220 (F5), HR 4134 (F5), HR 8181 (γ Pav; F7), HR 8447 (τ PsA; F6) and HR 8969 (ι Psc; F7) — none appeared to have a significant peak in its periodogram, and this was confirmed by the randomization probability analysis where none of the F dwarfs was found to be variable. Furthermore none showed significant slope or curvature in their velocities with time. It is possible that the anomalously large velocity scatters of these stars are due not to real variability but merely to having underestimated the radial-velocity error bar ϵ_v. It turns out that it is exactly these early F dwarfs which had the broadest cross-correlation peaks. In Equation 2.11 it can be seen that in an F-type star, the smaller number of spectral lines and the increased width of those lines (due to rotational broadening) imply a larger photon-noise limited radial-velocity error-bar. However, even for the broadest-lined and earliest-type stars, for the typical signal-to-noise ratios of the spectra in this programme, the photon-noise limited error-bar was small compared to the total error-bar (around 100 m/s). It appears that there is an augmentation of the total error bar over and above the effect already accounted for in the calculation of the photon-noise limited error-bar. This is a phenomenon observed also by Duquennoy, Mayor & Halbwachs (1991), who find that even though they have calculated the photon-noise limited error bar and other relevant error bars, they need also to add a term dependent on $v_{\rm rot} \sin i$ (rotational velocity times sine of the orbital inclination) to obtain a correct total random error. In the case of the Mt John programme F dwarfs, the broadening of the spectral lines (as seen in the cross-correlation function peak) is probably also due to rotational broadening, as this is normally a noticeable effect in dwarf spectra to the end of the F class. It is not instructive to compare the estimations of $v_{\rm rot} \sin i$ for these stars in the literature, as these are somewhat poor in quality. Another explanation for the broadening could be duplicity[4] but one might expect, in this case, a more convincing peak in the periodogram. In summary, the early-type stars indicated above are unlikely to be radial-velocity variables since the relatively large scatter in their radial velocities is probably an artefact of the measurement process rather than true variability.

[4]The two sets of lines of a double-lined spectroscopic binary may not be resolved, but may appear as a noticeable broadening in the lines of an apparently single spectrum.

The most probable variables in the Mt John programme are among the giant and supergiant radial-velocity standard stars. α Hya (HR 3748), δ Oph (HR 6056) and β Aqr (HR 8232) are flagged as variables in every test, while γ Cru (HR 4763) and α Cet (HR 911) are very convincing variables by both the F-test and periodogram tests, or even by just looking at their velocity records by eye. None of these stars shows a very clear unique signal in its periodogram, although the periodograms of α Hya and β Aqr suggest that a long-period variation is dominant. The complicated periodograms of most of these stars is probably due to irregular intrinsic variability and this is discussed in Chapter 7.

The remaining stars found to be variable include β Hyi (HR 98), which was found to be variable by both the F-test and the Lomb-Scargle analysis, although it must be remembered that these two tests are not really independent. The periodogram of β Hyi shows a peak at about 45 d which is not well defined in height but nevertheless persists despite removal of any small number of points from the periodogram. Because of this and the fact that the velocity sampling is thorough so this is not likely to be an artefact of the window function, β Hyi is considered to be a 'possible' variable.

β Cet (HR 188) was a less convincing variable (it had larger probabilities) in the F-test and Lomb-Scargle analyses and in fact the variability status probably arises from the outlying positions of just 2 points. However, the star is bright, implying small intrinsic velocity scatter, and there is nothing to indicate that there is anything unusual about these two points. β Cet is thus also given the status of 'possible' variable.

Finally, δ Sgr (HR 6859) was found to have a significant slope in its velocity time-series. This is even apparent from looking at the velocities by eye. Since the number of observations of this star was not large, and the slope of the velocities small relative to the scatter in the data, its variability is also conservatively designated 'possible'.

In summary, Table 6.4 lists the variables and possible variables found in this study. The findings of this study conflict somewhat with the radial-velocity variability status indicated for many of these stars in *The Bright Star Catalogue* (Hoffleit 1982). The radial-velocity variability claimed for δ Oph is confirmed but there is no evidence in this work for the variability claimed for β Vir, β Oph or β Aql. Furthermore γ Aps does not appear to be a spectroscopic binary and this study finds no evidence to support the suspected variability of o Col,

Variables		
HR 911	(α Cet)	M1.5IIIa
HR 3748	(α Hya)	K3II/III
HR 4763	(γ Cru)	M3.5III
HR 6056	(δ Oph)	M0.5III
HR 8232	(β Aqr)	G0Ib
Possible variables		
HR 98	(β Hyi)	G1IV
HR 188	(β Cet)	G9III
HR 6859	(δ Sgr)	K2.5IIIa

Table 6.4: Summary of radial-velocity variables in the Mt John programme.

HR 3862, HR 4979 or α Cen B.

Campbell, Walker & Yang (1988) observe possible small long-period changes in the radial velocities of β Vir, 61 Vir and β Aql. The maximum observed range in radial velocity that they observed for these stars was about 20–30 m/s over the six years of observation at a precision of 13 m/s. If such variations are real, then they are too small to be confirmed by this study, whose results do not therefore conflict with the Campbell *et al.* (1988) findings.

Chapter 7

The variable giants

The most striking evidence of radial-velocity variability in the Mt John programme exists not in the *programme* stars, but paradoxically, in the International Astronomical Union radial-velocity *standard* stars. The latter were chosen as standards because they are bright[1] and therefore they are mostly giants or supergiants, as opposed to the programme stars which are dwarfs. As variability due to pulsation is common in evolved stars, *a priori* it seems possible that the radial-velocity variability observed in the standard stars in the Mt John programme is intrinsic to the stars, rather than being due to centre-of-mass motion.

The 'long period' or 'red variable' group of stars is traditionally thought to be made up of giants and supergiants of spectral class about M and later (see Figure 7.1). Red variables are believed to owe their variability to radial pulsation by a mechanism similar to that of Cepheid pulsation. They are normally identified from their photometric variations, which are large ($\Delta V > 2.5$) for the rare Mira variables which are probably asymptotic giant branch stars, but much smaller for the more common 'small-amplitude' red variables which are red giants. The proportion of variables increases with increasing spectral type, as does the amplitude and period of the (photometric) variation. Sub-classes of 'irregular' and 'semi-regular' variables have been defined to describe the commonly-occurring irregularities in period.

The standard stars in the Mt John programme found in Chapter 6 to be variable are α Cet (HR 911; M1.5III), α Hya (HR 3748; K3III), γ Cru (HR 4763; M3.5III), δ Oph (HR 6056; M0.5III) and β Aqr (HR 8232; G0Ib). All of these

[1] The brightness means that 1) no more observing time than necessary will be used to observe standards and 2) the stars are likely to have been well studied in past radial-velocity surveys.

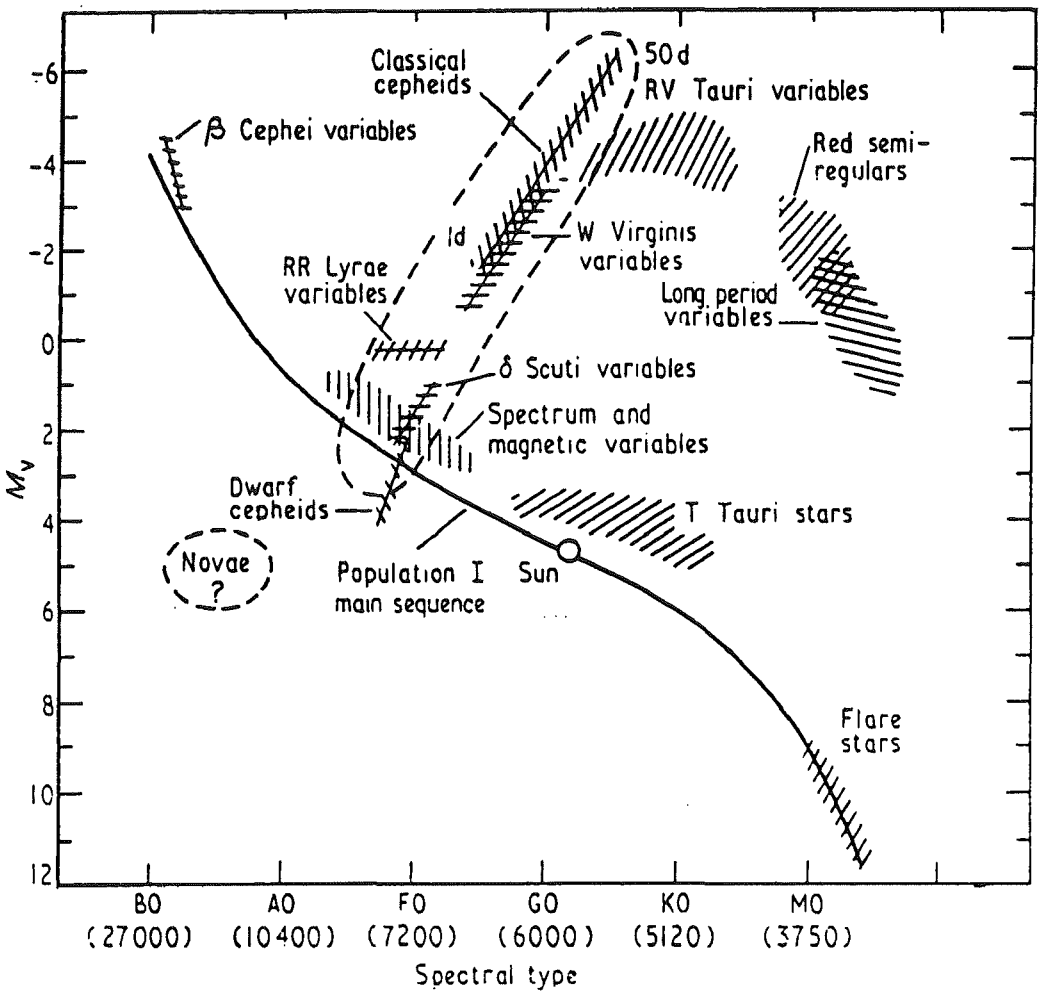

Figure 7.1: Location of the different types of intrinsic variables on the Hertzsprung-Russell diagram (from Cox 1974).

stars were included in the original list of International Astronomical Union radial-velocity standard stars (Pearce 1957) and appear on the revised radial-velocity standard star list of Mayor & Maurice (1985). All are included on the IAU list of future primary standard star candidates (McNally 1988), except for γ Cru which is excluded because of its southerly declination ($-57°$) since the list is restricted to stars within 20° of the celestial equator.

The Mt John programme observations suggest that none of these stars should be used as precise radial-velocity standards. Even classical representations of the regions of variability on the Hertzsprung-Russell diagram (for example Figure 7.1) indicate that the three M-giant standard stars are possible small-amplitude red variables. More recent work suggests that the blue edge of the red-variable region extends into the K spectral type, narrowing the gap between the red-variable region and the Cepheid instability strip (Hoffmeister, Richter & Wenzel 1985; Percy, Landis & Milton 1989; Walker *et al.* 1989). Thus even earlier spectral type evolved stars such as α Hya could be intrinsic variables. The stars will be considered individually.

7.1 γ Cru

γ Cru (Gacrux, HR 4763; spectral type M3.5III) is the brightest M giant in the sky[2]. Its radial-velocity variability is the most obvious of all the stars. All tests in Chapter 6 identified it as a certain variable. Even a naive look at the scatter of the raw data compared to the scatter of data of the other stars in the programme confirms this. Furthermore, the star was observed more intensively over the months 1991 March to 1991 July and fragments of a radial-velocity curve were able to be obtained. Figures 7.2 to 7.6 show (with identical scales) γ Cru velocities from data gathered during these months. The March data appear to define a broad maximum of a radial-velocity curve. The April data show nearly a linear change, while the June data suggest a radial-velocity minimum. The typically small scatter in radial velocity for data obtained at similar epochs (rms scatter about mean value of about 15 m/s — see Chapter 5) suggests that the variations are real and that the radial velocity of γ Cru was truly varying during these runs. Although the data in Figures 7.2 to 7.6 are insufficient for estimation of a period, an approximate upper limit to the typical cycle length can be inferred

[2]It is the red star at the apex of the Southern Cross.

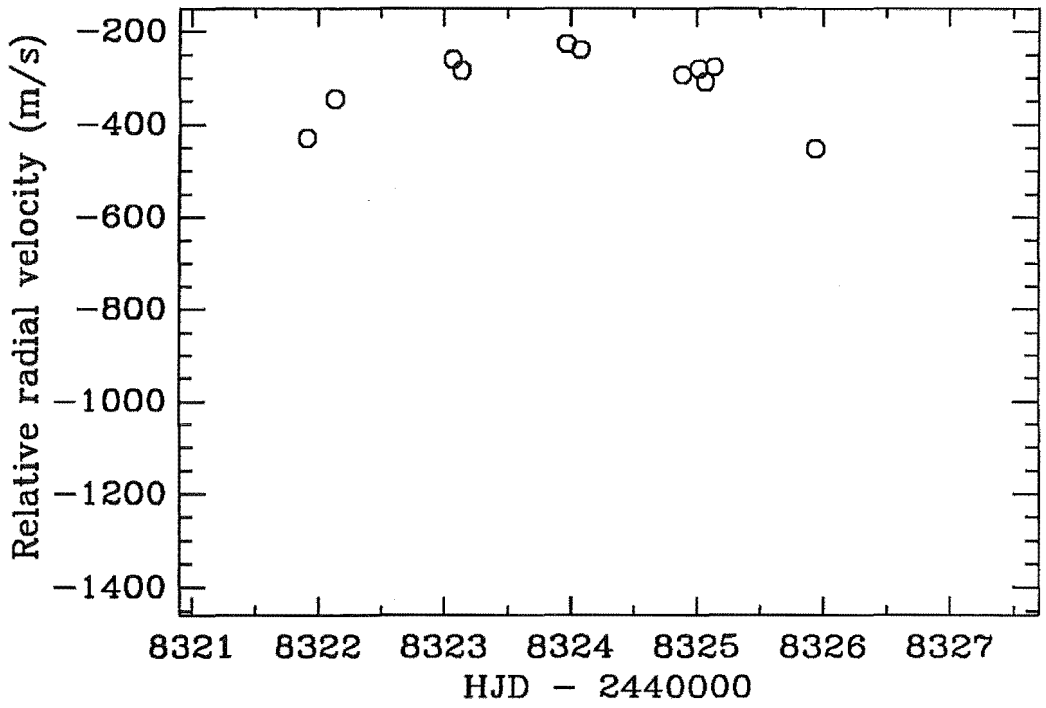

Figure 7.2: γ Cru radial velocities from 1991 March.

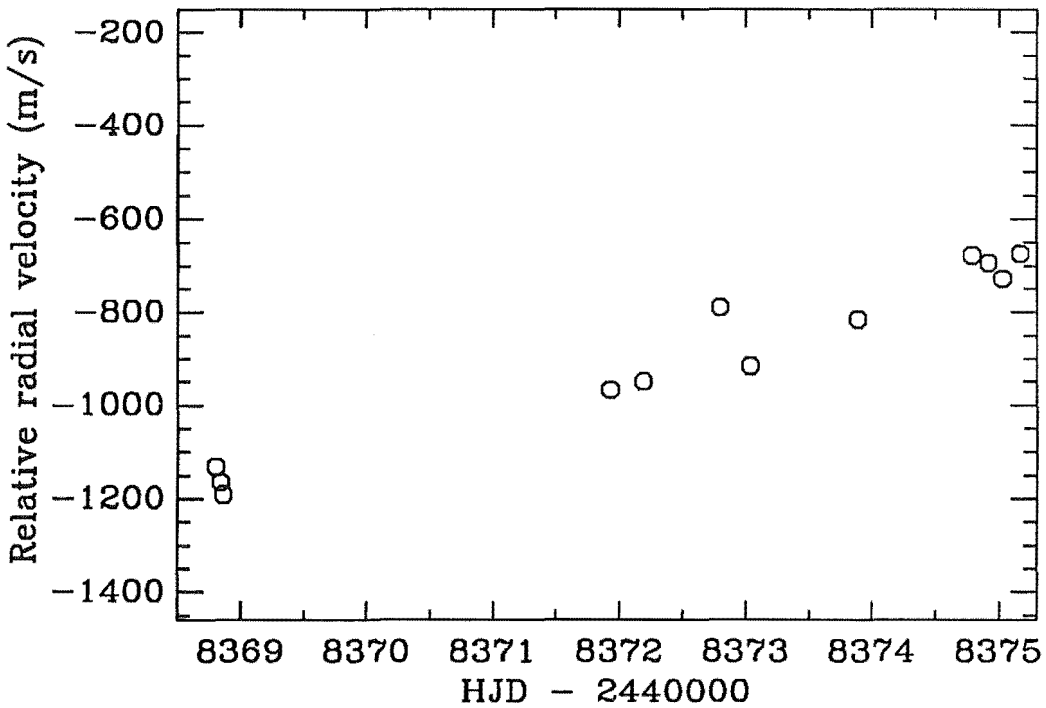

Figure 7.3: γ Cru radial velocities from 1991 April.

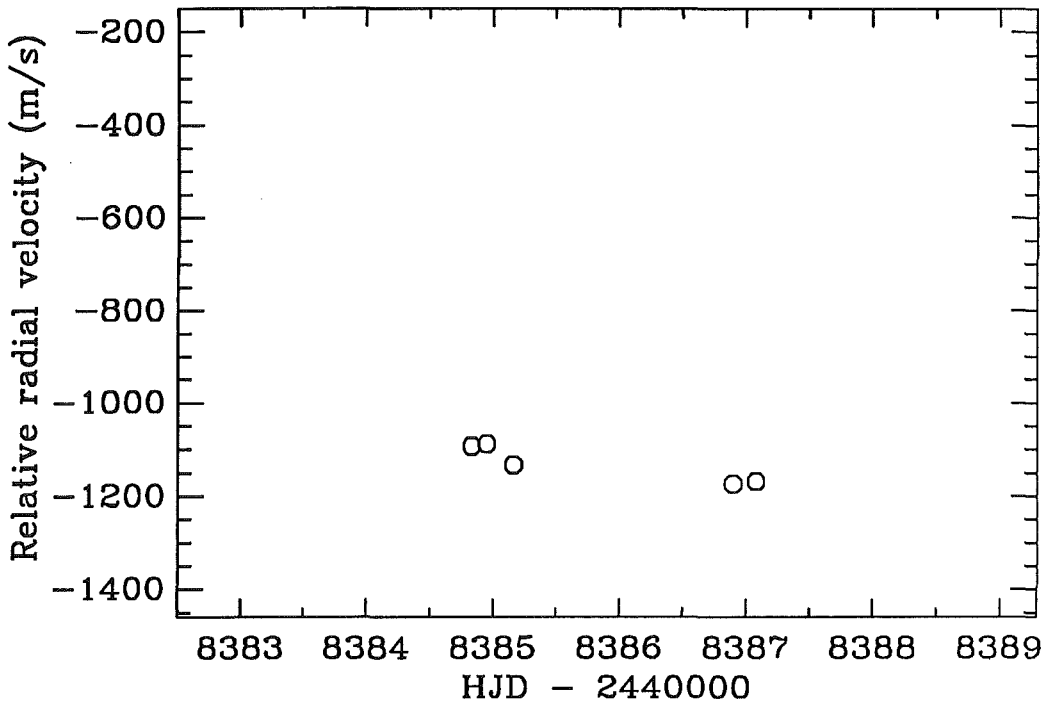

Figure 7.4: γ Cru radial velocities from 1991 May.

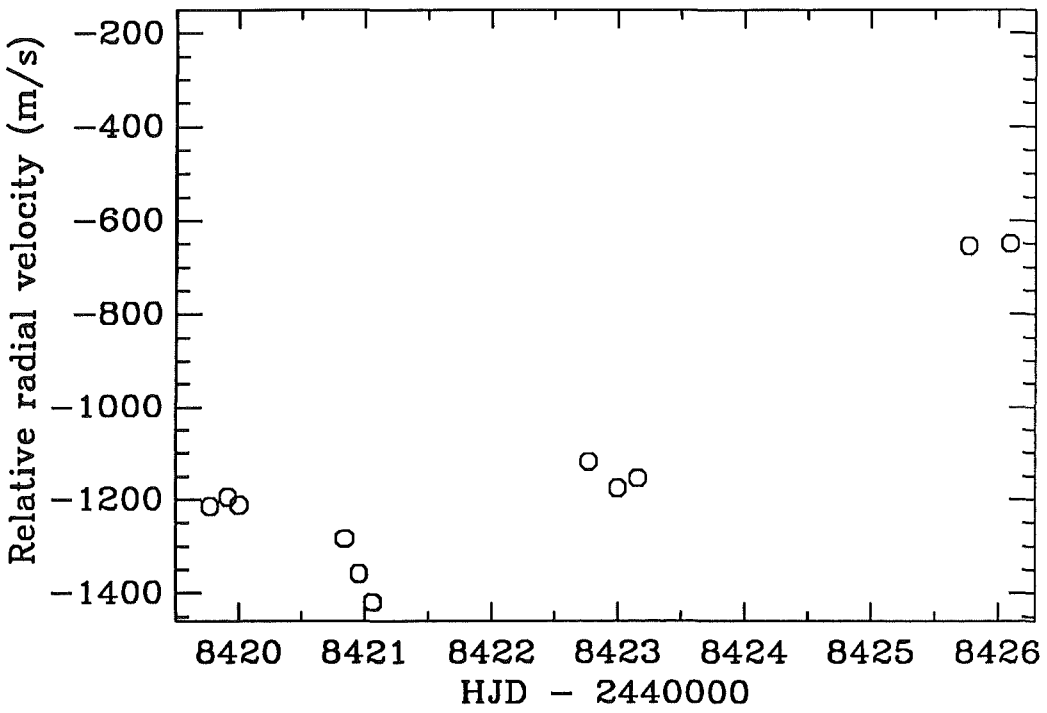

Figure 7.5: γ Cru radial velocities from 1991 June.

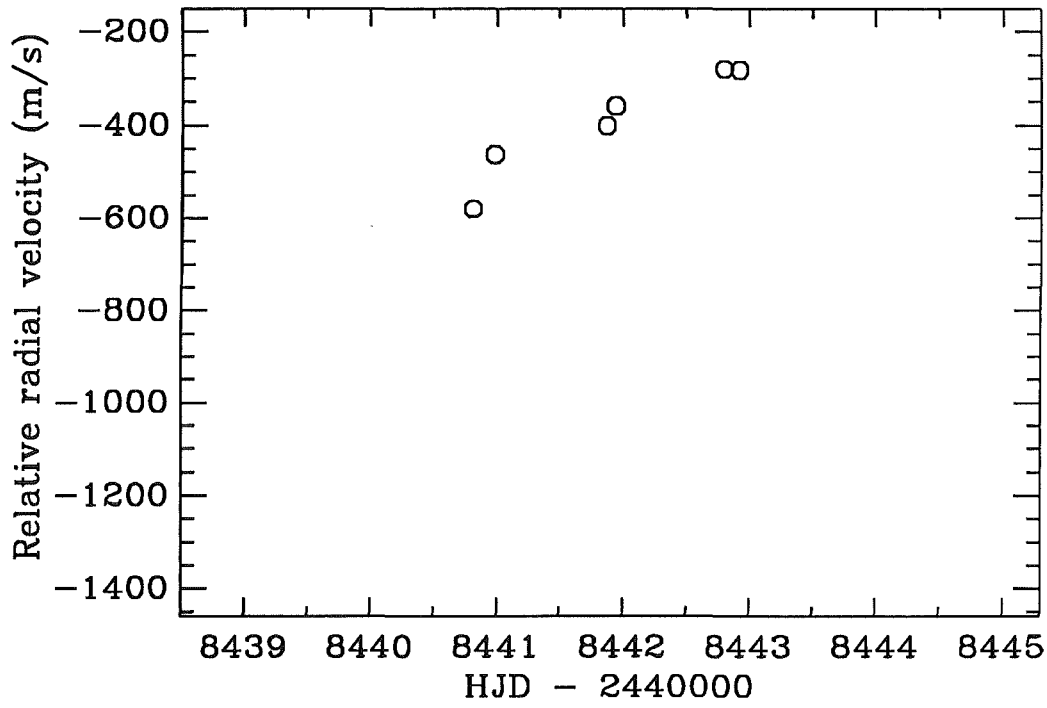

Figure 7.6: γ Cru radial velocities from 1991 July.

by assuming that data from adjacent runs form part of the same cycle. The most stringent limit to cycle length is obtained from the June and July runs, which although only 20 d apart, both show increasing velocities. This implies $P < 20$ d.

To investigate the existence and nature of periodicity over all the dates of observation, the power spectrum of the γ Cru velocities (see Figure 6.5) is examined more closely. There are three regions of high power — at 44 d, 17 d and 13 d — but none of these is particularly well-defined. Furthermore, it has been observed that the power spectrum is fairly unstable with time, the 17 d peak (probably corresponding to the variability observed in the 1991 April–July data) being the most persistent. The variability seems to be semi-regular or irregular in nature.

It is unlikely that the radial-velocity variation arises from orbital motion due to a companion. Using the mass and radius of γ Cru estimated below, for a companion to be in orbit outside of the star its orbital period would be at least 120 d. The March–July data have suggested at least one period shorter that this. The star is probably an intrinsic semi-regular variable of the small-amplitude red variable type. Indeed, γ Cru is suspected to vary in light (V band) by a few hundreths of a magnitude (Petit 1990).

An attempt has been made to predict the pulsation period of γ Cru based on

its mass M and radius R. The period of pulsation is given by

$$P_n = Q_n \sqrt{\frac{R^3}{M}}$$

where if R and M are in solar units, then Q and P are in days (Cox & Giuli 1972). The subscript n signifies the mode of pulsation since Q (and therefore P) depends upon whether the star is pulsating in the fundamental ($n = 0$) or first harmonic ($n = 1$) mode. Fox & Wood (1982) comment that Q_1 is approximately the same ($Q_1 \approx 0.04$) for all long period variables, but Q_0 depends in a more complicated way on the physical parameters of the star.

The angular diameter of γ Cru was estimated to be 0.034 arc s from application of the Barnes-Evans relation (Barnes and Evans 1976), from estimates of the star's effective temperature and bolometric correction (Flower 1975) and from the prediction of Ochsenbein & Halbwachs (1982) based on the star's spectral type. A spectroscopic parallax from the *Sky Catalogue 2000.0* (Hirshfeld & Sinnott 1982) was used to estimate the star's radius from all three methods as 100 ± 20 solar radii. Using an evolutionary mass of 1.3 ± 0.1 $M_\odot$ (Novotny 1973) and $Q_1 = 0.04 \pm 0.01$, the period of first harmonic pulsation was calculated to be 20 d $< P_1 <$ 60 d. $P_0/P_1 \approx 2$ for P_1 in this range (Fox & Wood 1982) so it can be expected that 40 d $< P_0 <$ 120 d.

The 1991 April–July data show radial-velocity periodicity which occurs on a time scale ($<$ 20 d) which is somewhat shorter than expected for fundamental or first-harmonic radial pulsation of a long period variable star. On the other hand, from inspection of the γ Cru periodogram, the radial-velocity variability of γ Cru observed in this programme did not appear to occur on a unique time-scale. Peaks occur at longer periods in the periodogram, although it cannot be said whether these periods are significant, and if so, whether they correspond to the expected periods for fundamental or first harmonic radial pulsation.

It does seem clear that γ Cru is of the semi-regular or irregular class of long-period variables. The radial-velocity variability is certainly real. The star's photometric amplitude is too small for it to be classified as a Mira and it lacks the emission features usually seen in the spectra of such stars. The time-scale of its radial-velocity variability is shorter than seen in Miras and yet is in the range in which variability is seen in several semi-regular stars (Hoffmeister *et al.* 1986). Hoffmeister *et al.* (1986) also comment that long-period variable stars with periods between 50 d and 90 d nearly always show irregularities. As one of

the periods of variability of γ Cru may fall within this range, it seems possible that the instability of the periodogram of the star with time could be due to real instabilities in the period of radial-velocity variations.

7.2 α Cet and δ Oph

The radial-velocity variations of the other two M-giants in the Mt John programme — α Cet (HR 911) and δ Oph (HR 6056) — are of a similar nature to those of γ Cru. Both show highly significant radial-velocity variations, but no unique period in the periodograms. They were both already suspected to be variable in radial velocity — Hoffleit (1982) (δ Oph), Scarfe, Batten & Fletcher (1989) (α Cet) and in light — Hoffleit (1982) (δ Oph), Eggen (1973) (α Cet). They are probably semi-regular red variables like γ Cru. The number of recorded velocities for these two stars is somewhat less than was recorded for γ Cru and therefore the stars do not warrant such a detailed analysis.

7.3 α Hya

Very high precision radial-velocity measurements have been made of α Hya by Walker *et al.* (1989). They find that the star exhibits radial-velocity variability with a total amplitude of about 300 m/s over the observation period of 5 years. This, along with the fact that this variability appears to be somewhat irregular and the star also shows variability in light (Hoffleit 1982), leads to the conclusion that α Hya is an intrinsic variable.

In the Mt John radial-velocity data of α Hya, there is also a 300 m/s range in the velocities, which is consistent with the variability reported by Walker *et al.* (1989).

7.4 β Aqr

This star has too early a spectral type to be a red variable — in fact it lies on or near the Cepheid instability strip, although it is not a Cepheid. The star shows no detectable photometric variability above 0.02 magnitudes (Fernie 1976). The apparent period (1000 d) of the radial-velocity variations observed in the Mt John programme is too long to be due to star spots or known pulsation mechanisms.

If the variations are real, it seems most likely that they are due to orbital motion with a companion, rather than to intrinsic variability of the star.

The tests in Chapter 6 have all indicated that the radial-velocity variations of the star are real. The data for β Aqr displayed in Figure 4.10 show the broad minimum of a radial-velocity curve whose period is at least 1000 d or so. Although the data were observed in 'clumps' around 4 main epochs, within each clump, data were obtained from between two and seven observing runs. The curvature is therefore not an artefact of systematic differences between runs. It is furthermore not an artefact of the run corrections — the mean of the velocities at each of the four 'clumps' has a range of about 300 m/s and no run correction was as large as this.

β Aqr has an 11th magnitude optical companion at a separation of 35.5 arc s (Hoffleit 1982). Since the spectroscopic parallax of β Aqr implies that it is 300 pc distant (Hirshfeld & Sinnott 1982), if the association of the visual pair is physical, then the companion is probably something like an F5 dwarf (mass about 1.4 $M_{\odot}$) and the period a matter of tens of thousands of years. The chance that the minimum of the radial-velocity curve of this orbit was observed over the course of the Mt John programme is small enough that the visual companion can be eliminated as a possible cause of the radial-velocity variations.

As less than one cycle was observed in the data, a reliable estimate of the period and semi-amplitude of the orbit cannot be made in order to derive a companion mass. The lower limit to the period is around 1000 d, which does at least imply an orbit well outside the approximately 75 $R_{\odot}$ star, assuming that the mass of the star is about 8 $M_{\odot}$ (Parsons & Bouw 1971). The minimum semi-amplitude of the orbit is about 150 m/s.

In order to consider what companion mass the data *might* imply, circular orbits of various periods were fitted to the data. Figure 7.7 shows how the period of the orbit is related to the companion mass M_2 (multiplied by the sine of the inclination i). Without knowledge of the orbital inclination, one can only say that there is a possibility of the companion being substellar (less than 0.08 $M_{\odot}$) as long as the period is less than about 2200 d.

There is some knowledge of the inclination of β Aqr's *rotational* axis. If one is prepared to make the assumption that the orbital and rotational axes are parallel (Campbell & Garrison 1985), then this can put a further constraint on the likely mass of the companion. Brosius, Mullan & Stencel (1985) have calculated the

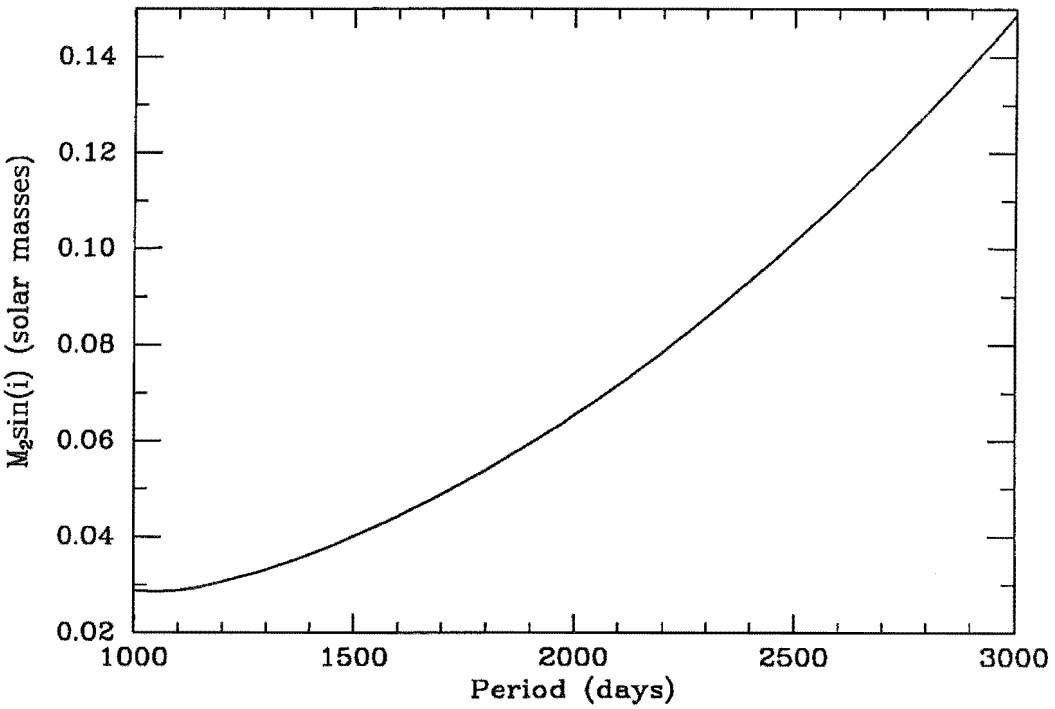

Figure 7.7: Dependence of mass of implied companion to β Aqr on best-fit circular orbits of different periods, assuming a primary mass of 8 $M_\odot$.

rotation period to be 390 d from variations in Ca II H and K emission. Gray & Toner (1986) have calculated $v \sin i$ to be 6.3 ± 1.3 km/s from analysis of line profiles. These two values, along with an assumed stellar radius of 75 $R_\odot$ imply that the rotational axis has an inclination of $\sin i = 0.65$. Assuming that this value can be adopted for the *orbital* inclination, the period of the circular orbit can be a maximum of 1800 d before the implied companion mass is stellar.

Obviously the true nature of the radial-velocity variability of β Aqr can only be determined by further spectroscopic and photometric observation.

Chapter 8

Discussion

8.1 Limits to companion masses in the Mt John programme

The radial-velocity perturbation induced by a brown-dwarf companion to a solar-mass star with a period less than 10 years is between a few hundred and a few thousand metres per second[1] for all inclinations except those nearly in the plane of the sky. Since the average radial-velocity error in the Mt John programme is about 65 m/s, any perturbation with a period of a few years and amplitude of the order of a couple of hundred metres per second or more should be easily discernible in the radial velocities of the primary star. In other words, if brown dwarfs are common as companions to solar-type stars then radial-velocity perturbations should have been obvious in some of the Mt John programme stars from the time series of radial velocities. In fact, the only *obvious* previously-undiscovered single-lined spectroscopic binary was HR 3220, whose companion is stellar. The lack of any other obvious spectroscopic binary is alone a strong negative statement regarding the presence of brown-dwarf companions to the Mt John programme stars.

In Chapter 6 the status of radial-velocity variability of the Mt John programme stars was examined by using tests which were aimed at the detection of very low amplitude variations in radial velocity. Only a single dwarf star (β Hyi) was indicated to be variable and even so its variability status is somewhat marginal. Figure 8.1, the union of Figures 6.2 and 6.8, summarizes the

[1] Example perturbations were listed in Table 1.2.

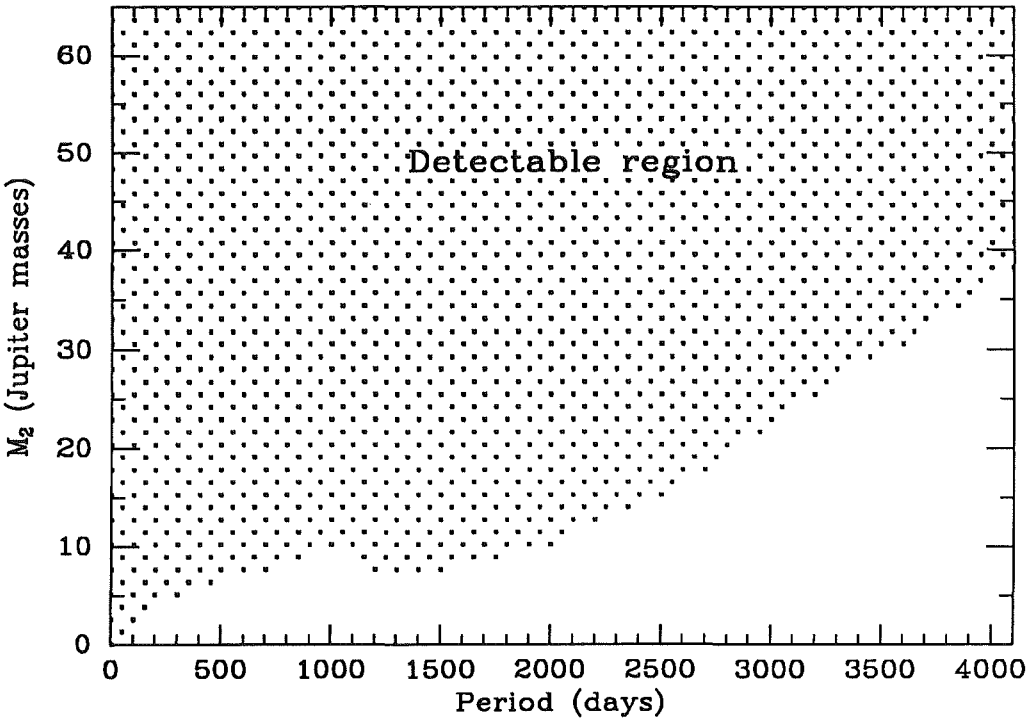

Figure 8.1: Net region of detectability of low-mass companions in the Mt John programme, assuming circular orbits, a primary star of 1 $M_\odot$, an average orbital inclination ($\sin i = \pi/4$) and Gaussian noise of 65 m/s.

orbits on the companion mass - period plane that were detectable[2] in the Mt John programme. Note that Figure 8.1 is a calculation for *average* orbital inclination and so for a given companion mass, the programme could detect longer period orbits for more favourably inclined systems (i closer to 90°). Furthermore, the shaded area represents detectability at the 95 per cent confidence level. In practice, the probability of detecting an orbit decreases smoothly over the boundary from the shaded region, meaning that orbits are in fact detectable in this region, but with a smaller probability. The programme should have found all companions with masses greater than 10 $M_{\mathcal{Y}}$ and periods shorter than 2000 d (5.5 years). If the lower mass boundary for brown dwarfs[3] is about 20 $M_{\mathcal{Y}}$, it can be said that the programme could have picked up all companions of brown dwarf mass or greater with periods shorter than 3000 d (8.2 years). In other words, apart the from possibility of a companion to β Hyi, it is very unlikely that brown dwarfs with periods less than 8 years are in orbit about the dwarf stars in the

[2]By F-test, periodogram and slope/curvature tests.
[3]See comments in Chapter 1 on the lower mass boundary for brown dwarfs.

Mt John programme. On the other hand, two of the evolved IAU standard stars (β Aqr, a G0 supergiant and δ Sgr, a K giant) show long-period radial-velocity modulation that could be due to low mass companions. The only effects that could conceivably mask significant numbers of companion brown dwarfs from detection are preferential orientation of their orbits in the plane of the sky or that they have large eccentricities[4] with a longitude of periastron close to $\pm 90°$. However, these effects can be discounted as they assume the sun is in a 'special' position.

For a small number of the dwarf stars in the Mt John programme, the conclusion concerning the existence of companion brown dwarfs can be strengthened by considering astrometric data. While radial-velocity analyses such as the Mt John programme are more sensitive to shorter-period orbits, astrometric analyses are more sensitive to longer-period ones[5]. A star which has been included in a long-term astrometric programme will have a determinable upper limit to possible perturbations due to a companion, over periods comparable to the length of the astrometric survey. Since the companion mass is proportional to the astrometric perturbation, knowledge of the maximum likely astrometric perturbation gives an estimate of the maximum likely companion mass. At long periods, this maximum companion-mass limit is inevitably a stronger constraint on the nature of possible companions than is the maximum companion-mass limit set by radial velocities.

Unfortunately the long-term astrometric coverage of southern hemisphere stars is very poor (Heintz 1992) and there are only four stars in this sample for which an astrometric limit to perturbations exists. These are α Cen A, α Cen B and α CMi (due to the measurements of their visual orbits) and δ Eri (which is included in the study of long-term astrometric perturbations by Lippincott & Worth 1980). No astrometric perturbation other than the visual orbit has been observed in either the α Cen system from over 100 years of data[6] or the Procyon system from 34 years of data (Strand 1951). Again, no astrometric perturbation has been found in the orbit of δ Eri by Lippincott & Worth (1980) from 38 years

[4]In very eccentric orbits the stellar velocities change only very slowly (and perhaps imperceptibly) over most of the orbit (around apastron) and one might not be observing when the rapid changes in velocity occur at periastron passage.

[5]See Chapter 1 for comments on the complementarity of astrometric and radial-velocity techniques

[6]Heintz 1982 comments that the system has been observed through 'nearly two revolutions'.

Star	π_p	Reference	M_1	Reference
α Cen A	+0.750	Hoffleit (1982)	1.09	Heintz (1982)
α Cen B	+0.750	Hoffleit (1982)	0.90	Heintz (1982)
α CMi	+0.292	Hoffleit (1982)	1.74	Strand (1951)
δ Eri	+0.113	Hoffleit (1982)	0.79	Lang (1992)

Table 8.1: Data used to derive astrometric limits to companions for those stars which were in long-term astrometric programmes. All parallaxes are trigonometric. The mass of δ Eri is based on its spectral type, the other masses are from the visual orbits.

of data. These results are interpreted to mean in each case a maximum angular perturbation due to an unseen companion (a third companion in the case of the α Cen and α CMi systems) of 0.02 arc s. The value of 0.02 arc s is chosen (following the reasoning of Marcy & Benitz 1989) because a perturbation would have to be several times larger than the typical error in the programme to be discovered. 0.02 arc s is about three times the typical positional error in the relevant photographic astrometry programmes in this case.

From this information, astrometric limits to the masses of possible companions were determined for α Cen A and B, Procyon and δ Eri. Assuming circular orbits, the minimum detectable mass via astrometry is

$$M_2 = \left(\frac{M_1}{P}\right)^{2/3} \frac{\theta}{\pi_p},$$

where M_1 and M_2 are the primary and secondary masses respectively, P is the period of the orbit, θ is the maximum likely astrometric perturbation for the system and π_p is the system parallax. Table 8.1 shows the data used for this calculation. Figure 8.2 shows the upper limits to the masses of companions of the four stars derived from astrometry, along with the area in the P-M_2 plane where companions are eliminated in this radial-velocity programme (from Figure 8.1). Even though the maximum angular perturbation for each star was assumed to be the same, the placement of the upper-limit line differs for each star mainly because of the stars' different distances.

The conclusions derived from Figure 8.1 regarding the existence of brown dwarfs (*e.g.* the statement that none of these stars has a brown-dwarf companion in an orbit with a period less than 8.2 years) still hold true for α Cen A, α Cen B, α CMi and δ Eri but the astrometric data has now allowed the companion-mass upper limit for these stars to be extended to longer period orbits. It can be seen

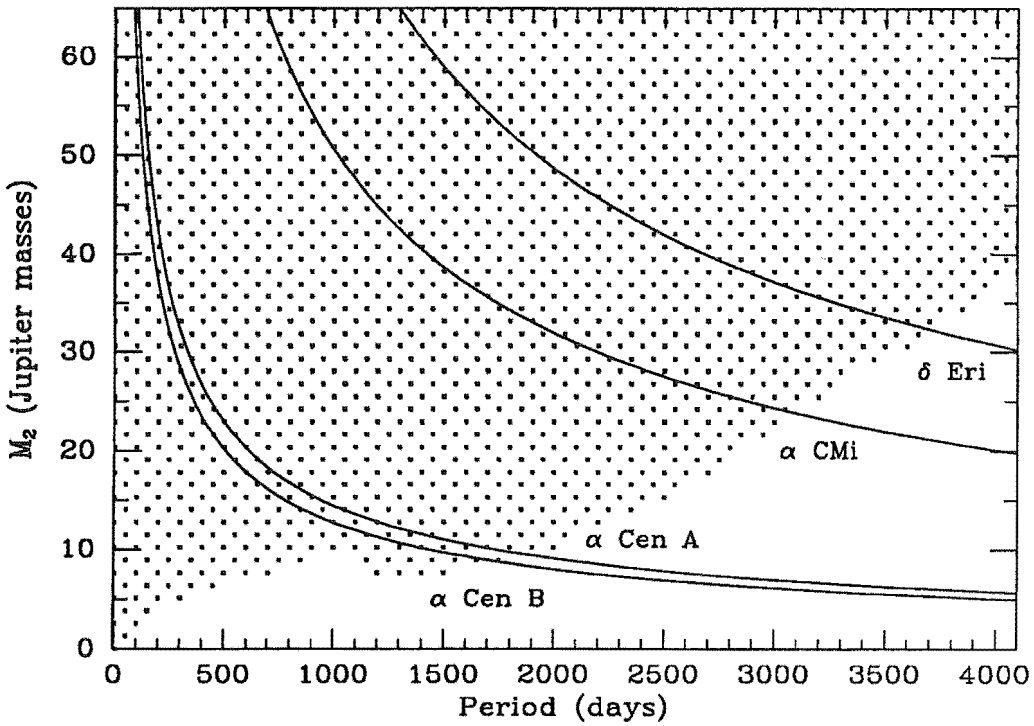

Figure 8.2: Limits to masses of companions of α Cen A, α Cen B, α CMi and δ Eri. The upper limit to the mass of companions as determined by this programme is the boundary of the shaded region while the lines are the upper mass limits as determined by astrometry.

that for both α Cen A and α Cen B, no companion of mass greater than about 10 $M_{\mathcal{Y}}$ exists with a period up to the duration of the astrometric coverage of the system which is more than a century. α CMi has no companion of mass greater than about 24 $M_{\mathcal{Y}}$ and period shorter than 34 years and δ Eri has no companion of mass greater than about 32 $M_{\mathcal{Y}}$ and period less than 38 years. Despite the fact that δ Eri has the highest upper mass limit, it is this star for which this calculation has most significance, since long period orbits would not be expected about α Cen A, α Cen B and α CMi because of the latter stars already having *stellar* companions in long-period orbits.

8.2 Previous surveys

In nearly every direct search for brown dwarfs[7] any putative brown dwarfs have been sufficiently similar in their surface properties that they are not distinguishable from low-mass main sequence stars. Part of the problem is that, as pointed out in Chapter 1, the easiest brown dwarfs to detect directly are the youngest ones but the theoretically expected luminosities, colours and spectra of young brown dwarfs are not well understood. However in the one case where the direct survey has been combined with a dynamical method to determine the masses of the candidate brown dwarfs, the masses turned out to be right at the star-brown dwarf dividing line, suggesting that this may be the reason that the objects have been difficult to classify.

Brown dwarfs have been looked for by direct means either in close spatial proximity to stars of known distance (as companions to the stars), or in deep surveys looking for 'free-floating' brown dwarfs. The earliest attempt at infrared surveying around stars was by Jameson, Sherrington & Giles (1983) who performed J, H and K photometry around 21 nearby stars and found no brown dwarf companions. Later surveys were performed on stars within 20 pc of the sun (Skrutskie, Forrest & Shure 1986, 1989) and on stars in the Taurus star cluster (Forrest *et al.* 1989). In the former survey, a candidate brown dwarf was found near Gliese 569, one of the sample of 60 stars (Forrest, Skrutskie & Shure 1988). The companion is obviously cool, from the observation of the molecular features in its spectrum (Henry & Kirkpatrick 1990) but the spectral evidence alone is not enough to distinguish it from a lower-main sequence star. Forrest *et*

[7] A direct search for brown dwarfs is one where the light from the brown dwarf is to be detected (See Chapter1).

al. (1989) found as many as 9 putative dwarfs in Taurus. Stauffer *et al.* (1991) obtained spectra of six of them but this time none of the carbon monoxide or water absorption expected for brown dwarfs was seen, which suggests that they are probably just highly reddened background stars. The similar survey of Rieke & Rieke (1990) in the ρ Ophiuchi star-formation region found three putative brown dwarfs but with a luminosities similar to low-mass stars.

It is the near-infrared speckle survey of Henry & McCarthy (1990) which has also used a dynamical method to find out more about apparently low-mass companions to stars. They observed brown-dwarf candidates at different epochs in order to estimate the visual orbits and hence the companion masses. The survey has identified via speckle interferometry, four brown dwarf candidates out of the 99 survey objects within 8 pc of the sun (Henry & McCarthy 1992). The orbits obtained for all of these companions suggest masses around the 80 $M_{\mathcal{Q}}$ hydrogen-burning minimum mass. Incidentally, it was the infrared speckle technique which led to the 'detection' of a brown-dwarf companion to the nearby M dwarf VB8 (McCarthy, Probst & Low 1985). Later attempts at the detection of the brown dwarf failed (*e.g.* Skrutskie, Forrest & Shure 1987; Perrier & Mariotti 1987) and the companion is no longer believed to exist.

Surveys for free-floating brown dwarfs are vulnerable in that the distances (and hence luminosities and colours) are less easy to determine. Jameson & Skillen (1989) conducted a deep CCD survey of the Pleiades cluster with a view to detecting young (the age of the Pleiades is around 7×10^7 years) free-floating brown dwarfs. Five candidate brown dwarfs arose from this survey but the brown-dwarf status of these is reliant on them being cluster members. Later studies (Hambly, Hawkins & Jameson 1991; Hambly & Jameson 1991) used proper motions to determine membership and claimed a lower limit of 10 candidate brown dwarfs in the Pleiades. Stauffer *et al.* (1989) also conducted a deep CCD survey of the Pleiades cluster and found four very faint, very red stars with luminosities similar to those of lower main sequence stars. It is not clear whether these objects are in fact lower main sequence stars or brown dwarfs before the degenerate cooling phase. In another deep survey (Boeshaar, Tyson & Seitzer 1986) found no companions, while in a search in the IRAS Point Source Catalog Shipman (1985) should have been able to find more massive brown dwarfs, but found none.

Hawkins (1986) and Hawkins & Bessell (1988) have found large numbers of faint, red objects in the field from analysis of UK Schmidt plates. At least some

of these objects appear from both photometry and spectroscopy (Bessell 1991) to match expectations of the appearance brown dwarfs.

Finally in terms of direct searches, the early photometric surveys of white dwarfs (Kumar 1987; Zuckerman & Becklin 1987a) for infrared excess indicative of brown-dwarf companions yielded no brown-dwarf candidates. Later, Zuckerman & Becklin (1987b) identified infrared excess in the emission from the white dwarf Giclas 29-38 and identified this as being due to an orbiting brown-dwarf companion. However no infrared companion was observed directly at > 3 astronomical units (Tokunaga *et al.* 1988) and no radial-velocity variations were observed in the primary (Wingert *et al.* 1990; Graham *et al.* 1990). Giclas 29-38 probably has a dust ring rather than a brown-dwarf companion. However, Becklin & Zuckerman (1988) also inferred a companion to another white dwarf, GD165, but this companion has actually been resolved as a compact object using an infrared array. The object's spectrum shows deep water bands at 2 μm (Tokunaga *et al.* 1990) so it is not a background galaxy.

Of indirect techniques, astrometry has the most potential for correctly identifying the mass of a companion. The technique gained some prominence in the search for substellar companions due to the apparent astrometric discovery of low-mass companions to Barnard's star reported by Van der Kamp (1969) and the suggestion of a brown-dwarf companion to the M-dwarf VB8 (Harrington, Kallarakal & Dahn 1983). Support for the existence of both of these companions has since evaporated and in fact there is at present only one case where there astrometric evidence alone supports the existence of a brown dwarf. This case is that of the binary system Wolf 424, the members of which may both be brown dwarfs. Heintz (1989) calculated the visual orbit of the 50 year-period binary system and concluded that the masses of the components are at 50 $M_{\downarrow}$ and 60 $M_{\downarrow}$ (± 10 $M_{\downarrow}$). However the data for this orbit are sparse and the objects are of similar brightness and so their identities could have been confused. Even though there has been no astrometric survey designed specifically to look for brown dwarfs, it is interesting and significant that this is the only case of a brown dwarf candidate found by astrometry.

Recent radial-velocity surveys for brown dwarf companions to stars have also been significantly unsuccessful. Campbell, Walker & Yang (1988) observed 16 solar-type stars over a period of six years with a mean radial-velocity error

of only 13 m/s. They found radial velocity variations indicative of stellar companions to two of the stars but the possible radial-velocity variations found in a further 7 stars would probably be due to objects with *less* mass than brown dwarfs, that is, planets. Other radial-velocity surveys have typically been more extensive, but with a poorer precision. Tokovinin (1988) observed 162 K and M dwarfs over 2 years with a radial-velocity error of 500 m/s. He concluded that there was no substellar companion in the sample with period less than one year. Marcy & Benitz (1989) observed, with an error of 230 m/s, 65 M-dwarf stars. M dwarfs were chosen on the basis that less massive stars suffer larger and therefore more easily-visible gravitational perturbations and since there are many nearby, known limits to astrometric perturbations put tighter constraints on the nature of possible companions. They found no companions to their stars except for Gliese 623 (Marcy & Moore 1989) which has a mass close to the hydrogen-burning minimum mass, but a luminosity larger than theory would suggest (McCarthy & Henry 1987). The companion is probably a low-mass main sequence star. Mazeh *et al.* (1990) found no periodicities in the radial velocities of 24 M-dwarf stars observed to a precision of a few hundred metres per second over four years, although they did find one or two low-amplitude variability candidates.

Finally, Duquennoy & Mayor (1991) have presented their results on a study of multiplicity of solar-type stars in the solar neighbourhood. Their study was conducted using the CORAVEL spectrometer (Baranne, Mayor & Poncet 1979) which enables the measurement of radial velocities to better than ± 300 m/s. They find, from a complete sample of 280 stars of spectral type from F0 to G9, that 8 ± 6 per cent of stars probably have substellar companions, although they report no certain detection. They furthermore report the secondary mass function increasing towards low masses.

Perhaps the most convincing substellar mass companion to a star from radial-velocity evidence came from a programme that was not specifically looking for low-mass companions to stars. The companion to the solar-type dwarf HD 114762 found by Latham *et al.* (1989) in a programme of monitoring IAU radial-velocity standard stars has a mass of at least 11 $M_{\mathcal{Y}}$ in an 84-day orbit. From arguments relating to the probability of the orbital inclination, not only is there a very small chance that the inclination is small enough that the companion is stellar, but also a large chance that the orbit is nearly edge on, meaning that the mass is unlikely to be much more than the 11 $M_{\mathcal{Y}}$ minimum. The companion is therefore likely

to be a low-mass brown dwarf or high mass planet. The same group also found evidence for a companion to another star, the late K-type dwarf SAO 76206. In this case the lower limit to the companion mass is around 15 $M_{\mathcal{Y}}$, but again the inclination is unknown.

In summary, direct searches for brown dwarfs have come up with a few candidates as companions to stars, but in every case the surface properties of the companions are very close to what is expected at the hydrogen-burning minimum stellar mass. All these objects could in fact be stars of very low mass. This is supported by the interpretation by Henry & McCarthy (1992) of the visual orbits of 4 candidate brown dwarfs and their primary stars as being due to companions near the hydrogen-burning minimum mass. Indirect surveys to look for brown dwarfs have come up with no convincing brown dwarf candidates. On the other hand, up to three may have been found serendipitously. The Wolf 424 system must be a pair of substellar mass objects if the orbit for the system is correct and the star HD 114762 has a companion that is substellar unless the orbit is nearly in the plane of the sky, which is statistically unlikely but by no means impossible.

8.3 Status of the existence of brown dwarfs

In the Mt John programme no certain brown dwarf companions and only one possible brown dwarf companion (to β Hyi) was found despite sensitivity to brown-dwarf companions of any mass with a period less than 8.2 years (orbital distance less than 4 AU).[8] It can be said that close brown-dwarf companions to the Mt John programme stars are therefore at least rare. The Mt John programme sample is not large, but because the stars are nearly all typical solar-type dwarfs it could be suggested that brown dwarfs closer than 4 AU are rare in orbit around *any* solar-type dwarf. This conclusion is strengthened in the light of the almost identical results from the other radial-velocity searches listed above. In every case, brown-dwarf companions appear to be rare. Duquennoy & Mayor (1991) have put a number on the substellar companion frequency to solar-type stars: 8 ± 6 per cent. Although the dwarf stars in the Mt John programme do not form a complete sample like those in the Duquennoy & Mayor (1991) study, from their results, out of the 29 dwarfs in this programme, one would expect

[8] More massive brown dwarfs at greater orbital distances could have been discovered, for example all 45 $M_{\mathcal{Y}}$ objects out to 5 AU (equivalent to the orbit of Jupiter) or all 80 $M_{\mathcal{Y}}$ objects out to 6 AU.

2.3 ± 1.7 stars with radial-velocity variations suggesting possible brown dwarf companions. The single possible brown dwarf in the Mt John programme is therefore not inconsistent with the Duquennoy & Mayor (1991) results.

While dynamical surveys have found only a few candidate brown-dwarf companions to stars, the few brown-dwarf companion candidates which have arisen from photometric searches look a lot like low-mass stars themselves. Marcy & Benitz (1989) have pointed out that these results are very significant when viewed together, since radial-velocity, astrometric and photometric methods are complementary: radial-velocity methods being sensitive to orbits within about 5 AU of the primary, astrometric methods covering 5–10 AU and photometric searches being sensitive from about 10 AU to nearly 50 AU. Note, however, that although the dynamical techniques are sensitive to all brown-dwarf masses, that the photometric techniques tend to be sensitive to luminosities corresponding to brown-dwarf masses above about 40 $M_{\mathcal{Q}}$.

The interpretation of the results of searches for brown dwarfs as companions to stars is facilitated by remembering that brown dwarfs are thought to form like stars and as such, might be expected to have the same orbital characteristics that stars have. Some recent results on *stellar* companions to stars are:

- The binary fraction of late-type stars is large — between two-thirds (Duquennoy & Mayor 1991) and all (Abt 1983) of solar-type dwarf primaries have companions.
- The frequency distribution of periods of binary systems approximates a broad bell-shaped curve peaking at 180 years and is independent of the companion mass (Duquennoy & Mayor 1991).
- The mass function of secondary stars is identical to the mass function of field stars (Abt 1979; Halbwachs 1983, 1986, 1987; Duquennoy & Mayor 1991).

If the orbital characteristics of stellar companions also apply to *brown dwarf* companions then the first and second results imply that if brown dwarfs are fairly common, they should exist as binary companions in any moderately sized sample of stars and the most common period of such binary systems would be about 180 years (an orbital separation of about 30 AU for solar-type stars). However, it has been pointed out that separations of up to about 50 AU have been covered by current techniques but few brown-dwarf candidates have been found. Since

most *stellar* secondaries are closer than 50 AU, this implies that the frequency of at least high-mass ($> 40\ M_{\odot}$) brown dwarfs is in fact rather low. The third result suggests that the frequency of brown-dwarf companions as secondaries can be used as an indicator of the frequency of field brown dwarfs, implying that they are rare as well. Indeed the surveys for field brown dwarfs mentioned above (mainly deep CCD surveys) have not found many brown-dwarf candidates.

The existence of large numbers of *low-mass* brown dwarfs has not been ruled out. Although they would have been discovered in close orbits by astrometry and radial velocities, brown dwarfs with masses less than about 40 $M_{\odot}$ would not necessarily have been discovered in orbits with separations larger than 10 AU, nor would they have necessarily been discovered in the field. The existence of large numbers of low-mass brown dwarfs in the face of the rarity of higher-mass brown dwarfs would suggest either a bimodal mechanism of star-like formation by fragmentation (one mechanism for stellar masses and another for substellar masses) or simply that the upper limit for masses formed like planets is in the brown-dwarf mass range. These hypothetical low-mass brown dwarfs might in the latter case more properly be called planets.

The scarcity of high-mass brown dwarfs has implications for star formation and for the solar neighbourhood mass density. Several objects have been discovered near the hydrogen-burning minimum mass but very few are certainly below it. Assuming the discovered objects are actually stars then either the expected luminosities of high-mass brown dwarfs have been overestimated or there is a real discontinuity in the mass function at the hydrogen-burning minimum mass. The question that would need to be answered in the latter case is why should stars not be formed just because their mass won't be large enough for hydrogen fusion reactions?

Next, the 'missing mass' in the solar neighbourhood was estimated to be around 100 $M_{\odot}\mathrm{pc}^{-3}$ (Bahcall 1984a). Certainly nowhere near this density of brown dwarfs is observed in the form of high-mass brown dwarfs. It is interesting that although low-mass brown dwarfs in the field or in wide orbits could still account for the solar-neighbourhood missing mass, a recent re-calculation (Kuijken & Gilmore 1989) has suggested that the local missing mass problem might not exist anyway. If this is true, the motivation behind the suspicion of large numbers of brown dwarfs virtually disappears (as long as a discontinuity of the mass function across the hydrogen-burning minimum mass can be accepted).

Although evidence for local missing mass is unclear, evidence for massive haloes is still overwhelming. The problem has been examined theoretically whether these massive haloes could be made up of baryonic matter. The general answer is that they cannot, unless the matter is in compact objects (like brown dwarfs). No one has yet ruled out the possibility of the existence of brown dwarfs in the halo (Adams & Walker 1990) which might be looked for by searches for the gravitational microlensing of Magellanic Cloud stars, for example (Gott 1981).

The point may be raised whether brown dwarfs (in the sense of substellar objects *formed like stars*) exist *at all.* In the Mt John programme and in other programmes there is in nearly every case a simple reason why a candidate brown dwarf might truly be a star. This might be due to poor theoretical expectations of brown-dwarf colours, luminosities or spectra, or simply to a poorly-determined system distance or a large orbital inclination. Marcy & Benitz (1989) have considered the fact that there are so many objects identified near the hydrogen-burning minimum mass (*e.g.* in direct searches) and yet so few suggested beneath it. They point out the similarity between the theory (Shu, Adams & Lizano 1987) which suggests that objects should not form with masses less than the mass at which deuterium-burning can occur (15 $M_{\downarrow}$) and the fact that objects (other than planets) do not seem to be observed with masses less than the mass at which hydrogen-burning can occur. As yet there is in fact no theory to suggest that objects should not form by fragmentation below the hydrogen-burning minimum mass. Such a theory could accommodate the observation of some 'brown-dwarf' mass objects as long as these turned out to be formed like planets rather than like stars.

Chapter 9

Summary and future work

9.1 Summary

In the Mt John radial-velocity programme it has been demonstrated that by using relatively simple equipment, very precise relative radial velocities (random error around ± 50 m/s) can be obtained of bright stars over the years required for a dynamical search for low-mass companions. Other recent programmes aiming to obtain radial velocities with errors less than 100 m/s have primarily approached the problem by imposing wavelength fiducials on the stellar spectrum to trace accurately the instrumental and other instabilities which thwart high-precision velocities. In many cases this has required complex instrumentation and reduction procedures. In this programme however, it has been demonstrated that by merely reducing the instabilities while retaining simple, conventional techniques for applying a wavelength reference, radial velocities of high precision can still be obtained.

The placement of an optical fibre feed between the telescope and spectrograph in the Mt John programme enabled the spectrograph to be mounted in a mechanically and thermally stable situation. This, and the fact that scrambling of starlight in the fibre dramatically reduces guiding errors has reduced radial-velocity errors from the few hundred metres per second typical for this kind of set-up without a fibre feed, to around 50 m/s. At this level the radial-velocity error is still not dominated by the photon noise in the stellar spectrum but is principally made up of a term from the error in the run-to-run correction and an exposure-time dependent term from instrumental sources (from the inability of the averaged dispersion solution to fully describe the dispersion throughout the

stellar exposure).

Using this system, 29 solar-type dwarfs and sub-giants (spectral types F5–K5, luminosity classes IV–V) and 10 giant International Astronomical Union standard stars were observed approximately monthly over a period of about 2.5 years. The aim was the discovery of low-amplitude single-lined spectroscopic binaries indicative of substellar mass companions to the stars. However, although the precision and timing of observations in the Mt John programme allowed the detection of secondaries with (for example) mass greater than 10 $M_{\mathcal{Q}}$ in orbits of periods less than 5.5 years (see Figure 8.1), only one previously unknown single-lined spectroscopic binary was actually found without ambiguity (HR 3220). The lower limit[1] to the mass of the companion of HR 3220 is 0.20 $M_{\odot}$, that is, the companion is a star. Another dwarf (β Hyi) emerged from the tests for variability (Chapter 6) as a possible low-amplitude radial-velocity variable. If the velocity variation is real then a substellar mass companion to the star could be implied, but the variability status is considered to be provisional.

In contrast, what is probably intrinsic variability was found in at least four and possibly five of the ten giant IAU radial-velocity standard stars. The variables include the three M giants in the programme (γ Cru, α Cet and δ Oph) which are probably radial pulsators of the irregular red variable type and a K giant (α Hya), which was also studied by Walker *et al.* (1988) and deemed to belong to a new class of 'yellow' intrinsic variable. Another G9 giant (β Cet), which was classified as a marginal variable in Chapter 6, may also be a yellow variable. Two further standard stars (δ Sgr and β Aqr) show rather longer period variability than the others. In both cases the variability is probably indicative of centre-of-mass motion of the star. δ Sgr has a slope to its velocities suggesting a variation of indeterminately long period but the curvature of β Aqr's velocity suggests that the period may not be much longer than the observing time-span of 1000 d. Unfortunately, less than one cycle of the variation was observed for β Aqr so no orbit could be obtained. This result is tantalizing as the companion could very well be substellar if the period of the variation turns out to be less than 1800 d.

The results of the Mt John programme are consistent with those of other radial-velocity programmes by Campbell, Walker & Yang (1988), Tokovinin (1988), Marcy & Benitz (1989) and Duquennoy & Mayor (1991). Brown dwarfs seem to be at the most rare as close (> 10 AU) companions to stars. Considering also the

[1] Since the inclination of the orbit is unknown.

results of photometric surveys for brown dwarfs, it appears that high-mass brown dwarfs are rare at best in the field and in orbits of all separations. High-mass brown dwarfs are unlikely to contribute significantly to the local mass density. Low-mass brown dwarfs, on the other hand, could have escaped detection until now in long-period orbits or in the field and could therefore possibly comprise the solar neighbourhood 'missing mass' (if there really is a missing mass problem). In this case the lack of continuity in the frequency distributions of low-mass brown dwarfs and low-mass stars would imply two different formation scenarios. This could be the difference in formation mechanisms between stars and planets. In this case the abundant low-mass brown dwarfs might more properly be called planets.

9.2 Future work

It has been suggested (Walker 1992) that the procedures employed in this study for obtaining high-precision radial velocities achieve the limiting precision for such a classical technique[2]. While a typical radial-velocity error bar of 55 m/s is up to a factor of ten better than might routinely be obtained without a fibre feed, this error could conceivably be reduced further to about 10–15 m/s while retaining the 'classical' technique. It was noted in Chapter 5 that the root-mean-squared velocity scatter of exposures of bright stars taken over a couple of days was about 10–15 m/s. The error is only larger in the longer term and for fainter stars because of longer exposures and the need for corrections between runs. Exposure times could however be decreased if the throughput of the system were improved with for example, an image slicer, or through installing a larger format detector, in which case the increased spectral coverage would relax the spectrum signal-to-noise requirements for a given photon noise-limited radial-velocity precision. The error in run corrections could be reduced by stabilizing the pressure of the spectrograph and keeping it always on the fibre feed system so that the fibre alignment on the slit need not be different from one run to the next. This would have the second-order effect of further decreasing exposure times as eliminating the fibre alignment problem would allow the spectrograph slit to be opened up to its optimum value (see Section 3.3.1).

[2]'Classical' referring to the fact that wavelength reference is obtained by recording a comparison spectrum before and after the stellar spectrum, rather than by wavelength fiducials being applied to the stellar spectrum.

It is clear that long-term radial-velocity programmes of high precision still have their place in searching for substellar companions to stars. The radial-velocity technique is one of the two techniques available where the most relevant parameter of the companion, the mass, can be determined dynamically, and because it is more sensitive to shorter-period orbits, can deliver orbits over relatively small time scales. The ambiguity of the orbital inclination is often considered to be a problem, but in practice putative brown dwarfs found by the radial-velocity technique can be observed by a complementary technique in order to provide more complete information.

Radial-velocity programmes have already produced a significant negative result for brown-dwarf companions in close orbits to stars. Although further programmes with more stars, longer-term coverage and greater sensitivity would be enlightening in making further comment on the existence of companion brown dwarfs to stars, in future the companions to search for would be the upper planetary masses rather than brown-dwarf masses, which appear scarce. This will require correspondingly better precision. Another use for very precise radial velocities would be the study of low-amplitude radial-velocity variability in late-type giants. This might allow a more fuller understanding of the nature of their pulsations.

The other technique where the mass of the companion is determined dynamically is astrometry. Most astrometric programmes so far have not been specifically designed for searches for brown dwarfs. Part of the problem is that the astrometric perturbation is largest for longer period orbits and therefore observing programmes are necessarily long as well as requiring high precision over their duration. However astrometric programmes have a unique role to play in searches for low-mass companions. The possibility of brown dwarfs in long-period orbits has only been investigated by programmes of infrared imaging around stars. Such programmes are sensitive mostly to high-mass brown dwarfs and have found few candidates. Astrometric programmes (possibly space-based) could look for low-mass brown dwarfs in long-period orbits. Astrometry would also be of use to searches for planetary systems, since the little we already know about planets suggests that the 'gas giants' should form at larger radii.

Acknowledgements

Thanks to my supervisor, John Hearnshaw, for initiating this project and providing support and advice throughout its duration.

Thanks to Mike Clark for making half of the observations and helping out with my observing problems. Peter Cottrell got the diode array functional again — thank you, and thanks to Dave Latham for his hospitality in Massachussetts. Warrick Lawson provided me with a programme for the analysis of periodicities in unevenly spaced data and gave me advice on its use, for which I am grateful.

For the duration of this work I was supported by a New Zealand Vice Chancellor's Committee Scholarship (*ex* University Grants Committee Scholarship) and a Ministry of Research, Science and Technology Women's Study Award (ex. Department of Scientific and Industrial Research Women's Study Award). I am indebted to Zonta International for their support in 1989 via an Amelia Earhart Award, in particular to the New Zealand branches of Zonta who fund-raise every year to maintain the Amelia Earhart Awards. During my seven months at the Harvard-Smithsonian Center for Astrophysics in 1989 and 1990 I was supported by a Smithsonian Pre-doctoral Fellowship. I also acknowledge financial support from: the Kingdon-Tomlinson Bequest of the Royal Astronomical Society of New Zealand towards my visit to the Dominion Astrophysical Observatory, Victoria, Canada in 1989; the Vatican Observatory and the Royal Society of New Zealand's Young Scientists' Fund for attendance at the Vatican Observatory's 1990 Summer School in Observational Astronomy and Astrophysics at Castel Gandolfo, Italy; the Mars group of companies for eating their chocolate bars, 1991; the International Astronomical Union, the University of Canterbury's Physics and Astronomy Department, the Kingdon-Tomlinson Bequest of the RASNZ and the Frank Bradshaw and Elizabeth Pepper Wood Fund for attendance of IAU Colloquium 135 at Pine Mountain, Georgia, U.S.A. in 1992.

Lastly, thanks to my fellow astronomy students for light relief — Warrick,

Jason, Steve, Alan, Donna, Karen, Michael, David and Lyndon. Thanks also to Jason for computer help (although he never *did* set any of my processes at priority 14) and for being a fish.

References

Abt, H. A., 1979. *Astron. J.*, **84**, 1591.

Abt, H. A., 1983. *Ann. Rev. Astron. Astrophys.*, **21**, 343.

Adams, F. C. & Walker, T. P., 1990. *Astrophys. J.*, **359**, 57.

Allen, C. W., 1973. *Astrophysical Quantities*, Ch.4, (London: Athlone Press).

Bahcall, J. N., 1984a. *Astrophys. J.*, **276**, 169.

Bahcall, J. N., 1984b. *Astrophys. J.*, **287**, 926.

Bahcall, J. N. & Soneira, R. M., 1980. *Astrophys. J. Suppl. Ser.*, 44, 73.

Barden, S. C. 1988. In *Fiber Optics in Astronomy*, edited by S. C. Barden, p. 40, (San Francisco: Astronomical Society of the Pacific).

Ball, J. A., 1976. In *Methods of Experimental Physics*, edited by M. L. Meeks, **12**, p308, (New York: Academic Press).

Balona, L. A., 1987. *South African Astronomical Observatory Circulars*, **11**, 1.

Baranne, A., Mayor, M. & Poncet, J. L., 1979. *Vistas in Astron.*, **23**, 279.

Barnes, T. G. & Evans, D. S., 1976. *Mon. Not. Roy. Astr.. Soc*, **174**, 489.

Batten, A. H., Fletcher, J. M. & MacCarthy, D. G., 1989. *Publ. Dominion Astrophysical Observatory*, **17**, 1.

Beckers, J. M., Bridges, C. A. & Gilliam, L. B., 1976. *A High Resolution Spectral Atlas of Solar Irradiance from 380 to 700 nanometers* Res. Pap. No. 565 AFGL-TR-76-0126(II) (Sacramento Peak Observatory: Sunspot).

Becklin, E. E. & Zuckerman, B., 1988. *Nature*, **336**, 656.

Benz, W., 1979. *Rotation Stellaire par la méthode de corrélation*, Geneva Observatory.

Bessell, M. S., 1991. *Astron. J.*, **101**, 662.

Boeshaar, P. C., Tyson, J. A. & Seitzer, P., 1985. In *Astrophysics of Brown Dwarfs* edited by M. C. Kafatos, R. S. Harrington & S. P. Maran, p. 76, (Cambridge: Cambridge University Press).

Borchers, H. & Schmidt, E., 1964. eds *Landolt-Börnstein: Numerical Data and Functional Relationships in Physics, Chemistry, Astronomy, Geophysics and Technology*, **IV, 2b**, 46 (Berlin: Springer-Verlag).

Boss, A. P., 1986. In *Astrophysics of Brown Dwarfs* edited by M. C. Kafatos, R. S. Harrington & S. P. Maran, p. 206, (Cambridge: Cambridge University Press).

Brault, J. M. & White, O. R., 1971. *Astron. Astrophys.*, **13**, 169.

Brosius, J. W., Mullan, D. J. & Stencel, R. E., 1985. *Astrophys. J.*, **288**, 310.

Brown, R. A., 1989. in *Joint Workshop on Planetary Science*, Moscow.

Burrows, A., Hubbard, W. B. & Lunine, J. I., 1989, *Astrophys. J.*, **345**, 939.

Campbell, B. & Garrison, R. F., 1985. *Publ. Astr. Soc. Pac.*, **97**, 180.

Campbell, B. & Walker, G. A. H., 1979. *Publ. Astr. Soc. Pac.*, **91**, 540.

Campbell, B., Walker, G. A. H. & Yang, S., 1988. *Astrophys. J.*, **331**, 902.

Carney, B. W., Laird, J. B., Latham, D. W. & Kurucz, R. L., 1987. *Astron. J.*, **94**, 1066.

Clerke, A. M., 1903. *Problems in Astrophysics*, p. 400., (London: Adam & Charles Black).

Cochran, W. D., 1988. *Astrophys. J.*, **334**, 349.

Cochran, W. D. & Hatzes, A. P., 1990. *Proc. SPIE*, **1318**, 148.

Collier, A. C., 1982. *Ph.D. thesis*, University of Canterbury.

Connes, P., 1985. *Astrophys. Space Sci.*, **110**, 211.

Cox, J. P., 1974. *Rep. Prog. Phys.*, **37**, 563.

Cox, J. P. & Giuli, R. T., 1968, *Principles of Stellar Structure*, **2**, p. 1033, (New York: Gordon & Breach).

Da Costa, G. S., Freeman, K. C., Kalnajs, A. J., Rodgers, A. W. & Stapinski, T. E., 1977. *Astron. J.*, **82**, 810.

D'Antona, F., 1987. *Astrophys. J.*, **320**, 653.

D'Antona, F. & Mazzitelli, I., 1985. *Astrophys. J.*, **296**, 502.

Duquennoy, A. & Mayor, M., 1991. *Astron. Astrophys.*, **248**, 485.

Duquennoy, A., Mayor, M. & Halbwachs, J.-L., 1991. *Astron. Astrophys. Suppl. Ser.*, **88**, 281.

Diego, F., 1985. *Publ. Astr. Soc. Pac.*, **97**, 1209.

Eggen, O. J., 1973. *Astrophys. J.*, **184**, 793.

Enard, D., Lund,. G. & Tarenghi, M., 1983. *ESO Messenger*, **33**, 32.

Fernie, J. D., 1976. *Publ. Astr. Soc. Pac.*, **88**, 116.

Flower, D. J., 1975. *Astron. Astrophys.*, **41**, 391.

Forrest, W. J., Garnett, J.D., Ninkov, Z., Skrutskie, M. & Shure, M., 1989. *Publ. Astr. Soc. Pac.*, **101**, 877.

Forrest, W. J., Skrutskie, M. F. & Shure, M., 1988. *Astrophys. J.*, **330**, L119.

Fox, M. W. & Wood, P. R., 1982. *Astrophys. J.*, **259**, 198.

Gott, J. R., 1981. *Astrophys. J.*, **243**, 140.

Graham, J. R., McCarthy, J. K., Reid, I. N. & Rich, R. M., 1990. *Astrophys. J.*, **357**, L21.

Gray, D., 1972. (ed.) *American Institute of Physics Handbook 3rd ed.*, p. 6-111, (New York: McGraw-Hill).

Gray, D. F., 1976. *The Observation and Analysis of Stellar Photospheres*, Ch.11, (New York: Wiley).

Gray, D. F. & Toner, C. G., 1987. *Astrophys. J.*, **322**, 360.

Griffin, R., 1967. *Astrophys. J.*, **148**, 465.

Griffin, R. & Griffin, R., 1973. *Mon. Not. Roy. Astr. Soc*, **162**, 243.

Grossman, A. S., 1970. *Astrophys. J.*, **161**, 619.

Grossman, A. S., Mutschlecner, J. P. & Pauls, T.A., 1970. *Astrophys. J.*, **162**, 613.

Grossman, A. S. & Graboske, H. C. Jr., 1971. *Astrophys. J.*, **164**, 475.

Halbwachs, J. L., 1983. *Astron. Astrophys.*, **128**, 399.

Halbwachs, J. L., 1986. *Astron. Astrophys.*, **168**, 161.

Halbwachs, J. L., 1987. *Astron. Astrophys.*, **183**, 234.

Hambly, N. C., Hawkins, M. R. S. & Jameson, R. F., 1991. *Mon. Not. Roy. Astr. Soc.*, **253**, 1.

Hambly, N. C. & Jameson, R. F., 1991. *Mon. Not. Roy. Astr. Soc.*, **249**, 137.

Harrington, R. S., Kallarakal, V. V. & Dahn, C. C., 1983. *Astron. J.*, **88**, 1038.

Hawkins, M. R. S., 1986. *Mon. Not. Roy. Astr. Soc.*, **223**, 845.

Hawkins, M. R. S. & Bessell, M. S., 1988. *Mon. Not. Roy. Astr. Soc.*, **234**, 177.

Hearnshaw, J. B., 1977. *Proc. Astron. Soc. Australia*, **3**, 102.

Hearnshaw, J. B., 1978. *Sky and Telescope*, **56**, 6.

Heintz, W. D., 1982. *The Observatory*, **102**, 42.

Heintz, W. D., 1989. *Astron. Astrophys.*, **217**, 145.

Heintz, W. D., 1992. Private communication.

Henry, T. J. & McCarthy, D. W., 1992. In *Complementary Approaches to Double and Multiple Star Research, IAU Colloquium 135*, edited by H. A. McAlister & W. I. Hartkopf, p. 10, (San Francisco: Astronomical Society of the Pacific).

Henry, T. J. & Kirkpatrick, J. D., 1990. *Astrophys. J.*, **354**, L29.

Henry, T. J. & McCarthy, D. W. Jr., 1990. *Astrophys. J.*, **350**, 334.

Hill, G., 1982. *Publ. Dominion Astrophysical Observatory*, **16**, 59.

Hirshfeld, A. H. & Sinnott, R. W., 1982. (eds.) *Sky Catalogue 2000.0*, (Cambridge: Cambridge University Press).

Hoffleit, D., 1982. *The Bright Star Catalogue*, (New Haven: Yale University Observatory).

Hoffmeister, C., Richter, G. & Wenzel, W., 1985. *Variable Stars*, Ch. 2, (Berlin: Springer-Verlag).

Houk, N. & Cowley, A. P. 1975. *Michigan Spectral Catalogue*, (Ann Arbor: University of Michigan).

Innis, J. L., Isaak, G. R. & Isaak, K., 1990. *The Observatory*, **110**, 188.

Isobe, T., Feigelson, E. D., Akritas, M. G. & Babu, G. J., 1990., *Astrophys. J.*, **364**, 104.

Jameson, R. F., Sherrington, M. R. & Giles, A. B., 1983. *Mon. Not. Roy. Astr. Soc.*, **205**, 39P.

Jameson, R. F. & Skillen, I., 1989. *Mon. Not. Roy. Astr. Soc.*, **239**, 247.

Kapany, N. S., 1967. *Fiber Optics: Principles and Applications*, (New York: Academic Press).

Kershaw, G. M. & Hearnshaw, J. B., 1989. *Southern Stars*, **33**, 89.

Kroupa, P., Tout, C. A. & Gilmore, G., 1990. *Mon. Not. Roy. Astr. Soc.*, **244**, 76.

Krum, N. & Salpeter, E. E., 1976. *Astrophys. J.*, **208**, L7.

Krum, N. & Salpeter, E. E., 1977. *Astron. Astrophys.*, **56**, 455.

Kuijken, K. & Gilmore, G., 1989. *Mon. Not. Roy. Astr. Soc.*, **239**, 651.

Kumar, S. S., 1963. *Astrophys. J.*, **137**, 1121.

Kumar, S. S., 1972. *Astrophys. Space Sci.*, **17**, 216.

Kumar, C. K., 1987. *Astron. J.*, **94**, 158.

Kurtz, D. W. & Marang, F., 1987. *Mon. Not. Roy. Astr. Soc.*, **228**, 141.

Kurucz, R. L., 1979. *Astrophys. J. Suppl. Ser.*, **40**, 1.

Lang, K. R., 1992. *Astrophysical Data: Planets and Stars*, p. 132, (New York: Springer-Verlag).

Latham, D. W., 1985. In *Stellar Radial Velocities, IAU Colloquium 88*, edited by A.G.D. Philip & D. W. Latham, p. 21, (Schenectady: L. Davis Press).

Latham, D. W., Mazeh, T., Stefanik, R. P., Mayor, M. & Burki, G., 1989. *Nature*, **339**, 38.

Lawson, W. A., Cottrell, P. L., Kilmartin, P. M. & Gilmore, A. C., 1990. *Mon. Not. Roy. Astr. Soc*, **247**, 91.

Leggett, S. K. & Hawkins, M. R. S., 1988. *Mon. Not. Roy. Astr. Soc.*, **234**, 1065.

Liebert, J. & Probst, R. G., 1987. *Ann. Rev. Astron. Astrophys.*, **25**, 473.

Lippincott, S. L., 1978. *Space Sci. Rev.*, **22**, 153.

Lippincott, S. L. & Worth, M. D., 1980. *Astron. J.*, **85**, 171.

Lomb, N. R., 1976. *Astrophys. Space Sci.*, **39**, 447.

Low, C. & Lynden-Bell, D., 1976. *Mon. Not. Roy. Astr. Soc.*, **176**, 367.

MacQueen, P. J., 1986. *Ph.D. thesis*, University of Canterbury.

Marcy, G. W. & Benitz, K. J., 1989. *Astrophys. J.*, **344**, 441.

Marcy, G. W, & Butler, R. P., 1992. *Publ. Astr. Soc. Pac.*, **104**, 270.

Marcy, G. W., Lindsay, V. & Wilson, K., 1987. *Publ. Astr. Soc. Pac.*, **99**, 490.

Marcy, G. W. & Moore, D., 1989. *Astrophys. J.*, **341**, 961.

Martinez, P., 1989. *Mon. Not. Roy. Astr. Soc.*, **238**, 439.

Mayor, M., 1985. In: *Stellar Radial Velocities, IAU Colloquium 88*, eds Philip, A.G.D. & Latham, D.W., p. 35, (Schenectady: L. Davis Press).

Mayor, M. & Maurice, E., 1985. In: *Stellar Radial Velocities, IAU Colloquium 88*, eds Philip, A.G.D. & Latham, D.W., p. 299, (Schenectady: L. Davis Press).

Mazeh, T., Latham, D. W., Stefanik, R. P., Torres, G. & Wasserman, E., 1990. *NATO Advanced Study Institute on Active Close Binaries*, edited by C. İbanoğlu, p.267, (Dordrecht: Kluwer).

McAlister, H. A., 1988. *American Scientist*, **76**, 166.

McCarthy, D. W. & Henry, T. J., 1987. *Astrophys. J.*, **319**, L93.

McCarthy, D. W., Probst, R. G. & Low, F. J., 1985. *Astrophys. J.*, 348, L37.

McMillan, R. S., Smith, P. H., Frecker, J. E., Merline, W. J. & Perry, M. L., 1985. In *Stellar Radial Velocities, IAU Colloquium 88*, edited by A.G.D. Philip & D.W. Latham, p.63, (Schenectady: L. Davis Press).

McNally, D., 1988. (ed.) *Trans. I.A.U.*, **20b**, 267.

Merline, W. J., 1985. In *Stellar Radial Velocities, IAU Colloquium 88*, edited by A. G. D. Philip & D.W. Latham, p.87, (Schenectady: L. Davis Press).

Murdoch, K. & Hearnshaw, J. B., 1991a. *Astrophys. Space Sci*, **186**, 137.

Murdoch, K. & Hearnshaw, J. B., 1991b. *Astrophys. Space Sci*, **186**, 169.

Murdoch, K. , Clark, M. & Hearnshaw, J. B., 1992. *Mon. Not. Roy. Astr. Soc*, **254**, 27.

Nankivell, G. R. & Rumsey, N. J., 1986. In *Instrumentation and Research Programmes for Small Telescopes, IAU Symposium 118*, edited by J. B. Hearnshaw & P. L. Cottrell, p.101, (Dordrecht: Reidel).

Nelson, L. A., Rappaport, S. A. & Joss, P. C., 1986. *Astrophys. J.*, **311**, 226.

Novotny, E., 1973. *Introduction to Stellar Atmospheres & Interiors*, p. 350, (New York: Oxford University Press).

Ochsenbein, F. & Halbwachs, J. L., 1982. *Astron. Astrophys. Suppl. Ser.*, **47**, 523.

Oort, J. H., 1932. *Bull. Astr. Inst. Neth.*, **6**, 249.

Oort, J. H., 1960. *Bull. Astr. Inst. Neth.*, **16**, 45.

Ostriker, J. P. & Peebles, P. J. E., 1973. *Astrophys. J.*, **186**, 467.

Parsons, S. B. & Bouw, G. D., 1971. *Mon. Not. Roy. Astr. Soc.*, **152**, 133.

Paczyński, B., 1991. *Astrophys. J.*, **371**, L63.

Pearce, J. A., 1957. *Trans. I.A.U.*, **9**, 441.

Perrier, C. & Mariotti, J.-M., 1987. *Astrophys. J.*, **312**, L27.

Percy, J. R., Landis, H. J. & Milton, R. E., 1989. *Publ. Astr. Soc. Pac.*, **101**, 893.

Petit, M., 1990. *Astron. Astrophys. Suppl. Ser.*, **85**, 971.

Pollack, J. B., 1984. *Ann. Rev. Astron. Astrophys.*, **22**, 389.

Press, W. H., Flannery, B. P., Teukolsky, S. A. & Vetterling, W. T., 1988. *Numerical Recipes.*, Ch.14, (New York: Cambridge University Press).

Press, W. H. & Teukolsky, S. A., 1988. *Computers in Physics*, Nov/Dec, p. 77, (New York: American Institute of Physics).

Reid, N. & Gilmore, G., 1984. *Mon. Not. Roy. Astr. Soc.*, **206**, 19.

Rieke, G. & Rieke, M. J., 1990. *Astrophys. J.*, **362**, L21.

Roberts, M. S., 1976. *Comments Astrophys.*, **6**, 105.

Robinson, E. L., Cochran, A. L., Cochran, W. D. & Shafter, A. W., 1990. *Astron. J.*, **99**, 672.

Rubin, V. C., Ford, W. K. Jr. & Thonnard, N., 1978. *Astrophys. J.*, **225**, L107.

Salpeter, E. E., 1955. *Astrophys. J.*, **121**, 161.

Scalo, J. M., 1986. *Fundamentals of Cosmic Physics*, **11**, 1.

Scarfe, C. D., Batten. A. H. & Fletcher, J. M., 1989. *Publ. Dominion Astrophysical Observatory*, **18**, 21.

Scargle, J. D., 1982. *Astrophys. J.*, **263**, 835.

Serkowski, K., 1976, *Icarus*, **27**, 13.

Shipman, H. L., 1985. In *Astrophysics of Brown Dwarfs* edited by M. C. Kafatos, R. S. Harrington & S. P. Maran, p. 71, (Cambridge: Cambridge University Press).

Shu, F. H., Adams, F. C. & Lizano, S., 1987. *Ann. Rev. Astron. Astrophys.*, **25**, 23.

Simkin, S. M., 1974. *Astron. Astrophys.*, **31**, 129.

Skrutskie, M. F., Forrest, W. J. & Shure, M., 1986. In *Astrophysics of Brown Dwarfs* edited by M. C. Kafatos, R. S. Harrington & S. P. Maran, p. 82, (Cambridge: Cambridge University Press).

Skrutskie, M. F., Forrest, W. J. & Shure, M., 1987. *Astrophys. J.*, **312**, L55.

Skrutskie, M. F., Forrest, W. J. & Shure, M., 1989. *Astron. J.*, **98**, 1409.

Smith, M., 1982. *Astrophys. J.*, **253**, 727.

Smith, M., 1983. *Astrophys. J.*, **265**, 325.

Smith, S., 1936. *Astrophys. J.*, **83**, 23.

Soderblom, D. R., 1982. *Astrophys. J.*, **261**, 259.

Stauffer, J., Hamilton, D., Probst, R., Rieke, G. & Mateo, M., 1989. *Astrophys. J.*, **344**, L21.

Stauffer, J., Herter, T., Hamilton, D., Rieke, G. H., Rieke, M. J., Probst, R. & Forrest, W., 1991. *Astrophys. J.*, **367**, L23.

Stevenson, D. J., 1978. *Proc. Astr. Soc. Australia*, **3**, 227.

Stevenson, D. J., 1991. *Ann. Rev. Astron. Astrophys.*, **29**, 163.

Strand, K. A., 1951. *Astrophys. J.*, **113**, 1.

Stumpff, P., 1980. *Astron. Astrophys. Suppl. Ser.*, **41**, 1.

Tarter, J. C., 1975. *Ph.D. thesis*, University of California, Berkeley.

Tokovinin, A. A., 1988. *Astrophys.*, **28**, 173.

Tokunaga, A. T., Brooke, T. Y., Becklin, E. E. & Zuckerman, B., 1990. *Bull. Amer. Astr. Soc.*, **22**, 1078.

Tokunaga, A. T., Hodapp, K. W., Becklin, E. E., Cruickshank, D. P., Rigler, M. Toomey, D., Brown, R. H. & Zuckerman, B., 1988. *Astrophys. J.*, **332**, L71.

Trimble, V., 1987. *Ann. Rev. Astron. Astrophys.*, **25**, 425.

Tull, R. G., 1969. *Appl. Optics*, **8**, 1635.

Van der Kamp, P., 1969. *Astron. J.*, **74**, 757.

Walker, G. A. H., 1992. In *Complementary Approaches to Double and Multiple Star Research, IAU Colloquium 135*, in press.

Walker, G. A. H., Yang, S., Campbell, B. & Irwin, A. W., 1989. *Astrophys. J.*, **343**, L21.

Wetherill, G. W., 1980. *Ann. Rev. Astron. Astrophys.*, **18**, 77.

Wilson, O. C., 1941. *Astrophys. J.*, **93**, 29.

Wingert, D. E., Natter, R. E., Clemens, J. C., Provencal, J., Kleinman, S. J., Bradley, P. A., Wood, M. A., Claver, C. F., Robinson, E. L., Graver, A. D., Hine, B. P., Fontaine, G., Achilleos, N., Marar, T. M. K., Seetha, S., Ashoka, B. N., O'Donoghue, D., Warner, B., Kurtz, D. W., Martinez, P., Vauclair, G., Chevreton, M., Kanaan, A., Kepler, S. O., Augusteijn, T., van Paradijs, J., Hansen, C. J. & Liebert, J. 1990. *Astrophys. J.*, **357**, 630.

Wolszczan, A. & Frail, D. A., 1992. *Nature*, **355**, 145.

Wyatt, W. F., 1985. In *Stellar Radial Velocities, IAU Colloquium 88*, edited by A.G.D. Philip & D.W. Latham, p.123, (Schenectady: L. Davis Press).

Zuckerman, B. & Becklin, E. E., 1987a. *Astrophys. J.*, **319**, L99.

Zuckerman, B. & Becklin, E. E., 1987b. *Nature*, **330**, 138.

Zwicky, F., 1933. *Helv. Phys. Acta*, **6**, 110.

Appendix A

Symbol definitions

Below are listed the mathematical symbols used in this thesis. Along with each symbol is listed its meaning and the chapter in which it first appeared.

Symbol	Chap.	Definition
α	6	Constant in equation relating ϵ_v with m and $\epsilon_{\rm run}$.
a	4	Orbital semi-major axis.
A	2	height of normalized cross-correlation function.
c	2	Speed of light in a vacuum.
C	6	Curvature in a time-series of radial velocities.
C_l	2	lth normalized element of the discrete cross-correlation function.
D	2	Root-mean-squared line depth.
$\epsilon_{\rm bc}$	5	Random error in radial velocity from uncertainties in the barycentric correction.
ϵ_C	2	Random error in the cross-correlation function.
ϵ_C	6	Random error in the estimation of the curvature in a time series of radial velocities.
$\epsilon_{\rm disp}$	5	Random error in radial velocity from uncertainties in the dispersion solution.
$\epsilon_{\rm instr}$	5	Random error in radial velocity from instrumental sources.

Symbol	Chap.	Definition
ϵ_p	2	Random error in radial velocity from photon noise only.
ϵ_{run}	5	Random error in radial velocity from differences in the run-to-run set-up.
ϵ_S	6	Random error in the estimation of the slope in a time-series of radial velocities.
ϵ_v	5	Overall random error in radial velocity.
e	4	Orbital eccentricity.
$f(M)$	1	Spectroscopic mass function.
F	2	Continuum signal.
F_0	6	F-statistic = ratio of the observed variance σ^2_{obs} of radial velocities to the variance of the presumed random error in radial velocites ϵ^2_v such that $F_0 > 1$.
i	4	Inclination of orbit to the plane of the sky.
I_λ	2	Spectral intensity at wavelength λ.
K	4	Radial-velocity semi-amplitude of spectroscopic orbit.
λ	2	Wavelength.
$L_\odot$	1	Solar luminosity unit.
m	2	Magnification between the slit and the image at the detector.
m	6	Stellar magnitude.
M	1	Mass.
$M_\odot$	1	Solar mass.
$M_\jmath$	1	Jupiter mass.
M_1	1	Primary star mass.
M_2	1	Secondary (companion) mass.
N	2	Number of points in a discretely-recorded spectrum.
N_{lines}	2	Number of spectral lines in recorded spectrum.
ω	4	Longitude of periastron of a spectroscopic orbit.
π_p	1	Parallax in arc s.
P	4	Period of orbit.

Symbol	Chap.	Definition
$P(F > F_0)$	6	Probability that the F-statistic would be as large as F_0 were the observed scatter due to random noise only.
P_C	6	Probability that $\|C\|/\epsilon_C$ in randomized radial-velocity time series of a star would exceed $\|C\|/\epsilon_C$ in the true radial-velocity time series.
P_S	6	Probability that $\|S\|/\epsilon_S$ in randomized radial-velocity time series of a star would exceed $\|S\|/\epsilon_S$ in the true radial-velocity time series.
ρ	2	Proportionality constant between spectrograph slit width and portion of stellar line width dependent on spectrograph slit width.
R	2	Root-mean-squared value of the signal in a recorded spectrum.
σ_0	2	Portion of stellar line half-$\frac{1}{e}$-width which is independent of spectrograph slit width ($= \sqrt{\sigma_{\rm pixel} + \sigma_{\rm Dopp}}$).
σ_*	2	Seeing half-$\frac{1}{e}$-width.
$\sigma_{\rm Dopp}$	2	Doppler half-$\frac{1}{e}$-width of a spectral line.
$\sigma_{\rm line}$	2	Half-$\frac{1}{e}$-spectral line width.
$\sigma_{\rm obs}$	4	Observed root-mean-squared scatter of a star's radial velocities.
$\sigma_{\rm pixel}$	2	Half-$\frac{1}{e}$ recorded line width due to the finite width of pixels of the detector.
S	6	Slope in a time series of radial velocities.
S/N	2	Spectral signal-to-noise ratio.
θ	1	Astrometric perturbation in arc s.
T_0	4	Julian day -2440000 of periastron passage for a spectroscopic orbit.
T_λ	2	Fractional transmission of starlight through the atmosphere and all optical elements other than the slit.
$T_{\rm slit}$	2	Fractional transmission of starlight through spectrograph slit.

Symbol	Chap.	Definition
v	2	Radial velocity.
$v_{\rm rot}$	6	Rotational velocity.
w	2	Spectrograph slit width.
$w_{\rm opt}$	2	Optimum spectrograph slit width for radial-velocity work.
$\xi(M)$	1	The stellar mass function.
Δx	2	Spectral sampling interval in velocity space.

Appendix B

Reduction programs

B.1 Programs

B.1.1 Program DISPFIT.PAS

The program calculates the dispersion solutions appropriate for all stellar spectra in a run (on a diskette) and needs to be run before the cross correlation program (CROSS.PAS).

```
program dispfit;
{  Program reads parameters from DPAR.DAT and automatically calculates a
parabolic least-squares fit to fourteen emission lines in all the *.LMP files
in the stated directory, throwing out lines where the pixel error is greater
than a certain stated value.  The other parameters in the file state the
directory you want the dispersion files to be written to and whether or not you
want to see the fitted lines on the screen (this is slower).  Finally the
program takes a mean of any degenerate files *A.LMP and *B.LMP.  These files
are of Th-Ar spectra taken before and after (respectively) the stellar
exposure.  The resultant dispersion file is called simply *.DIS (just the A or
B deleted).

The program is set for lines in a 4989 - 5030 angstrom window although
could easily be adjusted for another window or order of fit.

Last updated 1/90   KAM      }

uses
  Crt, LDA, Plot, Fit, Dos, Epar;
var
  i                              : integer;
  finished,beenherebefore, view  : boolean;
  specfile                       : PathStr;
  D,DisD                         : DirStr;
  N                              : NameStr;
  E                              : ExtStr;
```

```
  covar                          : glncabynca;
  maxsig, dev                    : real;
  DirInfo                        : SearchRec;
  a                              : glnparam;

procedure Initialise;
begin
  ClrScr;
  finished:= false;
  beenherebefore:=false;
  DosError:=0;
end;

procedure DispLSQ;
var
  disp         : text;
  chisq   : real;
  lista   : gllista;
  x,y,sig : glndata;
  ndata   : integer;
begin
  assign(disp,'disp.dat');
  reset(disp);
  i:=1;
  repeat
    read(disp,y[i],x[i],sig[i]);
    x[i]:=x[i]-5010;
    inc(i);
  until eof(disp);
  ndata:=i-2;
  close(disp);
  for i:=1 to 3 do
    lista[i]:=i;
  lfit(x,y,sig,ndata,a,3,lista,3,covar,3,chisq);
  dev:=0;
  for i:=1 to ndata do
    dev:=dev + sqr(y[i]-a[1] - (x[i])*a[2] - sqr(x[i])*a[3]);
end;

procedure WriteDispersionFile;
var
  result               : text;
begin
  FSplit(specfile,D,N,E);
  assign(result,DisD+N+'.DIS');
  rewrite(result);
  for i:=1 to 3 do
    if i=1 then
      writeln(result,a[i]:9:3,' ',sqrt(covar[i,i]):12:3,' ')
    else
```

```
      writeln(result,a[i]:15,' ',sqrt(covar[i,i]):10,' ');
  writeln(result);
  writeln(result,sqrt(dev):6:3);
  writeln('Dispersion solution written to ',DisD+M+'.DIS');
  close(result);
end;

  procedure MakeMeans;
  var
    root, fileID  : string;
    t             : text;
    a,b,ae,be     : array[1..3]of real;
    Marker        : string[1];
    j             : integer;
  begin
    FindFirst(D+'*.LMP',AnyFile,DirInfo);
    While DosError = 0 do
      begin
        Marker:=Copy(DirInfo.name,Length(DirInfo.name)-4,1);
        root:=Copy(DirInfo.name,1,Length(DirInfo.name)-5);
        If (Marker = 'A') or (Marker= 'a') then
        begin
          for j:=1 to 2 do
            begin
              if j=1 then
                fileID:= root+'A.DIS'
              else
                fileID:= root+'B.DIS';
              assign(t,fileID);
              reset(t);
              While IOResult <>0 do
                begin
                  write(fileID,' not found.  Enter name of file:');
                  readln(fileID);
                  assign(t,fileID);
                  reset(t);
                end;
              if j=1 then
                for i:=1 to 3 do
                  readln(t,a[i],ae[i])
              else
                for i:=1 to 3 do
                  readln(t,b[i],be[i]);
              close(t);
            end;
            assign(t,root+'.DIS');
            rewrite(t);
            for i:=1 to 3 do
              if i=1 then
                writeln(t,(a[i]+b[i])/2:9:3,' ',(ae[i]+be[i])/2:12:3)
```

```
            else
              writeln(t,(a[i]+b[i])/2:15,' ',(ae[i]+be[i])/2:10);
          close(t);
          writeln('Mean dispersion solution written: ',root+'.DIS');
       end;
   FindNext(DirInfo);
 end;
     end;

procedure ReadDPar;
var
  t           : text;
  OK          : boolean;
  answer      : word;
begin
  if beenherebefore= true then
    begin
      FindNext(DirInfo);
      If DosError = 18 then
        begin
          MakeMeans;
          writeln('  All .LMP files processed');
          writeln('      Press <return>');
          readln;
          Halt;
        end;
      specfile:=D+DirInfo.name
    end
  else
    begin
      assign(t,'dpar.dat');
      reset(t);
      readln(t,specfile);
      readln(t,DisD);
      while pos(' ',disD) <> 0 do
        DisD:= Copy(DisD,1,Length(DisD)-1);
      readln(t,maxsig);
      readln(t,answer);
      if answer=1 then
        view:=true
      else
        view:=false;
      close(t);
      repeat
        OK:=true;
        FSplit(specfile,D,N,E);
        If E<>'' then
        begin
          If (E='.LMP') or (E='.lmp') then
            finished:=true
```

```
          else
            begin
              writeln('File must be .LMP file.  Enter name again');
              readln(specfile);
              OK:=false
            end
          end
      until OK;
      If E='' then
        begin
          if D='' then
            begin
              writeln('Enter directory you want .DIS files for');
              readln(D);
            end;
          FindFirst(D+'*.LMP',AnyFile,DirInfo);
          specfile:=D+dirInfo.name;
        end;
    end;
  beenherebefore := true;
end;
{*****************************************************************************}
begin   {  main  }
  Initialise;
  EditPars(true);
  repeat
    ReadDPar;
    LinePositions(specfile,maxsig,view);
    DispLSQ;
    WriteDispersionFile;
  until finished;
end.
```

B.1.2 Program CROSS.PAS

This is the main cross correlation program described in Chapter 3.

```
program cross;
 uses DOS, Epar, LDA, Fit, Prepare, CRT, Plot, BarCor;

 type
    spectrum2  = record
      name          :       string[35];
      x             :       pspectrum2;
    end;
    spectrum  = record
      name          :       string[12];
      x             :       pspectrum;
    end;
 var
```

```
    t, pairfile                                  : text;
    specfile                                     : charfile;
    i,d,bins,answer                              : integer;
    xcor                                         : spectrum2;
    spec1,spec2,c                                : spectrum;
    velocity,fitrange,dlglambda, li, lf, dev,
                              v, v1, JD, JD2     : real;
    dispfile1,dispfile2,veldir,comname           : string;
    dis1,dis2                                    : vector3;
    autofit,filt,finished                        : boolean;
    name                                         : string[7];
    DirInfo                                      : SearchRec;

{*****************************************************************************}
 procedure ModifyNames(ext : ExtStr);
 var
   D      : DirStr;
   N      : NameStr;
   E      : ExtStr;
 begin
   while Pos(' ',spec1.name) > 0 do
     spec1.name:=Copy(spec1.name,1,Pos(' ',spec1.name)-1);
   FSplit(spec1.name,D,N,E);
   spec1.name:= D+N+Ext;

   while Pos(' ',spec2.name) > 0 do
    spec2.name:=Copy(spec2.name,1,Pos(' ',spec2.name)-1);
   FSplit(spec2.name,D,N,E);
   spec2.name:= D+N+Ext;
end;
{*****************************************************************************}
 procedure AutoDispSelect(sname  :string; var dispf :string; ext  : ExtStr);
 { Finds the name of the dispersion solution file implied by the
 spectrum file name: eg KAM0001.SPC implies KAM0001.DIS}
 begin
   dispf:=Copy(sname,1,Length(sname)-4)+ext;
 end;
{*****************************************************************************}
procedure ReadParFile;

begin
   ClrScr;
   assign(t,'par.dat');
   reset(t);
   readln(t,spec1.name);

   assign(pairfile,spec1.name);
   reset(pairfile);

   autofit:=false;
```

```
  filt:=true;
  readln(t,d);
  readln(t,fitrange);
  readln(t,li);
  readln(t,lf);
  readln(t,veldir);
  while Pos(' ',veldir) <> 0 do
    veldir:=Copy(veldir,1,Length(veldir)-1);
  close(t);
end;

{*****************************************************************************}
procedure BarycentricCorrection;
var
  u                                          : text;
  today                                      : datetype;
  tim1,tim                                   : timetype;
  elevation,latdeg,latmin,longdeg,longmin,
          epoch,rahrs,ramin,decdeg,decmin    : integer;
  latsec,longsec,rasec,decsec                : real;
procedure StarPosition;
var
  finished : boolean;
  name2    : string[7];
  b,C      : integer;
begin
  finished:=false;
  b:=1;
  while Pos(' ',name) >0 do
    Delete(name,Pos(' ',name),1);
  name:= Copy(name,1,6);
  assign(u,'coord.dat');
  reset(u);
  for c:=1 to 2 do
    readln(u);
  while not finished do
    begin
      for c:=1 to 7 do
        readln(u);
      readln(u,name2);
      if (Pos(name,name2)>0) then
        begin
          readln(u,comname);
          readln(u,rahrs);
          readln(u,ramin);
          readln(u,rasec);
          readln(u,decdeg);
          readln(u,decmin);
          readln(u,decsec);
          finished:=true;
```

```
          close(u);
          Exit;
        end;
        If eof(u) then
          begin
            if (b=1) or (b=2) then
                name:=Copy(name,1,Length(name)-1)
            else
              begin
                writeln('info on ',name,' not found');
                writeln('Enter correct star name');
                readln(name);
              end;
                close(u);
                assign(u,'coord.dat');
                reset(u);
                for c:=1 to 2 do
                  readln(u);
                inc(b);
           end;
    end;
end;

procedure ObservatoryPosition;
begin
 readln(u,elevation);
 readln(u,latdeg);
 readln(u,latmin);
 readln(u,latsec);
 readln(u,longdeg);
 readln(u,longmin);
 readln(u,longsec);
end;

procedure Time;
begin
  readln(t,name);
  readln(t,today.day);
  readln(t,today.month);
  readln(t,today.year);
  today.year:=today.year+1900;
  readln(t,tim.hours); readln(t,tim.minutes); readln(t,tim.seconds);
  readln(t,tim1.hours);readln(t,tim1.minutes);readln(t,tim1.seconds);
  tim.minutes:=30*tim1.hours + tim.minutes + trunc(0.5*tim1.minutes);
  tim.seconds:=tim.seconds+(0.5*tim1.minutes)-trunc(0.5*tim1.minutes);
  writeln(tim.hours,' ',tim.minutes,' ',tim.seconds:5:2);
end;

begin
 assign(u,'coord.dat');
```

```
  reset(u);
  readln(u,epoch);
  ObservatoryPosition;
  assign(t,'header.dat');
  reset(t);
  for i:=1 to 2 do
    begin
      v:=0;
      Time;
      StarPosition;
      radial_velocity(epoch,rahrs,ramin,decdeg,decmin,rasec,decsec,tim,today,
              elevation,latdeg,latmin,longdeg,longmin,latsec,longsec,v,JD);
      if i=1 then
        begin
          v1:=v;
          JD2:=JD;
        end;
    end;
  close(t);
end;
{*****************************************************************************}
 procedure GetVel;

  procedure SetUp(       ID               : string;
                  var arr                 : pspectrum;
                      dispfile            : string;
                  var disparr             : vector3;
                      second              : boolean);
  {Directs the massaging of the data that precedes cross correlation }
  var
       starfile                                    : charfile;
  begin
   If second then
     assign(specfile,'B:\'+ID)
   else
     assign(specfile,'C:\KAM\'+ID);
  read_data(specfile,arr,second);
  bins:=d;
  if second then
    assign(t,'B:\'+dispfile)
  else
    assign(t,'C:\KAM\'+dispfile);
  reset(t);
  While IOResult <> 0 do
    begin
      writeln('File ',dispfile,' not found');
      writeln('Enter name of dispersion file');
      readln(dispfile);
      assign(t,'B:\'+dispfile);
      reset(t);
```

```
   end;
 for i:=1 to 3 do
   readln(t,disparr[i]);
 close(t);
 rebin(arr,li,lf,dlglambda,bins,disparr);
 for i:=bins+1 to 2048 do
  arr^[i]:=0;
 subtractmean(arr,1,bins,second);
 cosinebell(arr,1,bins,second);
end;

procedure FitVelocity;
begin
   new(c.x);
  for i:=1 to 2048 do
   if i<1025 then
    c.x^[i+1024]:=xcor.x^[i]
  else
    c.x^[i-1024]:=xcor.x^[i];
  dispose(xcor.x);

  Xfit(c.x,dlglambda,autofit,xcor.name,fitrange,velocity);
  dispose(c.x);
end;

begin
  new(spec1.x);
  SetUp(spec1.name,spec1.x,dispfile1,dis1,false);
  new(spec2.x);
  SetUp(spec2.name,spec2.x,dispfile2,dis2,true);
  xcor.name:=spec2.name+' relative to '+spec1.name;
  new(xcor.x);
  Correl(spec1.x, spec2.x, 2048, xcor.x,filt,xcor.name);
  dispose(spec1.x);
  dispose(spec2.x);
  FitVelocity;
end;

procedure StarRun;
var
  velocity1             : real;
  b                     : integer;

procedure WriteVelFile;
begin
  velocity:=(exp(velocity*dlglambda) -1)*2.997925e5;
  spec1.name:=Copy(spec1.name,1,Pos('.',spec1.name)-1);
  spec2.name:=Copy(spec2.name,1,Pos('.',spec2.name)-1);
  assign(t,veldir+name+'.VEL');writeln(veldir+name+'.VEL');readln;
  Append(t);
```

```
  If IOResult<>0 then
    begin
      rewrite(t);
      writeln(t,comname);
      writeln(t,' VEL (km/s)      HJD                Files           (Vapp,BC1,BC2)');
    end;
  writeln(t,v-v1-velocity:7:3,'     ',JD:13:5,'     '
      ,spec1.name,',',spec2.name,' (',velocity:7:3,' ',v1:7:3,' ',v:7:3,')');
  close(t);
end;
{*************************************************************************}
  begin {Main cross correlation program}
    EditPars(false);
    finished:=false;
    ReadParFile;
    While not finished do
      If not eof(pairfile) then
        begin
          ClrScr;
          readln(pairfile,spec1.name,spec2.name);
          ModifyNames('.SPC');
          AutoDispSelect(spec1.name,dispfile1,'.DIS');
          AutoDispSelect(spec2.name,dispfile2,'.DIS');
          filt:=true;
          writeln(spec1.name,' ',spec2.name);
          GetVel;
          BarycentricCorrection;
          WriteVelFile;
        end
      else
        finished:= true;
    Close(pairfile);
  end.{Main cross correlation program}
```

B.2 Unit files

B.2.1 The unit file BARCOR.PAS

```
UNIT Barcor;
{ Computes the projection in the direction of the star of the velocity of
the telescope relative to the solar system barycentre.}
Interface
TYPE
 datetype = RECORD
             day : 1..31;
             month : 1..12;
             year  : integer
            END;
sexaginter = RECORD
```

```
             degrees : integer;
             minutes : -60..60;
             seconds : real
            END;
 timetype = RECORD
             hours   : integer;
             minutes : -60..60;
             seconds : real
            END;

PROCEDURE radial_velocity( epoch,rahrs,ramin,
                           decdeg,decmin   : integer;
                           rasec,decsec    : real;
                           tim             : timetype;
                           today           : datetype;
                           elevation,
                           latdeg,latmin,
                           longdeg,longmin : integer;
                           latsec,longsec  : real;
                          VAR truevelocity,JD : real);

Implementation

PROCEDURE radial_velocity( epoch,rahrs,ramin,
                           decdeg,decmin   : integer;
                           rasec,decsec    : real;
                           tim             : timetype;
                           today           : datetype;
                           elevation,
                           latdeg,latmin,
                           longdeg,longmin : integer;
                           latsec,longsec  : real;
                          VAR truevelocity,JD : real);
(* * * * * * * * * * * * * * * * * * * * * * * * * * * * * * * * * * * * * * )
(*                                                                           *)
(*   Purpose : To reduce radial-velocity measurements from spectra to *)
(*             barycentric radial velocities.                                *)
(*                                                                           *)
(*   Author  : Translated by V. McIntyre from a FORTRAN subroutine    *)
(*             by J.A.Ball listed on pp 308 & ff of:                         *)
(*               Methods of Experimental Physics,vol 12: Astrophysics *)
(*              edited by M.L. Meeks (Academic Press,1976)                   *)
(*             Corrections and 'Jupiter' procedure by Kaylene Murdoch.*)
(*                                                                           *)
(*   Note    : References are made in the program to the Astronomical *)
(*             Almanac,1986 (denoted by AA),  the 'Explanatory Sup-   *)
(*             plement to the Astronomical Ephemeris & American       *)
(*             Ephemeris and Nautical Almanac', 1961 (EE) ,the        *)
(*             paper by P.Stumpff on his heliocentric correction      *)
(*             subroutine BARVEL: A.A.Suppl.Ser. v41 p1 (1980)        *)
```

```
(*             and to S. Newcomb Astron. Papers vol VI B part 1 (1898)*)
(*                                                                     *)
(*   Maximum uncertainty: 8m/s over 3 or more years                    *)
(*                        <5m/s over less than a year                  *)
(*                        <1m/s during a night                         *)
(*                                                                     *)
(** * * * * * * * * * * * * * * * * * * * * * * * * * * * * * * * * *)

VAR
 rashift, decshift,
 dc,                      {eqn. of equinoxes(add to mean lst to get last)}
 lst,                     {Local Sidereal Time                          }
 smalld,jc_smalld,        {time from epoch to present (days&jul. cent.)}
 object_ra,object_dec,    {object's position in the starfield           }
 object_long,object_lat,  {object's position in geographic coords       }
 latitude,longitude,      {observer's geographic position               }
 light_time,              {between earth and sun                        }
 deltav1,
 deltav2,                 {velocity terms obtained for each correction  }
 deltav3,
 deltav4   : real;        { in km/sec                                   }
 earthlongsun,         {true long. as seen from sun         (radians)  }
 obliq                 {mean obliquity of the ecliptic}          : real;
(************************************************************************)
FUNCTION daynumber( today : datetype ) : integer;
{ Calculates the day-number of any date in the year }
VAR
 x : integer;
BEGIN
 CASE today.month OF
  1 : x:=0;
  2 : x:=31;
  3 : x:=59;
  4 : x:=90;
  5 : x:=120;
  6 : x:=151;
  7 : x:=181;
  8 : x:=212;
  9 : x:=243;
 10 : x:=273;
 11 : x:=304;
 12 : x:=334
 END; {case}
 IF today.month > 2 THEN {check for leapyear}
  IF ((today.year) mod 4)=0 THEN
   IF ((today.year) mod 100) <> 0 THEN
    x := x + 1;
 daynumber := x + today.day
END; {daynumber}
```

```
FUNCTION juldate( year,month,day,hour,min : integer; sec:real) : real;
var
  A,B                  :integer;
{ This function calculates the julian date for specified date in the     }
{specified year. The full form of the formula is :                       }
{                                                                        }
{    juldate = trunc(365.25*y) + trunc(30.6001*(m+1)) + day              }
{                + time(U.T.)/24 + 1720994.5  - B                        }
{                                                                        }
{   where : if the month is Jan or Feb, y = year - 1, m = month + 12,    }
{           otherwise y = year and m = month     ;                       }
{                                                                        }
{           and B = 2 - trunc(y/100) + trunc((trunc(y/100))/4),          }
{           as long as the date is after 15 Oct 1582, which is when      }
{           the Gregorian Calendar was introduced. Otherwise B=0.        }
{   The formula as described finds  J.D. at 0h UT on the specified day   }
BEGIN {juldate}
 if (month=1) or (month=2) then
   begin
     year:= year -1;
     month:=month+12;
   end
 else;
 A:= trunc(year/100);
 B:= 2 -A + trunc(A/4);
 if ((year=1582)and(month<10)and(day<15)) or (year<1582) then
   B:=0
 else;
 juldate := trunc(365.25*year) + trunc(30.6001*(month+1)) + day
            + (hour +(min/60) + (sec/360))/24 + 1720994.5 +B;
END; {juldate}
{*********************************************************************}
PROCEDURE coord( origina,originb,            {origin of new system in
                                                    the old coordinates  }
                 newpolea,newpoleb,   {coords of north pole of new system
                                                     in old coordinates  }
                 long,lat           : real;{star position in old coords  }
                VAR newlong,newlat     : real);{star pos'n in new coords }
VAR
 snewlat,              { sin of the latitude in the new system          }
 saa,caa,              { sin and cos of the angles which make up the    }
 sbb,cbb,              { angle newlong/2                                }
 sa2,ca2,ta2 : real;   { sin,cos and tan of newlong/2                   }

BEGIN {coord}
 snewlat := sin(newpoleb)*sin(lat) + cos(newpoleb)*cos(lat)*
    cos(newpolea - long);
 newlat := arctan(snewlat/(sqrt(1 - snewlat*snewlat)));
 saa := sin(newpolea-long)*cos(lat)/cos(newlat);
 caa := (sin(lat)-sin(newlat)*sin(newpoleb))/
```

```
      (cos(newlat)*cos(newpoleb));
 cbb := sin(originb)/cos(newpoleb);
 sbb := sin(newpolea - origina)*cos(originb);
 sa2 := saa*cbb - caa*sbb;
 ca2 := caa*cbb + saa*sbb;
 IF ca2 <= 0 THEN ta2 := (1 - ca2)/sa2
     ELSE ta2 := sa2/(1 + ca2);
 newlong := 2*arctan(ta2);
END; {coord}
{*********************************************************************}
PROCEDURE precess( epoch,                {initial epoch                }
                   year,
                   month,day  : integer; {current date                 }
                  VAR ra,dec,            {position to be precessed(rad)}
                      dc      : real   );{equation of equinoxes, also
                                         called the nutation in right ascension }
VAR
 csd,snd,tnd,      {sin,cos and tan of declination                     }
 daynum,
 cst, snt,
 a,ar,
 b,w,w1,w2,
 snr,csr,          {sin,cos and tan of right ascension                 }
 snl,csl,          {sin,cos and tan of longitude                       }
 t0,               {time from 1900 to epoch date in trop. centuries    }
 timtonow,         {time from epoch date to current date in trop.centuries}
 zeta, z,          {precessional angles, taken from ESE-29 and         }
 theta,            {measured in arcseconds                             }
 prcessm,prcessn   {precessional numbers, in radians(cf AA-B19)        }
           : real;
 c         : integer;
{ Precesses the coordinates of the mean epoch EPOCH to those of the mean epoch
 of date using rigorous formulae from AA-B19 (actually my translation of a
 CfA code). The formulae in Ball's code were approximate and not valid at
 high declinations.

 The reason why the coordinates need to be precessed at all is that in the
 procedures Orbital_motion and Motion_about_earthcenter formulae are used to
 determine the orbital elements of the earth and the moon relative to the mean
 equinox of date.  Therefore the star's coordinates are needed in that same
 frame of reference.

 Note that in the original code of Ball, the corresponding FORTRAN subroutine
 included corrections for nutation and aberration.  The correction for
 nutation was in error, as the coordinates in the Orbital_motions and
 Motion_about_earthcenter routines are referred to the MEAN equator and equinox
 (See Newcomb 1898 or ESE p98).  The correction for aberration is not required
 if one inputs mean coordinates rather than apparent ones.  Pre-1984 catalogs
 may not correct for annual aberration.(See AA glossary)
```

```
                                        K.M. 8/89                    }
BEGIN {precess}
 snd := sin(dec);
 csd := cos(dec);
 t0 := (epoch - 1900)/100;
 timtonow :=abs((year - epoch) + daynumber(today)/365.2421988)/100;
{    365.2421988 is the number of ephemeris days in a tropical year   }
 if (epoch > year) then
   c := -1
 else
   c :=  1;

 zeta  := c*((2304.25 + 1.396*t0)*timtonow + 0.302*sqr(timtonow) + 0.018*timtonow*
                   sqr(timtonow))*pi/(60*60*180);
 z     := zeta + c*0.791*sqr(timtonow)*pi/(60*60*180);
 theta := c*((2004.682 - 0.853*t0)*timtonow - 0.426*sqr(timtonow)
                 - 0.042*timtonow*sqr(timtonow))*pi/(60*60*180);

  snt := sin(theta);
  cst := cos(theta);
  ar := ra/pi + 0.5;
  a  := trunc(ar);
  ar := pi * a;
  a  := ra + zeta;
  w  := cos(a);
  w1 := cst*csd*w - snt*snd;
  w2 := csd*sin(a);

  if (w1 = 0) and (w2 = 0) then
    begin
      if (dec < 0) then
        dec := -pi/2
      else
        dec := pi/2;
      ra := 0;
    end
  else
    if (w1 = 0) then
      if (a - zeta -ar) < 0 then
        w2 := - pi/2
      else
        w2 := pi/2
    else
        w2 := arctan(w2/w1);
  a := w2 + ar + z;
  w1 := a - ra;
  w2 := abs(w1);
  if (w2 > 1.5) and (w2 < 4.5) then
    if w1 > 0 then
      a := a - pi
```

```
    else
      a := a + pi;
  b := w*snt*csd + cst*snd;
  dec := arctan(b/sqrt(1-b*b));
  w := 2*pi;

  if (a < 0) then
    ra := a + w
  else
    if (a > w) then
      ra := a - w
    else
      ra := a;

END; {precess}
{*************************************************************************}
PROCEDURE time_calculations( today : datetype; {date of observation    }
                             tim   : timetype; {time of observation(UT)}
                             longitude : real; {observer's longitude   }
                            VAR lst,       {Local Sidereal Time of obs.}
                                smalld,       {Days from epoch to TODAY}
                                jc_smalld : real {smalld in Julian
                                                  Centuries});
CONST
 solartosidereal=0.99726956634;           {from 1985-1988 AA  }
VAR
 jan0thisyr,         {Time from J1900 Jan 0.5 to Jan0.0 of today.year, in J.D}
 Tu,                 {the above, in Julian centuries (AA-B6 notation)  }
 uttoday,            { GMT from jan 0.0 to present date, in days       }
 start,              { Greenwich mean sidereal time on jan 0.0         }
 gsiderealt : real;  { Greenwich mean sidereal time,in days            }

 { Calculates mean LST and time in Julian centuries since  epoch 1900.0  }
BEGIN {time_calculations}

 { 1) LST calculation needs Tu relative to J2000.0 =JDN 2451545.0 }

 jan0thisyr := (juldate(today.year,1,0,0,0,0) - 2451545.0);
 Tu := jan0thisyr/36525;
 {the next line calculates the GMT from Jan 0.0 to today }
 uttoday    := daynumber(today) + tim.hours/24 + tim.minutes/1440 +
    tim.seconds/86400;
 JD:=juldate(today.year,1,0,0,0,0)+uttoday;
 start     := (24110.54841 + 8640184.812866*Tu + 0.093104*sqr(Tu) -
    6.2E-6*sqr(Tu)*Tu)/3600/24;              {In days}
 gsiderealt := start + uttoday/solartosidereal;
 lst := gsiderealt + longitude/(2*pi);           {In days}
 lst := lst - trunc(lst);

 { 2) Corrections for motion of EMB and of moon need j_smalld relative to
```

```
        J1900.0  Jan 0.5 = JDN 2415020.0 }

 janOthisyr := (juldate(today.year,1,0,0,0,0) - 2415020.0);
 Tu := janOthisyr/36525;
 {the next line calculates the GMT from Jan 0.0 to today }
 uttoday    := daynumber(today) + tim.hours/24 + tim.minutes/1440 +
    tim.seconds/86400;
 smalld     := janOthisyr + uttoday;
 jc_smalld  := smalld/36525;

end; {time_calculations}

PROCEDURE motion_about_earthcentre( elevation  : integer;
                                    latitude,
                                    lst,
                                    object_ra,
                                    object_dec : real;
                                   VAR deltav1      : real  );
{ Calculates the projection on the line of sight to the star of the
  telescope's motion with respect to the earth's center               }
CONST
 siderealtosolar = 0.99726956634;

VAR
 rho,              {radius vector from earthcentre to observer and     }
 vrho,             { the corresponding angular velocity                }
 dlat,             {correction to geographic latitude to give          }
 gcntlat : real;   {geocentric latitude                                }

 {  Checked 8/89 using AA-K }

BEGIN
 rho := 6378160*(0.998327073+0.001676438*cos(2*latitude) -
  3.519E-6*cos(4*latitude) + 8.0E-9*cos(6*latitude)) + elevation;{metres}
 vrho := 2*pi*rho/24/3600/siderealtosolar/1000;
 dlat := -1*(11*60+32.743)*sin(2*latitude) + 1.1633*sin(4*latitude) -
    0.0026*sin(6*latitude);
 gcntlat := latitude + dlat*pi/3600/180;

 deltav1 := vrho*cos(gcntlat)*cos(object_dec)*sin(object_ra - (lst*2*pi));
 {note that last factor is opposite in sign cf original code of Ball}

 writeln('dv1=',deltav1:10:3,' km/s  (rotational)')
END; {motion_about_earthcentre}

PROCEDURE orbital_motions( smalld,
                           jc_smalld,
                           object_ra,
                           object_dec    : real;
                          VAR object_long,
```

```
                              object_lat,
                              deltav2,
                              light_time    : real;
                            VAR earthlongsun  : REAL);
{ Calculates the projection on the line of sight to the star of the
Earth-Moon barycenter (EMB) relative to the sun    }

CONST
 semimajax=149598500;    {semimajor axis of EMB's orbit (km)         }

VAR
{ The following elements refer to the orbital motion of the EMB        }
 mean_anom,             {mean anomaly                                  }
 perilong,              {mean longitude of perihelion                  }
 e,                     {eccentricty                                   }
 true_anom,             {true anomaly                                  }
 angrate,               {mean angular rate about sun         (rdn/day) }
 sunlongearth,          {true long. of sun as seen from EMB  (radians) }
 hop          : REAL;   {component of the EMB's velocity perpendicular
                                                    to radius vector }
BEGIN {orbital_motions}
 angrate := 2*pi/365.2564;
 mean_anom := (358.47583 + 0.985600267*smalld - 0.00015*sqr(jc_smalld) -
    3.4E-6*sqr(jc_smalld)*jc_smalld)*pi/180; {radians}

 perilong :=(281.220844 + 0.0000470684*smalld + 0.000453*sqr(jc_smalld) -
    3.0E-6*sqr(jc_smalld)*jc_smalld)*pi/180;{radians}

 e := 0.01675104 - 4.18E-5*jc_smalld - 1.26E-7*sqr(jc_smalld);

 obliq := (23.452294 - 0.0130125*jc_smalld - 1.64E-6*sqr(jc_smalld) +
    5.03E-7*sqr(jc_smalld)*jc_smalld)*pi/180;{radians}

 true_anom := mean_anom + (2*e-0.25*e*e*e)*sin(mean_anom) +
    1.25*e*e*sin(2*mean_anom) + 13/12*e*e*e*sin(3*mean_anom);{radians}

 earthlongsun := perilong + true_anom;{radians}
 sunlongearth := earthlongsun + pi; {radians}

 coord(0,0,(-0.5*pi),(pi/2-obliq),object_ra,object_dec,object_long,object_lat);
 hop := semimajax*angrate/sqrt(1-e*e)/86400; {km/sec}

 light_time :=-semimajax*(1 - e*e)*cos(object_lat)
      *cos(sunlongearth-object_long)/(2.997925e5 * (1 + e*cos(true_anom)));
 light_time:=light_time/86400;
 deltav2 := -1*hop*cos(object_lat)*(sin(sunlongearth-object_long)
    - e*sin(perilong - object_long));

 writeln('dv2 = ',deltav2:9:3,' km/s  (orbital)');
```

```
END; {orbital_motions}
{************************************************************************}
PROCEDURE moon_effects( smalld,jc_smalld,object_long,object_lat : real;
                        VAR deltav3                              : real );
{ Calculates the projection on the line of sight to the star of the motion
of the earth relative to the EMB                                         }
CONST
 emoon          = 0.054900489; {eccentricity of lunar orbit              }
VAR
 omega,                       {long. of mean ascending node of lun. orbit}
 amon,                        {omega+mean lunar longitude of moon       }
 gammaprime,                  {omega + lunar long. of lunar perigee     }
 lunarperilong,               {mean lunar long. of lunar perigee        }
 luninclin,                   {inclination of lunar orbit to ecliptic   }
 lunarangrate,                {angular rate of moon's orbiting          }
 lunrsemimajax,               {semi-major axis of lunar orbit           }
 approxmeananom,sa,           {approx. mean anomaly of lunar orbit. It is
                               approx. because lunarperilong should be
                               the true rather than mean value          }
 trueanom,                    {true anomaly of lunar orbit              }
 lunarlongmoon,               {mean lunar longitude of moon             }
 truelunlongmoon,             {true lunar longitude of moon             }
 lunobj_long,                 {lunar longitude of object                }
 lunobj_lat,                  {lunar latitude of object                 }
 moonhop           : real;    {cpt of lunar vel. perp. to radius vector }
BEGIN
 luninclin := 5.1453964*pi/180;
 lunarangrate := 2*pi/27.321661;
 lunrsemimajax := 60.2665*6378.388;{km}
 omega := pi/180*(259.183275 - 0.0529539222*smalld + 0.002078*sqr(jc_smalld) +
    2.0E-6*sqr(jc_smalld)*jc_smalld);
 amon := pi/180*(270.434164 + 13.176396527*smalld - 0.001133*sqr(jc_smalld) -
    1.9E-6*sqr(jc_smalld)*jc_smalld);
 gammaprime := pi/180*(334.329556 + 0.1114040803*smalld - 0.01325*sqr(jc_smalld)
    - 1.2E-5*sqr(jc_smalld)*jc_smalld);
 lunarperilong := gammaprime-omega;
 lunarlongmoon := amon-omega;
 approxmeananom := lunarlongmoon-lunarperilong;
 sa := sin(approxmeananom);
 trueanom := approxmeananom + (2*emoon-0.25*sqr(emoon)*emoon)*sa +
    1.25*sqr(emoon)*sin(2*approxmeananom) + 13/12*sqr(emoon)*emoon
    *sin(3*approxmeananom);
 truelunlongmoon := lunarperilong + trueanom;
 coord(omega,0,(omega-(pi/2)),((pi/2)-luninclin),object_long,
    object_lat,lunobj_long,lunobj_lat);
 moonhop := lunarangrate*lunrsemimajax/sqrt(1-sqr(emoon))/86400;{km/sec}

 deltav3 := moonhop/81.300436836*cos(lunobj_lat)*(sin(truelunlongmoon -
  lunobj_long) - emoon*sin(lunarperilong-lunobj_long));
```

```
 writeln ('dv3=',deltav3:10:3,' km/s  (moon)')
END; {moon_effects}
(*************************************************************************)
procedure Jupiter(jc_smalld,
                  object_long, object_lat           :real;
          var     deltav4                           :real);
{ deltav4 is the projection in the direction of the star of the velocity of
the sun as it orbits the sun-Jupiter barycenter.                          }
const
  jupsemimajaxis        =  7.7832392e8;  { km }
var
  juphelilong,          {  heliocentric longitude of Jupiter  }
  juperilong,           {  longitude of perihelion of Jupiter's orbit }
  theta,                {  longitude of ascending node  }
  ejup,                 { eccentricity  }
  jupinc,               { inclination of the orbit to the ecliptic }
  meananom, trueanom,
  truelong,             { true heliocentric longitude of Jupiter in J coords}
  jupobj_long,jupobj_lat,{ coords of object in J coords }
  juphop                { circular velocity of Jupiter about sun  }: real;
begin
  juperilong := 2.220221e-1 + jc_smalld*(2.809917e-2 + 1.852532e-5*jc_smalld);

  juphelilong := 4.1547339 +jc_smalld*(52.993466764997 + 5.8845e-6*jc_smalld);

  theta := 1.735614 + jc_smalld*(1.763719e-2 + 6.370440e-6*jc_smalld);

  ejup := 4.833473e-2 + jc_smalld*(1.641773e-4  - 4.654200e-7*jc_smalld);

  jupinc := 2.284178e-2 + jc_smalld*(-9.941590e-5 + 6.787400e-8*jc_smalld);

  meananom := juphelilong - juperilong;

  trueanom := meananom + (2*ejup - 0.25*ejup*ejup*ejup)*sin(meananom) +
        1.25*ejup*ejup*sin(2*meananom) + 13/12*ejup*ejup*ejup*sin(3*meananom);

  truelong := trueanom + juperilong - theta;

  coord(theta,0,(theta-(pi/2)),((pi/2)-jupinc),object_long,object_lat,
          jupobj_long,jupobj_lat);

   juphop := 2*pi*jupsemimajaxis/(4332.59*86400*sqrt(1-sqr(ejup)));
   { 3145.533 is an APPROX(so far) sideareal rate of J in days  }

   deltav4 := juphop/1047.35*cos(jupobj_lat)*(sin(truelong - jupobj_long)
                        - ejup*sin(juperilong - theta - jupobj_long));
 { 1047.35 is the mass ratio  Sun : Jupiter   }

   writeln('dv4= ',deltav4:9:3,' km/s  (jupiter)');
end;
```

```
{*************************************************************************}
BEGIN {radialvelocity}
 object_ra :=2*pi*(rahrs+ramin/60+rasec/3600)/24; {radians}
 object_dec := pi*(abs(decdeg)+decmin/60+decsec/3600)/180; {radians}
 IF (decdeg<0) OR (decmin<0) OR (decsec<0) THEN
  object_dec := -1*object_dec;

 precess(epoch,today.year,today.month,today.day,object_ra,object_dec,dc);
 latitude :=pi*(abs(latdeg) + latmin/360 + latsec/3600)/180;
 IF (latdeg<0) OR (latmin<0) OR (latsec<0) THEN
  latitude := -1*latitude;
 longitude :=(abs(longdeg) + longmin/60 + longsec/3600)*pi/180;
 IF (longdeg<0) OR (longmin<0) OR (longsec<0) THEN
  longitude := -1*longitude;

 time_calculations(today,tim,longitude,lst,smalld,jc_smalld);

 motion_about_earthcentre(elevation,latitude,lst,object_ra,object_dec,
    deltav1);

 orbital_motions(smalld,jc_smalld,object_ra,object_dec,object_long,
     object_lat,deltav2,light_time,earthlongsun);

 moon_effects(smalld,jc_smalld,object_long,object_lat,deltav3);

 Jupiter(jc_smalld,object_long,object_lat,deltav4);

 truevelocity := truevelocity + deltav1 + deltav2 + deltav3 + deltav4;
 JD := JD + light_time;
END;{radialvelocity}

end.{Initialisation section}
```

B.2.2 The unit file EPAR.PAS

```
Unit Epar;
{To edit the parameters that define how a cross correlation will be done}
interface
uses
  CRT,TCScreen,Win;
type
  par                 = string[14];
  info                = object
    pars : array[1..8]of par;
    description  : array[1..8]of string;
    procedure WriteXY(X,Y:integer;cell   : string; highlight: boolean);
    procedure descriptions;
    procedure pdescriptions;
    procedure displaydata(dispersiondata : boolean);
    procedure writedata(dispersiondata  : boolean);
```

```
    procedure edit;
  end;
procedure InitScreen;
procedure HelpLine;
procedure EditPars(Dispersiondata : boolean);

implementation

var
  number  : integer;
  parfile   : text;

procedure info.WriteXY;
  begin
    if highlight then
      begin
        TextColor(Black);
        TextBackground(White);
      end
    else
      begin
        TextColor(White);
        TextBackground(Black);
      end;
    GoToXY(X,Y);
    Write(cell);
  end;

  procedure info.descriptions;
  var
    i     : integer;
  begin
    description[1]:='.PRS file listing .SPC pairs';
    description[2]:='Number of bins';
    description[3]:='Fraction of peak to be fitted';
    description[4]:='Wavelength of bluest Th-Ar line';
    description[5]:='Wavelength of reddest Th-Ar line';
    description[6]:='Left edge of mask    (Th xcor only)';
    description[7]:='Right edge of mask   (Th xcor only)';
    description[8]:='Directory for Stellar velocity files';
  end;

procedure info.pdescriptions;
var
  i        : integer;
begin
  description[1]:='Directory containing .LMP files to be reduced';
  description[2]:='Directory where dispersion files are to be written';
  description[3]:='Maximum pixel error in line before rejection';
  description[4]:='Visual presentation on (1) or off (0)?[NB 1 is slower]';
```

```
end;

procedure info.displaydata(dispersiondata : boolean);
  var
    parfile   : text;
    i         : integer;
  begin
    If dispersiondata then
      begin
        pdescriptions;
        number:=4;
        assign(parfile,'dpar.dat');
      end
    else
      begin
        descriptions;
        number:=8;
        assign(parfile,'c:\kam\par.dat');
      end;
    reset(parfile);
      for i:=1 to number do
        begin
          readln(parfile,pars[i]);
          writeXY(1,i,pars[i],false);
          writeXY(16,i,description[i],false);
          writeln;
        end;
      close(parfile);
     writeXY(1,1,pars[1],true);
   end;

  procedure info.writedata(dispersiondata : boolean);
  var
    parfile  : text;
    i        : integer;
  begin
    if dispersiondata then
      assign(parfile,'dpar.dat')
    else
     assign(parfile,'par.dat');
    rewrite(parfile);
    for i:=1 to 8 do
      writeln(parfile,pars[i]);
    close(parfile);
  end;

  procedure info.edit;
  var
    done     : boolean;
    answer   : char;
```

```
  i,j     : integer;
begin
  i:=1;
  done:=false;
  while not done do
  begin
    answer:=ReadKey;
    if answer= #0 then
      begin
        answer:=ReadKey;
          case Ord(answer) of
          3   : halt; {emergency stop!}
          15,         {shift-TAB}
          72  : begin {UP arrow}
                  writeXY(1,i,pars[i],false);
                  if i=1 then
                    i:= i+number-1
                  else
                    dec(i);
                  writeXY(1,i,pars[i],true);
                end;
           80 : begin {DOWN arrow}
                  writeXY(1,i,pars[i],false);
                  if (i=number) then
                   i:=i-number+1
                  else
                    inc(i);
                  writeXY(1,i,pars[i],true);
                end;
           45 : begin {ALT-X}
                  done:=true;
                  InitScreen;
                end
             else
               write(#7);
             end;  { case}
           end {if extended key}
          else
            begin
              if answer in [^C,#27] then begin ClrScr; halt; end;
              GoToXY(1,15);
              for j:=1 to 14 do
                write(' ');
                GoToXY(1,15);
              readln(pars[i]);
              for j:=1 to (14- Length(pars[i])) do
                pars[i]:=pars[i]+' ';
              writeXY(1,i,pars[i],true);
              GoToXY(1,15);
              TextBackground(Black);
```

```
              for j:=1 to 14 do
                write(' ');
              TextBackground(White);
            end;
          end;
        end;

procedure InitScreen;
  begin
    TextBackground(Black);
    TextColor(White);
    ClrScr;
    SetCursor(NoCursor);
  end;

 procedure HelpLine;
 begin
   GoToXY(1,20);
   write('  Arrow keys to select        Alt-X to quit and save');
   writeln('       Ctrl-Break to quit ');
 end;


procedure EditPars(Dispersiondata : boolean);
var
  parameters           : info;
begin {EditPars}
  InitScreen;
  HelpLine;
  with parameters do
    begin
     displaydata(dispersiondata);
     edit;
     writedata(dispersiondata);
   end;
end;
{initialisation}
end.
```

B.2.3 The unit file FIT.PAS

Several procedures and functions in this unit are from *Numerical Recipes* (Press *et al.* 1988). Some of these (these are marked within the program) have been slightly modified to fit in with the unit. The modifications are:

- Types `glnpbynp`, `glnpbymp`, `glcovar` and `glnalbynal` are replaced by type `glncabynca`.
- Type `glnp` is replaced by type `gllista`.

- Type **glmma** is replaced by type **glnparam**.
- Constant **mma** is replaced by **na**.
- Procedures **fgauss**, **mrqcof** and **mrqmin** call the extra parameter ycont: **real** in the formal parameter list and where these are called, the parameter list is extended accordingly.
- Procedure **fgauss** has the line `y:= y + a[i]*ex;` replaced by `y:= ycont + y + a[i]*ex;`.

```
unit Fit;
{Contains procedures that can be used for determining a least-squares fit
to a polynomial or fitting a gaussian function by the Levenberg-Marquardt
method}
interface
  uses
    Graph, CRT, LDA;
  const
    na = 3; nca = 3; ma = 3; ndata = 100;
  type
    glndata                          = array[1..100] of real;
    gllista                          = array[1..na] of integer;
    glnparam                         = array[1..na] of real;
    glncabynca                       = array[1..nca,1..nca] of real;
    sqmatrix15                       = array[1..15,1..15]of real;
    vector3                          = array[1..3]of real;
    vector15                         = array[1..15]of real;
    vector25                         = array[1..25]of real;
    dataarray                        = array[1..15,1..1]of real;
  var
    glochisq                         : real;
    lista                            : gllista;
    glbeta, a                        : glnparam;

FUNCTION gammln(xx: real): real;

PROCEDURE gcf(a,x: real; VAR gammcf,gln: real);

PROCEDURE gser(a,x: real; VAR gamser,gln: real);

FUNCTION gammq(a,x: real): real;

procedure gaussj(var  a : glncabynca; n, np : integer; VAR  b : glncabynca;
                     m, mp : integer);
{ Solves a system of linear equations by Gauss-Jordan elimination }

PROCEDURE covsrt(VAR covar: glncabynca; ncvm: integer; ma: integer;
       lista: gllista; mfit: integer);
```

```
{  Repacks covar matrix to true order of the parameters  }

PROCEDURE fgauss(x: real; a: glnparam; VAR y: real;
       VAR dyda: glnparam; na: integer;ycont  :real);
{ Gaussian function}

PROCEDURE mrqcof(x,y,sig: glndata; ndata: integer;
       VAR a: glnparam; na: integer; lista: gllista;
       mfit: integer; VAR alpha: glncabynca;
       VAR beta: glnparam; nca: integer; VAR chisq: real;ycont:real);
{  Used by  mrqmin to evaluate the linearised fitting matrix alpha and the
vector beta  }

PROCEDURE mrqmin(x,y,sig: glndata; ndata: integer;
         VAR a: glnparam; na: integer; lista: gllista;
         mfit: integer; VAR covar,alpha: glncabynca;
         nca: integer; VAR chisq,alamda: real;ycont:real);

PROCEDURE funcs(z:real;var afunc : glnparam;na: integer);
{ Polynomial function }

PROCEDURE lfit(x,y,sig: glndata; ndata: integer; VAR a: glnparam; na: integer;
      lista: gllista; mfit: integer; VAR covar: glncabynca;
      ncvm: integer; VAR chisq: real);
{ Linear least-squares fitting procedure}
implementation
{*************************************************************************}
{'Numerical recipes' procedures}
{$I gammln}
{$I gcf}
{$I gser}
{$I gammq}
{$I gaussj}  {See note in text}
{$I covsrt}  {See note in text}
{$I fgauss}  {See note in text}
{$I mrqcof}  {See note in text}

PROCEDURE funcs(z:real;var afunc : glnparam;na: integer);
var  l,i  : integer;
begin
  for i:=1 to na do
    begin
      afunc[i]:=1;
      for l:=1 to (i-1) do
      afunc[i]:=afunc[i]*z;
    end;
end;

{$I mrqmin} {See note in text}
{$I lfit}   {See note in text}
```

```
{*****************************************************************************}
end.
```

B.2.4 The unit file LDA.PAS

```
unit LDA;
{ To convert to ascii format from the hexidecimal format of spectrum files
from the Mt John University Observatory's Linear Diode Array.  Reference
MacQueen (1986) p211}
interface
  type    spectrum        = array[1..2048] of real;
          pspectrum       = ^spectrum;
          charfile        = file of Char;
 procedure read_data (var hexfile               : charfile;
                      var y                  : pspectrum;
                          second                : boolean);
implementation
 {*****************************************************************}
 procedure read_data (var hexfile               : charfile;
                      var y                     : pspectrum;
                          second                : boolean);
 {Reads data from LDA hexidecimal format}
 var
   a,b,x                                        :char;
   i                                            :integer;
   outfile                                      :text;
   factor                                       :real;
   ID                                           :string;

 procedure Initialise;
 var i   : integer;
 begin
   for i:=1 to 1872 do
        y^[i]:=0.0;
    reset (hexfile);
    While IOResult <> 0 do
      begin
        writeln('Spectrum file not found');
        writeln('Enter name of file');
        readln(ID);
        assign(hexfile,ID);
        reset(hexfile);
      end;
 end;

 procedure Header; {Read LDA frame header information}
 var    i    : integer;
 begin
    assign(outfile,'header.dat');
    if not second then
```

```
      rewrite(outfile)
    else
      append(outfile);
  for i :=1 to 144 do
    begin
      read(hexfile,a);
      read(hexfile,b);
      case i of
        7                : write(outfile,b);
        8..11            : write(outfile,a,b);
        12               : writeln(outfile,a);
        19..22           : begin
                             writeln(outfile,ord(a));
                             writeln(outfile,ord(b));
                           end;
        23               : begin
                             writeln(outfile,ord(a));
                             x:=b;
                           end;
                       else;
    end;
  end;
  close(outfile);
end;

procedure Data;{Read actual data}
var   i    : integer;
begin
  for i:=1 to 1872 do
    begin
      read(hexfile,a,b);
      y^[i]:=(ord(b)+256*(ord(a)))*1.0;
    end;
  close(hexfile);
end;
{*********************************************************************}
begin
  Initialise;
  Header;
  Data;
end;
{*********************************************************************}
end.
```

B.2.5 The unit file PLOT.PAS

```
unit PLOT;
interface
uses
  Graph, Fit, LDA, CRT;
```

```
type
  linearray     = array[1..14]of real;

procedure SetGraphics;
procedure SetHighlightColor;
procedure SetDefaultColor;
procedure DrawBox;
procedure SetWindow(ID : string);
procedure graphgaussian(c :pspectrum; xlarge,xsmall:integer;a: glnparam;
                                                              ycont:real);
procedure graphcrosscorrelation( x  : pspectrum;  xl,xs  :integer);
procedure FindDimension(a,b : integer; c: pspectrum; var  greatest,least:real;
                                                    var  greatesti:integer);
procedure FitGaussian(xlarge,xsmall:integer; var a: glnparam; c: pspectrum;
     ycont  : real; var covar :glncabynca;sig   : glndata; var chisq : real);
procedure Xfit(c : pspectrum;dlglambda  :real;autofit  : boolean;
                    specfile:string; fitrange : real;var velocity : real);
procedure Boundaries(var restlambda:glndata;
                    var linepos   : linearray);
procedure LinePositions(specfile:string;maxsig: real;view:boolean);
procedure DisplayResult(a : glnparam;dlglambda : real; error : real);
{************************************************************************}
implementation
var
          MaxX,MaxY,MaxColor        : word;
          ID, xlabel, ylabel        : string;
          VertScale,HorizScale,
          Xstart,Ystart,Xend,Yend,
          OptionLine,IDLine,
          CursorLine,XLabelLine,
          ResultLine,XScaleLine,
          i,xl,xs,xlarge,xsmall      : integer;
          greatest,least,chisq       : real;
          sigl                       : linearray;
{************************************************************************}
procedure SetGraphics;
var
  graphdriver, graphmode, errorcode           : integer;
begin
  graphdriver := Detect;
  initgraph(graphdriver, graphmode,'c:\TURBO');
  Errorcode:= GraphResult;
  If Errorcode <> grOK then
    begin
      writeln('Graphics error');
      writeln(GraphErrorMsg(Errorcode));
      writeln('Hit <return>');
      readln;
    end;
  MaxX:=GetMaxX;
```

```
  MaxY:=GetMaxY;
  MaxColor:=GetMaxColor;
end;
{*****************************************************************************}
procedure SetHighlightColor;
begin
  SetColor(MaxColor);
end;
{*****************************************************************************}
procedure SetDefaultColor;
begin
    SetColor(Maxcolor);
end;
{*****************************************************************************}
procedure DrawBox;
var
  i                              : longint;
  xcoord,ycoord, scale, limit    : integer;
  istring                        : string[7];
  scaleoption                    : array[1..9]of integer;
  cor                            : boolean;
  iy                             : real;
begin
{  Set the screen parameters and draw the box }
  SetHighlightColor;
  SetLineStyle(SolidLn,0,NormWidth);
  Xstart:=trunc(1.5*TextWidth('-1.00'));
  Xend:= MaxX;
  Ystart:=5*TextHeight('M');
  Yend:=MaxY-10*TextHeight('M');
  VertScale:=Yend-Ystart;
  HorizScale:=Xend- Xstart;
  Rectangle(Xstart,Ystart,Xend,Yend);
  OptionLine:=1*TextHeight('M');
  IDLine:= 4*textHeight('M');
  Cursorline:=Yend + ((MaxY - Yend) div 6);
  XscaleLine:=Yend + ((MaxY - Yend) div 4);
  XlabelLine:=Yend + ((MaxY - Yend) div 2);
  ResultLine:=MaxY -2*TextHeight('M');

{draw tick-marks in x}
 scaleoption[1]:=1;
 scaleoption[2]:=2;
 scaleoption[3]:=5;
 scaleoption[4]:=10;
 scaleoption[5]:=20;
 scaleoption[6]:=50;
 scaleoption[7]:=100;
 scaleoption[8]:=200;
 scaleoption[9]:=500;
```

```
cor:=false;
if ((greatest-least)/0.02 <= 100) then
  cor:=true;
scale:=0;i:=1;
while (scale=0) do   { Determine interval between x axis tick-marks }
  begin
    if (xl-xs)/scaleoption[i] <100 then
    scale:=scaleoption[i];
    inc(i);
  end;
 for i :=xs to xl do
   begin
     xcoord :=round(HorizScale*(i - xs)/(xl - xs)) + Xstart;
     if (i  mod scale = 0) then
       begin
       {label every second tick-mark and make these tick-marks larger}
         if ((i mod (10*scale) = 0) and (not cor))
           or (((i-1024) mod (10*scale) = 0) and cor) then
           begin
             moveto(xcoord - 5, XscaleLine);
             if cor then
               str (i-1024,istring)
             else
               str(i,istring);
             outtext(istring);
             moveto(xcoord,Yend);
             lineto(xcoord,Yend-5);
             moveto(xcoord,Ystart);
             lineto(xcoord,Ystart+5);
           end
         else  {smaller tick-marks}
         begin
           moveto(xcoord,Yend);
           lineto(xcoord,Yend-3);
           moveto(xcoord,Ystart);
           lineto(xcoord,Ystart+3);
         end;
       end
    else; {skip to next bin}
   end; {for}

 {  Write the labels   }
  settextstyle(0,1,0);
  OutTextXY(Xstart div 4,(Yend div 2)+((Yend-VertScale)div 2),ylabel);
  settextstyle(0,0,0);
  OutTextXY((MaxX div 2)+(Xstart div 2),XLabelLine,xlabel);
scale:=0;i:=1;
while (scale=0) do
  begin
    if (greatest-least)/scaleoption[i] <50 then
```

```
      scale:=scaleoption[i];
      inc(i);
    end;

{ Draw tick-marks in y }
  i :=scale*(trunc(least/scale)+1);
  if cor then
    begin
      i:= scale*(trunc(least*50/scale)+1);
      limit:= trunc(50*greatest);
    end
  else
    limit:=trunc(greatest);
  while i<=limit do
     begin
       if cor then
         iy:=0.02*i
       else
         iy:=i;
       ycoord := Ystart + round(VertScale*(greatest-iy)/(greatest-least));
       moveto(Xstart, ycoord);
       if (i mod (10*scale))=0 then
         begin
           lineto(Xstart+5, ycoord);
           moveto(2*(Xstart div 3), ycoord);
           str(iy:5:1,istring);
           str(iy/100:5:1,istring)};
           outtext(istring);
           moveto(MaxX-5,ycoord);
           lineto(MaxX,ycoord);
         end
       else
         begin
           lineto(Xstart+3, ycoord);
           moveto(MaxX-3,ycoord);
           lineto(MaxX,ycoord);
         end;
       i:=i + scale;
     end;
end;
{*****************************************************************************}
procedure SetWindow(ID : string);
begin
  ClearDevice;
  SetTextJustify(CenterText,CenterText);
  SetViewPort(0,0,MaxX,MaxY,ClipOn);
  DrawBox;
  OutTextXY(MaxX div 2,IDLine,ID);
end;
{*****************************************************************************}
```

```
procedure graphgaussian;
var
  number, gauss, z                : real;
  i,j                             : longint;
  xcoord,ycoord,p,k, scale        : integer;
  istring                         : string[20];
  answer                          : string[1];
  dummy                           : glnparam;
begin
  SetHighlightColor;
  SetLineStyle(0,0,Thickwidth);
  for k:=1 to 2 do
    begin
  for i := xsmall to xlarge do
    begin     { assign coordinate values}
      z :=i;
      if i = xlarge then
        p:=1
      else
        p := 10;
      for j := 1 to p do   {plot at 10x frequency of data points}
        begin
          xcoord := round((z - xs)*HorizScale/(xl - xs)) + Xstart;
          fgauss(z,a,gauss,dummy,na,ycont);
          ycoord := Yend - round(VertScale*(gauss-least)/(greatest-least));
          if (z = xsmall) then
            moveto(xcoord,ycoord)
          else
            lineto(xcoord,ycoord);
          z := z + 0.1;
        end;
    end;
  end;
  SetDefaultColor;
  end;
{*****************************************************************************}
procedure graphcrosscorrelation;
var
  i                               : longint;
  xcoord,ycoord                   : integer;
  istring                         : string[20];
begin
  for i := xs to xl do
    begin
     { assign screen coordinates }
        xcoord := round((i - xs)*HorizScale/(xl - xs)) + Xstart;
        ycoord := Yend - round(VertScale*(x^[i] - least )/(greatest - least));
     { plot the data points }
        if (i = xs) then
          moveto(xcoord,ycoord)
```

```
        else
          lineto(xcoord,ycoord);
    end;
end;
{*************************************************************************}
  procedure FindDimension(a,b: integer; c: pspectrum; var  greatest,least:real;
                                                    var  greatesti:integer);
  {finds greatest and least values in an array c}
  var
    i  : integer;
  begin
     greatest :=-1.0E+10;least := 1.0E+10;
     for i:= a to b do
     begin
       if c^[i] > greatest then
         begin
           greatest := c^[i];
           greatesti := i;
         end;
       if c^[i] < least then
         least := c^[i];
     end;
   end;
  {*************************************************************************}
  procedure FitGaussian;
  var
   j,ndata, mfit           : integer;
   x,y                     : glndata;
   lista                   : gllista;
   alamda, lastchisq       : real;
   alpha                   : glncabynca;
   glbeta                  : glnparam;
   fitfile                 : text;
  begin
   ndata := xlarge - xsmall + 1;
   for i := xsmall to xlarge do  {  order  data to be fitted into its array }
     begin                                    {    and renumber x    }
       j := i - xsmall + 1;
       x[j] := i;
       y[j] := c^[i];
     end;
  a[1] := greatest;     {  Set initial values of the parameters  }
  a[2] := xsmall + trunc(ndata/2)+1;
  a[3] := 3;
  mfit := 3;            { Determine which are to be fitted}
  for i := 1 to mfit do
    lista[i] := i;
  alamda := -1.0;   { This prompts initialisation in mrqmin }
  chisq:=100; lastchisq:=1000;
  while abs(lastchisq-chisq) > 0.1 do
```

```
    begin
      lastchisq:=chisq;
      mrqmin(x, y, sig, ndata, a, na,lista, mfit, covar,
                                    alpha, nca, chisq, alamda,ycont);
    end;
  alamda:=0;
  mrqmin(x, y, sig, ndata, a, na,lista, mfit, covar, alpha, nca, chisq, alamda,
                                                          ycont);
end;
{*************************************************************************}
procedure Xfit(c : pspectrum;dlglambda  :real;autofit  : boolean;
                   specfile:string;fitrange: real;var velocity: real);
var
  a, dummy                          : glnparam;
  xcont, greatesti, i, j, b         : integer;
  covar                             : glncabynca;
  ycont, val, dev, Q, a1, weight    : real;
  answer                            : char;
  finished                          : boolean;
  sig                               : glndata;
  error                             : double;
  f,plot                            : text;
begin
  xlabel:='Bin number'; ylabel:='Correlation';
  FindDimension(1,2048,c,greatest,least,greatesti);
    finished:=false;
  while not finished do
    begin
      xl:=(greatesti + 30);xs:=(greatesti - 30);
      xlarge:=greatesti;
      while c^[xlarge]>((1-fitrange)*greatest) do
        inc(xlarge);
      xsmall:=greatesti;
      while c^[xsmall]>((1-fitrange)*greatest) do
        dec(xsmall);
      {Make sure that  peak is not unreasonably wide}
      while (xlarge-xsmall) > 45 do
        begin
          writeln ('NDATA = ',xlarge-xsmall);
          writeln('Fraction of peak to be fitted probably too high');
          write('Enter new fraction: ');
          readln(fitrange);
          xlarge:=greatesti;
          while c^[xlarge]>((1-fitrange)*greatest) do
          inc(xlarge);
          xsmall:=greatesti;
          while c^[xsmall]>((1-fitrange)*greatest) do
          dec(xsmall);
        end;
      dev:=0.0003;
```

```
      for i:=xsmall to xlarge do
        sig[i-xsmall+1]:=dev;
      ycont:=0;
      FitGaussian(xlarge,xsmall,a,c,ycont,covar,sig,chisq);
      SetGraphics;
      SetWindow(specfile);
      graphcrosscorrelation(c,xl,xs);
      graphgaussian(c,xlarge,xsmall,a,ycont);
      delay(1000);
      readln;
      CloseGraph;
      RestoreCrtMode;
      a[2]:=a[2]-1024;
      writeln('Gaussian half width= ',a[3]:4:3,' +/- ',sqrt(covar[3,3]):5:4);
      writeln('Height=',a[1]:4:3,' +/- ',sqrt(covar[1,1]):5:4);
      writeln('Position=',a[2]-1:4:3,' +/- ',sqrt(covar[2,2]):5:4);
      writeln('Q= ',Q);
      chisq:=0;
      writeln('Number of points = ', xlarge-xsmall+1);
      writeln;
      writeln('Error in velocity is +/-',sqrt(covar[2,2])*1557:6:5,' m/s');
      finished:=true;autofit:=false;
      velocity:=(a[2]-1);
    end;
end;
{*****************************************************************************}
 procedure boundaries (var restlambda   : glndata;
                       var linepos      : linearray);
 var
   i,j                                  : integer;
 begin
   restlambda[1]:=4989.31; linepos[1]:=66.65;sigl[1]:=25;
   restlambda[2]:=4993.749;linepos[2]:=233.05;sigl[2]:=25;
   restlambda[3]:=4999.937;linepos[3]:=466.82;sigl[3]:=25;
   restlambda[4]:=5002.097;linepos[4]:=548.74;sigl[4]:=25;
   restlambda[5]:=5003.597;linepos[5]:=605.94;sigl[5]:=25;
   restlambda[6]:=5004.128;linepos[6]:=625.96;sigl[6]:=25;
   restlambda[7]:=5009.334;linepos[7]:=825.62;sigl[7]:=25;
   restlambda[8]:=5015.888;linepos[8]:=1078.78;sigl[8]:=25;
   restlambda[9]:=5017.51;linepos[9]:=1141.81;sigl[9]:=25;
   restlambda[10]:=5019.806;linepos[10]:=1231.20;sigl[10]:=25;
   restlambda[11]:=5022.005;linepos[11]:=1317.21;sigl[11]:=25;
   restlambda[12]:=5023.709;linepos[12]:=1383.84;sigl[12]:=25;
   restlambda[13]:=5028.656;linepos[13]:=1578.57;sigl[13]:=25;
   restlambda[14]:=5029.893;linepos[14]:=1627.71;sigl[14]:=25;
 end;

{*****************************************************************************}
procedure LinePositions(specfile:string;maxsig: real;view:boolean);
var
```

```
  x                                : pspectrum;
  a, dummy                         : glnparam;
  greatesti, xcont, l, i, k        : integer;
  covar                            : glncabynca;
  ycont                            : real;
  restlambda, sig, yfit            : glndata;
  dispfile                         : text;
  linepos                          : linearray;
  correction                       : real;
  message                          : string;
  spec                             : charfile;
  accepted                         : boolean;
  ans                              : char;
begin
  new(x);
  assign(spec,specfile);
  read_data(spec,x,false);
  xlabel:='Pixel number';
  ylabel:='Intensity (%)';
  assign(dispfile,'disp.dat');
  rewrite(dispfile);
  Boundaries(restlambda,linepos);

  for l:=1 to 14 do
    begin
      xl:=round(linepos[l])+15;xs:=round(linepos[l])-15;
      if l=1 then
        begin
          xl:=xl+10;xs:=xs-10;  {To make sure the first line is found}
        end
      else
        begin
          xl:=xl + round(correction);xs:=xs + round(correction);
        end;
       FindDimension(xs,xl,x,greatest,least,greatesti);
      greatest:=greatest+(greatest/5);
      if l=1 then
        begin
         xlarge:=greatesti+5;xsmall:=greatesti-5;
       end
     else
       begin
        xlarge:=round(linepos[l]+correction)+ 5;
        xsmall:=round(linepos[l]+correction)- 5;
      end;
      for i:=1 to (xlarge-xsmall+1) do
        sig[i]:=sigl[i];
      accepted:=false;
      ycont:=0;
      while not accepted do
```

```
      begin
        FitGaussian(xlarge,xsmall,a,x,ycont,covar,sig,chisq);
        message:='';
        If sqrt(covar[2,2]) < maxsig then
          begin
            writeln(dispfile,a[2]:8:3,' ',restlambda[1]:8:3,' '
                 ,sqrt(covar[2,2]):8:3);
            accepted:=true;
          end
        else
          begin
            message:='  (rejected) ';
            writeln(#7);
          end;
          correction:=a[2] - linepos[1];
        if view then
          begin
            SetGraphics;
            SetWindow(specfile);
            graphcrosscorrelation(x,xl,xs);
            graphgaussian(x, xlarge, xsmall, a,ycont);
            If keypressed then
              Delay(2000);
            if not accepted then readln;
            ClearDevice;
            CloseGraph;
          end
        else
          begin
            clrscr;
            writeln(1,message);
          end;
ycont:=0;

        if not accepted then
          begin
            writeln('Try again (y/n)?');
            readln(ans);
            if ans='y' then
              begin
                writeln('Enter new values for xsmall: ');
                readln(xsmall);
                writeln('..xlarge: ');
                readln(xlarge);
                writeln('Enter ycont');
                readln(ycont);
              end
            else
              accepted:=true;
          end;
```

```
        end;
    end;
    close(dispfile);
    dispose(x);
end;
{*************************************************************************}
procedure DisplayResult(a              : glnparam;
                        dlglambda      : real;
                        error          : real   );
var
  binstring,velocitystring,errorv,errorb         : string;
begin
  SetFillStyle(1,MaxColor);
  Bar(0,ResultLine -TextHeight('M'),MaxX,ResultLine+TextHeight('M'));
  SetColor(0);
  Str((exp(dlglambda*(a[2]-1)) - 1)*2.997925e+05:6:3,velocitystring);
  Str(error*(exp(dlglambda) -1)*2.997925e+5:6:3,errorv);
  OutTextXY(MaxX div 2,ResultLine,velocitystring+' +/- '+errorv+' km/sec');
end;
{*************************************************************************}
{initialisation section}
end.
```

B.2.6 The unit file PREPARE.PAS

```
unit Prepare;
{Contains procedures used to prepare stellar spectra for crosscorrelating}
interface
 uses
   LDA, Fit, Plot;
 type
   spectrum2     = array[1..4096]of real;
   pspectrum2    = ^spectrum2;
 procedure cosinebell(     y                        :pspectrum;
                           n1, n2                   :integer;
                           second                   :boolean);
{applies a cosine bell to the first and last 10% of the data y from n1 to n2}


PROCEDURE correl(data1,data2: pspectrum; n: integer; VAR ans: pspectrum2;
                    filt: boolean;title :string);
{Performs the correlation}

 procedure rebin( var y                     : pspectrum;
                     li, lf                 : real;
                  var dlglambda             : real;
                     d                      : integer;
                     dis                    : vector3 );
 { rebins n data bins y in interval [li, lf], dispersion equation
   coefficients dis - to n bins linear in log(lambda)             }
```

```
 procedure subtractmean(var y                : pspectrum;
                            n1,n2            : integer;
                            second           : boolean);
 { subtracts the mean of the array y between n1 and n2 }

implementation
 {************************************************************************}
 procedure cosinebell(     y                       :pspectrum;
                           n1, n2                  :integer;
                           second                  :boolean);
var
  k, m1, m2                                        : integer;

begin
  m1 := (n2 - n1 + 1) div 10; { calculate how much is 10% of the data}

  if (not second) then
    m2 := n2 - m1 + 1
  else
    m2 := n2 - m1 + 1;

  for k := n1 to (n1 + m1 - 1) do
    y^[k] := y^[k] * ( 1 - cos(3.141592654 * (k - n1)/m1))/2;
  for k := m2 to n2 do
    y^[k] := y^[k] * ( 1 + cos(3.141592654 * (k - m2)/m1))/2;
end;{cosinebell}
 {************************************************************************}
PROCEDURE correl(data1,data2: pspectrum; n: integer; VAR ans: pspectrum2;
    filt:boolean; title:string);
VAR
   no2,i,ii,a                      : integer;
   dum                             : real;
   data                            : pspectrum;
   isign, nn                       : integer;
   fft1, fft2                      : pspectrum2;
{ NB in any pspectrum2 array, odd values are the real parts, even : imag}

 procedure filter;
  { constructs and applies an optimum filter s to ans (See Brault and White or
    Press et al)

    A constant is approximated to the noise N in the power spectrum by a least
    squares fit to 4 points.  A straight line is approximated to the signal
    S(i) in the power spectrum in the same way.  The optimum filter is then
                          sqr(S(i))/(sqr(S(i)) + sqr(N)          }

  var lgpower,s            : pspectrum;
      i, ii, alpha, step   : integer;
      c                    : glnparam;
```

```
    a, b, sig           : glndata;
    covar               : glncabynca;
    Cxx,Cyy             : real;
    norm                : real;
    d                   : real;
    chisq               : real;
begin
  if filt then
    begin
      writeln('begin FILTER');
      new(lgpower);
      alpha := 300;
      step := alpha div 20;
      for i := 1 to (n div 2) do
      begin
       ii:=2*i;
       if (sqr(ans^[ii-1])+sqr(ans^[ii]) ) <= 1.0e-5 then
          writeln( 'at i=',i:5,sqr(ans^[ii-1])+sqr(ans^[ii]) );
      lgpower^[i] := ln( sqr(ans^[ii-1]) + sqr(ans^[ii]) )/ln(10);
      end;
    for i:=1 to 20 do
      begin
        a[i] := lgpower^[alpha+200+i*step];
        b[i] := alpha + i*step;
      end;

    lfit(b,a,sig,20,c,1,lista,1,covar,1,chisq);
    d:=c[1];
    for i := 1 to 20 do
      begin
        a[i] := lgpower^[i*step];
        b[i] := i*step
      end;
    lfit(b,a,sig,20,c,2,lista,2,covar,2,chisq);
    dispose(lgpower);
    new(s);
  { Calculate optimum filter = signal^2/(signal^2 + noise^2) }
    for i := 1 to ((n div 2)+1) do
      s^[i] := exp( ln(10)*(c[1] + c[2]*i))
                    /(exp(ln(10)*(c[1]+c[2]*i)) + exp(ln(10)* d));
    for i := 1 to n div 2 do
      s^[n-i+1] := s^[i+1];
  end
    else
      begin
        new(s);
        for i:=1 to n do
          s^[i]:=1;
        end;
```

```
   Cxx:= 0;
   Cyy:= 0;
   for i := 1 to n  do
     begin
       ii:=2*i;
       cxx := cxx + s^[i]*(sqr(fft1^[ii-1])+ sqr(fft1^[ii]));
       cyy := cyy + s^[i]*(sqr(fft2^[ii-1])+ sqr(fft2^[ii]));
     end;
     norm:=2048/(sqrt(Cxx)*sqrt(Cyy));
   for i := 1 to n do
     begin
       ii:=2*i;
       ans^[ii-1] := ans^[ii-1]*s^[i]*norm;
       ans^[ii]:= ans^[ii]*s^[i]*norm;
     end;
   dispose(s);
 end; { filter }
{*****************************************************************************}
PROCEDURE four1(VAR data: pspectrum2; nn,isign: integer);
(* Programs using routine FOUR1 must define type
TYPE
   pspectrum = ARRAY [1..nn2] OF real;
in the calling routine, where nn2=nn+nn. - nn := 1024 in this case*)
VAR
   ii,jj,n,mmax,m,j,istep,i: integer;
   wtemp,wr,wpr,wpi,wi,theta: real {double};
   tempr,tempi: real;
BEGIN
   n := 2*nn;
   j := 1;
   FOR ii := 1 to nn DO BEGIN
      i := 2*ii-1;
      IF (j > i) THEN BEGIN
         tempr := data^[j];
         tempi := data^[j+1];
         data^[j] := data^[i];
         data^[j+1] := data^[i+1];
         data^[i] := tempr;
         data^[i+1] := tempi
      END;
      m := n DIV 2;
      WHILE ((m >= 2) AND (j > m))  DO BEGIN
         j := j-m;
         m := m DIV 2
      END;
      j := j+m
   END;
   mmax := 2;
   WHILE (n > mmax) DO BEGIN
      istep := 2*mmax;
```

```
      theta := 6.28318530717959/(isign*mmax);
      wpr := -2.0*sqr(sin(0.5*theta));
      wpi := sin(theta);
      wr := 1.0;
      wi := 0.0;
      FOR ii := 1 to (mmax DIV 2) DO BEGIN
         m := 2*ii-1;
         FOR jj := 0 to ((n-m) DIV istep) DO BEGIN
            i := m + jj*istep;
            j := i+mmax;
            tempr := wr*data^[j]-wi*data^[j+1];
            tempi := wr*data^[j+1]+wi*data^[j];
            data^[j] := data^[i]-tempr;
            data^[j+1] := data^[i+1]-tempi;
            data^[i] := data^[i]+tempr;
            data^[i+1] := data^[i+1]+tempi
         END;
         wtemp := wr;
         wr := wr*wpr-wi*wpi+wr;
         wi := wi*wpr+wtemp*wpi+wi
      END;
      mmax := istep
   END
END;
 {*************************************************************************}
PROCEDURE realft(VAR data: pspectrum2; nn,isign: integer);
(* Programs using routine REALFT must define the type
TYPE
      pspectrum = ARRAY [1..2*nn] OF real;
where 2*n is the dimension of the input data array. When
routine FOUR1 is used with REALFT, its data type 'pspectrum'
should be set as in this program. *)
VAR
      wr,wi,wpr,wpi,wtemp,theta: real {double};  i,i1,i2,i3,i4: integer;
      c1,c2,h1r,h1i,h2r,h2i,wrs,wis: real;
BEGIN
      theta := 6.28318530717959/(2.0*nn);  c1 := 0.5;
      IF (isign = 1) THEN BEGIN
        c2 := -0.5;  four1(data,nn,1);  END   { forward transform  }
      ELSE BEGIN
        c2 := 0.5;  theta := -theta;  END;   { otherwise set up for inverse }
      wpr := -2.0*sqr(sin(0.5*theta));  wpi := sin(theta);
      wr := 1.0+wpr;  wi := wpi;
      FOR i := 2 TO (nn DIV 2)+1 DO BEGIN
        i1 := i+i-1;  i2 := i1+1;  i3 := nn+nn+3-i2;  i4 := i3+1;
        wrs := wr;  wis := wi;  h1r := c1*(data^[i1]+data^[i3]);
        h1i := c1*(data^[i2]-data^[i4]);  h2r := -c2*(data^[i2]+data^[i4]);
        h2i := c2*(data^[i1]-data^[i3]);  data^[i1] := h1r+wrs*h2r-wis*h2i;
        data^[i2] := h1i+wrs*h2i+wis*h2r;  data^[i3] := h1r-wrs*h2r+wis*h2i;
        data^[i4] := -h1i+wrs*h2i+wis*h2r;  wtemp := wr;
```

```
        wr := wr*wpr-wi*wpi+wr;  wi := wi*wpr+wtemp*wpi+wi  END;
      IF (isign = 1) THEN BEGIN
        h1r := data^[1];  data^[1] := h1r+data^[2];  data^[2] := h1r-data^[2]  END
      ELSE BEGIN
        h1r := data^[1];  data^[1] := c1*(h1r+data^[2]);
        data^[2] := c1*(h1r-data^[2]);  four1(data,nn,-1)  END {inverse transform}
END;


PROCEDURE twofft;
(* Programs using routine TWOFFT must define types
TYPE
   spectrum = ARRAY [1..n] OF real;
   spectrum2 = ARRAY [1..2*n] OF real;
where n is the dimension of the real-valued data arrays. *)
VAR
   nn3,nn2,nn,jj,j: integer;
   rep,rem,aip,aim: real;
BEGIN
  new(fft1);
  new(fft2);
   nn := n+n;
   nn2 := nn+2;
   nn3 := nn+3;
   FOR j := 1 to n DO BEGIN
      jj := j+j;
      fft1^[jj-1] := data1^[j];
      fft1^[jj] := data2^[j]
   END;
   four1(fft1,n,1);
   fft2^[1] := fft1^[2];
   fft1^[2] := 0.0;
   fft2^[2] := 0.0;
   FOR jj := 1 to (n DIV 2) DO BEGIN
      j := 2*jj+1;
      rep := 0.5*(fft1^[j]+fft1^[nn2-j]);
      rem := 0.5*(fft1^[j]-fft1^[nn2-j]);
      aip := 0.5*(fft1^[j+1]+fft1^[nn3-j]);
      aim := 0.5*(fft1^[j+1]-fft1^[nn3-j]);
      fft1^[j] := rep;
      fft1^[j+1] := aim;
      fft1^[nn2-j] := rep;
      fft1^[nn3-j] := -aim;
      fft2^[j] := aip;
      fft2^[j+1] := -rem;
      fft2^[nn2-j] := aip;
      fft2^[nn3-j] := rem
   END;
END;
```

```
BEGIN  {Correl}
   writeln(output,'Forward transform...');
   twofft;

   dispose(data1);
   dispose(data2);

   no2 := n DIV 2;
 FOR i := 1 to (no2+1) DO BEGIN
      ii := 2*i;
      dum := fft2^[ii-1];
      ans^[ii-1] := (fft1^[ii-1]*fft2^[ii-1]+fft1^[ii]*fft2^[ii])/no2;
      ans^[ii] := (fft1^[ii]*dum-fft1^[ii-1]*fft2^[ii])/no2
   END;

   ans^[2] := ans^[n+1];
  filter;
  dispose(fft1);
  dispose(fft2);

   writeln('Reverse transform...');
   realft(ans,no2,-1);

END;
 {*****************************************************************************}
 procedure rebin(var y                  : pspectrum;
                 li, lf                 : real;
             var dlglambda              : real;
                 d                      : integer;
                 dis                    : vector3);
 { rebins d data bins y in interval [li, lf], inverted dispersion equation
   coefficients dis - to d bins linear in log(wavelength).}
 var
     i,k,h                              : integer;
     scale                              : real;
     s, x, lambda                       : pspectrum;
begin
    dlglambda := (ln(lf) - ln(li))/d;
    new(x);
    new(lambda);
    for k := 1 to d+2 do
      begin
        lambda^[k] := exp(ln(li) + (k-1)*dlglambda);
        x^[k] :=dis[1]+(lambda^[k]-5010)*(dis[2]+(lambda^[k]-5010)*dis[3]);
      end;
    new(s);
     for k:= 1 to d do
       begin
        h:=trunc(x^[k]);
        scale:=x^[k+1]-x^[k];    { number of pixels in the bin }
```

```
      if (scale-1+x^[k]-h) <=0 then
        s^[k]:=scale*y^[h]
          else
            begin
              s^[k]:=(1-x^[k]+h)*y^[h];
              i:=0;
              for i:=1 to trunc(scale-1+x^[k]-h) do
                s^[k]:= s^[k] + y^[h+i];
              s^[k]:=s^[k] + (scale-1+x^[k]-h-i)*y^[h+i+1];
            end;

        s^[k]:=s^[k]/scale;
    end;
       for k:=1 to d do
         y^[k]:=s^[k];
  dispose(x);
  dispose(lambda);
  dispose(s);
end;{rebin}
{*****************************************************************************}
procedure subtractmean(var y                : pspectrum;
                           n1,n2            : integer;
                           second           : boolean);
{ subtracts the mean of the array y between n1 and n2 }
var
  i                                         : integer;
  sum,mean,rms                              : real;
begin
  sum := 0.0;
  mean := 0.0;
  rms := 0.0;
  if not second then
    begin
      for i := n1 to n2  do
        begin
          sum := sum + y^[i];
          rms := rms + sqr(y^[i] - 10000);
        end;
      mean := sum/(n2 - n1 + 1);
      rms := sqrt(rms/(n2 - n1 +1));
      writeln('RMS = ',rms);
      for i := n1 to n2 do
        y^[i] := y^[i] - mean;
      for i := (n2 + 1) to 2048 do
        y^[i] := 0;
    end
  else
    begin
     for i:=1 to (n1 -1) do
       y^[i] :=0;
```

```
      for i := n1 to n2 do
        begin
          sum := sum + y^[i];
          rms := rms + sqr(y^[i] - 10000);
        end;
      mean := sum/(n2  - n1 + 1);
      rms := sqrt(rms/(n2 - n1 + 1));
      for i := n1 to n2 do
        y^[i] := y^[i] - mean;
    end;
 end;{subtractmean}
 {*************************************************************************}
end.
```

Appendix C

Mt John programme velocities

The following six pages list the relative radial velocities obtained for the stars in the Mt John programme. These were displayed graphically in Chapter 4.

HJD −2440000	Velocity (km/s)	HJD −2440000	Velocity (km/s)	HJD −2440000	Velocity (km/s)	HJD −2440000	Velocity (km/s)
HR 77 (ζ Tuc)		8386.82	+0.042	8256.91	+0.221	7570.90	−0.051
7479.97	+0.050	8421.24	+0.067	8306.89	−0.172	7610.88	+0.167
7480.93	+0.154	8441.21	+0.002	8321.86	−0.336	7729.26	+0.091
7519.95	+0.030	HR 188 (β Cet)		8323.84	−0.161	8083.20	+0.133
7550.93	+0.090	7479.99	+0.050	8325.86	−0.132	8133.09	+0.073
7606.88	+0.178	7480.95	+0.019	8441.27	−0.147	8147.08	+0.090
7652.07	+0.076	7481.99	+0.043	8443.29	−0.044	8148.12	−0.001
7729.19	+0.096	7489.95	+0.087	8479.22	−0.035	8175.13	+0.075
7946.90	+0.234	7519.92	−0.158	HR 1008 (82 Eri)		8176.10	+0.054
8000.21	−0.028	7528.97	−0.051	7480.05	+0.050	8221.05	−0.038
8087.06	+0.094	7729.17	−0.025	7518.03	−0.068	8256.92	+0.108
8132.12	+0.055	7730.15	−0.049	7551.00	+0.008	8258.89	+0.048
8148.08	+0.008	8086.23	−0.034	7571.95	+0.139	8259.95	+0.070
8176.05	+0.231	8132.15	−0.026	7610.85	+0.040	8308.87	+0.086
8219.99	+0.017	8133.01	−0.015	7943.91	+0.052	8323.86	+0.111
8232.95	+0.071	8146.09	−0.042	7964.87	+0.030	8325.89	+0.099
8259.02	+0.044	8176.09	−0.067	8091.15	−0.052	8441.26	+0.114
8308.86	−0.008	8219.96	−0.177	8132.98	−0.051	8479.15	+0.133
8321.90	+0.221	8232.94	−0.045	8146.16	−0.102	HR 1674 (ζ Dor)	
8374.90	+0.257	8423.31	+0.017	8181.08	−0.110	7480.12	+0.050
8421.26	+0.243	8441.28	−0.006	8221.00	−0.141	7520.93	+0.012
8441.19	+0.103	HR 370 (ν Phe)		8233.02	−0.005	7570.94	−0.025
8477.83	+0.112	7481.96	+0.050	8258.97	−0.005	7603.95	+0.095
8478.82	−0.006	7517.97	+0.235	8306.91	−0.079	7640.85	−0.158
HR 98 (β Hyi)		8087.10	+0.267	8322.92	−0.131	7653.83	−0.004
7480.90	+0.050	8132.19	+0.271	8443.30	−0.097	7943.96	+0.119
7519.98	+0.026	8146.12	+0.188	HR 1083 (κ Ret)		8091.20	+0.089
7549.01	+0.139	8176.06	+0.292	7481.05	+0.050	8131.24	−0.089
7571.91	+0.196	8220.97	+0.123	7520.04	−0.082	8147.06	−0.005
7602.94	−0.044	8232.99	+0.298	7551.05	+0.004	8181.05	−0.004
7652.03	+0.089	8258.92	+0.138	7609.89	+0.191	8221.09	−0.284
7694.28	+0.049	8322.89	+0.074	7643.81	+0.084	8257.00	+0.018
7729.21	+0.083	8423.24	+0.344	7729.93	−0.041	8321.99	+0.020
8000.17	−0.070	HR 911 (α Cet)		7944.91	+0.198	8373.82	−0.161
8086.25	+0.065	7480.08	+0.050	8000.12	+0.181	8386.86	−0.237
8132.14	+0.031	7482.09	−0.056	8091.10	+0.126	8420.77	−0.042
8146.08	+0.061	7519.99	−0.219	8133.05	−0.042	HR 1743 (o Col)	
8176.08	−0.020	7529.92	−0.312	8146.22	+0.001	7481.11	+0.050
8219.94	−0.160	7547.91	+0.034	8176.12	−0.107	7520.98	−0.058
8232.97	+0.100	7552.93	−0.368	8221.03	−0.131	7547.97	−0.104
8259.05	−0.075	7570.88	−0.441	8233.06	−0.010	7603.88	+0.093
8306.86	+0.066	7571.88	−0.402	8259.00	+0.509	7643.85	+0.047
8320.89	+0.117	7729.24	−0.216	8308.95	+0.018	7964.95	+0.001
8321.88	+0.188	8131.20	+0.171	8321.96	−0.083	8133.13	−0.006
8322.87	+0.121	8146.18	+0.013	8374.87	−0.301	8147.11	−0.026
8323.87	+0.064	8147.17	+0.048	8423.28	+0.300	8181.13	−0.048
8324.87	+0.044	8175.10	+0.195	HR 1136 (δ Eri)		8256.94	+0.015
8325.88	+0.069	8176.09	+0.144	7480.01	+0.050	8260.01	+0.012
8373.01	+0.138	8219.90	−0.157	7520.08	+0.072	8308.90	+0.073
8384.82	+0.077	8232.91	+0.147	7549.91	+0.176	8323.89	+0.058

HJD −2440000	Velocity (km/s)
HR 1743 cont.	
8479.19	−0.004
HR 1829 (β Lep)	
7480.15	+0.195
7481.15	+0.059
7487.07	+0.063
7518.06	−0.024
7520.89	+0.091
7521.02	+0.015
7547.03	−0.040
7548.90	+0.079
7549.93	+0.190
7550.96	+0.017
7551.97	+0.040
7570.98	+0.016
7571.99	−0.049
7591.88	+0.056
7606.84	+0.044
7609.84	+0.047
7943.87	+0.061
7944.87	+0.045
7947.01	+0.042
7964.90	+0.014
7965.89	+0.065
7999.80	+0.004
8021.79	+0.006
8091.24	+0.011
8133.18	+0.068
8146.25	+0.035
8147.16	−0.016
8176.14	+0.052
8180.98	+0.066
8182.12	+0.015
8220.08	+0.009
8221.07	−0.086
8256.98	−0.001
8259.99	+0.019
8306.95	+0.033
8322.94	+0.001
8323.96	+0.091
8325.90	+0.015
8373.80	+0.052
8386.80	+0.051
8479.24	+0.064
HR 1983(γ Lep)	
7482.02	+0.050
7521.04	+0.098
7546.99	+0.093
7571.00	+0.261
7591.90	+0.164
7946.98	+0.020
7965.87	+0.177
8133.20	+0.154
8221.12	+0.033
8256.96	+0.132
8259.97	+0.220
8306.93	−0.217
8323.90	+0.174
HR 2906	
7487.11	+0.050
7521.07	+0.081
7551.10	−0.092
7591.93	−0.255
7643.91	+0.126
7944.97	+0.070
7965.92	+0.047
7999.86	+0.063
8021.84	+0.060
8133.23	+0.102
8147.23	+0.071
8182.10	+0.102
8257.03	−0.030
8260.03	−0.105
8306.98	+0.010
8323.92	−0.027
8373.84	+0.092
HR 2943 (α CMi)	
7481.17	+0.050
7518.13	−0.011
7547.05	+0.039
7571.02	+0.016
7591.97	−0.072
7945.00	+0.158
7965.94	+0.152
7998.83	+0.108
8021.81	+0.149
8133.26	+0.156
8181.18	+0.179
8257.04	+0.231
8260.04	+0.216
8306.96	+0.310
8323.93	+0.294
8372.79	+0.388
HR 3220	
7489.00	+0.050
7529.01	+0.476
7548.04	+0.943
7592.01	+1.763
7639.88	+2.697
7643.97	+2.564
7693.89	+3.506
7728.84	+3.747
7944.02	+3.361
8018.84	+2.087
8019.84	+1.898
8020.81	+1.737
8061.89	+0.706
8132.84	−1.109
8147.20	−1.186
8181.02	−1.681
8220.13	−2.185
8257.06	−1.948
8259.12	−2.102
8260.06	−2.132
8307.94	−1.736
8320.92	−1.154
8322.02	−1.079
8324.99	−1.294
8374.78	−0.391
8374.78	−0.391
8419.82	+0.506
8420.79	+0.541
8440.77	+0.641
HR 3748 (α Hya)	
7490.11	+0.050
7520.10	−0.057
7521.15	−0.083
7529.12	−0.049
7547.07	−0.154
7548.08	−0.135
7549.03	−0.102
7551.07	−0.186
7553.08	−0.013
7554.99	−0.096
7571.03	−0.101
7591.96	−0.219
7602.83	−0.160
7603.82	−0.242
7604.83	−0.254
7605.83	−0.214
7610.91	−0.164
7639.95	−0.263
7640.82	−0.033
7643.89	−0.158
7690.78	−0.251
7693.81	−0.183
7699.86	−0.106
7724.82	−0.162
7965.07	−0.159
7999.89	−0.127
8018.80	−0.066
8019.80	−0.211
8020.85	−0.165
8061.86	−0.212
8181.22	−0.165
8308.01	+0.091
8322.07	−0.031
8372.77	+0.125
8373.88	+0.033
8374.91	+0.100
8385.00	+0.102
8419.76	+0.002
8420.76	+0.031
8425.75	−0.101
8441.76	−0.010
8442.76	−0.111
HR 3862	
7489.07	+0.050
7529.07	−0.072
7555.03	+0.094
7654.98	+0.060
7699.80	+0.067
7965.02	+0.046
7999.92	+0.060
8020.89	−0.094
8061.82	−0.017
8086.82	−0.012
8181.20	−0.040
8257.12	+0.064
8308.97	+0.266
8322.04	−0.006
8374.84	+0.005
8384.92	+0.143
8420.82	+0.007
8441.78	+0.016
HR 4134	
7490.00	+0.050
7530.03	−0.035
7555.09	+0.160
7604.03	+0.169
7644.04	−0.148
7702.86	−0.118
7724.86	+0.166
7945.15	−0.061
7999.99	+0.102
8019.92	+0.314
8061.94	−0.233
8086.92	+0.292
8086.92	+0.292
8147.25	−0.106

HJD −2440000	Velocity (km/s)
HR 4134 cont.	
8182.14	+0.255
8257.10	+0.323
8308.07	+0.115
8322.09	+0.145
8372.91	−0.043
8385.01	+0.078
8419.84	+0.114
8440.79	+0.024
HR 4492	
8260.11	+ 0.059
8307.99	−16.794
8309.07	−16.156
8321.97	+ 0.310
8368.89	−17.283
8372.12	−13.476
8372.94	−12.402
8374.81	− 9.986
8384.86	+ 1.812
8387.01	+ 3.521
8419.87	−21.309
8421.03	−21.436
8422.79	−21.308
8425.79	−20.446
8441.00	− 3.569
8441.85	− 2.937
8442.78	− 1.699
8478.86	−19.730
HR 4523	
7490.08	+0.050
7552.97	−0.184
7606.06	−0.008
7653.91	+0.233
7690.87	+0.092
7728.91	−0.017
7944.13	+0.015
7995.96	+0.044
8020.95	−0.039
8082.90	+0.011
8133.83	−0.088
8146.84	−0.146
8182.18	+0.156
8257.17	+0.031
8309.00	+0.140
8323.17	+0.028
8372.96	+0.045
8374.98	+0.028
8384.97	+0.054
8422.87	+0.051

HJD −2440000	Velocity (km/s)
HR 4540 (β Vir)	
7530.11	−0.024
7555.15	+0.100
7603.00	+0.096
7651.94	+0.172
7690.81	+0.039
7729.80	+0.058
7945.10	+0.008
7966.03	+0.059
7997.92	+0.014
8085.80	+0.085
8090.80	+0.044
8259.15	+0.175
8309.02	+0.023
8321.99	−0.039
8323.05	+0.068
8323.94	+0.129
8325.09	+0.118
8325.91	+0.027
8373.05	+0.023
8374.96	+0.034
8384.88	+0.108
8386.96	+0.051
8420.86	+0.109
8422.84	+0.090
8441.80	−0.013
8442.77	+0.122
HR 4763 (γ Cru)	
7487.17	−0.321
7530.08	−0.155
7555.13	+0.038
7602.96	−0.489
7603.99	−0.402
7606.02	−0.172
7640.09	−0.389
7648.79	−0.367
7651.91	−0.567
7644.00	−0.485
7653.98	−0.661
7650.96	−0.449
7690.93	−0.391
7699.97	−0.543
7729.86	−0.871
7946.94	−0.968
7965.21	−0.634
7998.04	−0.942
8000.15	−0.800
8061.97	−0.785
8082.86	−0.149
8083.05	−0.138

HJD −2440000	Velocity (km/s)
8086.96	−0.735
8130.92	−0.333
8132.93	−0.466
8146.94	−0.186
8147.93	−0.244
8181.17	−0.638
8181.87	−0.734
8221.12	−0.271
8257.08	−0.645
8259.06	−0.098
8259.11	−0.103
8260.08	+0.055
8307.04	−0.240
8307.06	−0.386
8309.09	+0.027
8321.91	−0.429
8322.13	−0.345
8323.07	−0.260
8323.14	−0.283
8323.97	−0.226
8324.08	−0.239
8324.89	−0.293
8325.02	−0.280
8325.07	−0.308
8325.14	−0.275
8325.94	−0.452
8368.80	−1.132
8368.84	−1.165
8368.86	−1.192
8371.93	−0.968
8372.19	−0.950
8372.80	−0.790
8373.04	−0.916
8373.89	−0.816
8374.79	−0.678
8374.92	−0.694
8375.03	−0.728
8375.17	−0.674
8384.83	−1.093
8384.95	−1.088
8385.16	−1.133
8386.90	−1.173
8387.08	−1.168
8419.77	−1.215
8419.91	−1.195
8420.00	−1.212
8420.84	−1.284
8420.95	−1.359
8421.06	−1.420
8422.77	−1.119

HJD −2440000	Velocity (km/s)
8423.00	−1.176
8423.16	−1.155
8425.77	−0.655
8426.10	−0.650
8440.81	−0.580
8440.98	−0.463
8441.87	−0.401
8441.94	−0.359
8442.80	−0.279
8442.92	−0.282
8478.98	−0.882
HR 4786 (β Crv)	
7592.05	−0.094
7604.12	−0.129
7652.00	−0.088
7693.93	−0.048
7723.83	−0.156
7944.07	−0.045
7945.01	−0.100
7965.17	−0.091
7966.00	−0.087
7995.92	−0.052
7996.06	−0.103
7997.94	−0.061
8000.03	−0.114
8000.07	−0.031
8085.82	−0.116
8090.83	−0.144
8146.80	−0.084
8309.10	−0.134
8325.03	−0.073
HR 4979	
7553.05	+0.038
7606.13	−0.117
7640.04	+0.038
7651.97	+0.007
7702.94	−0.082
7724.93	+0.016
7965.12	−0.038
7995.99	−0.066
8020.05	−0.080
8082.97	−0.097
8132.90	−0.070
8146.89	+0.029
8260.14	−0.021
8309.05	+0.097
8323.20	−0.051
8372.98	+0.023
8375.01	−0.016
8385.04	0.070

HJD −2440000	Velocity (km/s)	HJD −2440000	Velocity (km/s)	HJD −2440000	Velocity (km/s)	HJD −2440000	Velocity (km/s)
HR 4979 cont.		8131.85	+0.023	7996.05	−0.204	7728.99	−0.008
8420.92	−0.158	8131.85	+0.017	7996.83	−0.201	7996.11	−0.017
8425.89	−0.034	8131.87	−0.001	7997.98	−0.224	8020.12	−0.067
8440.84	−0.015	8131.88	+0.013	7998.00	−0.189	8085.90	+0.008
HR 5019 (61 Vir)		8131.89	+0.008	7998.02	−0.196	8133.94	−0.049
7553.13	+0.043	8131.90	+0.001	8000.06	−0.178	8147.86	+0.021
7603.06	+0.098	8131.90	+0.034	8020.00	−0.249	8309.15	−0.082
7609.95	−0.010	8131.91	+0.089	8061.99	−0.269	8372.08	+0.009
7651.00	−0.041	8146.92	+0.073	8083.04	−0.261	8373.13	+0.003
7729.83	−0.069	8181.86	+0.023	8130.84	−0.209	8375.07	−0.106
7966.08	−0.326	8259.07	+0.062	8130.90	−0.269	8419.95	−0.164
7996.08	+0.010	8260.09	+0.058	8146.93	−0.225	8422.97	+0.012
8021.03	−0.162	8307.08	+0.149	8147.96	−0.285	8425.96	−0.121
8085.86	+0.041	8308.04	+0.193	8181.86	−0.318	8440.91	+0.202
8133.88	+0.066	8322.01	+0.037	8259.08	−0.375	8441.91	−0.011
8147.82	−0.045	8322.14	+0.024	8260.10	−0.309	8442.87	−0.014
8260.16	−0.001	8323.04	−0.009	8307.09	−0.487	HR 6056 (δ Oph)	
8309.11	−0.178	8323.13	+0.143	8308.05	−0.576	7604.24	−0.025
8323.09	−0.021	8323.98	+0.133	8322.02	−0.376	7606.18	−0.148
8373.07	+0.074	8324.06	+0.112	8322.15	−0.365	7651.11	−0.212
8385.07	−0.079	8324.95	+0.127	8323.04	−0.448	7652.11	−0.046
8420.89	−0.116	8325.05	+0.118	8323.14	−0.286	7690.99	−0.269
8422.93	−0.060	8325.95	+0.109	8323.99	−0.267	7702.99	−0.089
8440.86	+0.023	8368.81	+0.103	8324.07	−0.289	7724.98	−0.214
8442.85	−0.141	8372.81	+0.165	8324.96	−0.284	7728.95	−0.562
HR 5459 (α Cen A)		8374.93	+0.121	8325.06	−0.267	7743.91	−0.336
7487.15	+0.050	8384.84	+0.124	8325.96	−0.284	8132.95	−0.230
7520.12	−0.108	8384.94	+0.108	8368.82	−0.384	8145.82	−0.229
7548.11	−0.140	8385.13	+0.135	8372.82	−0.244	8147.90	−0.264
7603.11	−0.151	8386.92	+0.142	8374.94	−0.309	8309.17	−0.475
7649.15	−0.137	8387.05	+0.095	8384.84	−0.342	8322.12	−0.517
7690.95	−0.018	8419.78	+0.191	8384.94	−0.331	8323.11	−0.437
7725.01	−0.090	8420.01	+0.167	8385.14	−0.343	8323.16	−0.466
7945.21	+0.034	8420.98	+0.121	8386.93	−0.306	8324.09	−0.501
7996.04	+0.023	8421.07	+0.099	8419.79	−0.340	8325.12	−0.345
7996.82	+0.037	8423.04	+0.171	8420.02	−0.258	8372.10	−0.394
7997.97	+0.029	8425.92	+0.152	8420.99	−0.356	8373.09	−0.372
7997.99	+0.036	8426.11	+0.133	8421.07	−0.330	8375.09	−0.226
7998.01	+0.021	8441.89	+0.093	8423.05	−0.330	8385.10	−0.485
8000.05	+0.054	8442.81	+0.153	8423.18	−0.354	8387.10	−0.320
8019.99	+0.005	8478.99	+0.145	8425.92	−0.366	8419.92	−0.403
8061.98	−0.009	HR 5460 (α Cen B)		8426.11	−0.373	8420.87	−0.333
8083.01	+0.029	7487.15	+0.050	8440.88	−0.346	8420.97	−0.330
8130.83	+0.040	7520.13	−0.029	8441.89	−0.360	8422.90	−0.346
8130.89	+0.028	7548.12	−0.059	8442.82	−0.413	8423.01	−0.412
8131.82	+0.058	7603.12	−0.071	8478.99	−0.343	8425.99	−0.424
8131.82	+0.035	7649.16	−0.138	HR 5777 (37 Lib)		8426.05	−0.358
8131.83	+0.011	7690.96	−0.113	7606.22	−0.025	8440.94	−0.448
8131.83	+0.036	7725.02	−0.139	7651.06	−0.025	8440.96	−0.463
8131.84	+0.030	7945.22	−0.149	7693.98	+0.007	8441.03	−0.344

HJD −2440000	Velocity (km/s)
HR 6056 cont.	
8441.93	−0.422
8441.98	−0.395
8442.90	−0.495
8478.97	−0.263
HR 6102 (γ Aps)	
7482.07	+0.050
7529.97	+0.266
7603.17	+0.113
7610.98	+0.276
7649.10	+0.097
7691.03	+0.202
7729.05	+0.192
7996.18	+0.194
8020.21	+0.220
8083.09	+0.192
8130.95	+0.184
8146.97	+0.181
8181.90	+0.155
8257.16	+0.118
8309.14	+0.273
8322.17	+0.209
8373.03	+0.128
8375.05	+0.218
8387.14	+0.203
8419.98	+0.257
8421.00	+0.223
8423.06	+0.257
8426.02	+0.116
8440.93	+0.159
8441.96	+0.137
8442.89	+0.148
HR 6603 (β Oph)	
7649.14	−0.005
7729.07	−0.019
7996.14	+0.042
8020.17	−0.013
8062.05	−0.046
8083.12	+0.019
8085.94	−0.037
8090.90	−0.042
8322.20	−0.078
8147.91	−0.065
8372.20	−0.031
8373.11	−0.110
8375.10	−0.037
8387.16	+0.001
8420.08	−0.126
8421.05	−0.072
8423.03	−0.070
8426.07	−0.123
8441.01	+0.004
8442.96	−0.105
8479.02	−0.053
HR 6859 (δ Sgr)	
7649.18	−0.005
7652.23	−0.009
7692.09	+0.122
7694.09	+0.063
7700.08	+0.081
8021.08	+0.149
8062.13	+0.107
8086.03	+0.128
8131.98	+0.082
8145.90	+0.032
8181.94	+0.104
8324.11	+0.137
8372.21	+0.100
8420.10	+0.118
8423.11	+0.139
8426.13	+0.165
8441.06	+0.160
8441.99	+0.109
8443.01	+0.128
8478.95	+0.083
HR 7597 (ω Sgr)	
7487.91	+0.050
7488.91	+0.019
7700.12	+3.086
7729.11	+3.380
8021.19	+5.284
8062.10	+5.526
8085.97	+5.646
8090.93	+5.678
8131.00	+5.916
8145.85	+5.964
8180.94	+6.072
8372.23	+7.024
8420.05	+7.276
8441.08	+7.212
8442.01	+7.218
8479.03	+7.410
HR 7602 (β Aql)	
7652.26	−0.005
7692.14	−0.013
7729.97	−0.052
8021.14	+0.004
8062.15	−0.044
8086.01	−0.019
8131.93	−0.078
8145.88	−0.067
8147.97	−0.034
8181.92	−0.097
8372.17	−0.020
8375.19	+0.055
8420.13	−0.090
8421.11	+0.025
8423.13	−0.030
8441.04	+0.015
8442.02	−0.075
8479.06	−0.080
HR 7665 (δ Pav)	
7604.16	−0.025
7649.21	−0.020
7692.19	−0.040
7729.14	+0.021
7965.20	+0.042
8021.11	−0.018
8086.06	−0.005
8131.07	+0.025
8145.92	+0.020
8176.91	+0.017
8181.96	+0.013
8259.92	−0.030
8309.19	+0.001
8324.01	+0.086
8372.25	−0.045
8373.16	+0.016
8375.12	+0.019
8421.09	+0.008
8423.09	+0.009
8441.10	+0.017
8442.04	−0.043
8442.94	−0.041
8479.08	−0.021
HR 8181 (γ Pav)	
7486.96	+0.050
7604.20	+0.022
7652.15	−0.279
7694.16	−0.178
7725.16	−0.253
7744.00	−0.068
8021.26	−0.055
8083.24	−0.051
8131.10	−0.165
8145.94	−0.155
8176.03	−0.111
8176.94	−0.078
8181.98	−0.080
8259.94	−0.324
8309.21	−0.079
8324.04	−0.210
8373.19	−0.185
8375.15	−0.132
8420.18	+0.163
8441.11	−0.076
8442.95	−0.185
8479.09	+0.071
HR 8232 (β Aqr)	
7479.87	+0.050
7480.88	−0.136
7481.87	−0.057
7486.92	−0.118
7487.95	+0.063
7488.95	+0.027
7694.26	−0.231
7725.12	−0.440
7730.00	−0.197
8021.23	−0.452
8062.21	−0.424
8086.16	−0.250
8087.03	−0.154
8090.97	−0.256
8131.04	−0.340
8132.00	−0.407
8145.96	−0.302
8147.03	−0.207
8148.04	−0.325
8176.89	−0.318
8176.90	−0.160
8180.99	−0.402
8182.00	−0.284
8220.93	−0.414
8420.21	−0.148
8421.22	−0.072
8423.15	−0.201
8441.13	−0.115
8478.93	−0.161
HR 8387 (ϵ Ind)	
7487.02	−0.061
7528.94	+0.091
7700.23	−0.021
7730.18	+0.035
8086.11	+0.067
8131.15	+0.057
8145.98	+0.091
8176.96	−0.030
8182.03	+0.108
8258.95	+0.041
8324.14	+0.123

HJD	Velocity	HJD	Velocity	HJD	Velocity	HJD	Velocity
−2440000	(km/s)	−2440000	(km/s)	−2440000	(km/s)	−2440000	(km/s)
HR 8387 cont.		8062.19	−0.547	8421.18	+0.410	8147.01	+0.156
8373.21	+0.013	8087.00	−0.549	8441.17	−0.260	8148.01	+0.102
8421.14	+0.003	8132.07	−0.587	HR 8969 (ι Psc)		8177.01	+0.183
8441.15	+0.171	8146.02	−0.309	7479.90	+0.050	8182.08	+0.102
8479.12	+0.062	8176.99	+0.084	7730.08	+0.163	8421.29	+0.476
HR 8447 (τ PsA)		8182.05	−0.511	8086.19	+0.248		
7703.04	−0.021	8373.24	−0.598	8091.05	+0.180		
7725.20	−0.403	8420.24	−0.487	8132.02	+0.164		